INVESTIGATING THE ROLE OF HDAC4 SUBCELLULAR DISTRIBUTION IN *DROSOPHILA* DEVELOPMENT AND MEMORY

A thesis presented in partial fulfilment of the
requirements for the degree of

Doctor of Philosophy (PhD)

in

Biochemistry

At Massey University, Manawatū,
New Zealand

Patrick James Main

2019

"I sometimes feel, in reviewing the evidence on the localization of the memory trace, that the necessary conclusion is that learning is just not possible"

(Lashley, 1950)

Abstract

The class IIa histone deacetylase HDAC4 has been previously demonstrated to play an essential role in brain development, learning and memory. However, the molecular pathways through which it acts are unknown. HDAC4 undergoes activity-dependent nucleocytoplasmic shuttling, disruption of the balance of nuclear and cytoplasmic HDAC4 has been identified as a factor in developmental and neurodegenerative disorders. This project used *Drosophila melanogaster* as a model to investigate the effects of altered subcellular distribution of HDAC4 on neural development and memory formation through the overexpression of *Drosophila* HDAC4 and wild-type human HDAC4 (hHDAC4), as well as nuclear- and cytoplasm-localising mutants of hHDAC4 named 3SA and L175A, respectively. The nuclear or cytoplasmic abundance of HDAC4 was adjusted by expressing the mutants during development or in adult flies. It was established that increased nuclear abundance of hHDAC4 in the brain impaired long-term memory and development, whereas increasing the cytoplasmic abundance did not. Further investigation showed that, contrary to vertebrate models, HDAC4 does not appear to repress memory in *Drosophila* through inactivation of MEF2 or CREB. Investigation of the transcriptomic changes induced by nuclear and cytoplasmic HDAC4 via RNASeq on RNA isolated from fly heads showed that L175A unexpectedly up-regulates the expression of genes in transcription and DNA synthesis. The relatively low number of transcriptional changes induced by 3SA suggested that it may be acting through largely transcriptionally independent means to impair memory and development in *Drosophila*. The localisation of HDAC4 to punctate foci in nuclei, potentially forming protein aggregates similar to Marinesco bodies seen in Parkinson's Disease warrants further investigation. This project has shown that nuclear but not cytoplasmic HDAC4 impairs development and memory in *Drosophila*. Furthermore, cytoplasmic HDAC4 may play a role in transcriptional regulation of neurons, possibly regulation metabolic activity, suggesting that the activity-dependent nucleocytoplasmic shuttling of HDAC4 may not be primarily to remove HDAC4 from the nucleus and but instead to return HDAC4 to the cytoplasm.

Acknowledgements

Despite the single name in the authorship it is woefully inaccurate to consider a PhD the work of a single person. I do not believe for a single second I could have achieved this undertaking on my own, the support and input I received from friends, colleagues and family was essential to the completion of this project and I will utilise some space here to thank many of those who were part of this.

Firstly, my primary supervisor Dr Helen Fitzsimons without whom none of this could have happened in a very literal sense. The regular meetings and suggestions for interesting articles were vital to my understanding of the field. I am also infinitely grateful for her persistence and patience in nudging me into becoming the scientist I am today. Thank-you.

My co-supervisor Dr Tracy Hale, who was invaluable in her assistance with tissue culture and protein work, providing vital feedback and troubleshooting advice for cell-culture experiments in addition to critiquing my immunohistochemistry figures to help me think about communication with a wider audience.

The *Drosophila* neurogenetics group and chromatin research group that constitute our lab space have seen a number of members while I've been there, it has been a pleasure working with you all, particular thanks to Sarah Bond, Silvia Schwartz and Patrick Freymuth for teaching me many of the basics when I was new to the lab and Ana Claasen for being an excellent sounding board for ideas and bravely reading through my thesis.

I would also like to thank the Manawatū Microscopy and Imaging Centre for training and assistance with microscopy techniques, the technicians and administration team in the School of Fundamental sciences for their assistance in training and help, as well as the maintaining of equipment that is so vital to all of this.

Furthermore, I have been fortunate to receive the Massey Doctoral Scholarship to fund me through my research, in addition to the SFS Travel Fund for partially

funding my trip to the *Drosophila* Neurobiology conference in Krakow which was an unforgettable experience.

Last, and absolutely not least, my family and friends. My family for their unconditional support, my friends for being there when I needed distracting. My loving wife, Ami, for her tolerance, patience and love and my son Wilfred, who changed my life in ways I never considered.

ABBREVIATIONS

°C	Degrees Celsius
3SA	hHDAC4-3SA
Ach	Acetylcholine
AD	Alzheimer's Disease
APL	Anterior paired lateral neuron
Arc1	Activity-regulated cytoskeleton protein 1
ASD	Autism spectrum disorder
Aβ	Amyloid-beta
BDSC	Bloomington Drosophila Stock Centre
bp	Base pair
Ca++	Calcium
CaMK	Calcium/Calmodulin-dependent kinase
cAMP	Cyclic adenosine monophosphate
CI	Courtship index
CIP	Calf intestinal phosphatase
CRE	cAMP response element
CREB	CRE binding protein
Canton S	Canton special
CS	Conditioned stimulus
DAL	Dorsal anterolateral neuron
DAN	Dopaminergic neuron
DmHDAC4	*Drosophila* histone deacetylase 4
DNA	Deoxyribonucleic acid
DPM	Dorsal paired medial neurons
EDTA	Ethylenediaminetetraacetic acid
Elav	Embryonic lethal abnormal vision
FASII	Fasciclin II
GABA	γ-amino butyric acid
GFP	Green fluorescent protein
GMR	Glass multimer reporter
HAT	Histone acetyltransferase

HDAC	Histone deacetylase
HDACI	Histone deacetylase inhibitor
hHDAC4	Human histone deacetylase 4
KC	Kenyon cell
KCl	Potassium chloride
KD	Knockdown
kDa	Kilodalton
L	Litre
L175A	hHDAC4-L175A
LTM	Long-term memory
M	Molar
mA	Milliampere
MAPK	Mitogen-activated protein kinase
MB	Mushroom body
MBON	Mushroom body output neurons
MEF2	Myocyte enhancing factor 2
$MgCl_2$	Magnesium chloride
MI	Memory index
MRE	MEF2-response element
mRNA	Messenger RNA
NaB	Sodium butyrate
NEB	New England Biolabs
NES	Nuclear export signal
NLS	Nuclear localisation signal
NMDARs	N-methyl-D-aspartic acid receptors
OAN	Octopaminergic neurons
OE	Overexpression
PAM	Protocerebral anteromedial neurons
PBS	Phosphate buffered saline
PCR	Polymerase chain reaction
PD	Parkinson's disease
PKA	Protein kinase A
PKC	Protein kinase C

PPL	Protocerebral posterior lateral neurons
RIPA	Radioimmunoprecipitation assay buffer
RFP	Red fluorescent protein
RNAi	RNA interference
Rpm	Rotations per minute
RT	Room temperature
SAHA	Suberoylanilide hydroxamic acid
SDS-PAGE	Sodium dodecyl sulfate – polyacrylamide gel electrophoresis
STM	Short-term memory
SUMO	Small ubiquitin like modifier
TARGET	Temporal and regional gene expression targeting
TBS	Tris-buffered saline
TRP	Transient receptor potential
^{ts}	Temperature sensitive
UAS	Upstream activating sequence
V	Volts
VDRC	Vienna *Drosophila* Resource Centre
WB	Western blotting
wt	wild-type

Table of Contents

Table of Figures

Table of Tables

1 INTRODUCTION

1.1 Neurodevelopmental disorders & neurodegeneration

Neurodevelopmental disorders are defined as "a group of conditions with onset in the developmental period characterised by developmental deficits that produce impairments of personal, social, academic, or occupational functioning" (American Psychiatric Association, 2013). Disorders such as intellectual disability, autism spectrum disorders, epilepsy, and others are well recognised as developmental disorders that place a significant burden on the health of the individual as well as their families and the healthcare system. Often these disorders are evident in children as they grow up but others, such as attention-deficit hyperactivity disorder and autism-spectrum disorders can be subtle and remain undiagnosed well into adulthood.

Neurodegenerative disorders such as Alzheimer's Disease (AD) and Parkinson's Disease (PD) are characterised by dysfunction and death of neurons. This breakdown of the nervous system results in many symptoms such as loss of co-ordination or motor function; loss of memory and impaired sensory input (Kumar *et al.*, 2015; Przedborski, 2017). These disorders predominantly affect the elderly and, whilst they share many outward symptoms, are the result of a complex and diverse set of underlying causes, many of which are yet to be identified.

In general, neurodegenerative disorders are the result of the body's repair systems failing. These systems often breakdown with ageing and, as such, the increasing average age of the population is a growing concern. It was recently determined over 45 million people worldwide live with dementia, an increase of over 100% since 1990 (Prince *et al.*, 2015). Parkinson's disease, Alzheimer's disease and other dementias more than doubled from 0.7% of all deaths in 2000 to 2.6% in 2015 (World Health Organisation, 2016) , a trend which is expected to continue as life expectancies increase. In developed nations the prevalence of Alzheimer's in individuals over the age of 65 has been reported to be as high as

11% (Hebert *et al.*, 2013). This increase is expected to be more marked in underprivileged populations that, thanks to more widespread healthcare, are undergoing a more rapid increase in average life-expectancy (Prince *et al.*, 2015).

While the reduction in overall lifespan caused by neurodegeneration is a major concern, an additional factor is the years of healthy life lost during the progression of the disease, caused by steadily declining cognitive and motor function. The slow creep of these disorders makes them challenging to diagnose early as the symptoms are often confused with signs of stress and aging. A complication often leading to delayed diagnosis that results in worse treatment outcomes (Bradford *et al.*, 2009).

Alzheimer's disease accounts for upwards of 60% of the 50 million dementia cases worldwide (Alzheimer's Association, 2018). Alzheimer's disease is highly associated with the development of β-amyloid plaques and neurofibrillary tangles in the brain that are thought to lead to neuron death and subsequent degeneration in many regions of the brain (Alonso *et al.*, 1996; Murphy and LeVine III, 2010). As these physiological signs of the disorder develop and spread, they lead to increasing cognitive impairment. This impairment manifests initially as a reduced ability to form long-term memories.

A complicating factor in the diagnosis of neurodegenerative disorders is the prevalence of age-associated memory impairment (AAMI) (Crook *et al.*, 1986), the impairment of learning and memory caused by age-related loss of neural plasticity (Tulving and Markowitsch, 1998; Price *et al.*, 2004). As mentioned, the presence of AD is often missed in early diagnoses due to misidentification of the symptoms as "normal" AAMI. Multiple studies have demonstrated that older humans perform poorly in spatial memory tasks and are typically outperformed by their younger counterparts (Uttl and Graf, 1993; Wilkniss *et al.*, 1997; Moffat *et al.*, 2001; Price *et al.*, 2004). It is suggested that this reduction in neural function is due to age-related reductions in synaptic plasticity (the ability of a synapse to change in strength) a process required for learning and formation of new memories (Deupree *et al.*, 1993; Rosenzweig *et al.*, 1997; Vance and Wright, 2009).

Current research on AAMI is aimed at elucidating the molecular mechanisms underpinning this condition and determining whether they are related to the pathological effects that cause neurodegenerative diseases.

Due to the complex nature of learning and memory, it is often more feasible to study from the ground up, investigating the machinery by playing with individual cogs and levers and observing the effects, usually with a simplified model, an approach that is aided by the conservation of molecular mechanisms in learning and memory across a wide array of organisms.

1.2 The study of learning and memory

Learning is broadly defined as the acquisition of knowledge. The subsequent recall of this acquired knowledge is referred to as memory. The retention time of this memory can be brief (Short-term memory, STM) or can endure for longer periods of time (Long-term memory, LTM). This allows an individual organism to modify their behaviour to the changing environment by altering behaviour in response to experience. This behavioural plasticity was first observed by Santiago Ramon y Cajal (1894) in a series of studies that form the basis of modern neuroscience, identifying the role of "histological alterations" in the malleability of an individual's behaviour. The cell-based changes in this case are fluctuations in synaptic strength and number, a mechanism that is critical to learning and memory (Bailey and Kandel, 1993).

Synapses are the connection points between neurons, this connection is carried out through the transmittance of neurotransmitters that allow the propagation of an electrical signal across the cleft between individual neurons (Figure 1.1).

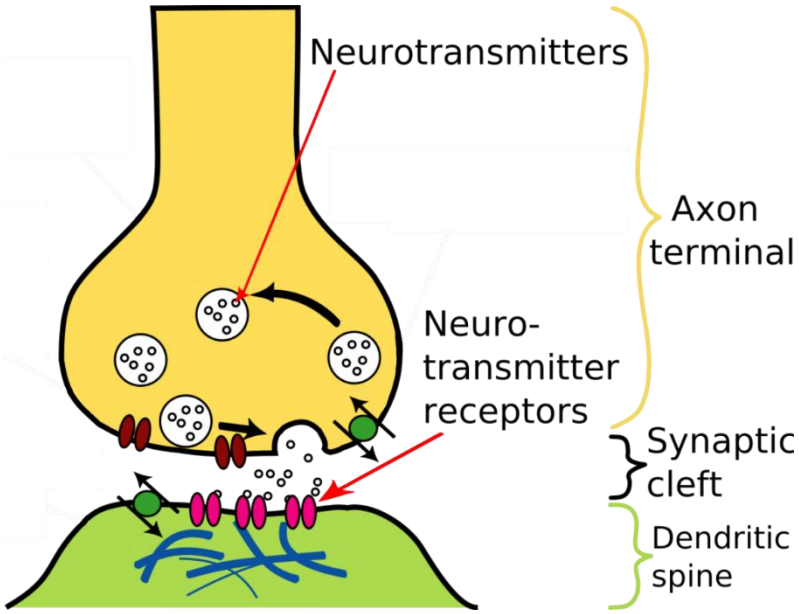

Figure 1.1 Schematic of an example synaptic junction.
A simplified figure emphasising the main components of synaptic transmission, notably the neurotransmitters (white circles) and the neurotransmitter receptors (purple) that are responsible for transmitting the electrical impulse from the axon (top) to the receiving dendrite (bottom) across the synaptic cleft. Figure modified from Osnimf, Wikipedia Commons, public domain.

Historically, the study of memory in invertebrates was believed to be futile. However, as the basic neural architecture is preserved across the animal kingdom it was proposed by Eric Kandel that the molecular mechanisms of memory are also conserved. Subsequently, he opted to study this conservation of systems in the sea snail *Aplysia californica*. This choice of organism seems unusual at first but *Aplysia* possess a number of large, easily identifiable neurons that permit the repeated testing of physiological responses within the same neuron across a range of individuals (Koester and Kandel, 1977).

In a simple but elegant series of experiments it was demonstrated that *Aplysia* exhibited long-term memory. This was done through exploitation of the gill-withdrawal reflex, a defensive, involuntary reflex in which the snail retracts its gill and siphon when disturbed to prevent damage to these sensitive structures. In these experiments, exposure to a noxious tactile stimulation caused the natural gill-withdrawal reflex (Kandel, 2001), (Figure 1.2). However, when this stimulation was repeated in an identical fashion the reflex response was reduced, a reduction that was shown to be independent of mechanical fatigue or sensory adaptation indicating a memory of the initial stimulus had been formed (Kandel and Tauc, 1965; Pinsker *et al.*, 1970; Frost *et al.*, 1985).

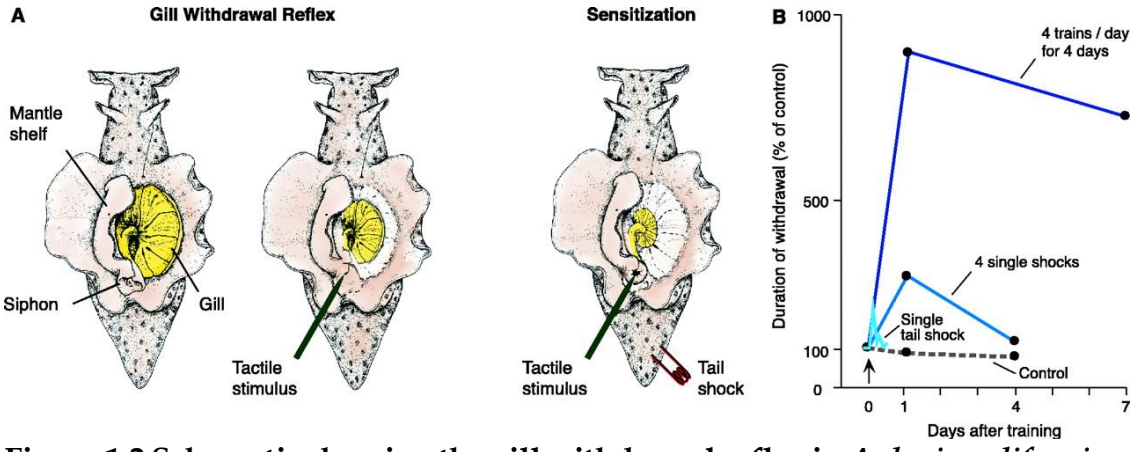

Figure 1.2 Schematic showing the gill withdrawal reflex in *Aplysia californica.*
A) Stimulation of the siphon results in rapid retraction of the delicate gill and siphon structures in an involuntary reflex. B) Repeat stimulation triggers a desensitisation characterised by reduced withdrawal of the gill (Kandel, 2001**)**. A) Reproduced with permission from AAAS, B) Copyright (1985) National Academy of Sciences (Frost *et al.*, 1985).

Further study showed that this training could be repeated in a fashion that would result in a much longer retention of the withdrawal reflex with a single training session being forgotten within minutes and multiple, time-spaced training sessions resulting in memories that last for days (Hawkins *et al.*, 2006).

Investigating further, it was shown that initial exposure to stimulus results in activation of the cyclic adenosine monophosphate (cAMP) kinase signalling cascade that involves activation of the cAMP-dependent protein kinase A (PKA) and subsequent phosphorylation of multiple targets (Abel and Lattal, 2001), which prevent the repolarisation of the neuronal membrane. This increases the release of neurotransmitters triggered by calcium ion influx when the wave of depolarisation reaches the synaptic cleft (Abel and Lattal, 2001). In addition to this, changes to the post-synaptic neuron's sensitivity to the released neurotransmitters can enhance this sensitisation (Kandel, 2012). These transient changes in neurotransmitter release and response result in short-term memory; a temporary memory in which the information is stored for approximately an hour (Rosenzweig *et al.*, 1993; Izquierdo *et al.*, 2002).

Continued activation of the same pathway (for example by repeat exposure to the same stimulus) results in a persistent increase in cAMP and PKA levels. This sustained increase results in the recruitment of a mitogen-activated protein kinase (MAPK) p42 that forms a complex that translocates into the nucleus and phosphorylates transcription factors such as cAMP response element binding protein (CREB). Phosphorylated CREB then binds to response elements in the genome and activates transcription of genes involved in dendrite growth and increasing synaptic density (De Roo *et al.*, 2008; Bourne and Harris, 2011; Chen *et al.*, 2017; Zhu *et al.*, 2018). The depth of study following Kandel's pioneer studies have shown that many of the mechanisms involved in learning and memory are conserved between vertebrates and invertebrates (Barco *et al.*, 2006), a high level overview of these similarities is shown in Figure 1.3.

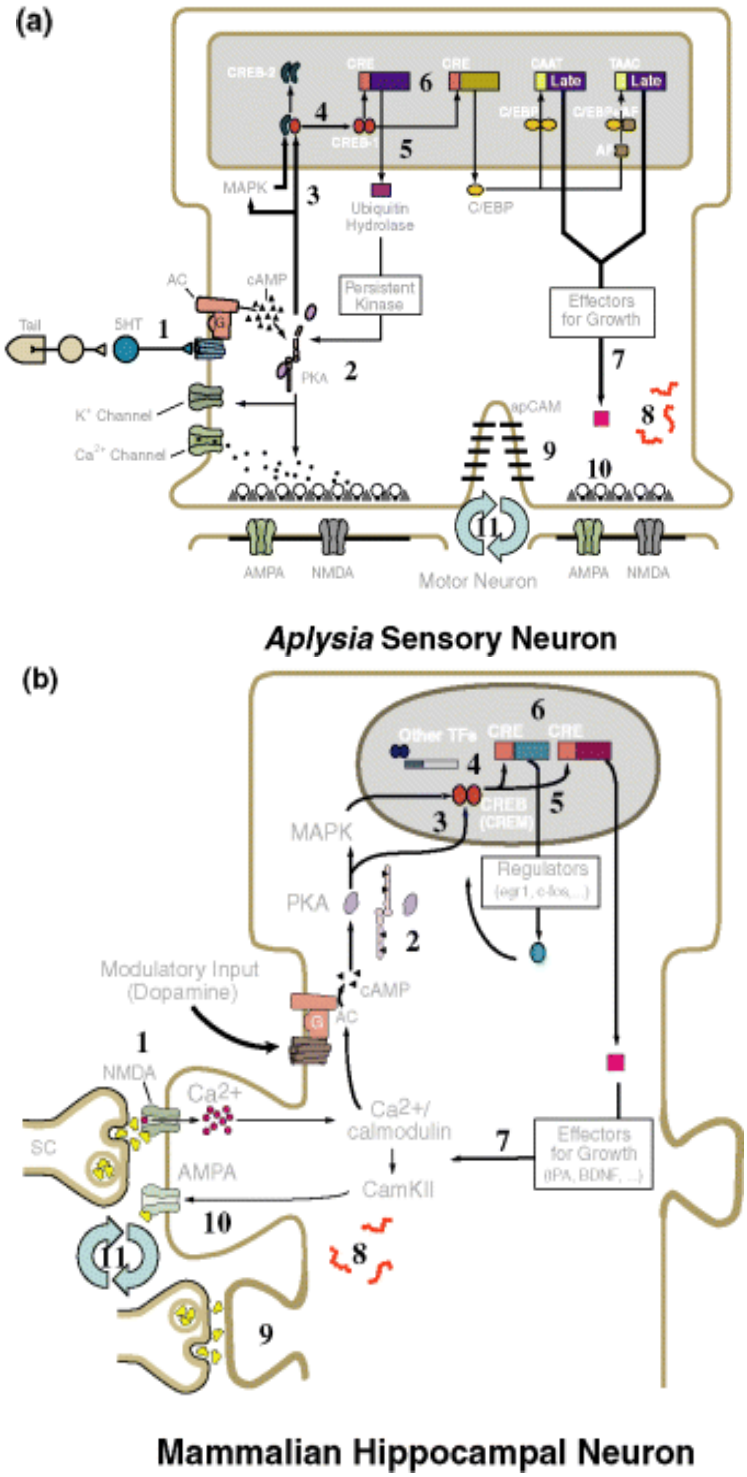

Figure 1.3 Molecular similarities between *Aplysia* and mammalian neurons.
Key factors in *Aplysia* neurons (a) and mammalian hippocampal neuron (b) signalling. 1) Release of neurotransmitters and short-term strengthening of synaptic connections; 2) maintained equilibrium between synaptic kinase and phosphatase activities; 3) transport of components from the synapse to the nucleus; 4) nuclear transcription regulation; 5) depolarisation induced gene expression; 6) epigenetic shifts in gene expression; 7) transport of newly transcribed products to synapse; 8) protein synthesis at synapses; 9) growth and development of new synapses; 10) activation of silent synapses; 11) memory persistence based on recurring mechanisms. These events move from the synapse (1-2), to the nucleus (3-6) and then back to the synapse (7-11). Figure from Barco *et al.*, 2006, reproduced with permission.

The cAMP pathway is also conserved in the fruit fly *Drosophila melanogaster*. Two of the first memory related mutants characterised in *Drosophila* were the cAMP associated genes *dunce* and *rutabaga* (Quinn *et al.*, 1974; Livingstone *et al.*, 1984). *dunce* was first identified in an olfactory learning assay and has since been shown to be a large, complex locus that encodes at least 10 differentially spliced variants of a cAMP phosphodiesterase, the enzyme responsible for the degradation of cAMP (Conti and Beavo, 2007). *rutabaga* plays a complimentary role, encoding a Ca^{2+}/Calmodulin-stimulated adenylate cyclase, an enzyme that makes cAMP and was first identified through learning deficiencies in the same assay as *dunce* (Quinn *et al.*, 1974).

This data supports the original hypothesis proposed by Eric Kandel in that the short- and long-term memory systems rely on a cAMP-dependent signalling cascade that is highly conserved between vertebrates and invertebrates allowing for the study of vertebrate learning and memory through invertebrate models.

1.2.1 SHORT AND LONG-TERM MEMORY

Although short and long-term memory are often referred to as a continuum of the same process, the two systems are independent from one another. This has been exemplified by the disruption of STM without affecting LTM and vice versa (Izquierdo *et al.*, 1999, 2000). This has been shown through pharmacological inhibition of memory formation by infusing rat brains with a range of treatments from receptor antagonists/agonists to enzyme inhibitors and stimulants and testing short- and long-term memory in the treated rats using an aversive memory assay. In this study it was observed that 11 treatments, including CNQX (a glutamate AMPA receptor blocker) and muscomil (a $GABA_A$ receptor agonist) inhibited the formation of short-term memory without altering LTM performance in the same animals (Izquierdo *et al.*, 2002). Paralleling these rat studies, it has been shown that treatment of *Aplysia* with serotonin during training was shown to disrupt the formation of STM without affecting LTM development (Emptage and Carew, 1993; Izquierdo *et al.*, 1998) once more

reinforcing the conservation of the molecular mechanisms involved in learning and memory.

1.2.2 THE PHYSIOLOGY OF MEMORY

Historically, it was believed that memory was stored in specific "memory neurons" that existed to facilitate information storage and recall. However, the potential for memory storage is built into the basic neural architecture (Kandel, 2012) and the formation of memory relies on the strengthening of connections in the existing neural pathway. This relies on increasing the sensitivity to stimulus, increasing the output from a single stimulation, or increasing the number of connections between neurons, all of which result in a greater neuronal output for a single stimulation (Hawkins *et al.*, 2006; De Roo *et al.*, 2008). In both mammal and insect models the formation and storage of memories occurs in specific structures within the brain. In *Drosophila melanogaster* the electrical impulses and gene expression associated with memory have been shown to be localised largely within the mushroom body (MB) (Davis, 2005; Plaçais *et al.*, 2012). These traces are modulated and acted upon by the extrinsic neurons that allow for the mushroom body to communicate with other brain regions (Aso *et al.*, 2014a; Masek and Keene, 2016).

In mammalian systems it is harder to pinpoint a single, specific structure in the brain associated with memory. This difficulty arises due to the complex interplay between structures of the mammalian brain and the tendency of individual stimulus associated impulses (traces) to pass through multiple structures (Shu *et al.*, 2003). In mammals, the hippocampus is particularly involved in converting short- to long-term memory as well as spatial memory (Berger *et al.*, 1976; Ergorul and Eichenbaum, 2004), the amygdala has been indicated as highly associated with emotional memories (McGaugh *et al.*, 1996; LaBar and Cabeza, 2006), the entorhinal cortex acts as a conduit from the hippocampus to the rest of the neo-cortex, as well as acting to retrieve memory (Segal, 1973; Takehara-Nishiuchi, 2014) and the cerebellum is highly associated with motor memories, physical responses to conditioned stimuli (Mishkin and Appenzeller, 1987; Attwell *et al.*,

2002). These four regions barely scratch the surface of the various regions in the mammalian brain involved in learning and memory. The complexity and diversity of the role these structures play can be shown by comparing the role of a single protein across the different structures. In a subset of neurons in the hippocampus, knocking out protein kinase C results in normal STM with defective LTM whereas in the entorhinal cortex PKC is required for both STM and LTM (Izquierdo *et al.*, 1999). It has also been shown that protein kinase A is involved in both forms of memory in the hippocampus, acting to generate STM in the first 90 minutes post-training and acting to generate LTM during training and approximately 180 minutes post-training (Vianna *et al.*, 1999). These studies show that the complexity of the mammalian system make determining the role of a protein challenging adding to the benefits of using the *Drosophila* model. Using a simplified model allows the characterisation of proteins with a key role in memory as a whole, without being concerned about the influence of that protein's role in different substructures.

1.3 The *Drosophila* mushroom body

The mushroom body is a bilateral neuropil structure initially identified by Félix Dujardin in 1850, who initially compared it to the cerebral cortex of vertebrates and considered it to be the major processing centre of the insect brain (Dujardin, 1850; Heisenberg, 1998). The mushroom body is part of the olfactory system which is a major pathway in courtship and olfactory memory (Section 1.7.1) It has subsequently been shown to be the main memory centre in *Drosophila* and is a structure present in other insects such as locusts and honeybees (Verlinden, 2018).

1.3.1 INTRINSIC NEURONS OF THE MUSHROOM BODY

The *Drosophila* mushroom body is comprised of approximately 5,000 neurons, making up approximately 2% of the neurons in the *Drosophila* brain (Alivisatos *et al.*, 2012). The intrinsic neurons of the mushroom body are the Kenyon cells. Their approximately 2,000 cell bodies are clustered in the dorsal posterior cortex of the brain and project bundles of axons to form the characteristic, L-shaped, mushroom body lobes (Aso *et al.*, 2009) (Figure 1.4, Figure 1.5). Their dendrites arborise to form a globular region known as the calyx and they receive input from the olfactory projection neurons (the antennocerebral tract) as well as visual input neurons that supply the ventral accessory calyx of the mushroom body (Vogt *et al.*, 2016).

There are three subtypes of Kenyon cell which are characterised by differential expression of eight gene markers (Crittenden *et al.*, 1998). The axons of all three subtypes are initially bundled together to form the pedunculus, which projects anteriorly from the cell bodies. Group 1 Kenyon cells (α/β neurons) project their axons anteriorly and then they bifurcate at the anterior region of the pedunculus to from the vertical α and medial β lobes. Group 2 (α′/β′ neurons) bifurcate similarly to form the α′ and β′ lobes and the group 3 Kenyon Cells (γ neurons) project a single medial γ lobe slightly anterior of the β/β′ lobes (Crittenden *et al.*, 1998).

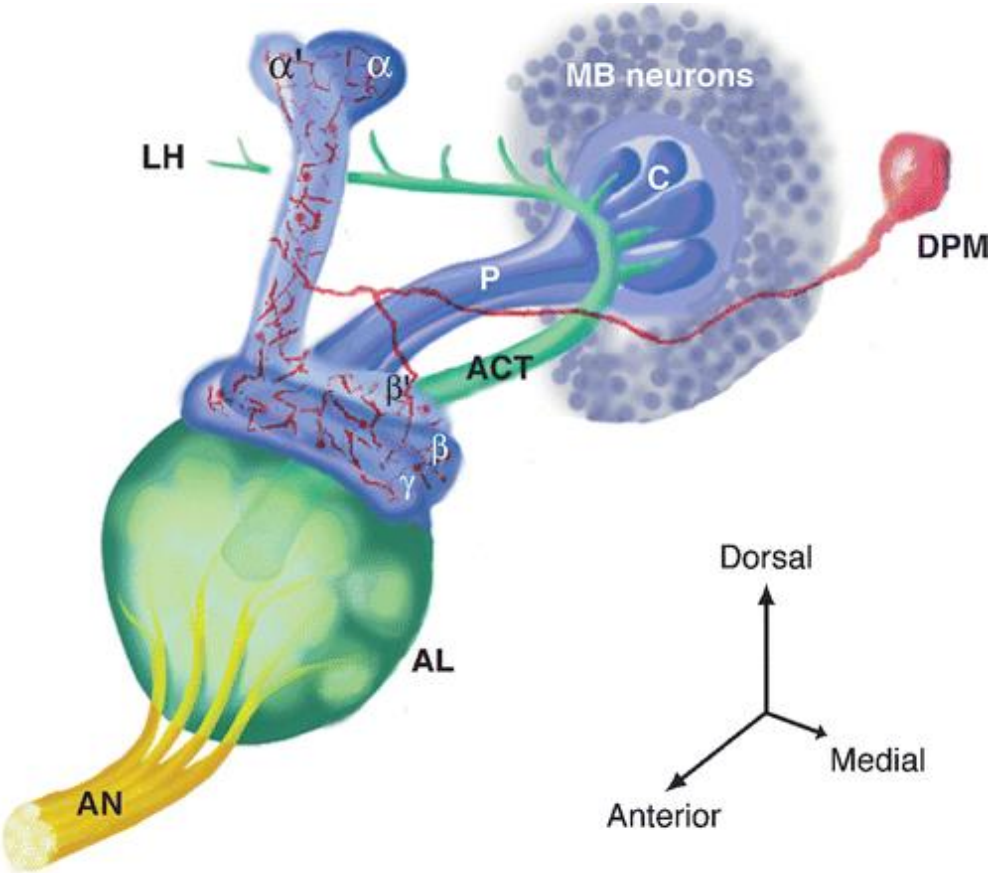

Figure 1.4 Lateral view of a single mushroom body and surrounding structure. Viewed anteriorly from the central line of the brain this schematic shows the Antennal neurons (AN), the antennal lobe (AL) the mushroom body lobes (α, α′, β, β′ and γ) as well as the pedunculus (P), calyx (C) and Kenyon cell bodies (Mushroom body neurons). Additionally, the dorsal paired medial neurons (DPM) are shown as an important input source to the mushroom body, as are the lateral horn (LH) and antennal cerebral tract (ACT). Figure from Davis, 2005, reproduced with permission from Annual reviews.

A crucial role for the mushroom body in learning and memory was initially suggested when single gene mutants that exhibited deformed mushroom bodies also demonstrated severely impaired olfactory associative learning (Heisenberg, 1985). In addition, the genes discovered early in the history of *Drosophila* memory research such as *dunce* and *rutabaga* are expressed highly in the mushroom body (Nighorn *et al.*, 1991; Han *et al.*, 1992; Qiu and Davis, 1993).

Since this time, memory researchers have focused their efforts on investigating the roles of specific Kenyon Cell subtypes, predominantly in the olfactory conditioning models, and found that they appear to be functionally distinct with the expression of different memory-related transcription factors in different

subtypes resulting in different memory phenotypes (Keleman *et al.*, 2007; Fitzsimons *et al.*, 2013; Guven-Ozkan and Davis, 2014).

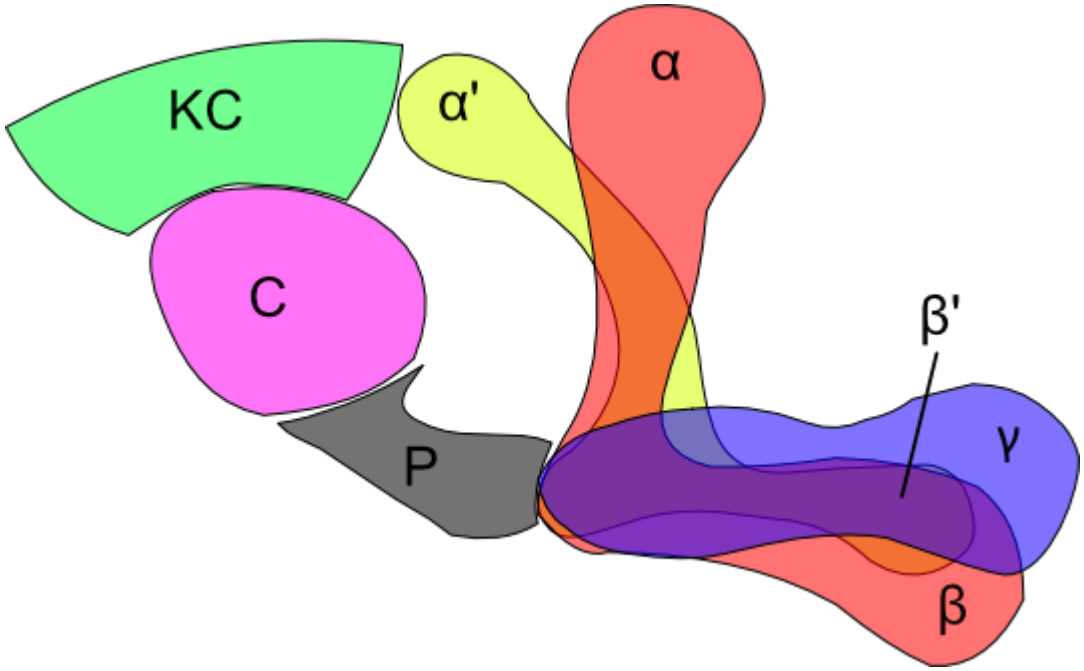

Figure 1.5 Simplified schematic of the MB from the anterior of the fly.
This figure provides a more representative image of what is observed in confocal microscope images of whole-brains. Each coloured region indicates a separate identifiable structure. Green is the Kenyon cells (KC), pink is the Calyx (C), and grey is the pedunculus (P) that projects from the KC to the MB lobes. The lobes are in yellow (α′/β′), red (α/β) and blue (γ), the image is artificially flattened for simplicity.

Courtship conditioning (described in detail in 1.3.2) is a method by which LTM can be assayed in *Drosophila*. The conditioning establishes a new behaviour pattern after the training period in a measurable, consistent manner. From here on this will be referred to as courtship memory, a memory that is neither strictly aversive or appetitive. Previously many papers have identified the γ lobe as having a vital role in long-term courtship conditioning. For example, whole-brain expression of a mutant Orb2, a cytoplasmically localised protein that acts as a translational activator in *Drosophila*, results in severely reduced LTM performance, but restoration of wild-type expression in only the γ-lobes of the MB restores LTM performance (Keleman *et al.*, 2007). Additionally, overexpression of the histone deacetylase HDAC4 in only the γ-lobes of the MB severely disrupts LTM when measuring long-term courtship memory whereas

overexpression in the α/β or the α'/β' lobes did not significantly impair LTM performance (Fitzsimons *et al.*, 2013). Recently, a study carried out using new drivers that express in extremely specific subsections of the MB has suggested that synaptic firing in the γ-lobe is not required for short term courtship memory (Montague and Baker, 2016). However, it is required for the learning process as inhibition of the γ extrinsic neuron activity results in disrupted courtship memory (Montague and Baker, 2016). This could suggest that the γ-lobes are required for long-term, but not short-term, courtship memory.

1.3.2 GENETIC TOOLS FOR *DROSOPHILA* MEMORY RESEARCH

In addition to the small but well characterised brains and reproducible memory assays that have been developed, there are powerful genetic tools that allow for tightly controlled transgene expression of constructs in the living fly. The UAS-GAL4 system allows for the expression of a specific transgene in specific tissue groups.

GAL4 is a transcriptional activator from yeast that binds to a specific sequence known as an upstream activating sequence (UAS) (Brand and Perrimon, 1993). *Drosophila* do not have a paralogous transcription activator, allowing activation of the gene downstream of the UAS exclusively in the presence of GAL4. When this GAL4 expression is driven by a *Drosophila* promoter or enhancer this system allows for the tissue-specific expression of a target gene, small interfering RNA (RNAi) or effectors like shibire^{ts} (Koenig and Ikeda, 1978) and TrpA1 (Viswanath *et al.*, 2003; Rosenzweig *et al.*, 2004). The UAS-GAL4 system can be utilised to examine the tissue-specific effects of a gene as a reverse genetic approach by expressing the gene of interest only in specific tissues and tissue groups. This bipartite system uses two strains of modified flies (lines of flies harbouring transgene constructs in their genome) the first which has the gene of interest inserted downstream of the UAS and the second that carries a *gal4* gene under control of a tissue-specific promoter which is commonly referred to as the GAL4-driver (Figure 1.6). These two fly lines are crossed and the resulting F1 progeny possess single copies of both the promoter-GAL4 construct and the UAS-gene of

interest construct which facilitates transgene expression only in the tissue where the promoter normally drives expression. Maintaining the driver and gene of

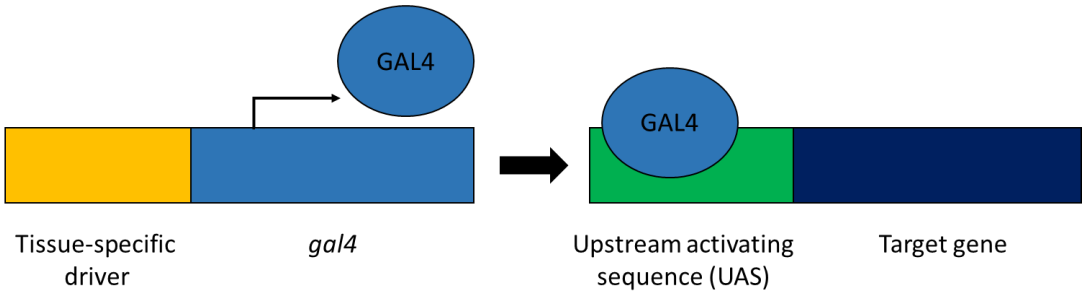

Figure 1.6 Schematic showing an example of the UAS-GAL4 system.
The tissue specific driver is activated based on its origin, allowing mimicry of expression patterns. The GAL4 is transcribed by the cell's transcription machinery and subsequently binds to the UAS, allowing transcription of the target gene (or construct) by the cell's transcription machinery.

interest in separate lines increases the utility of the system as it allows the combination of different transgenes with different driver lines without having to generate new transgenic organisms. This permits investigation of the role of different proteins in different tissue sets. Characterisation of the tissue-specific drivers can be carried out by expressing fluorescent proteins and then imaging the tissue to determine where the fluorescent protein is expressed. An example of this is shown below in which GFP and a nuclear-localising RFP are co-expressed using the OK107-GAL4 driver that expresses highly in the mushroom bodies. The expressed proteins are only present in the MB Kenyon cells and lobes, showing the tight spatial regulation provided by the UAS/GAL4 system (Figure 1.7).

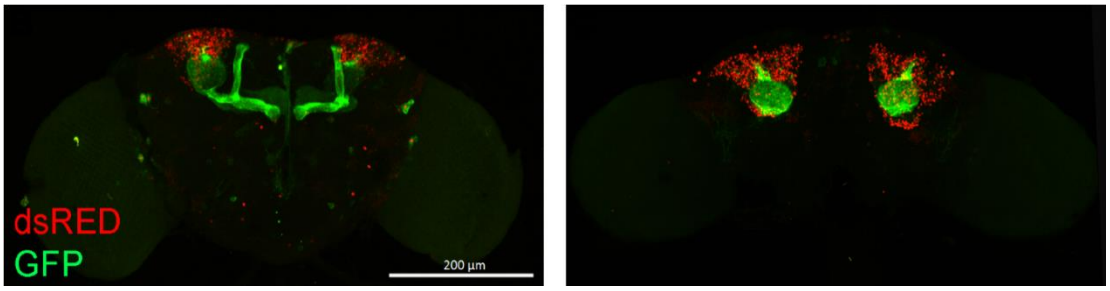

Figure 1.7 Whole mount confocal microscopy images showing the structure of the mushroom body in the adult brain.
Anterior on the left and posterior on the right. Nuclei are highlighted with a nuclear localised red fluorescent protein (dsRED) and cytoplasmic components are highlighted with GFP. Expression of both fluorescent proteins is driven by OK107-GAL4. Images from Fitzsimons *et al.*, 2013. Used under creative commons licence.

Recently, a finer method of construct activation called split-GAL4 has been developed. This is a modified version of the UAS-GAL4 system in which the broad expression patterns of many characterised drivers can be refined. The GAL4 activator can be split into two main components, the DNA binding domain (DBD) and the activator domain (AD) which cannot independently activate transcription but can when present in the same cell, thus, transcription is inactive unless the two domains are both present. Thus, crossing two lines, one which harbours the DBD under a tissue specific driver and a second that carries the AD under a different driver allows expression of a UAS-transgene only in the tissue in which the drivers overlap. This allows for the regulation of expression in single cell-types and even single neurons making the previous UAS-GAL4 system appear like a sledgehammer to the split-GAL4's scalpel (Luan *et al.*, 2006). Further refinement of this system is possible through the usage of a modified version of this technique referred to as temporal and regional gene expression targeting (TARGET).

TARGET makes use of a protein known as GAL80, this is a protein produced in yeast in the absence of galactose which binds to GAL4, preventing transcription. Using a temperature sensitive mutant of the GAL80 protein ($GAL80^{ts}$) allows the inhibition of GAL4 activated transcription by housing the flies at 18°C. Raising the temperature to 28-30°C inactivates $GAL80^{ts}$ and disrupts this interaction between GAL80 and GAL4, allowing GAL4-activated transcription to occur (Figure 1.8). Thus, regulating the incubation temperature of the flies allows for temporal regulation of the expression of GAL4-activated genes (McGuire *et al.*, 2004). The $GAL80^{ts}$ protein is totally inactivated at 30°C but the efficiency of its binding is reduced as temperature increases, allowing a sliding scale of activation. This tight, spatiotemporal control of expression allows for investigation of the effects of the gene of interest at specific points in development as well as interrupting pathways in mature organisms without inducing developmental defects.

The UAS-GAL4 system can also be used to drive expression of effectors that modulate cellular function such as *shibire*^{ts} and TrpA1 which mediate synaptic transmission and have been key in establishing the role of the intrinsic and extrinsic mushroom body neurons in learning, memory and behaviour (Aso *et al.*, 2014a; Montague and Baker, 2016; Pavlowsky *et al.*, 2018). The *shibire* gene encodes dynamin, a protein involved in the recycling of synaptic vesicles that is essential to synaptic function (Bliek and Meyerowrtz, 1991). A temperature sensitive mutant of this protein called *shibire ts1* (*shi*^{ts1}) was characterised in the early 1980's (Koenig and Ikeda, 1978) and shown to inhibit synaptic function in whole flies, leading to paralysis when the flies are incubated at a restrictive temperature (>29°C). It was subsequently shown that using the UAS-GAL4 system in combination with *shi*^{ts1} allowed for the rapid induction of a reversible temperature sensitive block in specific subsets of neuron (such as cholinergic neurons using the *Cha*-GAL4 driver or photoreceptors using the *ninaE*-GAL4 driver).

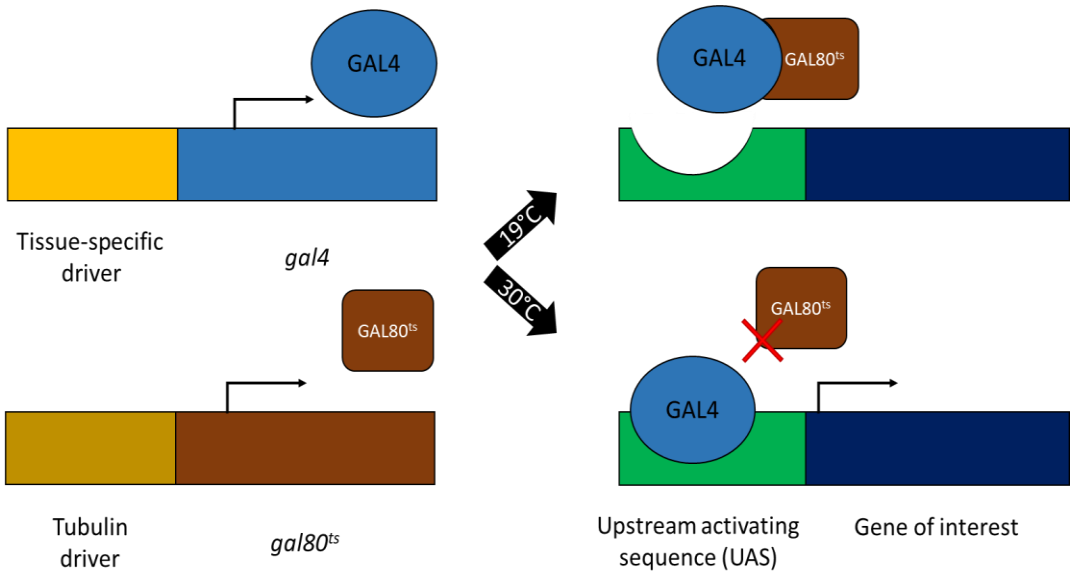

Figure 1.8 Schematic of the mechanism behind the TARGET system.
The TARGET system expands upon the UAS-GAL4 system by co-expression a temperature sensitive mutant of the GAL80 protein (GAL80^{ts}) that binds to GAL4 and prevents it binding to the UAS.

While *shi*^{ts1} can be used to reliably turn off synaptic function and thus dampen signalling at the single neuron level, a transient receptor potential (TRP) family ion channel called TRPA1 can be used to depolarise neurons and subsequently activate synaptic transmission. The TRP proteins in *Drosophila* were first identified in the early 2000's and rapidly characterised as having a key role in thermotaxis in *Drosophila* larvae by triggering movement away from excessive (>30°C) temperature by instigating nerve signalling in specific larval brain regions when above 25°C (Viswanath *et al.*, 2003; Rosenzweig *et al.*, 2004). This temperature dependent neuron activation can be manipulated using the UAS-GAL4 system to tightly regulate spatial expression of the *TrpA1* gene, which allows for temperature dependent activation of TRPA1 by increasing the temperature, opening the TRPA1 cation channel and causing rapid depolarisation of the neuron, leading to neuron signalling (Hamada *et al.*, 2008).

These tools have been vital in teasing apart the tissue-specific role of proteins in learning and memory in *Drosophila*. Such as characterising cell-specific roles of proteins using the UAS-GAL4 system to identify specific neuronal circuitry required for synaptic output during different phases of memory formation and retrieval using shibire^{ts} and TrpA1.

1.3.3 EXTRINSIC NEURONS OF THE MUSHROOM BODY

While the Kenyon cells are the intrinsic neurons of the mushroom body, extrinsic neurons also play an important role in learning and memory. Extrinsic neurons are neurons that either innervate the mushroom body from other parts of the brain or project to other parts of the brain from within the mushroom body (Ito *et al.*, 1997). An increasing number of extrinsic neurons have been shown to play critical roles in learning and memory. They are classified based on their grouping, location in the brain, and their primary neurotransmitter production. Neurons that generate dopamine are referred to as dopaminergic neurons (DANs), neurons that produce octopamine are referred to as octopaminergic neurons (OANs), neurons that produce γ-amino butyric acid (GABA) are known

as GABAergic neurons and neurons that utilise acetylcholine (Ach) are termed cholinergic neurons.

The first main division of extrinsic neurons is the divide between input and output neurons. The input neurons of the MB are responsible for the modulation of inputs to the MB as well as regulating the MB pathways themselves. One of the roles played by these is processing raw sensory information before feeding it into the MB. For example, the olfactory neurons (AN in Figure 1.4) do not feed straight into the MB but first project into the antennal lobe (AL in Figure 1.4) where they terminate in discrete glormeruli that, in turn, are innervated by the projection neurons via the antennocerebral tract (ACT in Figure 1.4) that send processed olfactory information into the MB and lateral horn (LH) (Davis, 2011).

The anterior paired lateral (APL) neuron is a large, inhibitory neuron that projects into the calyx, peduncle and lobes of the mushroom body and appears to be involved in habituation responses and required for formation of anaesthesia resistant memory in *Drosophila* (Liu and Davis, 2009; Wu *et al.*, 2013). Similar to APL neurons, dorsal paired medial (DPM) neurons projects into multiple sites of the mushroom body, however, in the case of DPM neurons this projection is exclusively into the lobes (Guven-Ozkan and Davis, 2014). DPM neurons have been implicated in memory recall, sleep regulation and memory consolidation (Keene *et al.*, 2004; Yu *et al.*, 2005; Haynes *et al.*, 2015).

The dorsal anterolateral neurons (DAL) project into the α and β lobes of the MB as well as the pedunculus. DAL neurons have been established as a site of protein synthesis required for olfactory associated LTM formation, and it has been proposed that the mushroom body receives the input and consolidates it into the DAL neurons which are then responsible for storage and subsequent retrieval of the memory (Chen *et al.*, 2012a). Protocerebral posterior lateral 1 (PPL1) neurons are dopaminergic neurons that project into the pedunculus and α-lobes of the MB. Activation of PPL1 neurons leads to reduced responses to noxious odours, silencing of the PPL1 has the reverse effect. Furthermore, PPL1 neurons have been shown to have a role in memory formation (Claridge-Chang *et al.*, 2009;

Fuenzalida-Uribe and Campusano, 2018). Finally, the protocerebral anteromedial (PAM) neurons are a large population of mostly (90 of the 130) dopaminergic neurons that project into multiple regions of the MB. PAM neurons have a multitude of roles in *Drosophila* behaviour, affecting both appetitive and aversive memory as well as regulating innate flight behaviour (Yamagata *et al.*, 2016; Fuenzalida-Uribe and Campusano, 2018; Manjila *et al.*, 2019).

It may be noticed that, in the above descriptions, some of these physically grouped extrinsic neurons are formed by neurons that produce different neurotransmitters. These neurons have distinct roles based on the neurotransmitter they secrete, modifying their activity in their bundle. Dopaminergic neurons (DANs) are specialised neurons in the brain that synthesise dopamine, in *Drosophila* these neurons are dispersed in fifteen clusters throughout the brain. Particularly relevant are the PPL1 and PAM1 DANs that innervate the MB (Mao and Davis, 2009). DANs are activated by aversive or rewarding stimuli in olfactory classical conditioning. Increased activity of DANs leads to increased dopamine which, in turn, increases the levels of cAMP and PKA (Tomchik and Davis, 2009; Gervasi *et al.*, 2010; Liu *et al.*, 2012). Furthermore, blocking DAN signalling during training with *shibire*^{ts} (a method by which to selectively silence neurons, detailed further in 1.3.3) impairs memory acquisition (Schwaerzel *et al.*, 2003). Formation of courtship conditioning induced memory requires the input of the sP13 dopaminergic neurons to DopR1 receptors on the MB γ-lobes and disruption of either element of this (either through inhibition of synaptic firing of sP13 or knockdown of DopR1) significantly impairs learning (Keleman *et al.*, 2012). Feedback from Kenyon Cells to DAN is cholinergic and this input is required for olfactory conditioning. DAN are both pre and post-synaptic to Kenyon Cell; acting as a closed circuit, much like the DAL neuron and the MB (Cervantes-Sandoval *et al.*, 2017). It has been proposed that DANs are required, not just for the formation of memory but also for the forgetting; and that the consolidation process requires the prevention of forgetting by blocking the activity of the dopamine receptor in the mushroom bodies (DAMB) (Berry *et al.*, 2012).

Octopamine is a neurotransmitter specific to protostomes that is similar in form and function to norepinephrine, readying the organism's nervous system and body for fight or flight responses (Claßen and Scholz, 2018). In *Drosophila,* octopaminergic neurons are involved in food attraction, appetite control and fat regulation (Zhang *et al.*, 2013; Claßen and Scholz, 2018; Youn *et al.*, 2018), but several studies have implicated octopamine and thus octopaminergic neurons in generating anaesthesia resistant memory (Wu *et al.*, 2013) and aversive olfactory conditioning (Iliadi *et al.*, 2017). These early results hint that, while predominantly involved in metabolic regulation, octopamine may have a role in learning and memory that is not yet well understood.

The output neurons of the MB have only been described in detail in a handful of studies, most thoroughly in Aso *et al.* in 2014 (2014a, 2014b) with further studies investigating the role these extrinsic neurons play in the learning and behaviour (Hige *et al.*, 2015; Montague and Baker, 2016; Saumweber *et al.*, 2018; Manjila *et al.*, 2019). In a pair of highly detailed studies into the mushroom body output neurons (MBONs) Aso *et al.* identified 21 MBON cell types using split-GAL4 lines then utilised the interruption of synaptic transmission by selective expression of *shibire*^{ts} using split GAL4 lines to preliminarily investigate the role of each cell-type in learning and memory. It was shown that the 2,000 Kenyon cells of the mushroom body output the information through only 34 neurons that extend their dendrites into the axons of the Kenyon cells and project to regions outside the mushroom body. The 34 neurons are comprised of 21 types, named for their origin in the mushroom body (Aso *et al.*, 2014a, 2014b). Initially, approximately three quarters of the characterised types had some role in aversive or appetitive memory but distinct roles such as sleep regulation, flight control and courtship behaviour being attributed to specific MBONs in subsequent studies (Aso *et al.*, 2014a; Montague and Baker, 2016; Berry *et al.*, 2018; Manjila *et al.*, 2019).

Kenyon cells are the intrinsic neurons of the mushroom body and are critical to the function of LTM. Their output is modulated by extrinsic neurons such as the DPM and DAL, and the output from the Kenyon cells is to 21 cell-types that

constitute the 34 output neurons. Overall the growing body of research on extrinsic neurons shows that, while not as simple as first believed, the circuitry plays an important role in memory function. Furthermore, with recent developments in the *Drosophila* toolkit it is become easier to alter the expression of candidate memory proteins in specific neuronal subtypes in order to further understand molecular memory pathway and correlate genetic changes with behavioural changes.

1.4 Epigenetic regulation of memory formation

Memory formation relies on the dynamic modification of gene expression to allow the precise temporal and spatial regulation of expression of subsets of genes within neurons. A major research focus of late has been into the epigenetic control of gene regulation. Epigenetic regulation is defined as the regulation of expression that is "above the genes" and refers to the control of gene expression through any means that not encoded in the sequence of that gene. The term epigenetics was previously strictly tied to the modification of chromatin but now broadened to include most regulation of transcription at a wide-spread level (Henikoff and Matzke, 1997; Choudhuri, 2011).

Chromatin is a superstructure in the nucleus that permits the organisation and tight packaging of DNA as well as playing a role in regulating DNA transcription, replication, and repair. Chromatin is comprised of nucleosomes, a repeating structure of DNA and protein in which the DNA wraps around an octamer of four histone subunits (two each of H2B, H2A, H4 and H3) 1.67 times, requiring 147 base pairs of DNA to complete the structure (Figure 1.9) (Marks *et al.*, 2003). The nucleosomes are connected to one another by a linking strand 20 – 30 bp in length. How tightly the nucleosomes are bound to one another varies depending on modifications made to the histone tails that control how accessible the DNA is to transcription factors and RNA polymerases (Marks *et al.*, 2001).

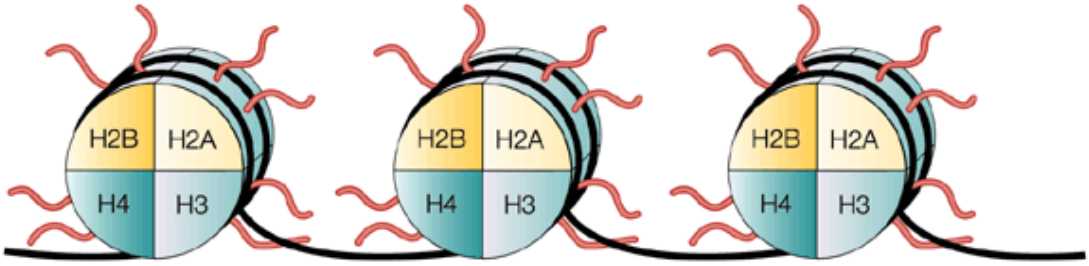

Figure 1.9 Schematic of the nucleosomes and their structure.
The four pairs of histone proteins are labelled (H2A, H2B, H3 and H4) and the histone protein tails are visible in pink. As shown in black the DNA wraps around not quite twice and connects each nucleosome with a flexible section approximately 25 bp in length. Figure from Marks *et al.*, 2001, reproduced with permission from Springer Nature.

The histone tails can be modified via acetylation/deacetylation (Gershey *et al.*, 1968); methylation/demethylation (Allfrey *et al.*, 1964); or phosphorylation/ dephosphorylation (Kleinsmith *et al.*, 1966). These modifications alter the charge and conformation of the histone tails leading to changes in the density of the chromatin structure, regulating the access of co-activators to the DNA and hence to activate gene transcription. Tighter interactions between the histones and the DNA result in the formation of transcriptionally inactive heterochromatin and looser interactions result in transcriptionally active euchromatin.

1.4.1 HISTONE ACETYLTRANSFERASES (HATS) AND HISTONE DEACETYLASES (HDACS)

Histone acetylation and deacetylation is kept in dynamic equilibrium by the activity of histone acetyl transferases (HATs) (which add acetyl groups) and histone deacetylases (HDACs) (that remove acetyl groups) on the ε amino group of conserved N-terminal lysine residues of histone tails (Haggarty and Tsai, 2011). Increased acetylation causes loosening of the chromatin structure by lowering the strength of the attraction between DNA and histones, leading to increased transcription. Deacetylation results in increased attraction between the histones and DNA and subsequently reduced transcriptional activity due to the inability of transcription factors to access the DNA (Shen *et al.*, 2015). The regulation of histone acetylation has been identified as an important mechanism in the regulation of LTM formation (Levenson and Sweatt, 2006).

1.4.2 HISTONE ACETYLATION AND MEMORY

An increase in histone acetylation was first correlated with memory formation nearly four decades ago, in which C^{14}-labelled acetate was used to detect changes in histone acetylation in various regions of rat brains post-training compared to pseudo-trained rats (Schmitt and Matthies, 1979). Since that time, immunoblotting studies have also determined that increased histone acetylase activity (and the resulting histone acetylation) is correlated with memory formation (Swank and Sweatt, 2001; Levenson *et al.*, 2004). Histone acetyltransferase activity is also implicated in learning and memory, as

deleterious mutations in CBP, a histone acetyltransferase, are associated with Rubinstein-Taybi syndrome, a condition that manifests as various physical defects as well as moderate to severe learning difficulties (Petrij *et al.*, 2000; Murata *et al.*, 2001). Furthermore, mice with insufficient levels of CBP display impairments in histone acetylation and LTM formation, both of which were rescued by administration of HDAC inhibitors (Alarcon *et al.*, 2004). Logically, as increased histone acetylation is correlated with increased learning and memory, increased histone deacetylation would be correlated with decreased learning and memory. However, many studies have shown that while reductions in deacetylase activity can improve cognitive function (Vecsey *et al.*, 2007; Guan *et al.*, 2009; Villain *et al.*, 2016), a total impairment of maternal histone deacetylation while mice are *in utero* can result in severe learning disabilities (Kataoka *et al.*, 2013; Takuma *et al.*, 2014). This variation is reflective of the diversity within HDACs which, compared to HATs, are more heterogenous in structure and function. This diversity makes them strong potential candidates for drug discovery for a host of diseases (Abe and Zukin, 2008). In addition to this, HDACs are not limited in function to deacetylating histones and have been shown to regulate other cellular processes in both the nucleus and cytoplasm by deacetylation independent means (Brandl *et al.*, 2009; Glozak and Seto, 2009; Delcuve *et al.*, 2012).

1.4.3 THE HDAC FAMILY MEMBERS

There are currently 11 known HDACs in humans which can be divided into four classes based on subcellular localisation and mechanisms of action (Gregoretti *et al.*, 2004; Morris and Monteggia, 2013)(Figure 1.10) .

Class I HDACs (HDAC 1, 2, 3, and 8) localise predominantly to the nucleus. Their activity is Zn^{2+} dependent and they have the highest deacetylase activity of all HDAC classes and are thus responsible for most of the histone deacetylation in the cell. Class II HDACs (HDAC 4, 5, 6, 7, 9 and 10) lack deacetylase activity of their own typically requiring recruitment of class I enzymes to carry out deacetylation and act as transcriptional repressors (Kao *et al.*, 2000; Fischle *et al.*,

2001). Class II HDACs are further divided into IIa (HDACs 4, 5, 7, and 9) and IIb (HDACs 6 and 10) based on their catalytic domains and subcellular distribution.

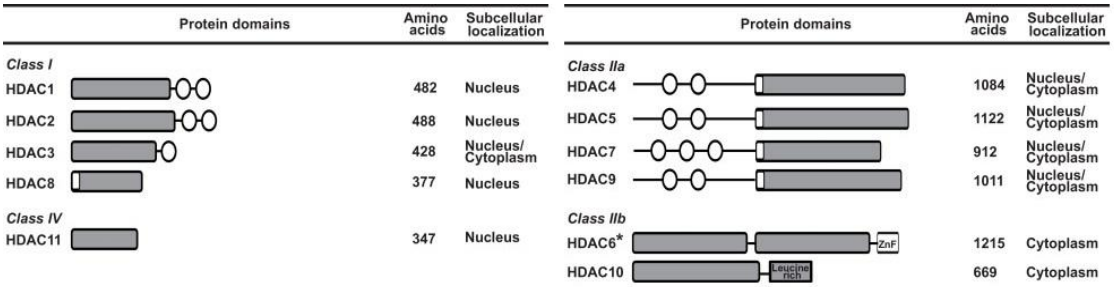

Figure 1.10 Simplified diagram comparing the 11 Histone Deacetylases in humans.

Listed are the 11 HDACs broken down into the four classes (I – IV). Deacetylase domains are highlighted in grey and the open circles and rectangles demarcate phosphorylation sites. Modified from Moris and Monteggia, 2013 with permission from Elselvier.

The class IIb HDACs possess two catalytic domains and are cytoplasmically restricted whereas the class IIa HDACs possess a large N-terminal extension that mediates protein-protein interactions and are actively shuttled between the nucleus and the cytoplasm. In addition to this the class IIa HDACs have a highly conserved C-terminal catalytic domain (Gregoire and Yang, 2005; Guo *et al.*, 2007; Bottomley *et al.*, 2008; Morris and Monteggia, 2013). Class IIa HDACs regulate the expression of a range of proteins through both direct binding to transcription factors to modulate their activity and recruitment of other HDACs (Fischle *et al.*, 2002; Majdzadeh *et al.*, 2008). This regulation has been shown to persist even when the recruitment of class I HDACs is blocked suggesting an alternative method of substrate modification (Fischle *et al.*, 2002). Class III HDACs are the sirtuins (Sirtuin 1-7), that are Zn^{2+} independent (Class I, II and IV are Zn^{2+} dependent) NAD^{+} dependent deacetylases that act on a wide range of proteins, not just histones (Herskovits and Guarente, 2013). HDAC11 is the sole member of class IV. It has similar properties to class I and II HDACs but distinct physiological roles that mean it cannot be classed alongside the previous groups.

1.4.4 HISTONE DEACETYLASES IN MEMORY

HDACs have increasingly been identified as important modulators of learning and memory and HDAC inhibitors (HDACIs) are commonly used as a tool to investigate the role of HDACs in animal models of memory. Treatment of mice with various HDACIs typically results in improved memory function (Vecsey *et al.*, 2007; Guan *et al.*, 2009; Villain *et al.*, 2016) strongly suggesting that histone acetylation is required for memory formation and learning. Early studies utilising the pharmacological inhibition of HDACs to study their role in learning and memory initially made use of HDACIs that lack specificity for individual HDACs with many studies focusing on class I HDACs as they have a higher activity. This broad-spectrum inhibition of the HDACs could result in complex up- and down-regulation of memory-related genes when administered at different time points relative to training (Dietz and Casaccia, 2010; Zovkic and Sweatt, 2013).

Efforts were therefore focused toward investigating the individual roles of HDACs via development of more specific HDACIs or targeting specific brain areas, approaches that have led to a number of potential uses for HDACIs as treatments for neurological disorders and indicated possible roles for HDACs in learning and memory. For example, reducing the hippocampal activity of HDACs using the class I-targeting HDACI sodium butyrate during consolidation improved long-term spatial memory formation in mice, most likely through a transient increase in histone acetylation (Villain *et al.*, 2016). Similarly, an infusion of trichostatin A into the basolateral amygdala of rats showed an increase in memory retention period (Valiati *et al.*, 2017). In addition to these direct investigations, many studies have investigated the potential of HDACIs as a treatment for neurodegenerative disorders. Recent research has shown that treatment of Alzheimer's model mice with the HDACI RGFP963 (inhibiting HDACs 1, 2 and 3) restored the wild-type memory function whereas inhibition of HDAC3 alone (with RGFP966) showed no recovery (Rumbaugh *et al.*, 2015).

While these studies have increased the understanding of how modulating histone acetylation can alter memory the use of HDACIs are limited they typically affect multiple proteins. To this end, it is beneficial to use genetic, rather than chemical, tools to increase or decrease the abundance of specific HDACs in the organism. Guan *et al.* (2009), showed that whole-brain overexpression of HDAC2 but not HDAC1 in mice impairs memory formation, reduces synaptic plasticity and reduces dendritic spine density and synapse number. Further investigation showed that the effects exhibited by overexpression of HDAC2 were due to the resulting transcriptional repression of multiple genes associated with memory formation such as *Fos, Cam2ka* and *Crebbp*. It was also shown that the treatment of these mice with SAHA (a hydroxamic acid-based HDAC inhibitor) could rescue the mouse from the effects of HDAC2 overexpression (Revenga *et al.*, 2018).

However, in contrast to this previous studies of overexpression, a similar result is observed with the knockdown of Rpd3 (an HDAC1 and HDAC2 homologue) in the *Drosophila* mushroom body, a memory impairment that could be overcome by rescuing the deficit by reintroducing Rpd3 (Fitzsimons and Scott, 2011). Additionally, treatment of *Drosophila* with either the class I HDACIs Sodium butyrate or Scriptaid prior to training prevented the formation of LTM without inhibiting STM (Fitzsimons and Scott, 2011). These results suggest that the role of deacetylation is vital for memory formation but that requirement is complex and tightly regulated in normal memory function.

HDAC3 is the most highly expressed class I HDAC in the mammalian brain (Broide *et al.*, 2007) and interacts with nuclear receptor corepressor 1 (NCoR), silencing mediator for retinoid and thyroid hormone receptors (SMRT) and class IIa HDACs such as HDAC4 to form a large protein complex that regulates gene expression via deacetylase activity (Li *et al.*, 2000; Guenther *et al.*, 2001). Inhibition of HDAC3 has been shown to reduce the presence of Alzheimer's Disease indicators (such as hyperphosphorylated Tau and $A\beta_{1\text{-}42}$ abundance) in cultured

cells and AD model mice (Janczura *et al.*, 2018), suggesting HDAC3 activity is a causative factor in AD biochemical symptoms.

Deletion of HDAC3 in the mouse hippocampus has been shown to enhance LTM performance over controls with normal expression of HDAC3. This increase in LTM performance could be replicated by preventing the interaction between NCoR and HDAC3 by disrupting the deacetylase activation domain (DAD) through which NCoR interacts with HDAC3 (McQuown *et al.*, 2011). Treatment with the HDACI RGFP136 lead to similar enhancements in LTM, as well as decreased HDAC4 expression, strongly suggesting that, potentially due to its interaction as a corepressor, HDAC3 activates the expression of HDAC4 (McQuown *et al.*, 2011).

Thus, it is known that class I HDACs modulate memory formation in a largely repressive fashion and have differing roles in different brain areas. This makes them promising targets for the development of specific HDACIs to treat specific memory conditions, however, more research is required to investigate their specific roles. Class II HDACs are, on the other hand, less well studied but there is increasing evidence that they, particularly HDAC4, play a critical role in LTM.

1.5 Histone deacetylase 4 (HDAC4) in the brain

The human class IIa histone deacetylase HDAC4 was first characterised in 1999 (Grozinger *et al.*, 1999). Since this initial paper a growing body of evidence shows that HDAC4 is involved in multiple neurological functions, from neuronal survival (Bolger and Yao, 2005; Chen and Cepko, 2009) to synaptic plasticity and memory formation (Kim *et al.*, 2012; Sando *et al.*, 2012; Fitzsimons *et al.*, 2013).

1.5.1 DOMAIN STRUCTURE AND CATALYTIC ACTIVITY OF HDAC4

Human HDAC4 (hHDAC4) is a 1084 amino-acid protein which has high similarity to the 1252-amino-acid *Drosophila* HDAC4 (DmHDAC4) (Figure 1.11). Both proteins possess a substrate-binding region at the N-terminus that has been shown to bind the complex formed by transcription factor myocyte enhancing factor 2 (MEF2) binding to DNA. HDAC4 binds these MEF2-DNA complexes, repressing MEF2-activated transcription (Backs *et al.*, 2011). It also contains a catalytic C-terminal domain (Wang *et al.*, 1999a), and a nuclear localisation sequence that resides in the N-terminus of the protein (Wang and Yang, 2001; Paroni *et al.*, 2007). This overall structure is highly conserved in *Drosophila* though the deacetylase domain is functional in *Drosophila* and inactive in vertebrates (Miska *et al.*, 1999; Lahm *et al.*, 2007).

While the vertebrate HDAC4 exhibits no deacetylase activity on its own (Lahm *et al.*, 2007) it can initiate deacetylation through the recruitment of a class I HDAC and formation of the NCoR1/HDAC3 complex. This interaction was shown by Fischle *et al.* in a series of experiments in which the deletion of the C-terminal of HDAC4 abolished its apparent deacetylase activity by preventing it from associating with HDAC3 (Fischle *et al.*, 2002). *Drosophila* HDAC4, much like all other non-mammalian HDAC4 paralogues, does display deacetylase activity. This difference is caused by a histidine to tyrosine mutation away from the canonical eukaryotic HDAC4 to the vertebrate HDAC4 at residue 976 in the mammalian HDAC4. Restoration of this tyrosine residue restores the deacetylase activity of mammalian HDAC4 (Lahm *et al.*, 2007).

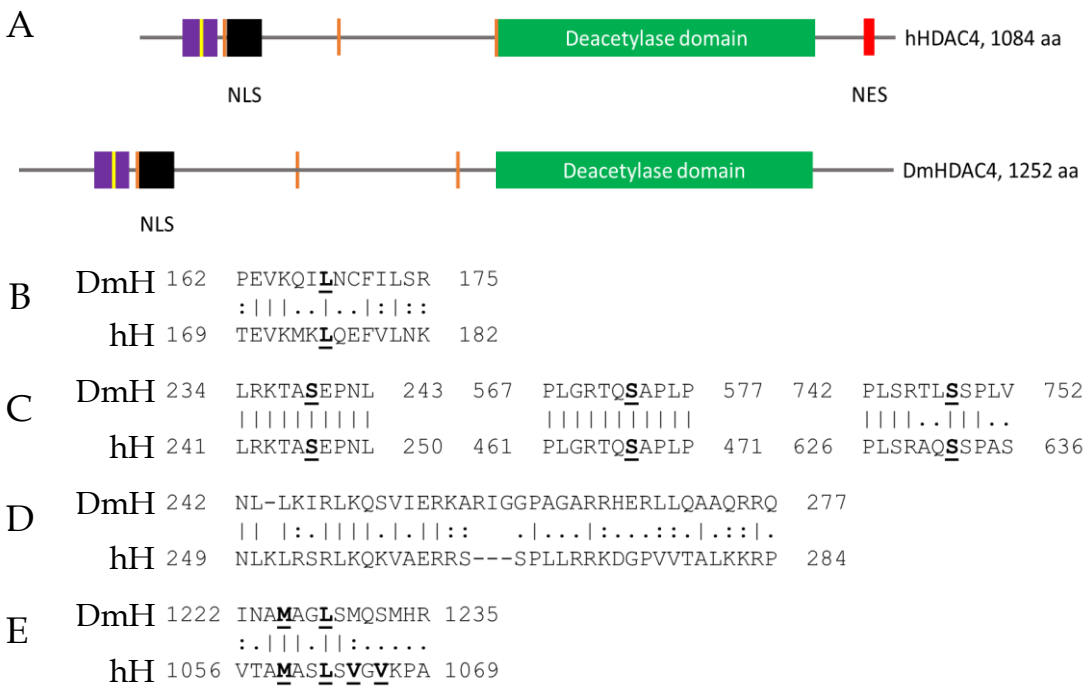

Figure 1.11 Comparison of human HDAC4 and *Drosophila* HDAC4.
A) showing an approximate alignment of the two proteins centred around the deacetylase domain, MEF2 binding domain in purple, NLS in black, 3 serine residues highlighted in orange, deacetylase domain shown in green and the hHDAC4 NES is in red. B) Alignment of the MEF2 binding site conserved between the two homologues, key leucine residue bold and underlined. C) Alignments of the 3 serine residues (and surrounding sequence) involved in 14-3-3 chaperone protein binding and subsequent nuclear exclusion, key serines are bolded and underlined. D) Alignment of the region harbouring the nuclear localisation sequence. E) Alignment of the region harbouring the nuclear export sequence. The four key residues in hHDAC4 and their two conserved counterparts in DmHDAC4 are bolded and underlined. Figure adapted from Fitzsimons *et al.*, 2013 under creative commons licence, with data from Miska *et al.*, 1999 and Wang and Yang, 2001.

Additionally, sequence alignment shows that the nuclear export sequence (NES) present in the C-terminus of human HDAC4 (hHDAC4) is disrupted in *Drosophila* HDAC4, with two valine residues mutated to methionine and serine (V1064 and V1066 in hHDAC4). A study characterising the NES of hHDAC4 showed that mutations in either of these two valine residues lead to the nuclear accumulation of hHDAC4 in cultured cells (Wang and Yang, 2001). The NES present in hHDAC4 shows a consensus sequence (MXXLXVXV) conserved between hHDAC4 and two other class IIa HDACs: hHDAC5 and hHDAC7 (Wang and Yang, 2001). This NES consensus is conspicuously absent from HDAC9, the fourth class IIa HDAC, yet HDAC9 also undergoes shuttling

between the nucleus and cytoplasm (Alchini *et al.*, 2011, 2017), strongly suggesting that the nuclear translocation of HDAC4 exerted by the 14-3-3 chaperone protein is sufficient to partially exclude it from the nucleus, as suggested by Miska *et al.* (1999).

The subcellular distribution of HDAC4 is kept in a dynamic equilibrium through the actions of the nuclear export sequence (NES) and nuclear localisation sequence (NLS) present at the C- and N-termini respectively (Paroni *et al.*, 2007). Nuclear export of HDAC4 is mediated through glutamate receptor (NMDAR) induced Ca^{2+}/Calmodulin-dependent kinase (CaMKII) phosphorylation of three specific serine residues on HDAC4 (S246, S467, and S632 in human HDAC4). This allows for subsequent association with the molecular chaperone 14-3-3ζ which exports HDAC4 from the nucleus (McKinsey *et al.*, 2001; Sando *et al.*, 2012). Nuclear import of HDAC4 relies on phosphorylation of S298 that leads to PP2A binding to the N-terminal region of HDAC4 in the cytoplasm. Following this, the PP2A dephosphorylates S298 (Paroni *et al.*, 2008) and allows the transcription factor MEF2C to bind and subsequently import HDAC4 into the nucleus. The binding of MEF2 to HDAC4 is vital to this process as the mutation of leucine 175 to alanine (L175A mutant) prevents MEF2C binding and causes cytoplasmic accumulation of HDAC4 (Wang and Yang, 2001).

1.5.2 EXPRESSION OF HDAC4 IN THE BRAIN

In a methodical study of HDAC4 distribution within multiple tissues and structures of the mouse brain it was shown that the distribution of HDAC4 between the cytoplasm and nucleus was highly variable dependent on cell type. For example, the CA1 neurons of the hippocampus exhibited no nuclear staining for HDAC4 yet immunoreactive puncta were observed, indicating deliberate exclusion of HDAC4 from the nucleus, however, subsets of Purkinje cells of the cerebellum showed strong nuclear staining for HDAC4 (Darcy *et al.*, 2010). HDAC4 immunoreactivity was also present at subsets of dendrites, suggesting that HDAC4 has a potential role in synaptic signalling (Darcy *et al.*, 2010). This varied and cell-specific regulation of HDAC4 subcellular distribution suggests

that HDAC4 has multiple roles in the mammalian brain. The same cell-by-cell differential subcellular distribution of HDAC4 has been shown in the *Drosophila* model in which FLAG-tagged HDAC4 was observed in the axons of MB lobes as well as largely cytoplasmic in the Kenyon cell bodies of the MB, but was shown to exhibit nuclear puncta in specific nuclei of Kenyon Cell when overexpressed (Figure 1.12) (Fitzsimons *et al.*, 2013).

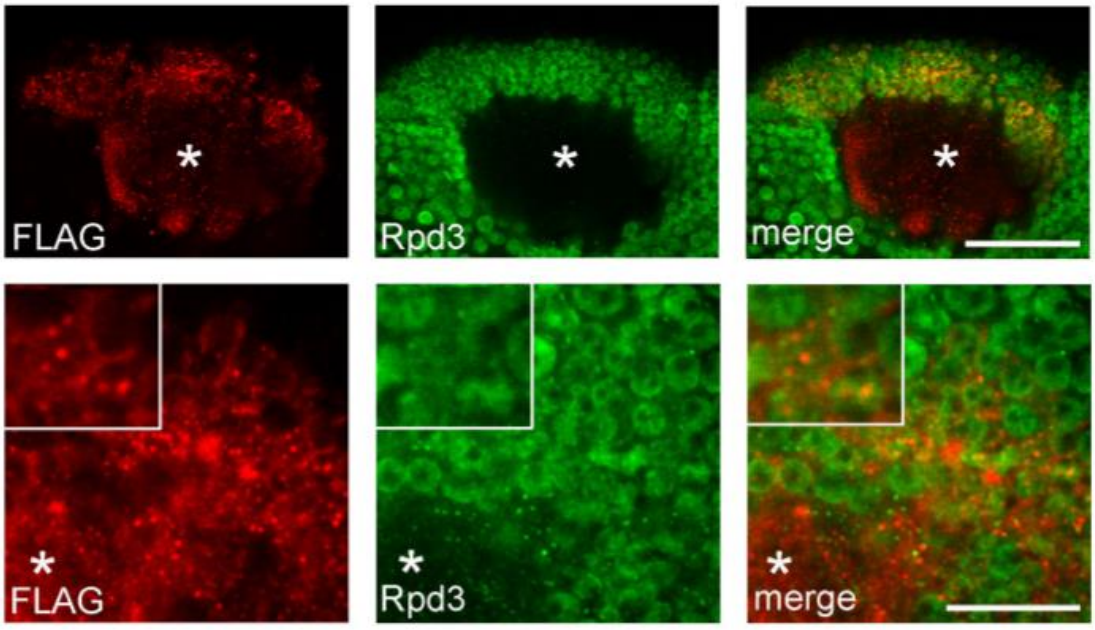

Figure 1.12 Subcellular distribution of HDAC4 in the *Drosophila* mushroom body.
Immunohistochemistry on a whole mount brain showing expression of the FLAG-tagged HDAC4 in the mushroom body (Left) counterstained with Rpd3, which is nuclear-localised (middle). A 1 µm section through the MB at the level of the cell bodies and calyx (dendritic field (asterisk) is shown in the top row (scale bar 25 µm). A magnified section of the image is shown (bottom) in which expression of Rpd3 is predominantly nuclear in all cells whereas the FLAG-tagged HDAC4 is largely cytoplasmic with nuclear punctate foci in a subset of cells. Figure modified from Fitzsimons *et al.*, 2013, reused under creative commons licence.

1.5.3 HDAC4 AND NEURONAL FUNCTION

Brachydactyly mental retardation syndrome (BDMR), also known as 2q37 deletion syndrome, is a developmental disorder in humans that presents symptoms including developmental delay, language difficulties, autism and impaired motor function (Williams *et al.*, 2010) that is associated with haploinsufficiency of HDAC4. Additionally, a maternally inherited case of BDMR was investigated in which both individuals exhibited greatly reduced

expression of HDAC4 when compared to non-affected individuals (Morris *et al.*, 2012). Haploinsufficiency of HDAC4 has also been highlighted as a potential causative factor in autism spectrum disorder (ASD), a similar maternally inherited 2q37 deletion was detected in this far-reaching study into the genetic factors behind ASD in North American and European families that directly implicates HDAC4 haploinsufficiency in ASD (Pinto *et al.*, 2014). Additionally, in a preliminary study of a Korean population, a single nucleotide polymorphism (SNP) of HDAC4 was suggested to increase the risk of schizophrenia (Kim *et al.*, 2010).

While BDMR is primarily associated with haploinsufficiency of HDAC4, one individual expressed a nuclear-restricted, transcriptionally active but truncated mutant of *hdac4* caused by a cytosine insertion leading to a frameshift that leads to a termination before the deacetylase domain and nuclear export signal (Williams *et al.*, 2010; Sando *et al.*, 2012).

As well as developmental disorders, HDAC4 has been implicated in neurodegenerative disorders. In a study by Shen *et al.* (2016), the examination of a number of human individuals with varying severities of Alzheimer's Disease (measured by Braak score) showed a positive correlation between the severity of the disease and the relative abundance of hippocampal cells exhibiting nuclear-accumulated HDAC4, suggesting that nuclear accumulated HDAC4 plays a significant role in the pathophysiology of Alzheimer's Disease in humans (Shen *et al.*, 2016). This data is supported by a proteomics study of 5XFAD AD model mice expressing human APP and PSEN1 with five-AD linked mutations. In this, investigation HDAC4 was predicted to be the most likely causative factor in memory loss associated with both AD and ageing (Neuner *et al.*, 2016).

The suggestion that HDAC4 is a candidate gene for neurological diseases has led to studies investigating HDAC4 function in vertebrates and invertebrates. A brain specific, conditional knockout of HDAC4 in mice has been shown to cause impaired LTM when either aversive or spatial memory were tested, as well as causing minor behavioural defects such as hyperactivity compared to control

mice (Kim *et al.*, 2012). However, the role of HDAC4 in learning and memory is not straightforward as a detailed investigation by Sando *et al.* (2012) showed that an overabundance of a truncated N-terminal fragment of HDAC4 with no deacetylase domain or NES led to severely impaired spatial memory performance in mice (Sando *et al.*, 2012). Thus, reduced HDAC4 is associated with BDMR and other neurological dysfunctions, indicating HDAC4 is required for normal development but an increased nuclear abundance is also causative, suggesting HDAC4 has deleterious effects when it is present in high nuclear concentrations.

The results of these studies in mammals were replicable in *Drosophila*. An experiment in which flies overexpressing HDAC4 in the mushroom body were tested for LTM performance using the courtship suppression assay showed that an overabundance of HDAC4 severely impaired the memory of male flies (Fitzsimons *et al.*, 2013). In addition to this, knockdown of HDAC4 in the mushroom body of adult flies caused a similar phenotype, with male flies unable to form LTM during the courtship suppression assay, supporting the proposition that the role of HDAC4 in learning and memory is complex (Fitzsimons *et al.*, 2013). It is likely that these effects are deacetylase independent as it was also demonstrated that overexpression of an HDAC4 variant with a mutated H968 residue that disrupts deacetylase activity (Miska *et al.*, 1999) also caused severe impairment of learning (Fitzsimons *et al.*, 2013).

It is still unclear how HDAC4 is causing these effects. Recent transcription analysis of whole fly heads from adult flies overexpressing DmHDAC4 has shown that only a small number of genes are significantly differentially expressed, indicating that HDAC4 is not a global regulator of transcription but, at a transcriptional level, might facilitate specific changes related to learning and memory (Schwartz, 2016). The relatively small number of transcriptional changes could be due to the relatively low nuclear abundance of HDAC4 across the brain (the nuclear abundance occurs in only small subsets of cells) leading to a dilution of the nuclear effects of HDAC4 or it could, in tandem with its cytoplasmic

abundance, indicate that HDAC4 works through predominantly transcriptionally independent means. Indeed, a screen of multiple genes shown to interact with HDAC4 identified Ubc9 as a candidate for investigation (Schwartz *et al.*, 2016). Ubc9 is an essential protein in SUMOylation (discussed in full in 1.6.3) the process through which SUMO molecules are added to proteins to alter their stability or activity (Wilkinson and Henley, 2010). The interaction between HDAC4 and Ubc9 is not unexpected as HDAC4 has been proposed to carry out SUMO E3 ligase activity previously (Gregoire and Yang, 2005). It is thus possible that in addition to the minor role that HDAC4 plays in transcription regulation, it regulates memory-associated proteins in the cytoplasm, altering their function and stability to affect memory formation.

1.6 Downstream targets of HDAC4

As discussed, HDAC4 lacks deacetylase activity in mammals and, while the deacetylase domain is intact in *Drosophila*, a variant of HDAC4 with a mutated deacetylase domain (H968A) causes the same phenotypes when overexpressed in the brain as the wild-type HDAC4 (Fitzsimons *et al.*, 2013). Indeed, it has been shown that HDAC4 can cause deacetylation of proteins through the recruitment of HDAC3 through a SMRT/N-CoR co-repressor complex. Blocking the formation of this complex results in an almost complete drop off in deacetylase activity (Fischle *et al.*, 2002). Despite this, it is becoming clear that much of HDAC4's activity may be mediated through the regulation of other transcription factors such as myocyte enhancing factor 2 (MEF2) (Miska *et al.*, 1999; Paroni *et al.*, 2007) and Runx2 (Jeon *et al.*, 2006) which have the potential for much finer regulation of transcription than histone deacetylation. This is an idea supported by the results from Schwartz *et al.*, (2016) in which the changes in transcription observed when HDAC4 was overexpressed in *Drosophila* were only significant for a small number of transcripts.

A further piece of the puzzle has been identified as it has been shown that a mutated variant of HDAC4, in which the three serines required for nuclear export are mutated to alanines (3SA) which results in nuclear accumulation of HDAC4, lead to changes in transcription. The ability of the 3SA mutant to cause these changes are abolished by C-terminal deletion which is unable to associate with MEF2 (Miska *et al.*, 1999; Backs *et al.*, 2011; Sando *et al.*, 2012). This suggests that at least some of the deleterious effects caused by nuclear localisation of HDAC4 occur through the interaction between HDAC4 and MEF2. The results from the Miska study also showed that the changes resulting from overexpression of HDAC4 are acetylation independent as the N-terminal deletion also removed the HDAC4 deacetylase domain, confirming the proposal that HDAC4-induced changes in the cell are independent of deacetylase activity (Miska *et al.*, 1999).

1.6.1 MEF2 AND ARC IN BRAIN DEVELOPMENT AND MEMORY

The association between MEF2 and HDAC4 has been investigated in the past as both are associated with memory and learning. As previously mentioned, MEF2 is required for the nuclear import of HDAC4, however the binding of HDAC4 to MEF2 also prevents MEF2 interacting with DNA, repressing MEF2-regulated transcription (Sando *et al.*, 2012).

MEF2 is a transcription factor originally identified for its role in transcription regulation in muscle cells but has since been shown to be involved in multiple developmental pathways, apoptosis and immune cell differentiation (McKinsey *et al.*, 2002). In vertebrates, four *mef2* genes have been identified (*mef2A-D*) which have highly conserved MADS-box and MEF2-DNA binding domains but variable transactivation domains (Black and Olson, 1998). MEF2 proteins have been shown to be required for many important facets of central nervous system function where they promote neuronal survival and regulate dendrite morphogenesis (Flavell *et al.*, 2006; Shalizi *et al.*, 2006). Furthermore, it has been suggested that MEF2 proteins regulate multiple synapse associated genes, promoting the development of inhibitory synapses and repressing excitatory synapse development (Barbosa *et al.*, 2008).

Mutations in genes regulated by MEF2 such as *lgi1, protocadherin 10* and *kcna1* have been associated with disorders such as epilepsy, autism and general intellectual disabilities. It is proposed that these disorders arise early in development due to increased dendritic spine density that results in an imbalance of excitatory and inhibitory signals in the brain (Flavell *et al.*, 2008).

MEF2 is regulated by phosphorylation, as increased MEF2 phosphorylation in the hippocampus or nucleus accumbens has been associated with the formation of spatial and fear memories (Cole *et al.*, 2012). This phosphorylation leads to a decrease in MEF2-mediated transcription, suggesting that MEF2 acts as a repressor of memory and that the reduction in MEF2 activity leads to memory formation. Interestingly, transgenic mice with brain specific deletions of MEF2A

and/or MEF2D showed no changes in hippocampal spine density or memory formation, suggesting that these two isoforms are not involved in learning and memory (Akhtar *et al.*, 2012). Conversely, mice with brain specific deletions of MEF2C show an impairment in certain types of fear memory formation as well as a reduction in dendrite density in the dentate gyrus (Barbosa *et al.*, 2008). These contrasting results strongly suggest different roles for the MEF2 subtypes in mammalian memory. As mentioned, the molecular pathways involved in *Drosophila* memory are highly conserved between *Drosophila* and mammalian models however, most MEF2 studies in *Drosophila* have focused on its role as a regulator of the circadian rhythm (Sivachenko *et al.*, 2013) and a muscle growth factor (Ranganayakulu *et al.*, 1995; Soler *et al.*, 2012) but the role of MEF2 in *Drosophila* memory has not been investigated.

In addition to being poorly studied in learning and memory, *Drosophila* has only one MEF2 isoform which means that alterations to the *mef2* gene affect all downstream MEF2 targets, for example point mutations in the conserved MADS box result in a non-viable fly (Nyugen *et al.*, 2002). This makes it an ideal target for study because, as briefly covered, alterations to *mef2* in vertebrates has varying effects depending on which of the genes is the target of the disruption, thus, use of the *Drosophila* model eliminates some of the complexities that arise through redundancy.

The *arc1* (activity regulated cytoskeletal protein 1) gene has been identified as a target of MEF2 during memory development in mice (Cole *et al.*, 2012). ARC1 reduces the synaptic efficacy of neurons by inducing endocytosis of AMPA receptors in the post-synaptic neuron (Wang *et al.*, 2008). Disruption of this endocytosis rescues MEF2-induced memory impairment suggesting that MEF2 acts to repress memory formation through activation of the *arc1* gene in mice (Cole *et al.*, 2012). Interestingly, overexpression of HDAC4 has been shown to reduce the abundance of *arc1* mRNA, consistent with the idea that HDAC4 represses MEF2, allowing memory formation to occur normally (Schwartz, 2016).

1.6.2 CREB IN MEMORY AND LEARNING

cAMP responsive element binding protein (CREB) is a transcriptional regulator that binds to promoter cAMP response element (CRE) sites upstream of target genes (Brindle *et al.*, 1993). Addition of exogenous CRE oligonucleotides (competing with endogenous CREB for binding) blocks LTM but not STM by sequence specific binding (Dash *et al.*, 1990), and phosphorylation and subsequent activation of CREB is observed in the hippocampus and cortical regions of the brain following training (Mayr and Montminy, 2001). CREB activity has been shown to be essential for LTM formation (Tully *et al.*, 1994; Yin *et al.*, 1994; Perazzona *et al.*, 2004) as well as the maintenance of four-day LTM (Hirano *et al.*, 2016). HDAC4 has been shown to bind to CREB in vertebrates (Sen and Sen, 2016) but this interaction has not been investigated in *Drosophila*.

1.6.3 HDAC4 AND SUMOYLATION

A non-transcriptional pathway that could be a candidate for HDAC4 activity is SUMOylation. In this process, small ubiquitin like modifier proteins (SUMO proteins) transiently alter the activity or stability of multiple transcription regulators in a process known as SUMOylation. During this process a member of the SUMO family of proteins is covalently bound to a specific lysine residue of the target protein which results in altered function, either by changing its stability, activity or binding affinity for its usual substrates (Wilkinson and Henley, 2010). The E3 enzyme in the machinery of SUMOylation is the enzyme that attaches the SUMO protein to the target substrate and is the primary source of target specificity as there is only one E2 enzyme in the SUMOylation system (Seufert *et al.*, 1995). Interestingly, it has been proposed that HDAC4 possesses E3 ligase activity (Gregoire and Yang, 2005).

Recently, some research has been carried out in our lab by Schwartz *et al.*, (2016) in which it was shown that HDAC4 interacted with the SUMOylation machinery. Furthermore, it has been observed that SUMOylation appears to have a role in the regulation of transcription factors important to neuronal survival as well as learning and memory (Craig and Henley, 2012). These results suggest that

HDAC4 could potentially regulate the activity of downstream regulators through SUMOylation, as SUMOylation is a translationally independent method of regulating protein abundance and activity in a rapid, reversible fashion.

Finally, it's also possible that HDAC4 has different mechanisms of activity in each cell. There is a significant body of evidence that shows the different subsets of Kenyon cells have different transcription profiles (Aso *et al.*, 2009; Montague and Baker, 2016). It is currently unknown whether or not the cells with nuclear HDAC4 are stochastic or patterned in each organism. The subcellular distribution may be another way through which the different neurons of the mushroom body are differentially programmed.

1.7 *Drosophila melanogaster* as a model to study memory

Drosophila melanogaster is a widely used model organism for the genetic analysis of development and disease. A short lifespan and rapid generation time, combined with the well-characterised genome and the genetic tools that have subsequently been developed make the fruit flies ideal for characterising both single genes and complex molecular pathways (Matthews *et al.*, 2005; Venken and Bellen, 2007; Dietzl *et al.*, 2007). Approximately 75% of the genes implicated in human genetic disorders are conserved in *Drosophila* (Adams *et al.*, 2000; Bellen *et al.*, 2010; Pandey and Nichols, 2011) and the availability of the full genome (Fisher *et al.*, 2012) allows the generation of transgenic lines to investigate uncharacterised genes through overexpression and knockdown.

Perhaps most relevant for this project, *Drosophila* can develop persistent associations between a conditioned stimulus and an unconditioned stimulus, first shown in the analysis of *Drosophila* fear response (Quinn *et al.*, 1974). As mentioned previously, two of the earliest memory-related mutants characterised in *Drosophila* were the *dunce* mutant (encoding a cAMP phosphodiesterase) (Dudai *et al.*, 1976) and *rutabaga* (encoding a calmodulin dependent adenylate cyclase) (Aceves-Piña and Quinn, 1979) highlighting the conservation of the cAMP pathway in learning and memory between vertebrates and invertebrates.

1.7.1 BEHAVIOURAL ASSAYS TO EVALUATE LEARNING AND MEMORY

Since it was first discovered that *Drosophila* can develop associations between conditioned and unconditioned stimuli, multiple assays have been developed to test facets of their memory formation including olfactory conditioning using the T-maze test, visual conditioning, and the courtship suppression assay. The T-maze test makes use of olfactory conditioning to associate a noxious odour with a stimulus (Figure 1.13), (Tully and Quinn, 1985; Schwaerzel *et al.*, 2003; Davis, 2005). In this assay, flies are exposed to two different odours (the conditioned stimulus, or CS) that are both mildly unpleasant. A mild electrical shock (the unconditioned stimulus, or US) is applied during exposure to one of the odours (CS^+) but not the other (CS^-). The number of times this training is repeated alters

the duration of the memory formed. A few training sessions over a brief period of time (minutes) permits the formation of STM lasting approximately 2 hours, whereas multiple training periods interspersed with rest periods (known as spaced training) (Davis, 2005) leads to the induction of protein synthesis to generate long term memory that can last several days (Tully *et al.*, 1994). Learning ability is tested by introducing the trained flies to the T-shaped maze in which one arm carries the CS^+ odour and the other carries the CS^- odour. The flies then choose which arm of the maze to proceed down for a set period of time before being trapped, anaesthetised and counted.

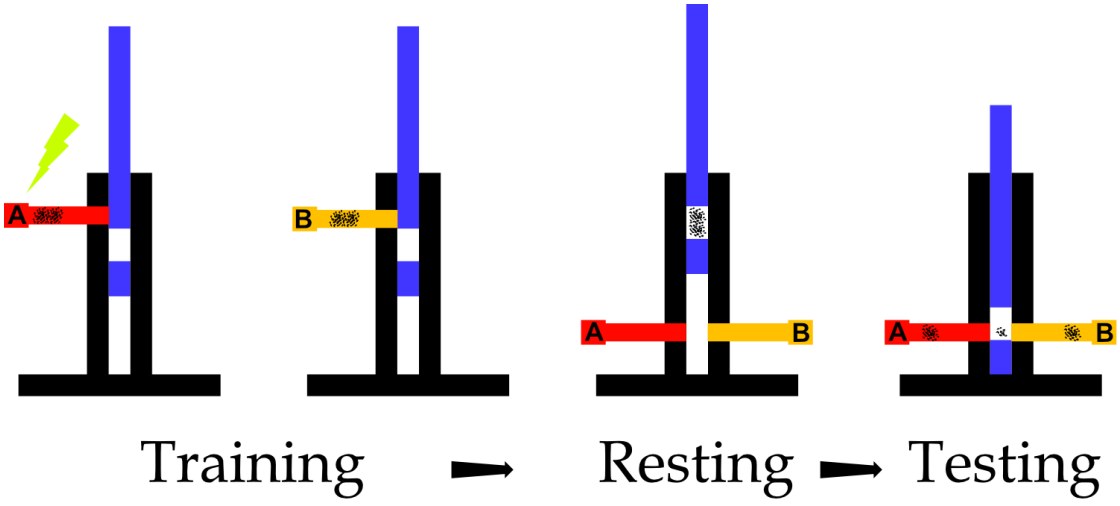

Figure 1.13 Schematic outlining the T-maze test used in olfactory conditioning. Flies are trained in a tube lined with an electrical grid and consecutively exposed to two different noxious odours. The first odour is present while the flies are exposed to a mild electric shock (A) then the second odour is pumped in without an electrical shock (B). Following this, the flies are released into a T-test in which one arm contains odour A and one contains odour B and provided a set amount of time to choose which arm to fly toward. Figure adapted from Malik and Hodge, 2014, under creative commons licence,

A measure of memory function is given by the following formula:

$$\frac{(Flies\ choosing\ odour\ A - flies\ choosing\ odour\ B)}{Total\ number\ of\ flies} = Performance\ Index$$

The experiment is also repeated with the odours swapped, so that odour B is paired with the electrical shock and odour A is unpaired, to remove any bias provided by the natural preference/aversion to the odours used. The average of

the two performance indices (from both repeats) gives a quantitative measurement of memory performance known as a memory index ranging from 0 to 1 in which 1 indicates that all flies chose the odour not associated with the electrical shock and thus, have perfect memories (Malik and Hodge, 2014). This test allows for the assessment of many (~100) flies at once but cannot be used if the gene of interest also affects the ability of the fly to detect the odour or the shock.

The courtship suppression assay is another method of measuring learning and memory. This assay monitors the changes in innate behaviour of male *Drosophila* after repeated rejection by a mated female (Keleman *et al.*, 2007; Ejima and Griffith, 2011). This method utilises the natural tendency of female *Drosophila* to be unreceptive towards courtship attempts from males after an initial copulation event, acting to repress courtship behaviour in the males (Tompkins *et al.*, 1972). The assay relies on the observation of easily identifiable courtship behaviours exhibited by the male fly (Figure 1.14) (Sokolowski, 2001).

During the courtship suppression assay individual male flies are placed with individual, freshly-mated female flies that will be unresponsive to the repeated mating attempts by the males. After training and a subsequent consolidation period, trained male flies are exposed to new, freshly-mated female flies and will make fewer attempts at courtship as they have learned from their previous exposure that attempts at courting unreceptive females are a waste of energy. The proportion of time that trained males spend trying to court is compared to that of untrained (or sham) male flies of the same genotype (Section 2.14), generating a memory index that provides an indicator of memory function (Figure 1.15).

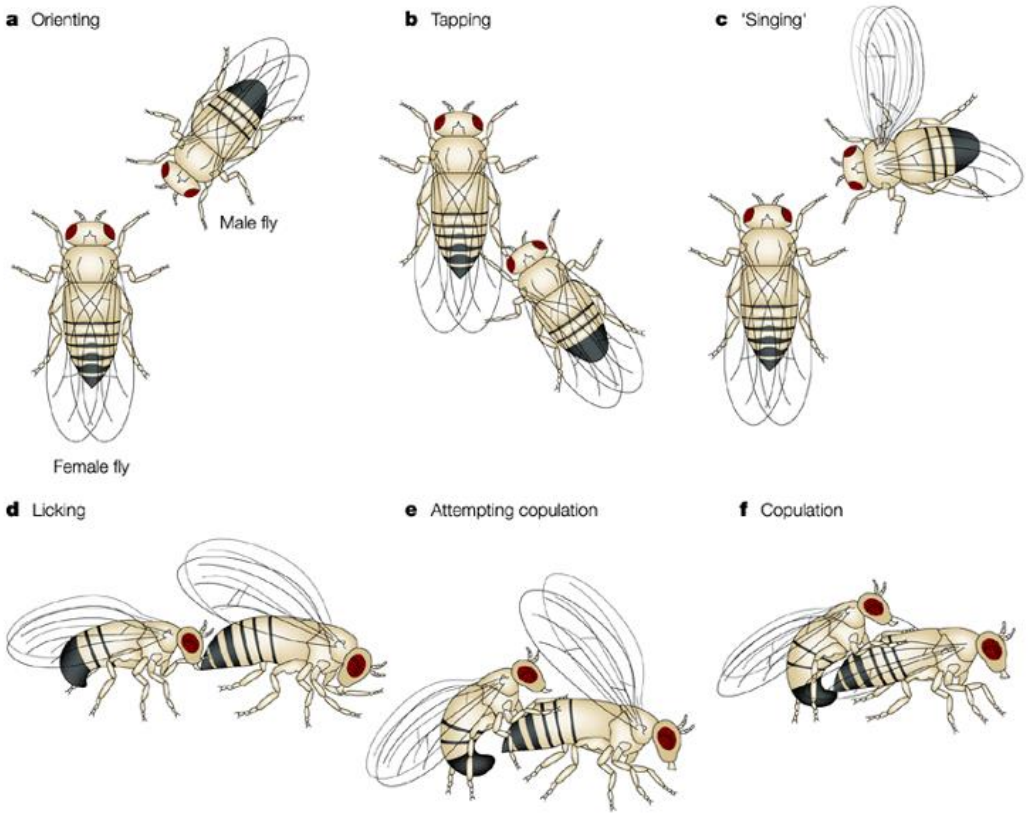

Figure 1.14 Characteristic courtship behaviours of a male *Drosophila*.
The naïve male (Dark posterior segment of the abdomen) will repeatedly attempt to court a novel female he is exposed to, exhibiting these characteristic behaviours. The absence of courting attempts is typically exemplified by cleaning and lack of orientation toward the female fly. Figure reproduced from Sokolowski, 2001 with permission from Springer Nature.

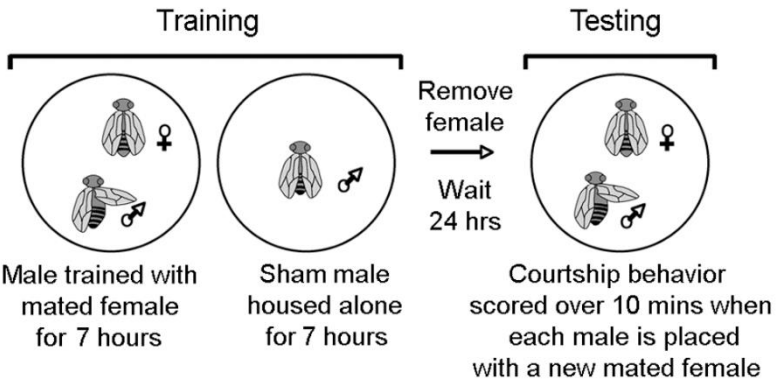

Figure 1.15 Schematic showing the courtship suppression assay.
In this assay the naïve males are housed in small chambers with food containing either a recently mated female (Trained) or no female (Sham). Following training and a rest period, the male flies are then exposed to a novel, freshly mated female and the frequency of their attempts at courtship are recorded for ten minutes to provide a courtship index (CI). Figure from Fitzsimons and Scott, 2011, reproduced under creative commons licence.

The courtship suppression assay can also be used to assess long- and short-term memory, altering the conditions and duration of training alters the formation of memory. A single period of training lasting up to 30 minutes has been shown to result in STM (Siegel and Hall, 1979). To assess protein-synthesis dependent LTM, longer training sessions of at least 5 hours or sequential training sessions with consolidation intervals (either through removing the males or using large chambers to give a natural respite) are used, generating behaviour patterns that persist for up to 8 days (Griffith and Ejima, 2009). The addition of food to the training chamber also leads to an increase in LTM formation, possibly because the presence of food allows for extended consolidation intervals between courtship attempts, or the presence of yeast alters the cues exhibited by the non-receptive female (McBride *et al.*, 1999). As discussed earlier, there are several neuronal subgroups that are required for learning in the courtship suppression assay. It was established by McBride *et al.* (1999) that flies with ablated mushroom bodies were behaviourally normal with respect to courtship activity, with the naïve males attempting to court when exposed to females but were unable to develop LTM after a 5-hour training session with a mated female (McBride *et al.*, 1999).

1.7.2 INVESTIGATING DEVELOPMENTAL PATHWAYS IN NEURONS

The complex network of genes involved in memory formation are often also involved in neuronal development. In *Drosophila*, the eye is a commonly used organ to evaluate neuronal development as it is rich in neuronal photoreceptors and defects in the eye structure provide an easy way to quickly and easily visualise defects in developmental pathway. The UAS-GAL4 system can be used in conjunction with the glass multimer reporter (GMR) driver to drive expression of a transgene or RNAi in the post-mitotic photoreceptor neurons of the *Drosophila* eye (Freeman, 1996; Laverty *et al.*, 2011). *Drosophila* eyes are composed of several hundred hexagonal ommatidia (or facets) with regularly spaced bristles between them. The disruption of these structures during development results in a "rough eye" phenotype in which the ommatidia may have irregular shapes, erratic spacing and often severe discolouration. A *Drosophila* eye screen

allows quick and easily observable assessment of the impact of overexpression and knockdown of specific genes on neuronal development and can identify genetic interaction between genes, in which the expression of two genes in a connected developmental pathway can disrupt development in a much more severe manner than each gene individually (Figure 1.16). Previous work has used this assay to provide *in vivo* evidence of genetic interaction to support the evidence of interactions provided by transcriptome analysis with the enhancement of the rough eye phenotype, providing evidence of genetic interactions during development (Schwartz *et al.*, 2016). The eye, therefore, provides a method to screen for genes involved in neuronal function prior to assessment in the brain.

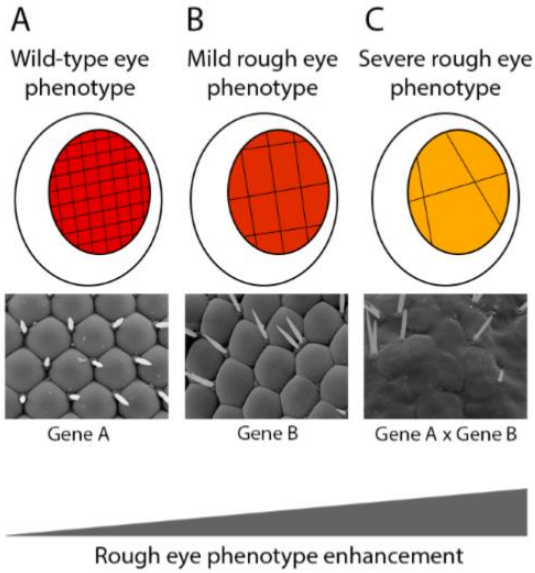

Figure 1.16 Schematic outlining the rough eye phenotype screen.
Column A shows an eye expressing a single gene with minimal interference to the development of the eye. Column B shows an eye expressing a gene that has a more significant role in the development of the eye, leading to impaired ommatidia and bristle development. Column C shows the expression of both genes, leading to a synergistic effect with severely disrupted eye development, very few bristles and severe discolouration as delivery of the pigment to the ommatidial surface is interrupted. Figure from Schwartz, 2016, reproduced with permission.

While the eye screen provides a quick assessment of developmental defects the photoreceptors are phenotypically distinct to central neurons and thus driving expression in the adult brain is necessary to ascertain if any effects observed in the eye phenotypes are carried through to affect the distribution and pathing of

axons in the brain. As described in 1.3.1 the fly mushroom body is an easily identifiable structure in the brain, and disruptions to this structure have been shown to negatively impact memory formation (Zwarts *et al.*, 2015). Using the GAL4 system to express constructs in all neurons allows for the analysis of the role of target genes in neuron structure and development. The fly brain can be dissected out of the headcase and gross structural morphology can be analysed using immunohistochemical approaches. Combined, the assays and tools described here allow a comprehensive way to analyse the role of a given gene in neuronal development, learning and memory.

1.8 Aims of this project

Previous research into HDAC4 has identified that it has a role in learning and memory (Kim *et al.*, 2012; Sando *et al.*, 2012; Fitzsimons *et al.*, 2013), affects transcription of a select group of memory-related genes (Sando *et al.*, 2012; Schwartz *et al.*, 2016) and undergoes activity-regulated nucleocytoplasmic shuttling (McKinsey *et al.*, 2001; Paroni *et al.*, 2007; Sando *et al.*, 2012). It has also been proposed that HDAC4 has the potential to act in the cytoplasm to affect protein activity and stability (Schwartz *et al.*, 2016).

However, the mechanisms through which HDAC4 influences brain development and whether this requires activity in the nucleus, cytoplasm or both is unknown. In this project, four variants of HDAC4 will be utilised, wild-type *Drosophila* HDAC4 (DmHDAC4), wild-type human HDAC4 (hHDAC4), a nuclear-localising mutant of the hHDAC4 that harbours 3 serine to alanine mutations that prevent nuclear export (3SA), and a cytoplasmically localising variant that harbours a leucine to alanine mutation that prevents nuclear import (L175A). Using these four variants and the *Drosophila* model this project will endeavour to uncover some of the effects of altering the subcellular distribution of HDAC4 in the brain and characterise their impact on neuronal development and memory.

Given the current evidence, it is hypothesised that nuclear HDAC4 is the primary cause of the deleterious effects observed when HDAC4 is overabundance in the brain, both during development and in the case of long-term memory formation.

To improve the understanding of the role of nuclear HDAC4, this project aims to:

1 - Characterise the subcellular distribution of four HDAC4 variants (DmHDAC4, hHDAC4, hHDAC4 – 3SA, and hHDAC4 – L175A) in the *Drosophila* brain.

2 - Characterise the effects of altered subcellular distribution of HDAC4 on *Drosophila* memory.

3 - Characterise the effects of altered subcellular distribution of HDAC4 on *Drosophila* neural development.

4 - Examine the effects of altered HDAC4 subcellular distribution on transcription in *Drosophila* brains.

5 - Establish the presence or absence of interactions with previously proposed downstream transcription regulators that may be targeted by HDAC4 such as MEF2 and CREB.

6 – Identify novel targets through which HDAC4 acts to affect learning, memory and neurological development.

2 METHODS AND MATERIALS

2.1 Fly strains

During this work, multiple established *Drosophila* lines were used, the full records of these are listed in Appendix 1. Here the specific genotype and any relevant data will be recorded along with a short-hand name that will be used to refer to each line in the body of this work.

Gene and protein nomenclature for all fly lines will follow the established protocols listed in Flybase (Thurmond *et al.*, 2019) in which the case of the first letter of a protein name indicates recessive (lower-case) or dominant (upper-case) and genes named after a protein product begin with an uppercase letter. Mammalian gene symbols are italicised and mammalian protein symbols are not.

2.1.1 FLY STRAIN MAINTENANCE

Experimental flies were maintained at 25°C and raised on standard fly media on a 12-hour light-dark cycle, unless otherwise indicated.

Standard fly media is made as follows: 10 g agar, 40 g yeast, 110 g cornflour is added to 1 L of dH_2O and brought to the boil. The mixture is simmered for 2 minutes with constant stirring before taking off the heat and adding 130 g sugar, 20 mL molasses, and 3.3 g of methyl 4-hydroxybenzoate (Sigma-Aldrich) dissolved in 37 mL of 96% ethanol. Mixture is stirred thoroughly before ~8 mL was poured into 30 mL vials (LabServ), allowed to set and then dusted with yeast to encourage egg-laying.

2.1.2 GENETIC CROSSES

Individual fly lines were crossed by introducing 4 males of one genotype with up to 6 virgin females of another line in a 30 mL vial (LabServ) containing 6-10 mL of standard media (2.1.1). Crosses requiring larger numbers of offspring were carried out in 100 mL bottles containing 30-40 mL of media. Adults were removed after 3-4 days and progeny started emerging after 10 days.

To guarantee the females collected were virgins, adult flies were removed in the morning and subsequent flies were collected within eight hours (as *Drosophila* do not mate for 10 hours after eclosion). During the clearing, any females with a clearly visible meconium (remnants of last larval meal) in their abdominal section were also collected as this is an obvious indicator of recent emergence.

2.2 Eye phenotype analysis

To assess the effects of altered gene expression on neuronal development a fly bearing the GMR-GAL4 driver was combined with a fly line harbouring a gene of interest (or RNAi) under control of an upstream activating sequence (UAS). The offspring of these flies were then examined for any aberrant phenotypes, examining for both colour (using light microscopy) and mis-regulated patterning of the ommatidia and bristles (using scanning electron microscopy).

2.2.1 LIGHT MICROSCOPY

The progeny expressing the construct of interest under control of the GMR driver were frozen at -20°C overnight and their eye phenotypes were analysed under the stereomicroscope (Olympus SZX12). Images were taken of representative eyes using an Olympus DP70 camera and DP controller imaging software. At least five offspring from each cross were examined in this manner.

2.2.2 SCANNING ELECTRON MICROSCOPY (SEM)

A dozen isolated flies were placed in new 30 mL vials (LabServ) containing only paper towel soaked with water. This method allowed for the acquisition of images of their eyes unobscured by food particles.

After this cleaning period, the flies were then anaesthetised using FlyNap (Carolina) and added to primary modified Karnovsky's fixative (3% gluteraldehyde, 2% formaldehyde in 0.1 M phosphate buffer, pH 7.2) with triton X-100 and vacuum infiltrated until soaked through. The flies were then placed in fresh fixative and incubated at RT for at least eight hours. Three 10-minute phosphate buffer (0.1 M, pH 7.2) washes were carried out followed by dehydration using a graded ethanol series for ten to fifteen minutes at each step

(25%, 50%, 75%, 95%, 100%) and a final 1-hour wash in 100% ethanol was carried out.

Following the ethanol dehydration, the samples were critical point dried using CO_2 and 100% ethanol (Polaron E3000 series II drying apparatus). The samples were then mounted onto aluminium stubs and sputter coated with gold (Baltex SCD 050 sputter coater) and imaged in the FEI Quanta 200 Environmental Scanning Electron Microscope at an accelerating voltage of 20kV.

After the initial fixing step, the drying and imaging process were conducted by Dr Matthew Savoian, Dr Pani Vijayan, Niki Minards and Patrick Main at the Manawatu Microscopy and Imaging Centre (MMIC) at Massey University, Palmerston North.

2.3 *Drosophila* brain isolation

To determine the effects of protein expression on the *Drosophila* brain whole fly brains were dissected out of flies for imaging using immunohistochemistry and confocal microscopy. To isolate the brains, whole flies were fixed in PFAT/DMSO (4% paraformaldehyde in 1x PBS with 0.1% Triton X-100 and 5% DMSO) for 1 - 2 hours and then washed 3 times for 15 minutes each wash in ice cold 1x PBS + 0.5% Triton X-100 (PBST). The washed flies were then placed in a 60 mm glass Petri dish and submerged in ice-cold PBST. The brains were then dissected out under stereomicroscope (Zeiss, Stemi 305) using a pair of Dumont #5 forceps with sharpened tips, taking care to remove the air sacs and fatty tissue around the brain.

Once free of the headcase the brains were moved into a 1.5 mL microfuge tube (Axygen) though a glass Pasteur pipette and post-fixed in PFAT/DMSO for 20 minutes. These could then be washed twice in 100% methanol for long term storage at -20°C or moved processed for immunohistochemistry (Section 2.3.1).

2.3.1 IMMUNOHISTOCHEMISTRY ON WHOLE FLY BRAINS

After dissection and post-fixing the brains underwent another wash step before being incubated in 5% normal goat serum in PBST (blocking solution) for 3 hours at room temperature. Brains were incubated with fresh blocking solution at room temperature overnight with primary antibodies (Table 11.3, Appendix 3). Primary antibodies were washed off with 3 x 5-minute washes in PBST and 1 x 2-hour wash with PBST, the brains were then incubated in fresh blocking buffer containing the appropriate secondary antibody (Table 11.4, Appendix 3) overnight at 4°C in a light-proof vessel.

Following the incubation with secondary antibody the brains underwent 3 x 20-minute washes in PBST, ensuring minimal exposure to light during this time. Once the final wash buffer was removed 50 µL of antifade (1 mL 10x PBS, 9 mL glycerol, and n-propyl gallate to a final concentration of 0.2 mg/mL) was added and the brains were allowed to equilibrate for 20 minutes in the dark before being mounted on a slide (Sail), coverslipped and sealed with nail-polish. The slide was mounted under the Leica SP5 DM6000B scanning confocal microscope and brains were imaged at 400x or 630x total magnification.

2.4 Protein extraction from flies

2.4.1 FLY HEAD ISOLATION

To isolate protein or RNA specifically from *Drosophila* heads (enriching for brain tissue) heads had to be isolated from the *Drosophila* body. This enrichment step involved anaesthetising the flies with CO_2 and placing in a 15 mL Falcon tube (Greiner) which was subsequently submerged in liquid nitrogen or a dry ice/ethanol bath for 10-15 minutes. The tubes were then vortexed three times for 10 seconds each. This takes advantage of the fragile connection between the head and thorax of *Drosophila* allowing the now brittle structure to snap, separating the head from the thorax. The flies were then passed through a fine-grade sieve through a chilled glass funnel and then into another 15 mL Falcon tube. This allowed the legs (which are also broken off in the process) to stick to the glass funnel and then the falcon tube, rather than being isolated with the heads. This

process results in minimal contamination from other tissue as well as permitting the rapid isolation of many heads. These heads were then transferred immediately to the -80°C freezer for storage.

2.4.2 PROTEIN ISOLATION

Protein isolation from whole flies or fly heads was carried out to analyse expression or knockdown levels of tagged proteins using a combination of SDS-PAGE and Western blots. This extraction could be either the total protein in the cell or a fractionation of the nuclear and cytoplasmic proteins, as follows.

2.4.2.1 Total protein isolation

Total protein was obtained by adding approximately 50 fly heads (or equivalent mass in bodies, 6 or 7 whole bodies) and adding 50 uL RIPA (150 mM NaCl, 0.1% Triton X, 0.5% Sodium deoxycholate, 0.1% SDS, 50 mM Tris, pH 8.0) with freshly added cOmplete EDTA-free protease inhibitor (Roche). These were homogenised with 3 x 10 second pulses with a homogeniser before being centrifuged at 13,000g at 4°C for 5 minutes to pellet the cellular debris. The lysate was then transferred to a fresh tube and this centrifugation was repeated to ensure the removal of all cellular debris. Once transferred to a fresh tube this supernatant can then be quantified using the BCA protein assay (2.11) immediately or stored at -80°C long term.

2.4.2.2 Nuclear and cytoplasmic fraction isolation

To isolate nuclear and cytoplasmic proteins for subcellular distribution analysis, a different method of protein extraction was used. 50 fly heads were isolated and collected in a 1.5 mL microfuge tube with 100 µL of Buffer I (1 mM dithiothreitol, 1.1 mM EDTA, 15 mM HEPES pH 7.6, 10 mM KCl, 5 mM $MgCl_2$, 0.5 mM EGTA, 0.35 M sucrose) with cOmplete EDTA-free protease inhibitor (Roche). The fly heads were homogenised using 3 x 5 second pulses with a homogeniser and then spun gently at 1,000 x g for 1 minute. The supernatant was isolated and re-homogenised (3 x 5 second pulses) once the bulk of the cellular debris had been separated. The resulting homogenate was then centrifuged at 7,700 x g for fifteen minutes at 4°C to pellet the nuclei. The cytoplasmic lysate was then collected in

a fresh 1.5 mL microfuge tube and was then ready for use in SDS-PAGE gels or was stored at -80°C for long-term storage. The nuclear pellet was then resuspended in RIPA buffer and homogenised with 3 x 5 second pulses with a homogeniser. The homogenate was then incubated on ice for 10 minutes before the nuclei were lysed by sonication in a sonicator bath (Elmasonic S 10 H, Emla) at < 4°C. This mixture was then centrifuged at 1,350 x g to separate out any remaining cellular debris and the supernatant (nuclear extract) was then transferred to a fresh 1.5 mL microfuge tube, whereupon it could be quantified (2.11) and used immediately or stored at -80°C long-term.

2.4.3 RNA EXTRACTION FROM FLIES

Fly heads were separated as described in section 2.4.1. Approximately 150-200 heads were submerged in 500 µL TRIzol and homogenised using 3 x 5 second pulses with a motorised pestle. Sample was centrifuged at 13,000 x g for 10 minutes to pellet cellular debris and supernatant was transferred to a fresh tube. 100 µL of chloroform was added to the supernatant and mixed well before being centrifuged at 13,000 x g for 15 minutes. The solution separated in several phases, the upper phase was pipetted into a column tube from a Qiagen RNAEasy kit and centrifuged at 8,000 x g for 15 seconds. The collection vessel was emptied the column re-inserted before 700 µL of buffer RW1 (Qiagen, RNAEasy) was added and the column was centrifuged as before. The collection vessel was emptied, and the column re-inserted before 500 µL of buffer RPE was added and the column was spun again, as before. This step was repeated but centrifuged for 2 minutes at 8,000 x g. The column was inserted into a fresh RNAse-free tube and 30 µL of RNAse-free water was added straight to the column and this was centrifuged at 8,000 x g for 1 minute to elute the RNA. This step was repeated using a second aliquot of RNAse-free water to maximise yield.

The RNA was then stored at -80°C until quantification and sequencing.

2.5 Plasmid subcloning

To generate GFP-tagged HDAC4 proteins for expression in fly models, pUAST-attB plasmids modified with a GFP sequence were ordered from Genscript (New Jersey, USA) See appendix 2. This is described in more detail in section 3.2.2 but, in brief, the HDAC4 variant sequences were then excised from plasmids already present in the lab and ligated into the pUAST-attB-GFP plasmids so that they all had a GFP tag at the N-terminal, the resulting plasmid was propagated in *E. coli* (Section 2.5.2) and stored at -20°C.

2.5.1 GENERATION OF COMPETENT CELLS

Competent *Escherichia coli* DH5α cells were generated in large batches that were then aliquoted into 300 µL volumes. DH5α cells were streaked out on LB Agar plates (1 g tryptone, 1 g NaCl, 0.5 g yeast extract and 1.5g agar per 100 mL) with no antibiotics, then incubated overnight at 37°Cand an individual, well separated colony was picked using a sterile toothpick and used to inoculate 5 mL LB (1 g tryptone, 1 g NaCl, 0.5 g yeast extract per 100 mL) with 100 µL 1 M $MgSO_4$ (final concentration of 20 mM) and 5 µL 1 M KCl added (final concentration of 10 mM). These were then incubated overnight at 37°C while oscillating at ~225 rpm.

The following day, 200 mL of LB + 20 mM $MgSO_4$ and 10 mM KCl was inoculated with 2 mL of the overnight culture and incubated at 37°C for 2-3 hours or until the OD_{600} was equal to 0.35 – 0.4. Cells were transferred to multiple 50 mL plastic tubes (Nunc) and pelleted by centrifugation at 4,400 x g at 4°C for 5 minutes and the media was removed. The cells were then resuspended in 25 mL (per tube) of ice-cold TFBI (100 mM RbCl; 50 mM $MgCl_2$; 10mM $CaCl_2$; 30mM KAc; 15% glycerol; pH 5.8) and incubated on ice for 10 minutes before being pelleted as before, TFBI removed and resuspended in 4 mL of ice-cold TFBII (10 mM RbCl; 10 mM MOPS, pH 7.0; 75 mM $CaCl_2$; 15% glycerol) then combined into one 50 mL tube.

The cells were aliquoted out into tubes submerged in a dry-ice/ethanol bath to snap freeze them and stored at -80°C.

2.5.2 PLASMID PREPARATION FROM *ESCHERICHIA COLI*

Plasmid DNA was extracted from transformed *E. coli* using an InTron Biotech DNA-Spin plasmid purification kit (for 3-5 mL cultures) or an Invitrogen PureLink Hi-Pure plasmid filter midi-prep kit (for 100 – 300 mL cultures) according to the manufacturer's instructions.

2.5.3 QUANTIFICATION OF DNA

DNA extracted from *E. coli* was quantified through using a Denovix DS-11 spectrophotometer. This device also provided a 260/280 measurement used to approximate the quality of the sample.

2.5.4 RESTRICTION ENDONUCLEASE DIGESTION OF DNA

Total plasmid DNA extracted from *E. coli* (2.5.2) was digested by combining 1 µg of DNA with 2 units of the desired restriction enzymes (Table 10.1, Appendix 2) and 5 µL of the appropriate buffer before making the mixture up to 50 µL with dH_2O. This solution was mixed briefly by tapping and centrifuged at ~1000 x g for 5 seconds to ensure the reagents were well combined. The reaction mixtures were then incubated in a 37°C water bath for 60 minutes then transferred to ice and subjected to agarose gel electrophoresis (Section 2.5.4).

In the case of samples where a fragment was being cut out to insert into a new plasmid the digestion reaction was treated to prevent re-ligation of the digested DNA if compatible cut sites remained. To do this, 2 µL of Calf intestinal phosphatase (CIP, NEB) was added to the reaction mixture and the mixture was incubated for a further hour at 37°C to dephosphorylate the 5' ends.

2.5.5 AGAROSE GEL ELECTROPHORESIS

Agarose gel electrophoresis was used to separate DNA based on size for analysis of ligated plasmids or separation of fragments from restriction endonuclease digestions. To do this, a gel was made by melting 1 g of agarose (BioRad) in 100 mL of 1x TAE buffer in a microwave before adding Ethidium Bromide (EtBr) to a final concentration of 0.3 µg/mL. This was then poured into a gel casting tray with a comb inserted and allowed to cool for 1 hour.

The set gel was then transferred to an electrophoresis apparatus (BioRad) which was filled with 1x TAE until the gel was covered to a depth of 1cm. 3 µL of EtBr was added to the reservoir at the positive electrode to enhance staining. Approximately 50 ng of DNA was combined with 6x purple loading dye (NEB) to a final concentration of 1x loading dye and these mixtures were pipetted into the wells alongside a 5 µL sample of the BioRad 1 kb+ ladder as a mass standard. If the samples were going to be purified from the gel for future use up to 300 ng was added per lane. The gel rig was then connected to a power pack (BioRad PowerPac HC) and run at 75 V for 60 minutes or until the dye front was ~3/4 of the way down the gel. Following this, the gel was visualised using BioRad Gel-doc and the ImageLab 5.1 software.

2.5.6 DNA PURIFICATION FROM AGAROSE GELS

Restriction endonuclease digested DNA fragments were separated using gel electrophoresis (Section 2.5.4) and subsequently excised from the gel using a scalpel blade. The DNA was purified from the agarose using the Invitrogen PureLink Quick Gel Extraction kit, according to manufacturer's instructions.

2.5.7 PLASMID LIGATION

The vector and insert fragments were combined by adding 50-100 ng of vector to 5x the concentration of insert and diluted with DNAse free water to 8 µL before adding 1 µL Ligation Buffer (NEB) and 1 µL of T4 DNA Ligase (NEB). Ligation was carried out at 18°C overnight.

2.5.8 TRANSFORMATION OF COMPETENT CELLS

Competent cells (Section 2.5.1) were thawed on ice and a 2 µL of the ligation reaction was added to a 50 µL aliquot of the competent cells and incubated on ice for 45 minutes. The cells were then heat-shocked in a 42°C water-bath for 40 seconds and then returned to the ice before 500 µL of LB was added. The cells were then incubated at 37°C for an hour, a 50 µL aliquot was taken and plated out on LB-agar plates containing 100 µg/mL of ampicillin to select for only transformed *E. coli*. These plates were inverted and incubated overnight at 37°C

and a several individual colonies were isolated and cultured overnight in 2 mL of LB containing 100 µg/mL ampicillin. These overnight cultures then had DNA extracted (Section 2.5.2) and subjected to an analysis restriction digest to select for successful transformations with the insert present and in the correct direction.

2.6 SDS-PAGE and Western Blots

Sodium dodecyl sulfate – polyacrylamide gel electrophoresis (SDS-PAGE) was used to separate proteins in a given sample by size. For this, 15 µg of total protein was added to 5 x Laemmli buffer (2% SDS, 5% 2-marcaptoethanol, 10% glycerol, 0.01% bromophenol blue, 60 mM Tris HCL, pH 6.8). This was diluted with RIPA buffer to make the final concentration of Laemmli buffer 1x. The resulting mixture was then boiled at 95°C for five minutes to reduce and denature the protein before being loaded into the wells of a pre-cast polyacrylamide gel (Mini Protean TGX 4%-20%, Bio-Rad) submerged in running buffer (25 mM Tris, 190 mM glycine, 0.1% SDS). It was instantly run for 30 minutes at 15V to allow steady access of the protein into the gel and then run at 120V for approximately 90 minutes or until the dye front reaches the bottom of the gel.

The proteins were transferred to a nitrocellulose membrane (Amersham Protran premium 0.45 µm nitrocellulose, GE Healthcare LifeScience) by inserting the gel and pre-soaked membrane between two pre-soaked fabric pads and clamping together in a cassette to ensure close contact. This cassette was then submerged in 4°C 1x Transfer buffer (25 Mm Tris, 190 Mm glycine, 0.1% SDS, 20% methanol) and a 100 mA current was applied for 60 minutes. The membrane was incubated with Ponceau-S stain (0.1% Ponceau, 5% acetic acid) to confirm the presence of protein on the membrane and then rinsed by sequential submersion in distilled H_2O until the bands were no longer visible.

The rinsed membrane was immediately incubated with 5% blocking buffer (5% (w/v) skim milk powder in TBST), completely submerged and gently agitated at RT for at least 1 hour to prevent non-specific binding of antibodies. To probe for the protein or tag of interest, the membrane was then incubated with the primary

antibody (Table 11.3, Appendix 3) diluted in 1% blocking buffer overnight at 4°C to reduce non-specific binding. The following day the membrane was washed for 3 x 5 minute washes with TBST (1x TBS, 0.1% Tween 20) and then incubated with the secondary antibody (Table 11.4, Appendix 3) diluted in 1% blocking buffer at room temperature for 1 hour. The membrane underwent the same wash step as before and the proteins were detected using a chemiluminescent substrate from either Amersham ECL Select Western blotting detection reagent (GE Healthcare) or ECL Prime (GE Healthcare). Chemiluminescence was visually detected using Azure c600 (azure biotech)

2.7 Sequencing of DNA

DNA was sequenced by Massey Genome Services (MGS) using the BigDye Sequencing Ready Reaction mix (ThermoFisher) and cycle sequencing PCR, with analysis by the ABI3730 DNA analyser (ThermoFisher). Primers used during this project are listed in Table 11.1 Appendix 3.

2.8 *Drosophila* transgenesis

Plasmids (designed and created in section 2.5) were amplified in *E. coli* and purified using a maxi-prep (Section 2.5.2)**.** The resulting DNA was then ethanol precipitated and resuspended in 50 µL of injection buffer (50 mM KCl, 0.1 mM sodium phosphate buffer, pH 6.8) to a final concentration of 0.8 µg/µL and stored at -20°C.

The fly stock used for microinjection in this project was VK37 (Venken *et al.*, 2006). VK37 harbours an attP docking-site at 22A3 on the left arm of chromosome 2. This docking site allows the integration of the attB containing DNA from a pUAS-attB plasmid via phiC31-mediated-integration.

Approximately 20 days before injection, multiple bottles of the VK37-attP stock were set to allow plenty of time for the flies to emerge, reach maturity and begin laying eggs at a high rate. Three days before injection extra yeast paste (dried

yeast with water added to generate a peanut butter-like texture) was added to each bottle to encourage more rapid egg laying.

On the day of injection the injection buffer was centrifuged at 13,000 x g for 15 minutes at 4°C to pellet any particulates that may block the injection needle. The injection buffer was then transferred to an ice bath for the day to keep it liquid but cold and reduce the risk of DNA degradation. While the DNA is being centrifuged, approximately 400 flies (6-8 bottles' worth) were decanted into polystyrene beakers with airholes and taped to a 60 mm diameter polystyrene petri dish (ThermoFisher) filled with egg-plate media (20 g agar; 60 g fine cornflour; 40 g molasses added to 1 L of dH_2O, brought to the boil and taken of the heat before adding 3.3 g methyl-4-hydroxybenzonate dissolved in 37 mL of 96% ethanol) and streaked with 2-3 mL of yeast paste.

These were incubated for about an hour and then the plates were cleaned of eggs, this prevents the collection of eggs stored by the female flies that would be too old for successful microinjection. The food plates were replaced with fresh plates and the flies were incubated for a further 20 minutes. After this period the eggs were removed from the plates with a small paintbrush and dechorionated by rolling on double-sided tape attached to a microscope slide using fine forceps. The dechorionated eggs were aligned at the end of the microscope slide which was subsequently transferred to a glass petri dish containing pre-dried silica beads to dehydrate the eggs for 3-6 minutes (depending on relative humidity on the day). Once slightly dehydrated the eggs were immediately covered in Halocarbon oil 700 (Sigma, H8898) to prevent further dehydration and reduce cytoplasmic leakage. The eggs were then injected as soon as possible. 2 µL of the prepared plasmid in Injection buffer was loaded into a pre-pulled quartz-glass needle with a 20 µL Eppendorf Microloader tip, the needle was then attached to a micro-manipulator (Leica). The needles were made from 1.0 mm x 0.75 mm, 10 cm long, thin-walled quartz capillary glasses with microfilament (A-M system) and pulled from a laser-based micropipette puller (P-2000, Sutter Instruments).

DNA injection into the embryos was carried out with a Femtojet express transjector (Eppendorf) using pressurised nitrogen gas. A small but unknown amount of DNA was injected into the posterior end of the embryos, visualised with a CK2 inverted compound microscope (Olympus). Embryos not successfully injected (or deemed too mature for injection) were destroyed with the forceps or the needle.

The slides were incubated overnight at 18°C in a humidity chamber under pressurised oxygen (~2 atm). The following day the chamber was placed at 21°C for another 24 hours. After this 21°C incubation, surviving larvae had shed their egg-casings and were collected onto moist tissue paper (Kimberly-Clark Kimwipe) using forceps. This paper was then transferred to a vial containing standard media and then incubated at 25°C.

2.8.1 CROSSES TO GENERATE STABLE FLY LINES

The transgenic flies that survived were collected and crossed with w(CS10) (Canton S line with a w^- mutant gene, exhibiting white eyes in the adults). The resulting progeny were examined and transformant flies with red eyes were collected as they should bear the inserted gene (as the pUAST vector used contains a w^+ gene, allowing expression of red pigment in the eyes leading to a red eye phenotype). The VK37 fly line these plasmids were injected into harbours an attP site on the second chromosome so the transformant offspring were crossed to w^{CS10}; *CyO*, *ScO* flies. The *CyO* and *ScO* genes on the 2nd chromosomes are part of balancers that prevent recombination across the chromosome. Red eyed, curly winged offspring were selected as these harbour both the inserted construct and the curly marker that allows for selection. These offspring were crossed together and non-curly offspring were selected from the progeny. The non-curly, red-eyed flies were homozygous for the GFP-Tagged HDAC4 variant on the second chromosome, allowing for the maintenance of the transgenic flies as a stable line.

2.9 Transient transfection of human cell lines

MCF7 or HeLa cells (kind gifts from Dr Tracy Hale) were seeded into a 24-well plate at a density of $1.0x10^5$ cells/well in Dulbecco's Modified Eagle Medium supplemented with 10% fetal bovine serum (FBS; Thermo Fisher) and 1% penicillin (Thermo Fisher). These were incubated for 24 hours to reach approximately 70-80% confluence and the media was flushed and replaced with fresh DMEM media. 0.5 µg of total DNA was then combined with transfection reagent X-TremeGene9 at a ratio of 1 µg of DNA to 3 µL of reagent in 50 µL of OptiMEM media. This mixture was then incubated for 15 minutes at RT to allow the transfection complexes time to form before being added to the cells. The cells were then incubated for a further 48 hours before being processed.

2.10 Total protein extraction of human cell lines

Human cells cultured in 24-well plates were harvested for protein analysis by washing the cells 2 x in 200 µL PBST to remove excess media before adding 100 µL of RIPA buffer + protease inhibitor and using a cell scraper to remove the cells from the base of the plate. The resulting slurry was transferred to a 1.6 mL microfuge tube and incubated on ice for 5 minutes. Following incubation, the sample was centrifuged at 7,000 x g for 5 minutes to pellet the cellular debris and the supernatant was isolated and either used immediately or stored at -80°C.

2.11 Quantification of protein

Protein concentration was quantified using the Pierce BCA Protein Assay Kit (ThermoFisher) to generate the standard curve and stain the cell lysates, according to manufacturer's instructions. Absorbance of the standard and all measured samples was measured using a BioTek PowerWave XS plate reader. This was used for both *Drosophila* and mammalian tissues with each unknown measured in triplicate.

2.12 Luciferase assay

Luciferase assays were carried out using the Promega Luciferase Kit. Tissue, either fly heads (2.4.1) or cultured human cells (2.16) were lysed by diluting 5 x reporter lysis buffer (Promega) to 1 x with dH_2O.

2.12.1 TISSUE PREPARATION FOR FLIES

Approximately 50 heads (2.4.1) (or 5 whole flies) were added to 100 µL of 1x Reporter Lysis Buffer and homogenised with a motorised mortar and pestle with 3 x 5 second bursts, this homogenate was then centrifuged at 1,450 x g for 10 minutes to pellet the head capsules. The supernatant was then transferred to a pre-chilled microcentrifuge tube and kept on ice until the luciferase activity was measured (Section 2.12.3).

2.12.2 TISSUE PREPARATION FOR HUMAN CELL CULTURE

The 24-well plate was removed from the incubator and checked to ensure the confluency was ≥90%. Once checked, the cells washed in 1 x PBS twice before being submerged in 1 x Reporter lysis buffer (Promega) and scraped from the base of the wells with manual scraping. The cell suspension was transferred to the freezer for a freeze-thaw cycle and the thawed suspension was transferred to new, pre-chilled microfuge tubes and centrifuged at 7,000 x g for 10 minutes to pellet the cellular debris. Following this, the supernatant was transferred to new pre-chilled microfuge tubes. From here the cell lysates were treated identically.

2.12.3 LUCIFERASE ASSAY

A 10 µL aliquot of each sample was aliquoted into a well of a white-plastic 96-well tray, keeping the samples in non-adjacent wells to avoid the bleeding over in the case of particularly bright samples. 50 µL of luciferase reagent was added to each sample immediately before reading using a PolstarOMEGA (BMG Labtech) and the Omega software package. Luminescence units were normalised either to transfection efficiency (for human cell culture) by comparing relative luminescence provided by the renilla luciferase transfected alongside at 0.2 µg/

culture well. Fly luminescence was normalised to the total protein measured in the sample (Section 2.11).

2.13 Transcriptome analysis

RNA extracted from *Drosophila* was quantified, initially, using a Denovix DS-11 spectrophotometer before being sent to Massey Genome Services for Labchip GX Touch HT (PerkinElmer) analysis. Following verification of RNA quality and quantity, samples were sent to Novogene (Hong Kong) for further QC and library assembly using paired-end sequencing.

Following library assembly, the library data was sent to NBSeq for read mapping and read count analysis. The process of this is detailed in section 6.3 but in brief, the reads were processed and trimmed using *fastqc* before being mapped to the *Drosophila* genome (release 92) downloaded from ENSEMBL using HAT2 in stranded mapping mode. The read count for each mapped read was measured and this was used to generate $\log_2$-fold changes in transcription used to measure transcriptional changes induced between treatment groups.

Further analysis of the changes in transcription to characterise subsets of enriched genes was done with DAVID (Huang *et al.*, 2009a, 2009b).

2.14 Courtship suppression assay

To assess memory and learning in *Drosophila melanogaster* fruit flies the repeat training courtship suppression assay was used. Courtship conditioning is a form of associative learning that conditions male flies to expect rejection by mated females. This conditioning trains the male flies to expect rejection when exposed to new courted female, and the male flies with fully functioning memories will recall this rejection and attempt to court subsequent non-receptive females less frequently. Thus, the frequency with which trained males attempt to court females compared to the attempt rate of untrained male flies provides a reliable measure of memory function.

Immature, virgin males of each genotype to be tested were collected for up to seven days before testing, flies were stored individually in cotton-plugged, 30 mL vials containing ~3 mL of food. To generate freshly mated females, virgin CS flies were collected and then housed with an excess of virgin males for 72 hours prior to training to ensure all female flies were mated and thus, unreceptive to courtship attempts. After 72 hours the flies were anaesthetised and separated by gender, discarding the males and keeping the females for training after 30 minutes to recover from the effects of the anaesthetic. Using an aspirator, an individual virgin male was added to a courtship chamber with 0.5 mL of food in the base. After this, a mated female was introduced to the chamber and they were left to court for 8 hours. A duplicate chamber, housing an individual male to remain untrained, was also set up. These are termed sham males. N > 20 males of each genotype were trained and N > 20 sham males of each genotype were left untrained.

These flies were left for 8 hours, either being trained through exposure to non-receptive females or in identical conditions on their own. After this period the female flies were aspirated out and discarded. The male flies were kept in their chambers and incubated overnight in isolation for 16 hours to permit consolidation of long-term memories. The following morning the male flies were individually aspirated into transparent testing chambers and exposed to fresh non-receptive females, prepared as before, and video recorded for the first ten minutes of courtship. This 10-minute video was analysed with the tester blind to the genotype and trained/sham nature of each fly and the proportion of time the male spent attempting to court the female was recorded as a percentage. Once analysis was complete the tester was unblinded to the original genotype and trained/sham status of the fly to provide an average proportion for each genotype in both the trained and sham flies known as a courtship index. The trained and sham courtship indices could be compared to one another to provide what is known as a memory index, providing a reliable measurement of memory function across several repeat training/testing experiments.

2.14.1 STATISTICAL ANALYSIS OF COURTSHIP DATA

Courtship data was amalgamated and the average of each genotype's un-trained courtship index (CI) was calculated. Following this, the memory index of each male fly was calculated as follows:

$$\frac{\overline{CI}_{naive} - CI_{trained}}{\overline{CI}_{naive}} = MI$$

In which $\overline{CI}_{naive}$ refers to the average courtship index of all naïve male flies and $CI_{trained}$ refers to the courtship index of an individual trained male fly.

These MI scores were averaged for each genotype to provide an indication of the memory performance, a score of 0 indicates no memory was formed and the average trained male fly spent 100% of the time trying to court the female. A score of 1 indicates perfect memory and that the average trained male fly spent 0% of the time trying to court the female. This value was used in plotting the graphs and generating the standard errors (SE).

As the memory index scores were typically not normally distributed, they were then Arcsine transformed to normalise the data and the same steps as before were then taken to calculate the memory indices for the trained individuals. These scores were tested using a one-way analysis of variants (ANOVA) followed by a post-hoc Tukey's HSD to determine significance.

2.15 Electrical stimulation of whole flies

Electrical stimulation of whole flies was carried out according to olfactory conditioning protocols (Tully *et al.*, 1994; Malik and Hodge, 2014) barring the inclusion of the noxious odours. Using a GRASS S48 stimulator connected to copper-lined tubes, flies were anaesthetised with CO_2 and sealed into the tube. The stimulator was set to train rate: 14; train duration: 1.2; stimulation rate: 2.0; delay: 0.01; duration 1.25 s; and voltage: 90V. Flies were allowed 5 minutes to recover from anaesthetic before being stimulated for 60s (with a 1.25 s shock

every 5 seconds). Flies were anaesthetised and transferred to a vial for recovery before being processed to measure luciferase activity.

2.16 TrpA1 activation

TrpA1 is a temperature-gated ion channel that, when under control of a UAS activator can be expressed in the fly in a tissue specific manner. Flies expressing a UAS-TrpA1 construct were raised at 21°C to avoid incidental activation. The method for activation is adapted from (Neely *et al.*, 2011) so that normal food vials containing the flies were submerged up to halfway in a 46°C water bath for four minutes. Following submersion, the food vial was removed and placed on ice to induce a rapid return to room temperature, avoiding incidental effects through extended activation of the TrpA1 ion channel.

3 THE SUBCELLULAR DISTRIBUTION OF HDAC4 VARIANTS

3.1 Investigating the effects of nuclear and cytoplasmic HDAC4 on neuronal development

HDAC4 is a class IIa histone deacetylase that undergoes activity dependent nucleocytoplasmic shuttling in neurons. Previous studies have shown that this protein impairs learning and memory in both mammals and *Drosophila* when overexpressed (Sando *et al.*, 2012; Fitzsimons *et al.*, 2013), suggesting it acts as a memory repressor. However, knockdown of the expression also impairs memory function, as do mutations in HDAC4 or deletion of HDAC4 (Kim *et al.*, 2012; Fitzsimons *et al.*, 2013), indicating that in *Drosophila* HDAC4 is vital for memory formation but that excess amounts have a repressive effect.

Complicating our understanding is that nuclear accumulation of HDAC4 goes hand-in-hand with cytoplasmic depletion, making it unclear whether the cytoplasmic shuttling of HDAC4 is required for learning and memory or whether it is merely being sequestered outside of the nucleus. As nuclear and cytoplasmically restricted human HDAC4 mutants have been previously developed and characterised (Chen *et al.*, 2012b; Sando *et al.*, 2012) these can be used to investigate the contribution of nuclear and cytoplasmic pools of HDAC4 to the development of *Drosophila* brains. These nuclear and cytoplasmic variants will be compared to WT *Drosophila* HDAC4 and human HDAC4 to untangle the separate roles of nuclear and cytoplasmic HDAC4 in development and memory, as well as directly comparing the activity of *Drosophila* and human HDAC4s. Both mammalian HDAC4 and DmHDAC4 have been demonstrated to repress memory in their respective models, however, their subcellular distribution and respective roles in neurons have not been directly compared.

As previous work has been carried out in mammalian systems this project will characterise the subcellular distribution in the *Drosophila* model and compare this to the expression of the wild-type *Drosophila* HDAC4 (DmHDAC4) which, like mammalian HDAC4, undergoes nucleocytoplasmic shuttling and has been

shown to be present in both the nucleus and the cytoplasm in *Drosophila* brains (Fitzsimons *et al.*, 2013).

The project will compare the *Drosophila* and human HDAC4 subcellular distribution and activity, in addition to characterising two human subcellular distribution mutants. One that is proposed to be largely nuclear, known as 3SA, and another that is proposed to be largely cytoplasmic, known as L175A.

The 3SA variant contains three serine to alanine mutations that prevents the phosphorylation of HDAC4 and subsequent association with the molecular chaperon 14-3-3ζ that is responsible for nuclear export, thus, the 3SA mutant accumulates in the nucleus and is very tightly restricted to the nucleus in cultured mouse neurons (Bolger and Yao, 2005). L175A (leucine 175 to alanine) interrupts the binding of MEF2 to HDAC4 and prevents the nuclear import of HDAC4. Subsequently, the L175A mutant is a cytoplasmically restricted variant of HDAC4.

The first aim of this thesis is to characterise and compare the subcellular distribution of the four constructs in the *Drosophila* brain, the second aim is to examine the effect of expression of each construct on neuronal development. Collectively, all four (DmHDAC4, hHDAC4, L175A, and 3SA) of these will be referred to as the HDAC4 variants (HDACv). Initial characterisation utilised fly lines harbouring FLAG-tagged HDACv that were generated in the lab by Helen Fitzsimons.

3.2 Characterisation of the subcellular distribution of wild-type and mutant HDAC4 in the *Drosophila* brain

3.2.1 A NOTE ON COLOUR SCHEMES

It has been observed by numerous research groups over recent years that the default colour schemes used in figures and graphs is often unfavourable to persons with altered colour perception (Okabe and Ito, 2002). Notably, and most relevant to this project, red and green is a frequently used colour pair for double-stained immunohistochemistry samples. In an effort to make figures more reader-friendly, many *Drosophila* researchers have adopted the use of magenta instead of red, allowing individuals with protanopia (difficulty distinguishing between red and green pigments) to identify the different stains, as shown below (Figure 3.1).

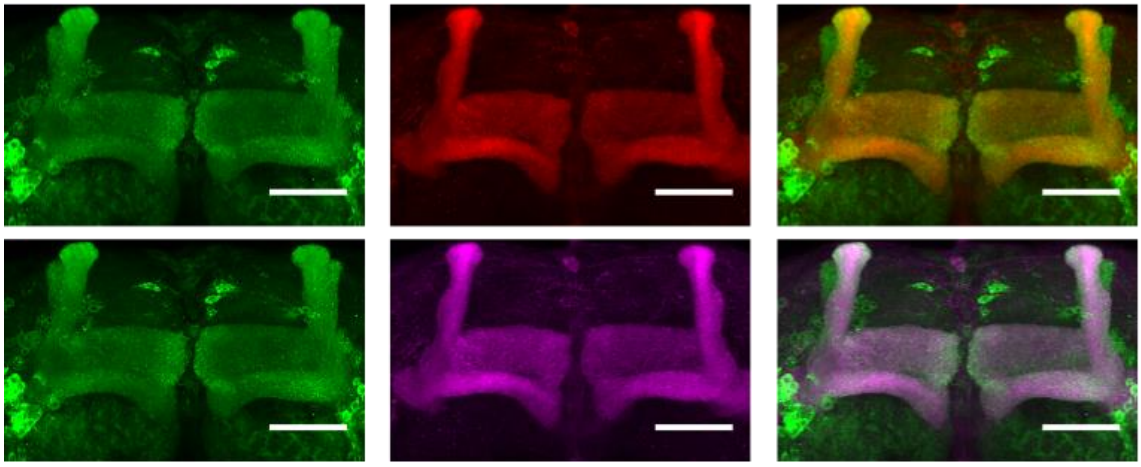

Figure 3.1 Confocal microscopy images showing the mushroom body.
Flies expressing a CD8::GFP fusion protein were counterstained with an anti-FASII antibody. The top row shows the traditional colour scheme of red and green, overlapping to generate orange/yellow. The bottom row shows the modified scheme common in *Drosophila* research in which the red and blue channels are merged to show magenta where the red fluorescence is detected. This is a much clearer image for individuals suffering from protanopia, or red-green colourblindness. Scale bar = 40 μm.

3.2.2 GENERATION OF N-TERMINAL GFP-HDAC4 FUSION

UAS-driven HDACv constructs were already present in out lab, however the FLAG-tags on the constructs proved to be unreliable as a tag in Western blots and initial assessment of HDAC4 subcellular distribution via

immunohistochemistry was hampered by poor staining with two different α-FLAG antibodies. Robust expression was observed but it was spotty and did not permit the visualisation of HDAC4 at the desired resolution in Kenyon cell nuclei. This was overcome by developing a strategy to generate GFP-fusions which would permit both the visualisation of HDAC4 in whole brain immunofluorescence and, in addition, would provide a more reliable tag for Western blotting.

Firstly, a plasmid containing GFP was designed and then synthesised by Genscript, such that each HDAC4 could be inserted in order to generate an in-frame, N-terminal fusion. The pUAST-attB plasmid contains a 5x GAL4 DNA binding domain (the upstream activating sequence, UAS), in addition to an attB site, which allows for transformation into *Drosophila* via the attB/attP recombination system mediated by PhiC31 integrase. Additionally, the plasmid harbours an ampicillin resistance gene for selection during cloning. Inserting the GFP open reading frame into this plasmid not only allows for the generation of the GFP-tagged HDACv constructs but would also permit the future addition of the GFP tag to other genes (overview of plasmid construction strategy in Figure 3.2).

The HDACv sequences were excised from their host plasmids using restriction digests (Section 2.5.3, details on restriction enzymes used in Table 10.1, Appendix 2). Fragment size was confirmed through agarose gel electrophoresis (Section 2.5.4), (Figure 10.2, Appendix 2). The verified fragment was cut from the gel and purified (Section 2.5.5) before being ligated into the pUAST-attB GFP plasmid (Section 2.5.6) and transformed into competent *E. coli* DH5α (Sections 2.5.1, 2.5.7) for amplification of the plasmid. The final plasmid product was then subjected to a three-part analytical digest: excising the fragment; linearising the whole plasmid to determine if it was the predicted length; and an internal digest to verify the orientation of the ligation (Figure 3.3).

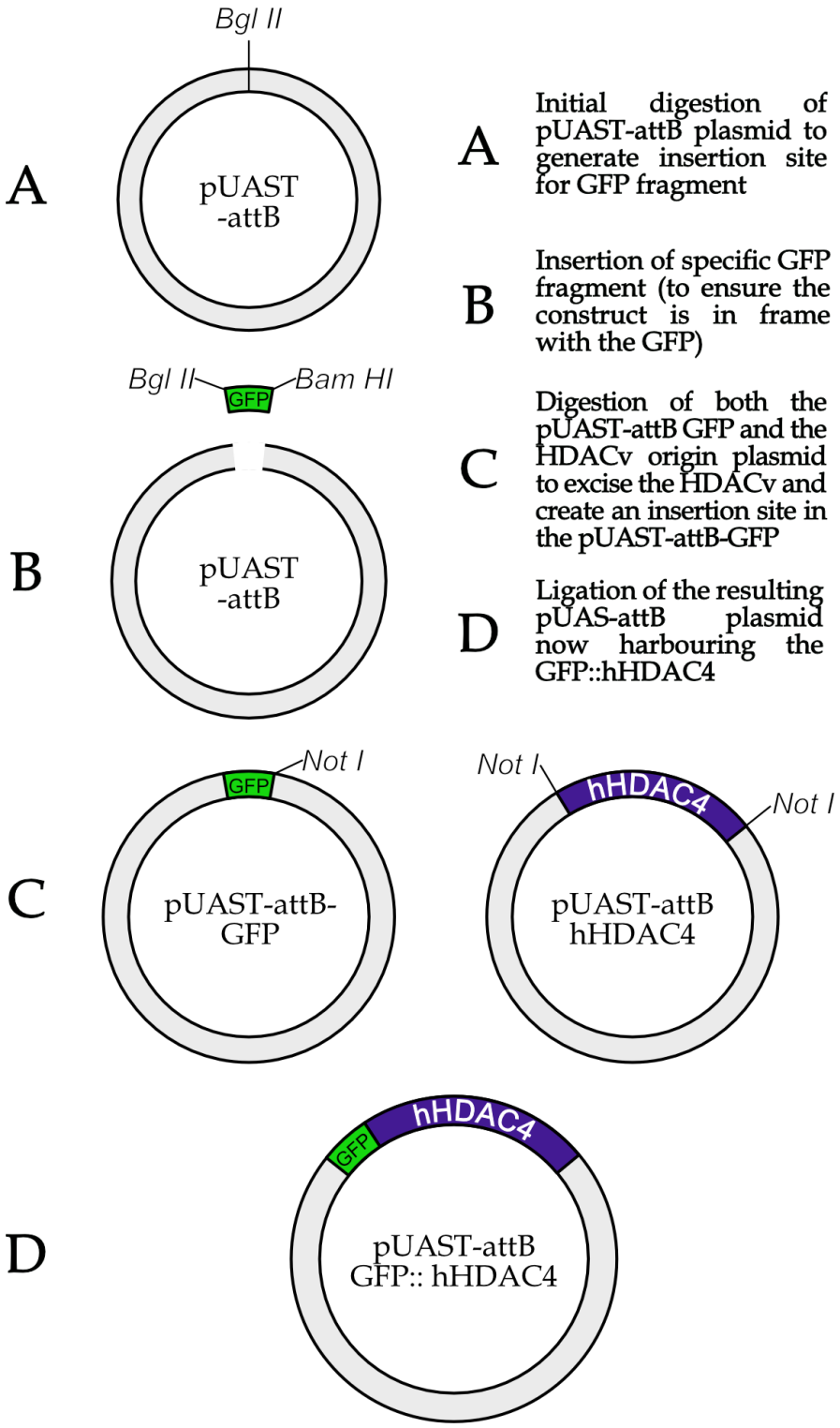

Figure 3.2 Visual summary of the cloning strategy.

Outline of the basic strategy used to generate the GFP::HDACv fusion constructs under UAS control. This figure uses hHDAC4 as the example but each HDACv used a slightly different GFP fragment and restriction enzyme due to differences in the sequences of the origin plasmids. Details in Appendix 3.

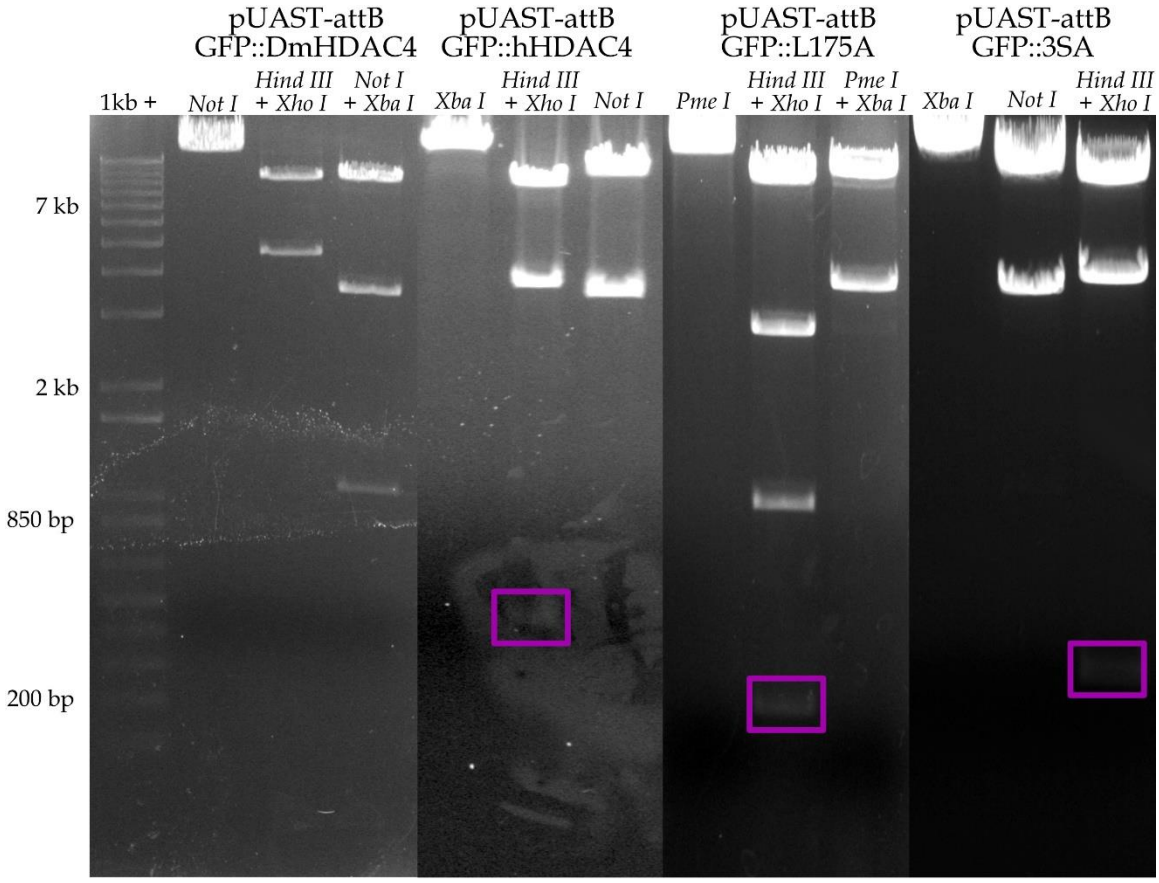

Figure 3.3 Restriction digests of pUAS-attB GFP::HDACv plasmid maxi-preps. Above are the combined gel images of the gel electrophoresis separated digests of the pUAST-attB GFP::HDACv plasmids. The enzymes used are listed and show a linearization, an excision of the fragment (plasmid + insert at different sizes) and an internal digest/direction of insertion check. Smaller, harder to visualise fragments are highlighted in magenta boxes. Several standard sizes are highlighted in white text, the line indicating the front of the band. Expected fragment sizes are listed in Table 3.1.

Transgenic flies were generated via microinjection of *Drosophila* embryos (See 2.9). Each construct was injected into the VK37 line which contains an attP site on the left arm of the second chromosome at position 2L (22A3). The PhiC31 system was used for homologous recombination into this genomic site for each construct in order to minimise differences in expression between the different constructs. If inserted into the same chromosomal location they will be influenced by an identical chromatin environment. This will minimise position effects that occur with the semi-random insertion of P-element constructs which require analysis of multiple lines for each construct. Newly generated flies were then outcrossed into the w[CS10] line to ensure that experiments were carried out in the same genetic background as previous works.

Plasmid	GFP::DmHDAC4	GFP::hHDAC4	GFP::L175A	GFP::3SA
Linearised	13,718 bp	12,513 bp	12,535 bp	12,513 bp
Construct excision	9,184 bp 4,534 bp	9,204 bp 3,309 bp	9,185 bp 3,350 bp	9,204 bp 3,309 bp
Internal digest	9,319 bp 3,212 bp 1,367 bp	8,471 bp 3,595 bp 447 bp	8,433 bp 2,524 bp 1,131 bp 447 bp	8,471 bp 3595 bp 447 bp

Table 3.1 Restriction digest predicted lengths for pUAS-GFP::HDACv.
Restriction fragment length predicted with SerialCloner 2.6.1 (Perez, 2013).

To express each variant in the *Drosophila* brain, the UAS-GAL4 system was utilised, with fly lines each harbouring an HDAC4v under control of a upstream activating sequence that allows for the induction of expression by GAL4, a yeast transcriptional activator. In order to provide temporal control, the TARGET system was used (McGuire *et al.*, 2004). This system incorporates a temperature sensitive variant of GAL80 ($GAL80^{ts}$) which binds to GAL4, preventing it from activating transcription at incubation temperatures less than 19°C but does not at higher temperatures, with full induction of expression at >29°C (Section 1.3.2). This allows expression to be induced in the adult brain without incurring developmental effects that could be caused expressing a construct through development.

The OK107-driver was used to express the HDAC4 variants in the mushroom body according to the crossing scheme below (Figure 3.4), this driver facilitates robust expression in all Kenyon cells, the intrinsic neurons of the mushroom body (Aso *et al.*, 2009; Fitzsimons *et al.*, 2013). $GAL80^{ts}$ under control of a tubulin promoter was also present in the driver line.

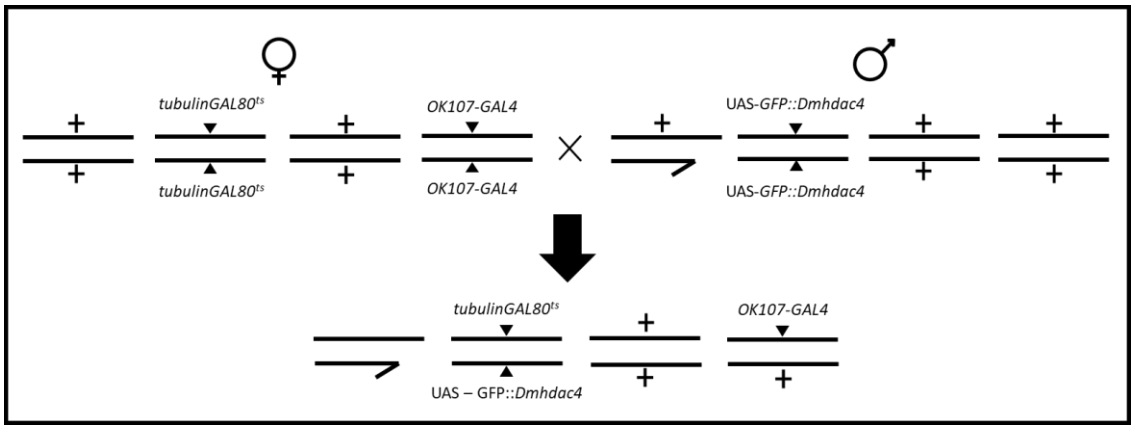

Figure 3.4 Schematic of *Drosophila* genetic cross.

In this the female fly harbours two copies of the driver-GAL4 and the tubulin-driven GAL80^{ts} and the male harbours two copies of the UAS-driven construct (in this case GFP::DmHDAC4). The resulting F1 progeny harbour one copy of each gene. ▲ indicates construct presence, + indicates wild-type chromosome.

Flies were raised at 18°C and then 3-5 day-old progeny were incubated at 30°C for 48 hours to induce transgene expression, and were split into two batches. Whole cell lysates were made (Sections 2.4.1, 2.4.2) and proteins were separated by SDS-PAGE and analysed by Western blot (Section 2.6) to confirm the fusion protein was being expressed in the flies (Figure 3.5). Verifying the GFP::hHDACv at ~146kDa and the GFP::DmHDAC4 at ~161 kDa. Subsequently, immunohistochemistry on whole-mount fly brains was carried out using an anti-GFP antibody and counterstaining with DAPI to highlight nuclei.

In whole *Drosophila* brain imaging, the cells and organised structures can be difficult to interpret. To help orient the reader Figure 3.6 has been included. This figure shows the whole brain, stained with DAPI to visualise nuclei, viewed from the posterior side in which the cell bodies of the Kenyon cells are visualised (white box) as a circular structure with the calyx (dendritic field of the Kenyon cells) in the centre. The figures below (Figure 3.7, Figure 3.8) show the relative distribution of the GFP-tagged HDAC4 in the Kenyon cells. Nuclei are counter-stained with DAPI. The expression pattern of GFP is observed in the top panel for comparison to that of the GFP-tagged HDAC4 variants.

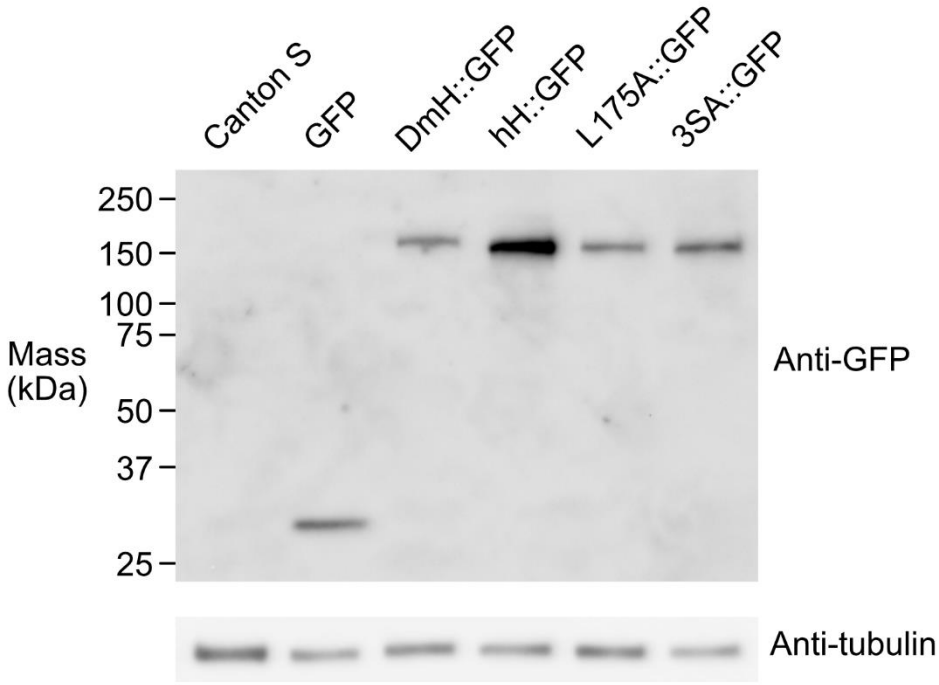

Figure 3.5 Western blot probed with anti-GFP antibody.
Whole protein extract from fly heads was run on an SDS-PAGE gel and underwent Western blotting using anti-GFP antibody to probe for the GFP::HDACv. UAS-GFP serves as a positive control for the anti-GFP antibody.

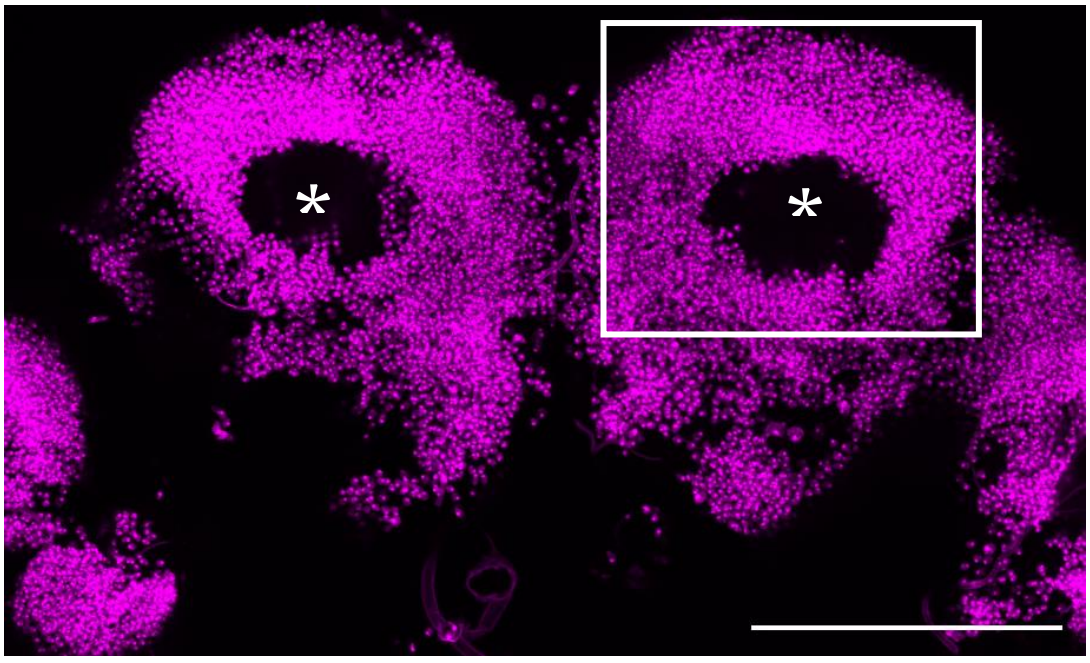

Figure 3.6 DAPI staining of a whole *Drosophila* brain from the posterior.
Note the nucleus-free calyces (asterisk) surrounded by Kenyon cell bodies. The dorsal side of the brain is at the top of the figure and ventral at the bottom. The white box highlights the calyx and Kenyon cell bodies shown in 3.7. Scale bar is 100 µm.

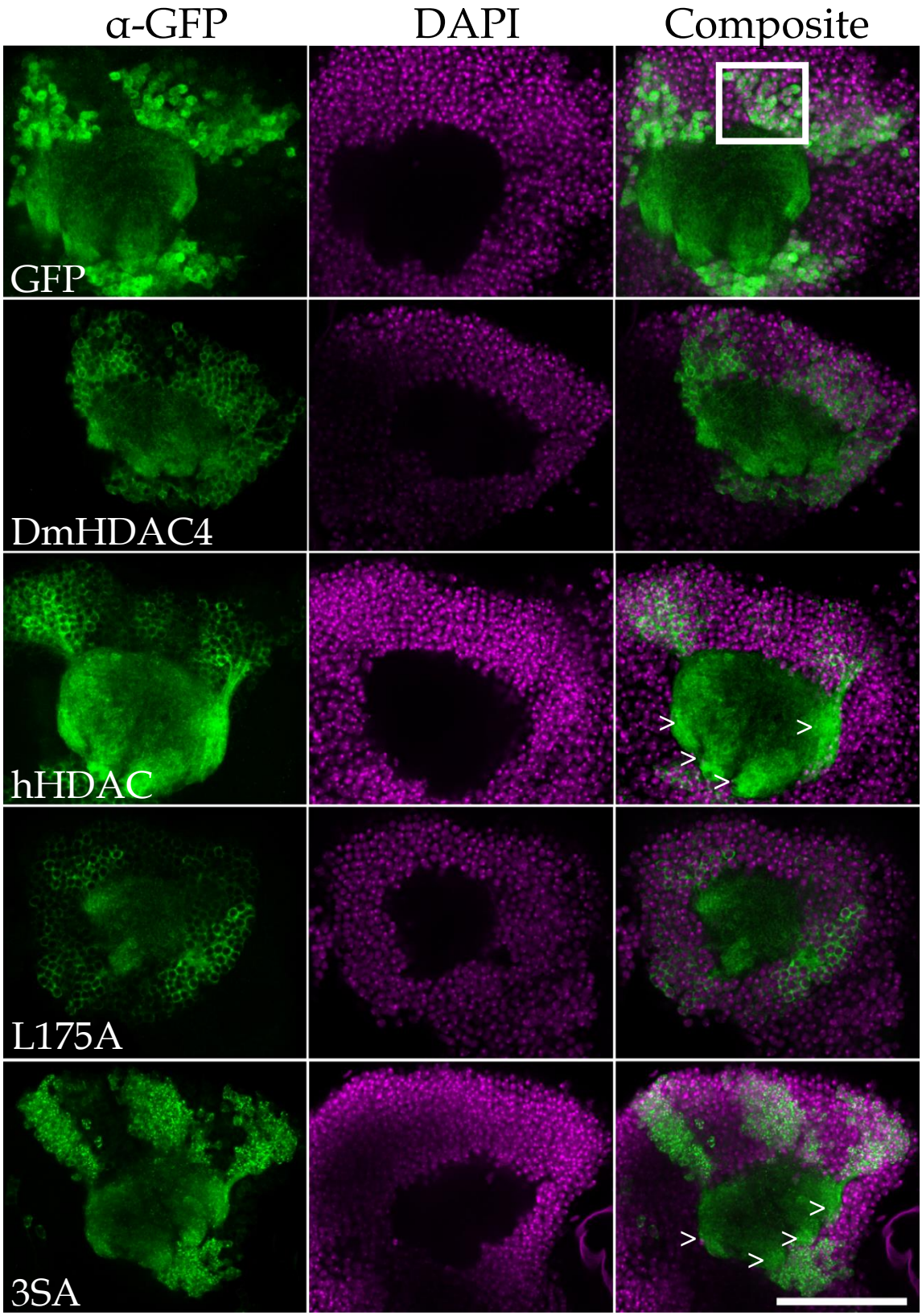

Figure 3.7 Subcellular distribution of HDACv in *Drosophila* KC bodies.
Immunohistochemistry on whole-mount brains using anti-GFP (Green) and DAPI (magenta). GFP-tagged construct expression driven by the OK107 driver. From top to bottom: GFP only, GFP::DmHDAC4, GFP::hHDAC4, GFP::L175A, and GFP::3SA. Scale bar = 40 µm. Highlighted box is magnified in following image (3.8). Chevrons in hHDAC4 and 3SA samples highlight beginning of the pedunculus.

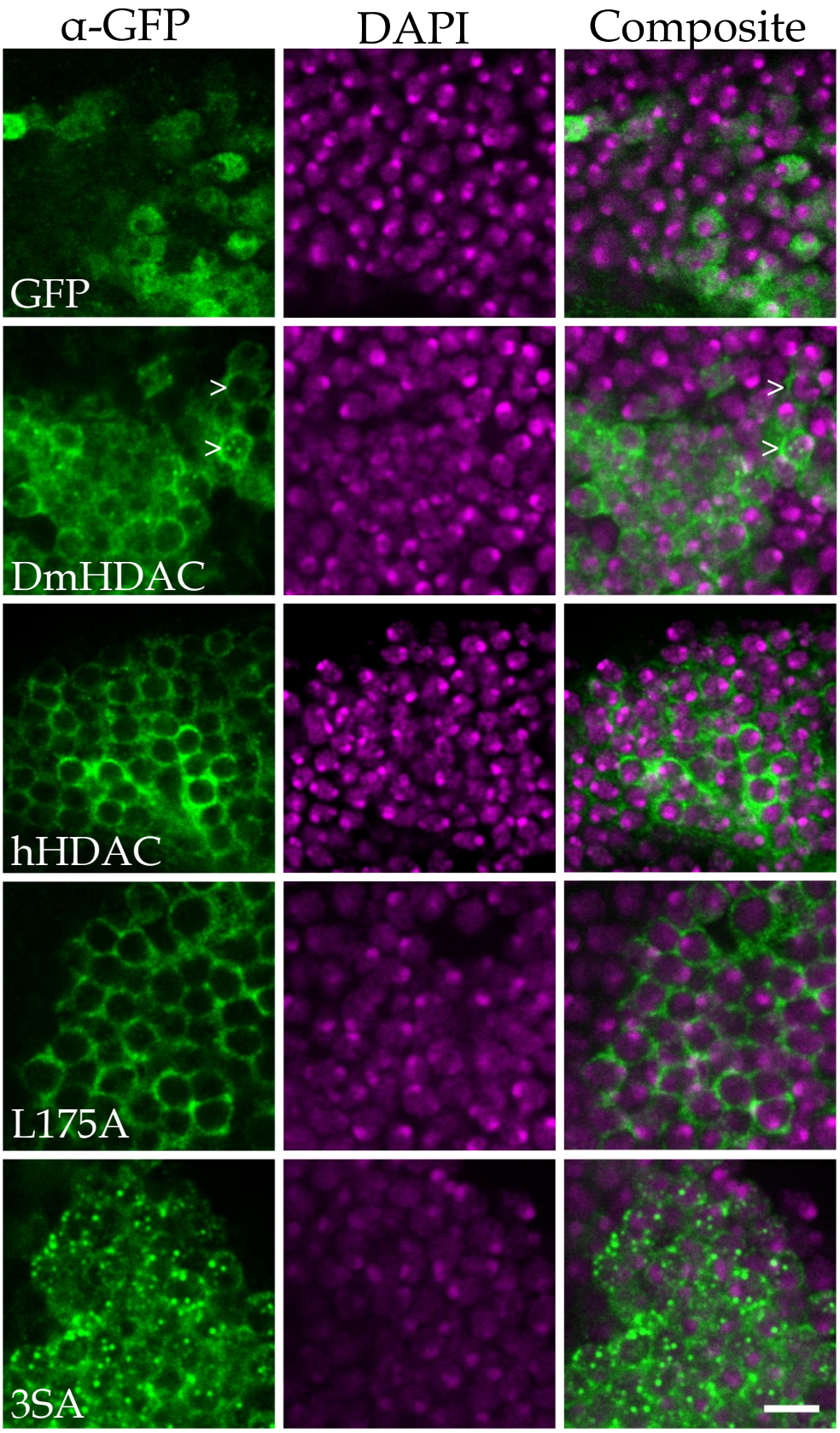

Figure 3.8 Single layer images to visualise HDACv subcellular distribution. Immunohistochemistry on whole-mount brains using anti-GFP (green) and DAPI (magenta). All expression is driven by the OK107 driver. From top to bottom: GFP only, GFP::DmHDAC4, GFP::hHDAC4, GFP::L175A, and GFP::3SA. Scale bar = 4 µm. Chevrons highlight two cell bodies in DmHDAC4, one with nuclear puncta and one without.

The GFP protein is observed in diffuse patterns in the nucleus and cytoplasm. GFP::DmHDAC has a mostly cytoplasmic localisation with some diffuse nuclear staining and several cells showing punctate foci of DmHDAC4 localisation, indicated by intense GFP staining. This is similar to subcellular distribution shown in earlier work (Fitzsimons *et al.*, 2013). The distribution of GFP::hHDAC4 was clearly different to DmHDAC4 having very low nuclear presence with no punctate foci, the cytoplasmic presence is obvious as cytoplasmic haloes clearly visible. Additionally, it was observed that hHDAC4 exhibited an increased presence in the axonal projections that constitute the pedunculus compared to DmHDAC4. GFP::L175A exhibited an exclusively cytoplasmic distribution with no nuclear presence at all, similar to the hHDAC4 wild-type localisation though without the occasional faint nuclear staining exhibited by hHDAC4. Finally, the 3SA::GFP fusion protein shows significantly altered distribution compared to the GFP::hHDAC4, with a much higher nuclear presence, even greater than the GFP::DmHDAC4 and exhibiting a high number of punctate foci in the majority of cells. Interestingly, it also exhibited significant cytoplasmic presence, as shown by haloes around cell bodies and presence in the pedunculus. This was not observed when 3SA was investigated in cultured mouse neurons, in which it was tightly and exclusively expressed in the nucleus (Bolger and Yao, 2005), suggesting that there is a secondary transport system or altered regulation of shuttling in *Drosophila*.

Combined with the Western blot, this data confirms the expression of the new GFP::HDACv fusion proteins and shows the subcellular distribution of each variant. This validation will allow for the analysis of the effects of each variant on *Drosophila* learning and development.

3.3 Effects of altered subcellular distribution on neuronal development.

Previous research in the lab has indicated that overexpression of HDAC4 impairs development of the mushroom body (Schwartz, 2016). To tease apart the role of nuclear and cytoplasmic HDAC4 during development and determine whether nuclear or cytoplasmic accumulation of HDAC4 is responsible for mushroom body defects, the individual HDAC4 variants were expressed using the UAS-GAL4 system. In order to express HDAC4 in the brain the elav-GAL4 driver was used (Robinow and White, 1988; Thurmond *et al.*, 2019). This is a pan-neuronal driver that drives expression from embryonic stage 10 (approximately 60 minutes after the egg has been laid), adults will be dissected and the effects of HDACv on mushroom body development will be assessed.

As described in section 1.3, the mushroom body is the primary centre of learning and memory in *Drosophila* and is also a large and easily identifiable structure in the brain. Disruption of normal mushroom body development is observed as interruption of axonal guidance, elongation and/or termination (Schwartz *et al.*, 2016; Freymuth and Fitzsimons, 2017).

3.3.1 CHARACTERISING THE EFFECTS OF ALTERED HDAC4 DISTRIBUTION ON *DROSOPHILA* MUSHROOM BODY DEVELOPMENT

Elav-GAL4 females were crossed with each HDACv as well as w(CS10) which is the genetic background into which the variant has been outcrossed as a control. After raising the larvae at 25°C mature adult brains of F1 flies were dissected out four days after eclosion (Section 2.3). The effects of HDACv expression were observed by staining with anti-FASII (Section 2.3.1), an antibody that targets Fasciclin II, a cell-cell adhesion protein that is expressed highly in the α, β and γ lobes, the bundled axons of the mushroom body. Highlighting this protein allows the visualisation of the axons that constitute the mushroom body as the adhesion between axons is vital to their normal pathing. Each brain was assessed for the normal development of each lobe and whether they were wild-type with respect to thickness (i.e. thin lobes indicate the presence of fewer axons) or whether

fusion of the β-lobes across the midline occurs, which is a commonly observed deficit that indicates impaired axon termination.

Initially, the frequency of each phenotype was observed to determine whether there was a predominant phenotype was observed (Table 3.2). This would indicate a specific role played by HDAC4 in one specific aspect of mushroom body development. However, no outstanding association between genotype and phenotype was observed (*i.e.* nuclear accumulation did not exclusively cause increased trimming but affected development by both impairing axon termination and impairing axon growth). In order to provide a semi-quantitative analysis, a scoring system was developed based on data from previous experiments with an increasing score reflecting increased disruption of mushroom body development (Bruckert *et al.*, 2015; Freymuth and Fitzsimons, 2017).

	Wild-type	Thin	Fused Beta	Thin and Fused	Single missing lobe	Multiple missing lobes	n
w(CS10)	100% (23)	0% (0)	0% (0)	0% (0)	0% (0)	0% (0)	23
DmHDAC4	5% (1)	19% (4)	14% (3)	52% (11)	10% (2)	0% (0)	21
hHDAC4	52% (12)	30% (7)	9% (2)	4% (1)	4% (1)	0% (0)	23
3SA	0% (0)	19% (6)	3% (1)	45% (15)	23% (7)	6% (2)	31
L175A	86% (18)	10% (2)	5% (1)	0%	0%	0%	21

Table 3.2 Frequency of the observed mushroom body phenotypes brains.
Frequency of each deficit is shown as a % with total sample number of MBs in the far-right column (n).

The scoring system is, as follows: in wild-type mushroom bodies the α and β lobes are 8-10 µm thick bundles of Kenyon cell axons in two mirrored L-shaped structures and are scored 0 as they have no apparent defects. Thinned lobes are less than 5 µm in width and often have misshapen or missing dorsal projections, indicating a reduced number of axons elongating in the vertical plane. As these thinned lobes can be caused by a small number of axons mis-pathing or not

growing, the phenotype was scored a 0.25. A lack of axonal termination which can result in fusion of the β-lobes, this was also scored a 0.25. The presence of both thin and fused phenotypes suggests a more severe disruption and so was assigned a score of 0.5. Absence or mis-pathing of a single lobe results in the absence of one of the two dorsally projected lobes in the L-structure was assigned 0.75. Similarly, the most severe disruption of axonal development observed was a full absence of multiple lobes, this extreme phenotype was scored a 1. The scores were averaged across all samples taken to provide a phenotype score (Figure 3.9)

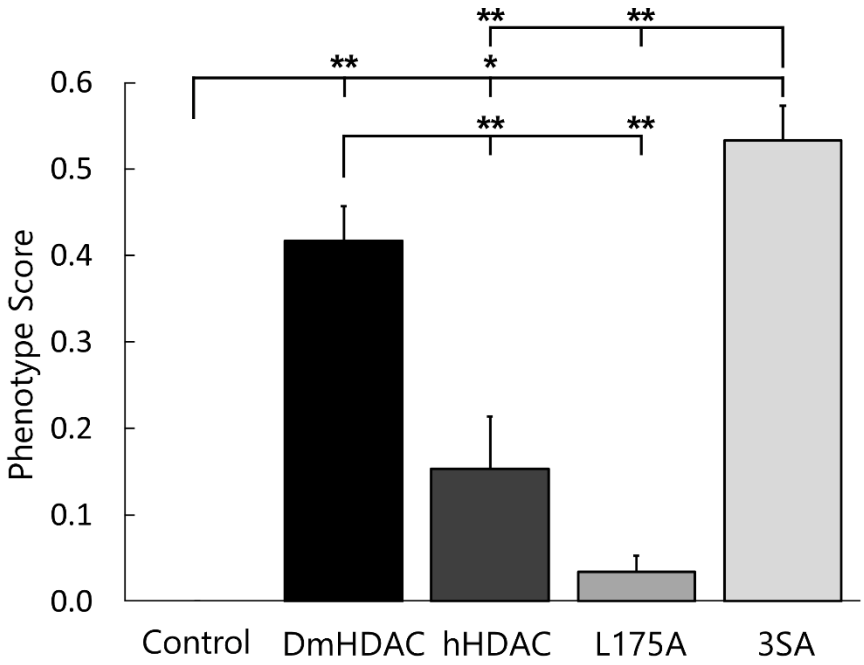

Figure 3.9 Averaged phenotype scores of the elav x HDACv F1 progeny.

The phenotype scores of brains of flies overexpressing each HDACv in comparison to control brains are shown. Bars indicate mean +/- SEM. * = $p < 0.05$, ** = $p < 0.01$ following one-way ANOVA and Tukey's post-hoc significance test. P-Values are: Control:DmHDAC4 = 0.001, Control:hHDAC4 = 0.016, Control:L175A = 0.900, Control:3SA = 0.001, DmHDAC4:hHDAC4 = 0.001, DmHDAC4:L175A = 0.001, DmHDAC4:3SA = 0.092, hHDAC4:L175A = 0.113, hHDAC4:3SA = 0.001, L175A:3SA = 0.001.

These data show that the nuclear accumulation of HDAC4 is a major causative factor in the negative effects caused by an overabundance of HDAC4 as the nuclear accumulated variant leads to a severe developmental phenotype while the cytoplasmically restricted HDAC4 does not significantly alter the phenotype from wild-type (Figure 3.9).

Representative images of the phenotypes observed are shown (Figure 3.10). It was observed during these experiments that overexpression of HDAC4 can down-regulate expression of FASII, potentially one of the pathways through which these disruptions are occurring. To ensure that the phenotypes observed were real and not a misinterpretation caused by the down-regulation of FASII a series of crosses were set including the expression of CD8::GFP, this is a fusion protein in which GFP is fused to a transmembrane glycoprotein that will highlight axons. At least 20 brains were characterised from each genotype and the scores were averaged to provide an overall phenotype score.

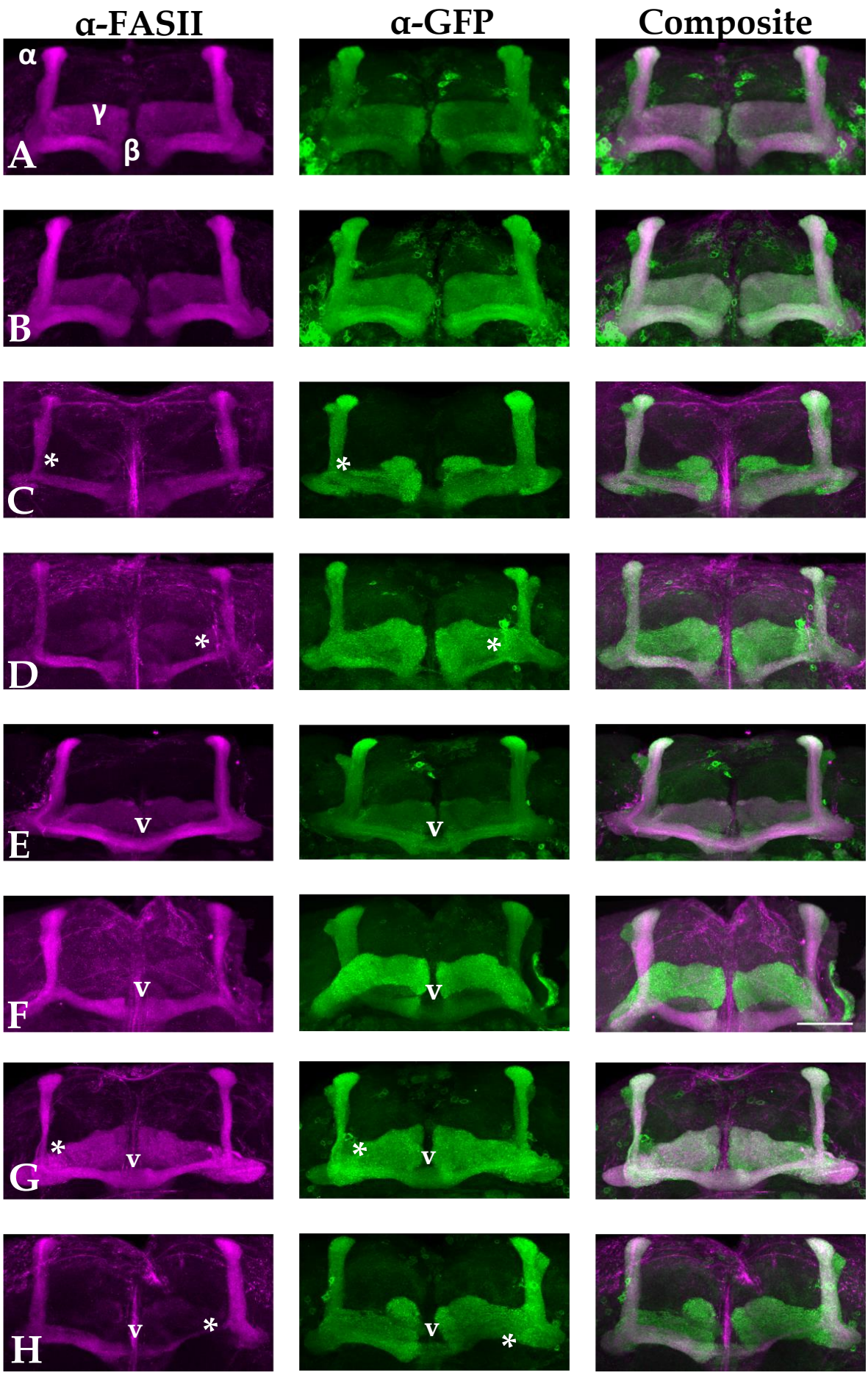
α-FASII
α-GFP
Composite
α
γ
β
A
B
C
D
E
F
G
H
*
v

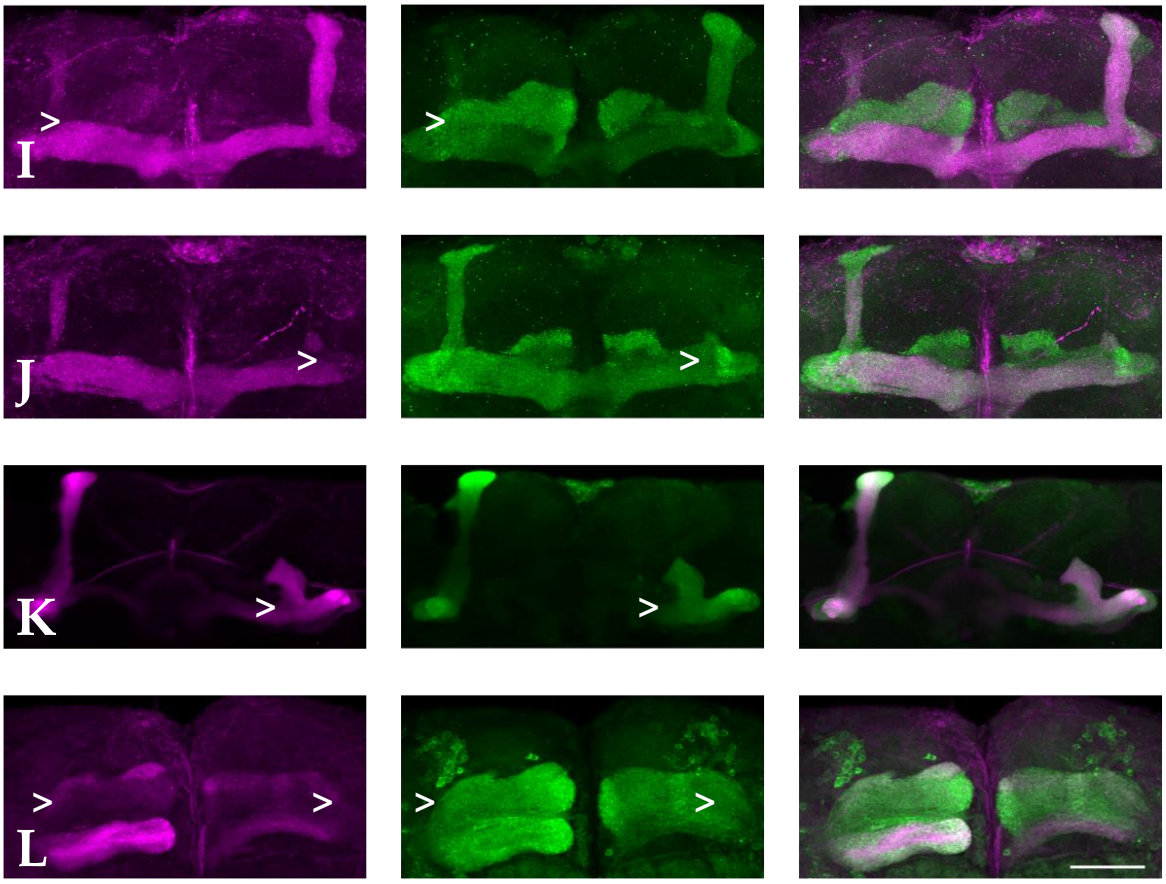

Figure 3.10 Typical phenotypes observed following overexpression of HDAC4v in mushroom bodies.

A & B represent wild-type brains with α and β and γ lobes labelled. C&D show typical mushroom bodies with thinned lobes, predominantly notable in the α-lobes, highlighted by *, note that it is harder to see thinned β-lobes in the GFP channel due to the presence of the γ-lobes. E & F show mushroom bodies in which the β-lobes appear to have fused, due to a lack of axonal termination (denoted by v). G and H show mushroom bodies with both thinned lobes (*) and fused β lobes (v). I and J show brain lacking elongation of one of the α lobes (> shows where the lobe should be). K and L show severely malformed brains missing multiple lobes (either from α or β lobes) (> indicates normal lobe position). Scale bar is 40 μm.

3.3.2 EFFECTS OF ALTERED SUBCELLULAR DISTRIBUTION ON *DROSOPHILA* EYE DEVELOPMENT

To further characterise the role of HDAC4 in neural development each HDACv was overexpressed in the fly eye during development. This was carried out as the eye is a highly sensitive to developmental disruption due to the highly organised ommatidia and bristles that constitute the surface of the eye, allowing for minor phenotypes to be characterised than in the mushroom body. In addition, we had previously characterised the phenotype resulting from overexpression of DmHDAC4 and showed severe disruption to ommatidia patterning and bristle formation. The eye is comprised of approximately 800 ommatidia, each surrounded by secondary and tertiary pigmentation cells and interspersed with bristles. Each ommatidia contains eight photoreceptor cells, four cone cells and two primary pigmentation cells.

Protein expression in the developing eye was driven using the glass multimer reporter (GMR) driver. GMR expresses predominantly in the post-mitotic eye disc and developing photoreceptors during the third instar larval stage (Ray and Lakhotia, 2015). In a control fly in which expression of any exogenous gene was not induced a single copy of the GMR driver resulted in very minor alterations to the phenotype of the eye when raised at 25°C. Previous work in this lab has shown that the rough eye phenotype induced by HDAC4 is specific to HDAC4 as the co-expression of the OE construct and an RNAi line targeted to HDAC4 resulted in a restoration of the wild-type phenotype (Schwartz, 2016). Therefore, the phenotype is a result of HDAC4 expression rather than an effect of the GMR-GAL4. Gross morphological and pigmentation changes were visualised using light microscopy (Section 2.2.1) and minor changes in ommatidia and bristle patterning were visualised with scanning electron microscopy (Section 2.2.2), (Figure 3.11).

Overexpression of DmHDAC4 resulted in a moderate rough eye phenotype with irregular ommatidia (unusual shapes and occasionally fused ommatidia) and bristle distribution (multiple bristles sprouting from one pore, unevenly spaced

bristles). The expression of the human HDAC4 did not severely alter the eye development, causing very occasional mis-regulation of the bristle patterning, breaking from the regular pattern of every other corner of an ommatidia. A similarly mild phenotype was observed when the cytoplasmically restricted L175A mutant was expressed. The nuclear mutant, 3SA, resulted in severe developmental disruption with fusing of many ommatidia and poorly patterned bristle distribution, a more severe phenotype than that observed in the DmHDAC4 OE model. Furthermore, it was noted that double homozygotes of the GMR driver and the UAS-3SA construct resulted in no viable offspring, emphasising the extent of the developmental disruption caused by nuclear accumulation of HDAC4.

The observed phenotypes suggest that, as in the mushroom body developmental assay, the increased nuclear HDAC4 resulted in severely disrupted development, causing fused ommatidia and multiple bristles growing from individual pores, while increased cytoplasmic HDAC4 caused no discernible disruption.

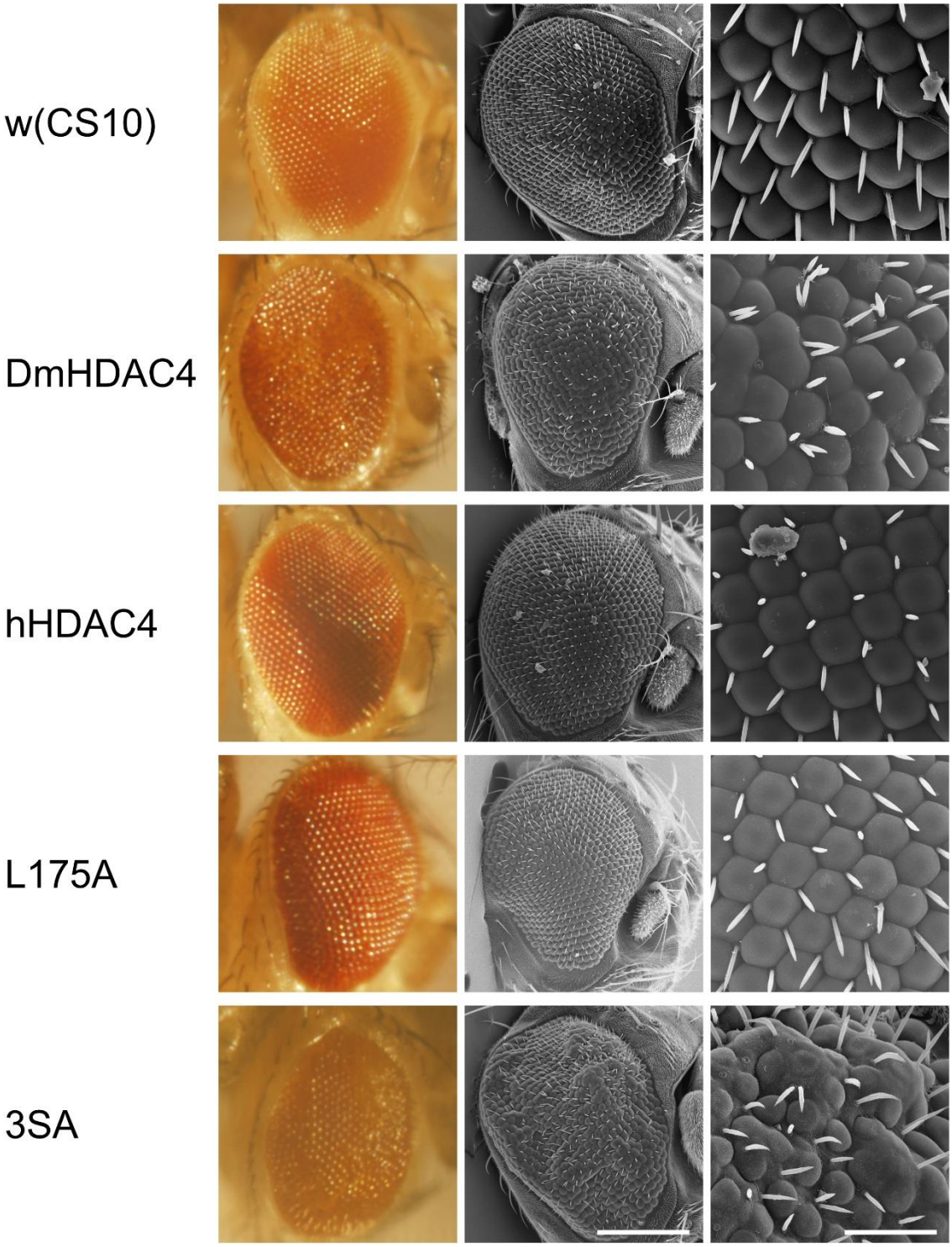

Figure 3.11 Light and scanning electron microscopy images of *Drosophila* eyes.

The genotype of each sample is listed on the left. Images presented are (left to right) 110x magnification light microscopy, 250x magnification SEM, 1500x magnification SEM. Scale bars are 200 μm and 30 μm in the middle and right-hand columns respectively.

3.4 Discussion

Previously, it has been shown in mice that HDAC4-null mice have impaired brain development caused by altered skull formation due to skeletal deformations (Vega *et al.*, 2004). Subsequently, it was determined that brain-specific conditional knockout of HDAC4 (that avoids the skeletal defects) has a minimal effect on brain development but impairs spatial memory (Kim *et al.*, 2012). The role of an overabundance of HDAC4 has not been investigated thoroughly in mouse brain development but recent studies have shown that increased nuclear abundance of HDAC4 alters neuron growth through regulation of vascular endothelial growth factor D (Litke *et al.*, 2018) and the nuclear accumulation of HDAC4 has been implicated in neurotoxicity in Parkinson's disease models in mice (Wu *et al.*, 2017). Thus, it can be assumed that HDAC4 has a role in cell-survival and development but, in mammals, is not required for the normal development of gross morphology of the brain.

Initially, it was shown that DmHDAC4 has a distribution that is mostly cytoplasmic but with some nuclear presence, the wt-hHDAC4 and L175A were largely cytoplasmic and the hHDAC4-3SA was abundantly nuclear but still retained a cytoplasmic presence. It was seen through the developmental assays that the overexpression of DmHDAC4 disrupts normal neuron development yet human HDAC4 had a minimal effect on mushroom body development. Furthermore, wild-type human HDAC4 had no effect on eye development and neither did L175A. However, the 3SA-hHDAC4 that exhibits high nuclear presence (Section 3.2.2) caused the most severe mushroom body development defects, with 29% missing one or more lobes entirely. This severity of disruption was also observed in the eye phenotype in which 3SA lead to a greater disruption of the ommatidia than DmHDAC4.

Typically, stocks are established as homozygotes with two copies of a construct and, for assays such as the eye screen, two copies of the driver as well. However, a further example of the disruption caused by the 3SA variant was observed in this instance as flies homozygous for both the GMR-driver and the 3SA construct

are non-viable. Given current research, it is presumed that this is due to exogenous expression of 3SA by the GMR driver Ray and Lahkotia (2015), who identified GAL4 driven expression in the larval spiracles or breathing tubes. As the hHDAC4 3SA mutant had severe effects on all other structures investigated it is not unreasonable to assume that this expression in the larval spiracles reduced the ability of the larvae to breathe, leading to their death through suffocation.

Taken together, these results indicate that the negative developmental effects observed when HDAC4 is overexpressed are predominantly due to an overabundance of HDAC4 in the nucleus, an observation that is supported by research highlighting the role of nuclear accumulated HDAC4 in development (Morris *et al.*, 2012; Sando *et al.*, 2012). The data also suggests that an overabundance of cytoplasmic HDAC4 does not exert an effect in development, possibly indicating that the cytoplasmic shuttling of HDAC4 is predominantly to remove it from the nucleus and prevent it regulating transcription.

4 Investigating the role of altered HDAC4 subcellular distribution on long-term memory

4.1 Courtship suppression assay

Overexpression of HDAC4 has been shown to impair long-term memory in mice (Sando *et al.*, 2012). Additionally, it has been shown that the nuclear export of HDAC4 in an activity-dependent fashion, in that synaptic activation of a neuron leads to the phosphorylation of the three, key serine residues, leading to association with the 14-3-3 chaperone protein and subsequent nuclear export (McKinsey *et al.*, 2001). This data suggested that nuclear HDAC4 is responsible for the repression of memory and it was subsequently shown by Sando *et al.*, that a nuclear accumulating variant of HDAC4 caused severe repression of spatial memory in mice (Sando *et al.*, 2012).

Previous work has been carried out in our lab establishing that the overexpression and knockdown of DmHDAC4 have a negative impact on long-term memory, suggesting that DmHDAC4 plays an essential role in learning and memory but requires a delicate balance of its activity (Fitzsimons *et al.*, 2013). With this in mind, it is logical to assume that altered subcellular distribution of HDAC4 will influence memory in *Drosophila*. It is yet unclear if these repressive effects of overabundant HDAC4 on memory are due to the increased nuclear abundance of HDAC4 or the cytoplasmic depletion of HDAC4. If the latter, it is possible that an increased cytoplasmic abundance of HDAC4 will lead to improved memory formation.

Investigating the subcellular distribution of HDAC4 in the fly allows the use of the genetic tools particular to *Drosophila*. Through the use of the UAS-GAL4 system, the expression of the HDACv can be restricted to the mushroom body by expressing GAL4 using the OK107 driver which expresses strongly in each of the mushroom body lobes (Aso *et al.*, 2009). Additionally the TARGET system (Section 1.3.2) will be used to prevent expression during development (McGuire

et al., 2004), allowing investigation of the role of altered HDAC4 subcellular distribution in the adult brain, independent of developmental effects.

To assay the effect of overexpression of HDACv on long-term memory the courtship suppression assay was utilised. As described in section 2.14 the courtship suppression assay takes advantage of the natural behaviour of male flies which, when exposed to an unreceptive female will reduce the frequency of their attempts at courtship. The female indicates unreceptiveness through a suite of behaviours, in addition to altered pheromone secretion. This reduction in courtship attempts is a measurable behaviour that, after extended training periods, is retained for up to 7 days (Keleman *et al.*, 2007; Griffith and Ejima, 2009; Ejima and Griffith, 2011). This behaviour change can be compared to males exposed to the same conditions but without exposure to non-receptive females before testing, to measure this the first 10 minutes of exposure to mated females is recorded and the proportion of time spent courting was noted with the tester blind to the genotype of the flies.

The naïve courtship index is calculated by averaging the proportion of time spent courting by the untrained flies, using this the memory index can be calculated by comparing the courtship index of the trained flies to the averaged courtship index of the naïve flies. This memory index provides an approximate measure of how well the flies recall their training from the day before with a memory index of 1 indicating perfect memory (complete reduction of courtship attempts in the testing period) and a memory index of 0 indicating no memory (the male fly spends the 10 minutes courting, regardless of refusal). A wild-type fly in normal conditions will typically exhibit a memory index of 0.4 – 0.6, spending an average of 40-60% of the testing period attempting to court the female fly.

4.2 *Drosophila* and human HDAC4 in long-term memory

In order to assess the impact of HDAC4 overexpression on LTM, each UAS-HDACv was crossed to Tub GAL80^{ts}; OK107-GAL4 flies and the progeny were raised at 18°C. Three days prior to the assay, male flies were shifted to 30°C incubation to induce expression of the constructs prior to being used in the courtship suppression assay. Naïve males were subjected to the courtship suppression assay. Initially, DmHDAC4 and hHDAC4 were compared.

The total dataset for each courtship assay was arcsine transformed to normalise the distribution and analysed using a one-way ANOVA followed by Tukey's post-hoc analysis to determine significant differences between genotypes.

As the courtship suppression assay relies on normal courtship behaviour, it was important to confirm that the expression of the constructs was not altering basal courtship behaviour. Thus, the proportion of time that naïve males spent attempting to court was recorded to validate the model (Figure 4.1). This showed that the fly lines expressing DmHDAC4 and hHDAC4 did not have significantly altered courtship behaviour. Having confirmed this, the memory indices for each group were compared (Figure 4.2) and it was observed that expression of both hHDAC4 and DmHDAC4 resulted in impaired LTM in comparison to the OK107-driver only control. This reinforced the understanding that hHDAC4 was functional in the *Drosophila* system and, subsequently, the effects of expression of the L175A and 3SA variants were tested.

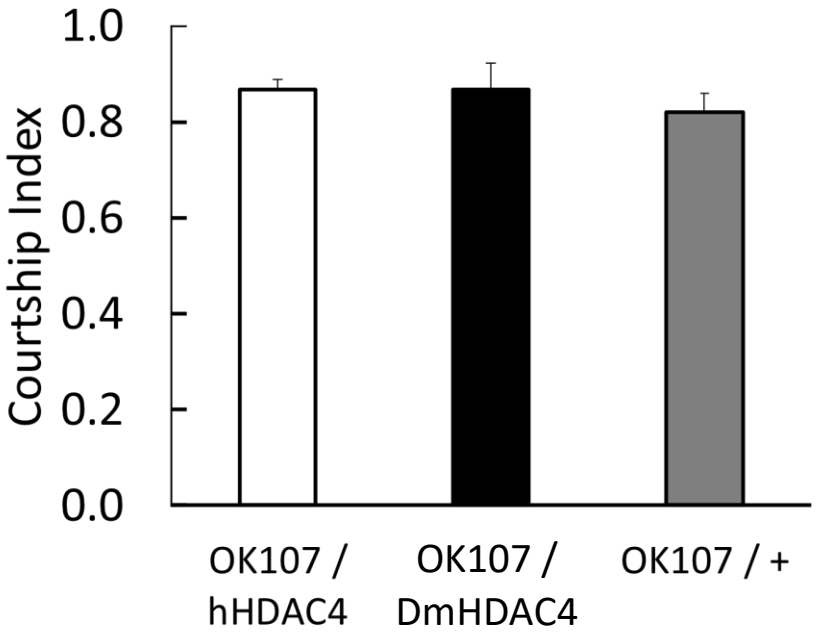

Figure 4.1 Courtship indices of flies tested in behaviour analysis.
The courtship index is the proportion of time naïve male flies spend trying to court females during the testing period, a wild-type naïve fly will have a courtship index of 0.8-0.9, indicating 80-90% of the testing period is spent courting the female. Bars represent mean courtship index ±SEM. (N > 25 per sample).

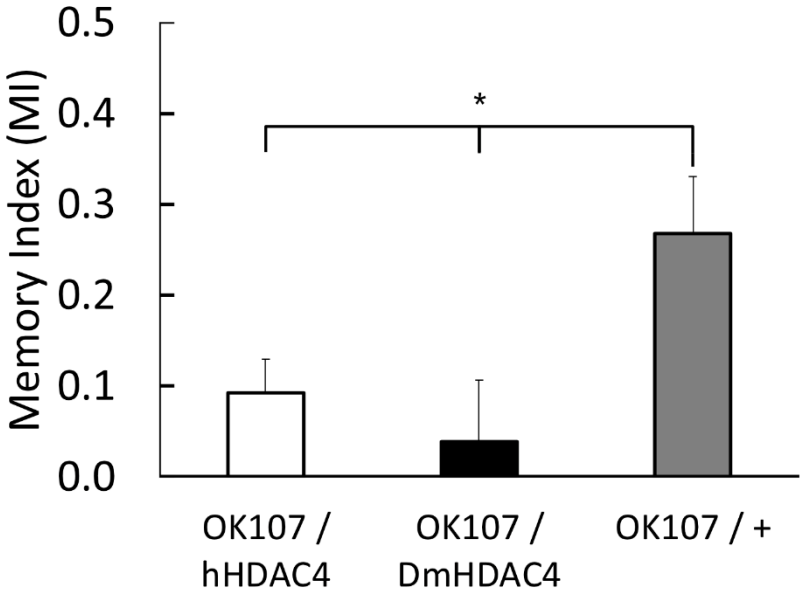

Figure 4.2 Memory indices of flies expressing hHDAC4 and DmHDAC4.
The overexpressed hHDAC4 and DmHDAC4 both impair memory, reducing the memory index to <0.1 compared to the driver-only control. Bars indicate mean ±SEM. N = >20, * = $p < 0.05$ between treatments, one-way ANOVA followed by Tukey's post-hoc significance test. P-values are hHDAC4 : OK107 / + = 0.028, DmHDAC4 : OK107 / + = 0.040, hHDAC4 : DmHDAC4 = 0.800.

4.3 Nuclear and cytoplasmic hHDAC4 in long-term memory

Once more, the effects of construct expression were tested to ensure normal courtship behaviour was not altered by expression of 3SA and L175A. It was confirmed that the expression of the two constructs did not significantly alter courtship attempts by naïve males (Figure 4.3).

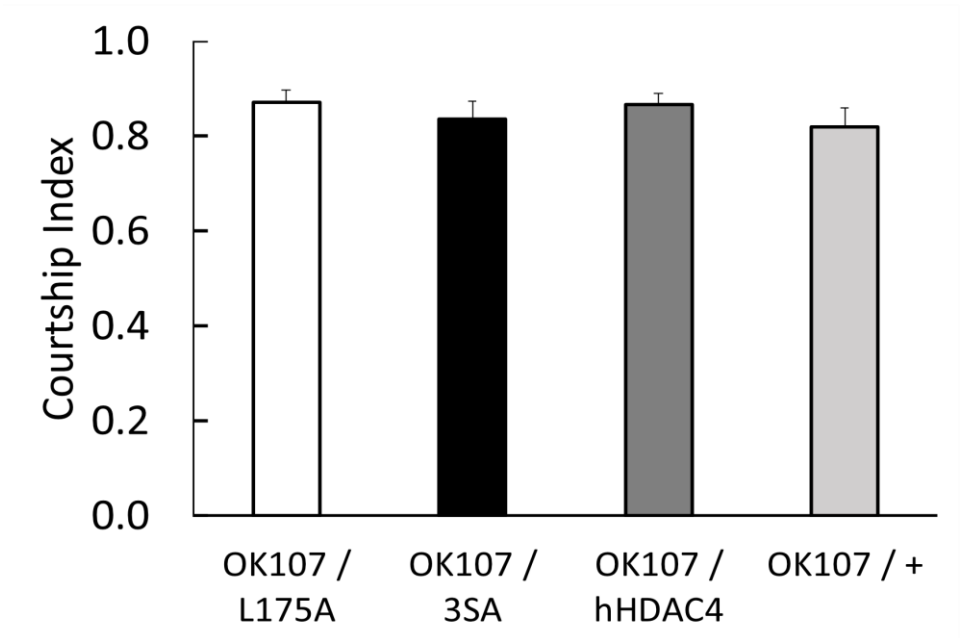

Figure 4.3 Courtship indices of flies expressing hHDACv.
The overexpressed 3SA, L175A and hHDAC4 proteins did not appear to significantly alter base courtship behaviour with courtship indices around 0.85 compared to the control line of 0.81. Bars represent mean memory index ±SEM, N = 25 per group.

Subsequently, memory indices of flies expressing hHDAC4, 3SA and L175A were compared to a control line harbouring only the driver line (Figure 4.4).This data shows that the increased nuclear abundance of hHDAC4-3SA in *Drosophila* mushroom bodies greatly impairs memory performance while the cytoplasmically restricted hHDAC4-L175A does not appear to significantly affect memory. This suggests that the negative effects of HDAC4 overexpression observed in previous work are largely due to an overabundance of nuclear HDAC4.

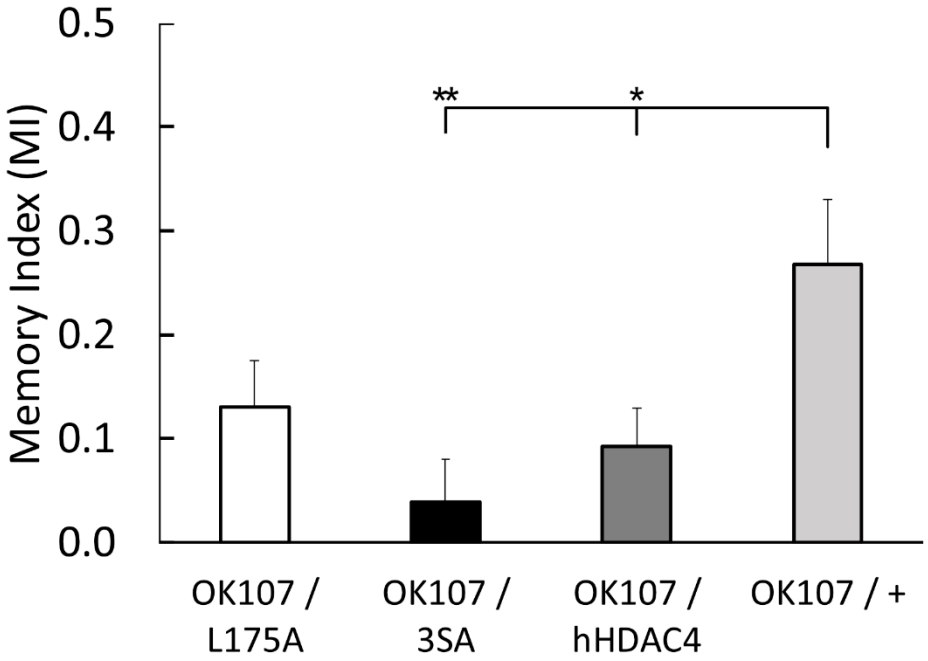

Figure 4.4 Memory indices of flies expressing hHDACv.

hHDAC4-3SA significantly impairs memory compared to driver-only control, as does hHDAC4-wt. However, hHDAC4-L175A does not. Bars represent mean memory index ±SEM. N = 25, * = $p < 0.05$, ** = $p < 0.01$ between treatments, one-way ANOVA followed by Tukey's post-hoc significance test. P-values compared to control are as follows, L175A:OK107/+ = 0.215, 3SA:OK107/+ = 0.009, hHDAC4:OK107/+ = 0.027.

4.4 Discussion

Having shown that increased nuclear HDAC4 is detrimental to neuronal development, the effects of altered subcellular distribution on learning and memory were subsequently investigated using the courtship suppression assay. Comparing flies overexpressing the DmHDAC4 and hHDAC4 exclusively in the adult mushroom body showed that expression of either the hHDAC4 or the DmHDAC4 significantly reduced the male fly's ability to form long-term memory. Subsequent performance testing of the nuclear and cytoplasmic variants showed that 3SA greatly impairing LTM function in adult *Drosophila.* This showed that the hHDAC4 construct is active in memory function but that it is the nuclear accumulation that correlates with impaired memory performance. The L175A construct appeared to disrupt learning somewhat but was not significantly different to controls, suggesting that nuclear HDAC4 is the main causative factor in disruptions to learning and memory when it is overexpressed in the brain.

This data supports the results from the developmental assays in Section 3, in which increased nuclear abundance of HDAC4 caused greater disruption to development and further supports studies (Sando *et al.*, 2012) showing that nuclear, not cytoplasmic HDAC4 impairs long-term memory formation in male *Drosophila*. On a physiological level, the memory impairment could be caused through dysregulated trimming of dendrites, a process key to forming robust memories (Bourne and Harris, 2011). This could be through the disruption of the same pathways that lead to cytoskeletal disruption that causes developmental disorders observed earlier (Section 3).

The means through which HDAC4 is acting to affect memory and development are not certain but several candidates are known in the literature. It was recently shown in our lab that HDAC4 interacts with Ubc9, the E2-enzyme of SUMOylation machinery to affect memory in *Drosophila* (Schwartz *et al.*, 2016). HDAC4 has been previously indicated to interact with the SUMOylation machinery and, as a method of transiently altering protein stability and binding,

SUMOylation has been proposed as a method of modifying learning and memory in a rapidly inducible and reversible manner (Gregoire and Yang, 2005; Craig and Henley, 2012; Loriol *et al.*, 2013; Chen *et al.*, 2014).

Alternatively, it has previously been suggested that the neuronal depolarisation induced nuclear export of HDAC4 limits its ability to bind to an repress the activity of MEF2, permitting the expression of genes required for LTM formation (Flavell *et al.*, 2006). Another possibility is that HDAC4 acts through modulation of CREB. It has recently been shown that nuclear accumulation of HDAC4 corresponds with inactivation of CREB following isofluorane exposure (Sen and Sen, 2016). This is not the first time that it has been proposed that CREB is modified by HDAC4 and, indeed, due to CREB's key role in memory, this makes it a prime candidate for further investigation (Silva *et al.*, 1998; Kassis *et al.*, 2016).

Thus, the potential repression of known transcription factors MEF2 and CREB by nuclear HDAC4 will be investigated as both are expressed in the fly mushroom body.

5 HDAC4 AND TRANSCRIPTIONAL REGULATORS

HDAC4 has been identified as a transcriptional regulator acts in the nucleus through the repression of other transcriptional regulators such as MEF2 (Miska *et al.*, 1999) and CREB (Sen and Sen, 2016). MEF2 has been identified as having a role in memory formation in addition to regulating dendrite growth and synaptic proliferation (Flavell *et al.*, 2006; Cole *et al.*, 2012). Furthermore, CREB has previously been shown to be key in memory formation (Tully *et al.*, 1994; Hirano *et al.*, 2016). It has been shown in our lab that MEF2 is expressed highly in the Kenyon cells but its role in brain development and memory in *Drosophila* has not been investigated. CREB is also expressed in the mushroom body and has been shown to be essential for long-term memory in *Drosophila* (Yin *et al.*, 1994; Hirano *et al.*, 2016) and has recently been shown to interact genetically with HDAC4 during development (Schwartz, 2016). Therefore, it is also a potential candidate for regulation by HDAC4. Subsequently, it was decided to investigate these proteins for possible interactions with HDAC4 in the *Drosophila* brain.

5.1 Co-localisation of HDAC4 and MEF2

5.1.1 A SECOND NOTE ON COLOUR SCHEMES

Earlier (Section 3.2.1) a section was given over to discussing some of the measures an author may take to make their paper more reader-friendly to a wider audience, specifically regarding colour images and individuals with difficulty perceiving the full spectrum of colour. In this previous chapter it was shown that instead of using red as a false-colour counterstain, magenta could be used to enable sufferers of protanopia to distinguish different channels in confocal images. However, this raises difficulties when attempting to highlight three distinct components of the sample as the magenta equally occupies the blue and red channels, using green leaves a very limited palette from which to select to show co-localised tags.

As this project moved on to attempt to provide evidence of the co-localisation (or lack thereof) of proteins relative to the nucleus of the cell it was deemed necessary

to find a colour scheme that would permit the viewing of three distinct components. Following guidelines proposed by Okabe and Ito (2002), a colour scheme using magenta, orange and blue was used for all triple-channel figures and this colour scheme was maintained throughout the rest of the images to provide consistency. This colour scheme, while significantly different to most observed in current literature, allows sufferers of protanopia and, to a lesser extent, sufferers of deuteranopia and tritanopia to distinguish between channels in the composite image (Figure 5.1).

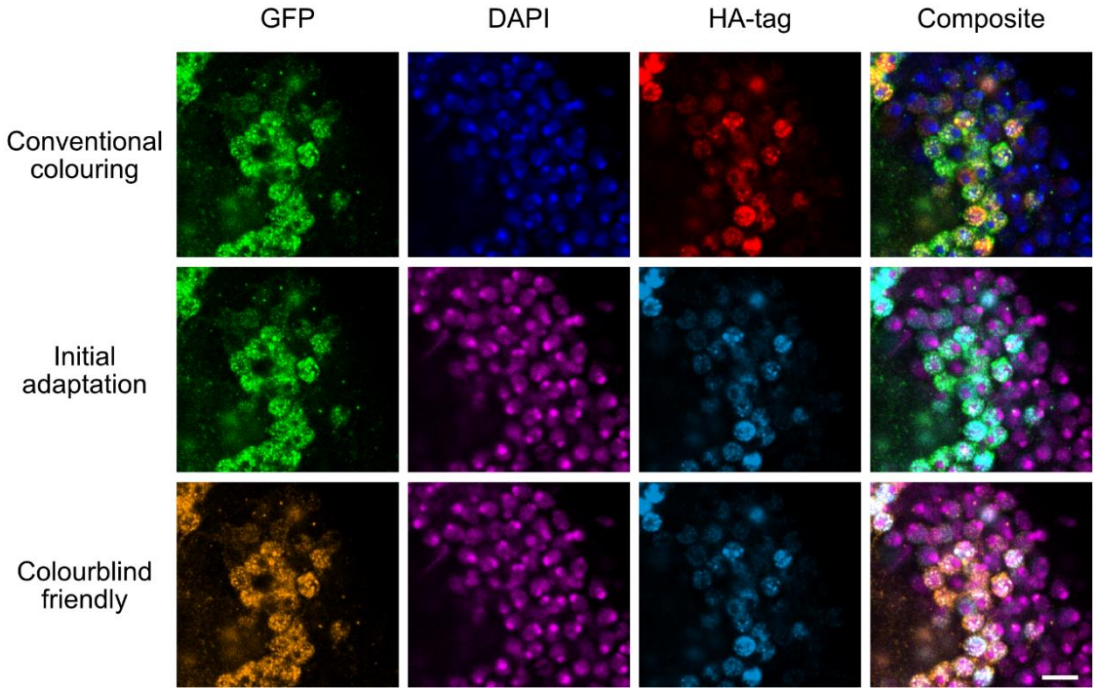

Figure 5.1 Confocal microscopy images with a single slice of the Kenyon cell bodies of the mushroom body.

Whole brains expressing GFP-tagged hHDAC4 – 3SA and HA-tagged MEF2 were stained with their appropriate antibodies and counterstained with DAPI to highlight the nucleus of the cell. The top row presents the traditional red, green, and blue colour scheme for image colourisation with a merge of all three channels on the right. The bottom row shows the same figures but altered to magenta, orange and sky-blue, again with the merge on the far right. The colour combination in the bottom row shows co-localisation of the 3 different components with high accuracy while also being colour-blind friendly, particularly to sufferers of protanopia. Scale bar is 5 μm.

5.2 Co-localisation of HDAC4 and MEF2 in the brain

MEF2 has been previously shown to co-localise in nuclear puncta formed by DmHDAC4 in the fly brain (Fitzsimons *et al.*, 2013). In addition to this, HDAC4 has been proposed to act through the repression of MEF2, potentially acting through MEF2 regulation to alter learning and memory (Sando *et al.*, 2012). To this end, it was decided to investigate if the co-localisation could also be observed in the nuclear-accumulating mutant, 3SA.

Fly-lines harbouring the GFP::HDACv and an HA-tagged DmMEF2 were generated and crossed with a fly line harbouring the OK107-GAL4 driver and Tubulin-GAL80^{ts}, as was done in the initial subcellular distribution study (Section 3.2). The progeny were dissected (Section 2.3), probed with α-GFP and α-HA antibodies and imaged (Section 2.3.1), (Figure 5.2, 5.3).

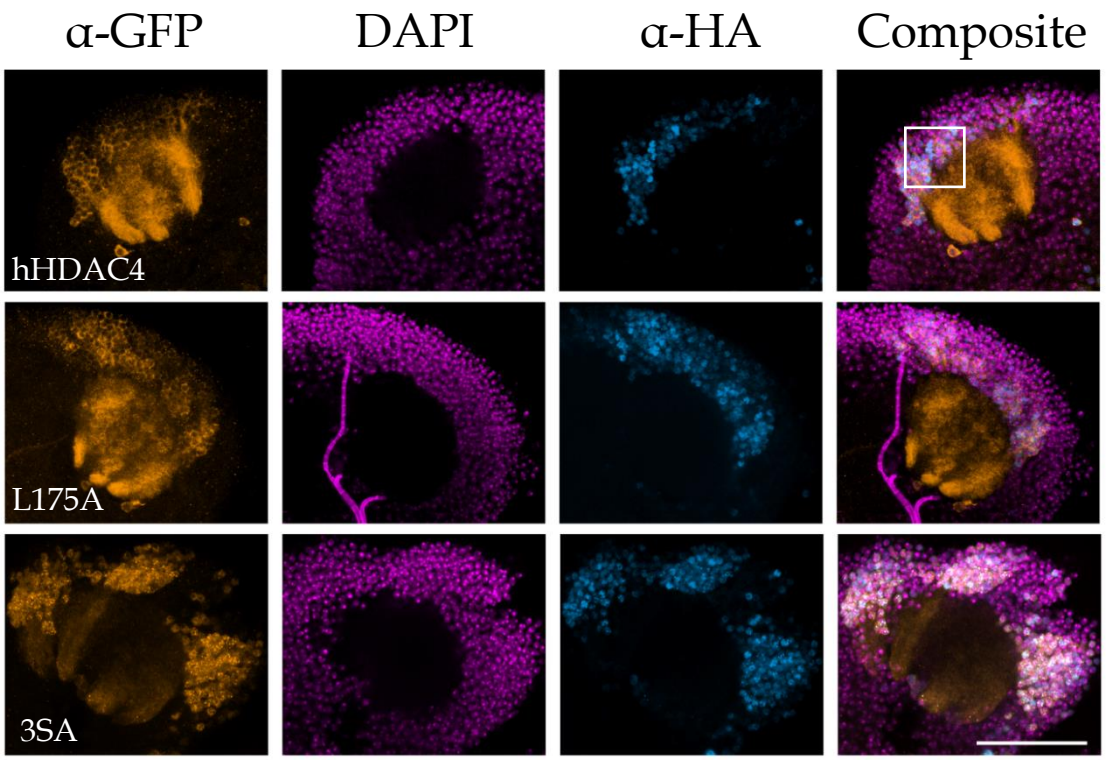

Figure 5.2 Confocal images of hHDAC4 variants and MEF2.
Multiple stacks of whole calyces of MB. Immunohistochemistry on whole mount brains was carried out with α-GFP (orange); DAPI (magenta); and α-HA. Highlighted box is shown in Figure 5.3. Scale bar is 40 μm.

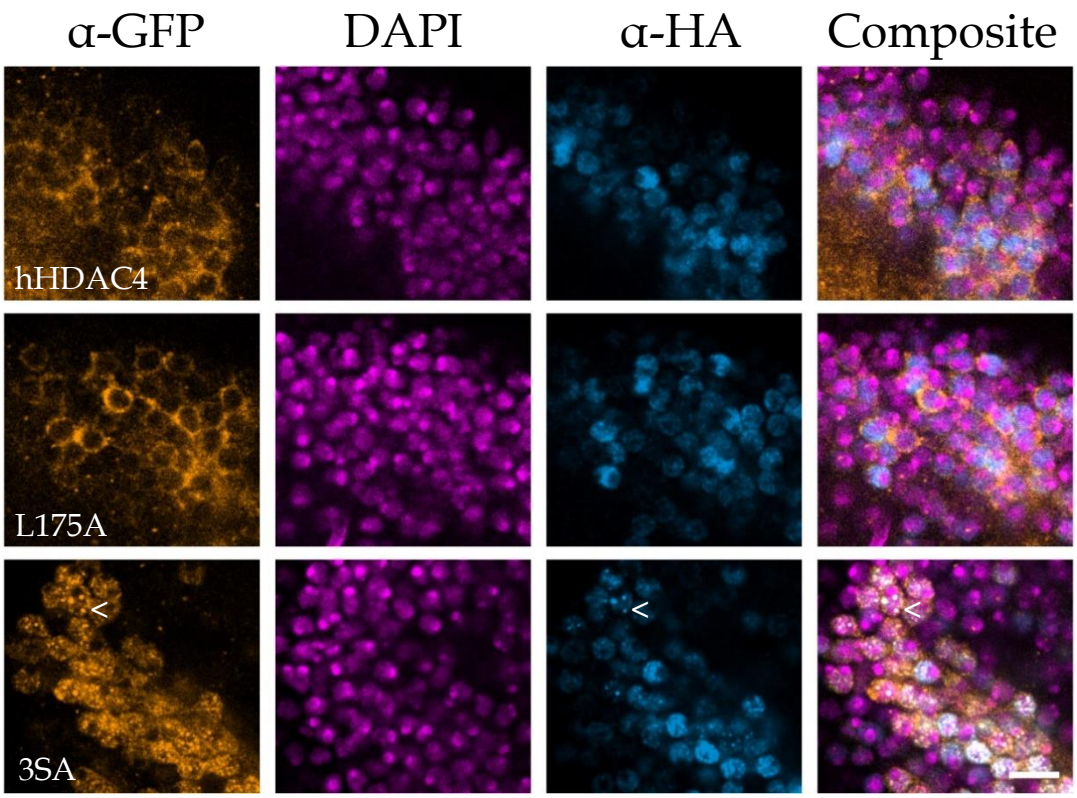

Figure 5.3 Confocal images of hHDAC4 variants and MEF2.
Single slice of magnified portion of KC bodies. Immunohistochemistry on whole-mount brains was carried out with α-GFP (orange); DAPI (magenta); and α-HA. Note nuclear puncta in 3SA sample co-localising with HA-tagged MEF2 (<). Scale bar is 4 μm.

The images from these brains show that the same overlap has been observed between MEF2 and DmHDAC4 was observed with MEF2 and the hHDAC4-3SA mutant with nuclear puncta of MEF2 co-localising with puncta of 3SA in the nucleus. This suggests that the mechanism through which DmHDAC4 and MEF2 co-distribute in the Kenyon cells is conserved between DmHDAC4 and hHDAC4. No co-localisation was seen between either the wt-hHDAC4 and MEF2 or the hHDAC4-L175A which are largely cytoplasmic. This data provides further evidence that HDAC4 acts through regulation of MEF2.

5.3 Effects of altered abundance of MEF2 on *Drosophila* mushroom body development

Both the behaviour and the courtship suppression assays suggest that the negative effects of HDAC4 overexpression are due to the nuclear accumulation of HDAC4 and potentially its regulation of other transcription factors. Following this, it was decided to investigate the role of MEF2 in mushroom body development as this transcription regulator has previously been highlighted as a potential target of HDAC4 activity. Furthermore, DmHDAC4 and MEF2 have been shown to interact genetically in a rough eye screen, indicating they act in the same molecular pathway during eye development (Schwartz, 2016).

Overexpression and knockdown (using a previously verified RNAi) (Schwartz, 2016) of MEF2, as well as expression of a constitutively active MEF2-VP16 (Made by Helen Fitzsimons) construct driven by the pan-neuronal driver elav was carried out in the brain of developing flies to assay the effects of altered abundance of MEF2 in brain development.

The MEF2-VP16 construct contains a human MEF2-DNA binding domain fused to the VP16 transactivation domain and has been demonstrated to activate MEF2 *in vitro* (Black *et al.*, 1996; Lam *et al.*, 2010). The severity of defects was assayed as previously described (Section 3.3.1) with the phenotype distribution shown in Table 5.1 and the average scores shown in Figure 5.4. Representative phenotypes shown in Figure 5.5

	Wild-type	**Thin**	**Fused Beta**	**Thin and Fused**	**Single missing lobe**	**Multiple missing lobes**	**Total**
MEF2 OE	58% (13)	25% (6)	0% (0)	0% (0)	13% (3)	4% (1)	23
MEF2 KD	38% (8)	38% (8)	8% (2)	0% (0)	8% (2)	8% (2)	22
MEF2VP16	33% (7)	33% (7)	14% (3)	0% (0)	14% (3)	5% (1)	21

Table 5.1 Phenotype frequency from altered MEF2 during development.
Values indicate percentage of total flies that exhibited this phenotype, raw number shown in brackets to the right.

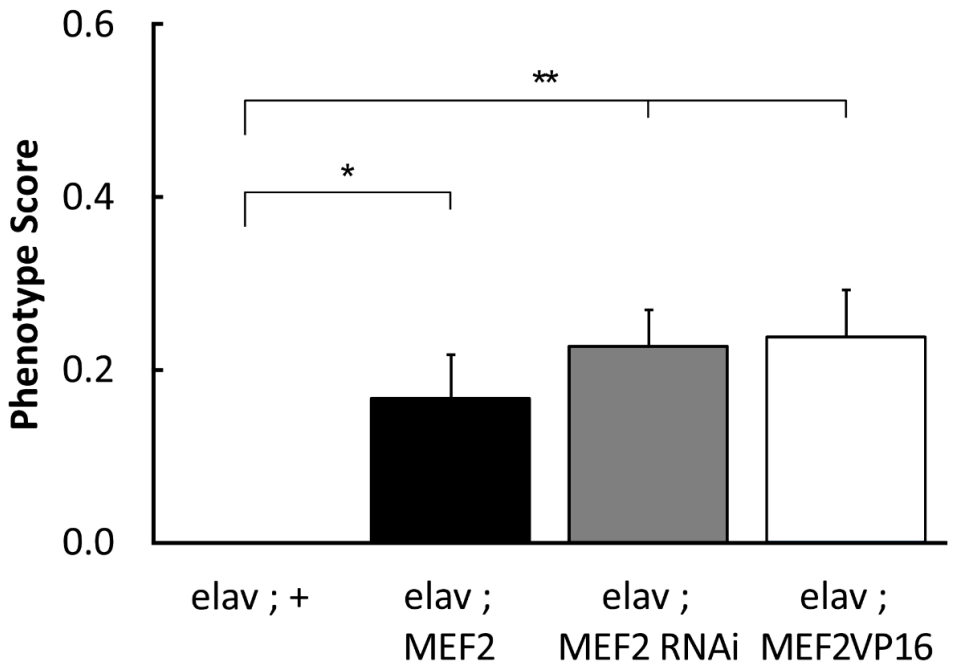

Figure 5.4 Phenotype scores from flies with altered MEF2 activity.
Flies harbouring an elav driver and either control (+), MEF2 OE (MEF2), MEF2 KD (MEF2 RNAi) or a construct with a MEF2-DNA binding domain and a VP16 transactivation domain (MEF2-VP16). Scores are generated as described in 3.4.1. Bars represent mean score ±SEM. * = $p < 0.05$; ** = $p < 0.01$, as calculated by one-way ANOVA and post-hoc Tukey's significance test. N > 20 for each genotype. P-values comparing samples to controls are MEF2OE:Control = 0.031, MEF2KD:Control = 0.002, MEF2VP16:Control = 0.001.

The resulting data shows that the severity of developmental phenotypes is mild compared to those observed in HDAC4 but still reflective of MEF2 being required for normal brain development as the knock-down of MEF2 resulted in developmental defects. This supports the hypothesis that HDAC4 regulates MEF2, as the overexpression of HDAC4 and the knockdown of MEF2 both cause developmental defects. However, overexpression of MEF2 and expression of a constitutively active MEF2 also resulted in developmental disruption also caused mild defects, suggesting that, similar to HDAC4, MEF2 is required for normal mushroom body development but in controlled amounts.

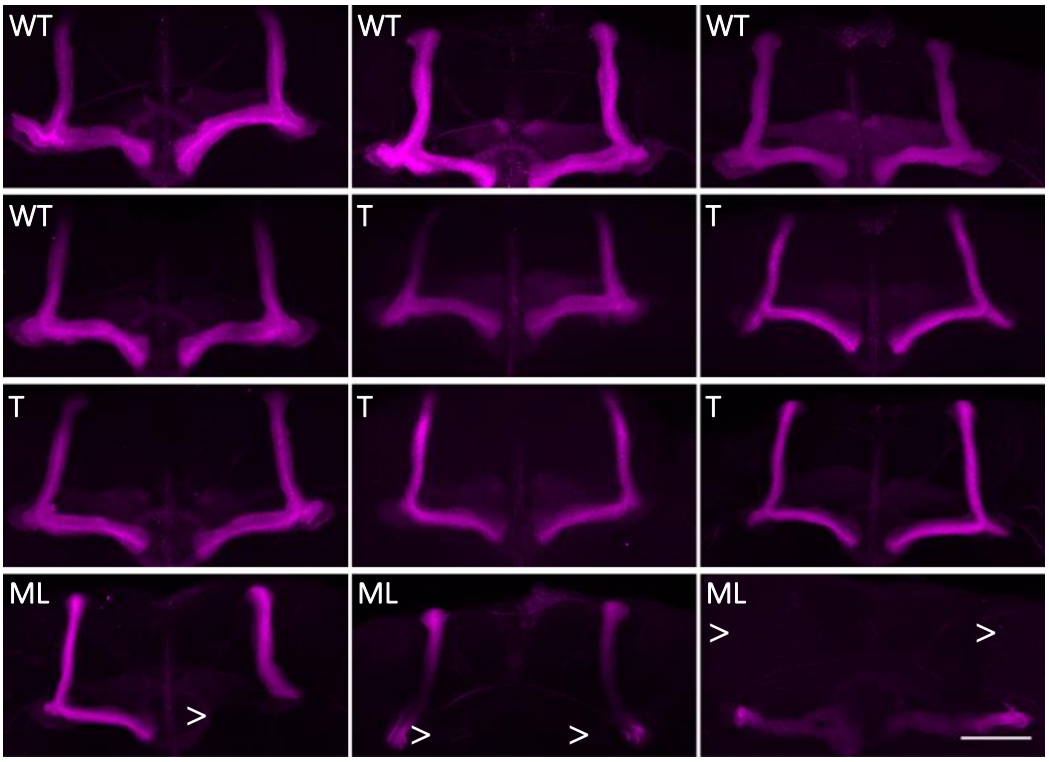

Figure 5.5 Representative phenotypes from altered MEF2 activity in mushroom bodies.

Immunohistochemistry on whole-mount brains using α-FASII antibody. Phenotype labels WT = wild-type, T = thin lobes, ML = missing lobe. Missing mushroom body lobes highlighted with >. Scale bar = 40 μm.

5.4 Investigating the role of MEF2 in memory

It was initially proposed that MEF2 is involved in memory because neuronal depolarisation leads to activation of many MEF2-regulated genes (Chawla *et al.*, 2003) and while studies in mice have shown that MEF2 is involved in spatial and fear memories (Barbosa *et al.*, 2008; Cole *et al.*, 2012), the role of MEF2 in *Drosophila* learning is poorly studied. It has also been proposed that HDAC4 represses MEF2 as the neuronal depolarisation induces nuclear export of HDAC4 that correlates with increased activity (Sando *et al.*, 2012) and nuclear HDAC4 has been shown to co-localise with endogenous MEF2 (Fitzsimons *et al.*, 2013). Logically, as increased nuclear abundance of HDAC4 represses memory the knockdown of MEF2 should mimic this and similarly impair the ability of *Drosophila* to learn. To determine this, female flies harbouring the OK107-GAL4 driver and the Tubulin-GAL80^{ts} construct were crossed with male flies harbouring either the UAS-DmMEF2-myc or UAS-MEF2-RNAi, the male progeny were then trained and their memory tested using the courtship suppression assay (Section 2.15). Once more, the baseline courtship index was measured to ensure that the MEF2 overexpression and knockdown constructs were not interfering with courtship behaviour (Figure 5.6).

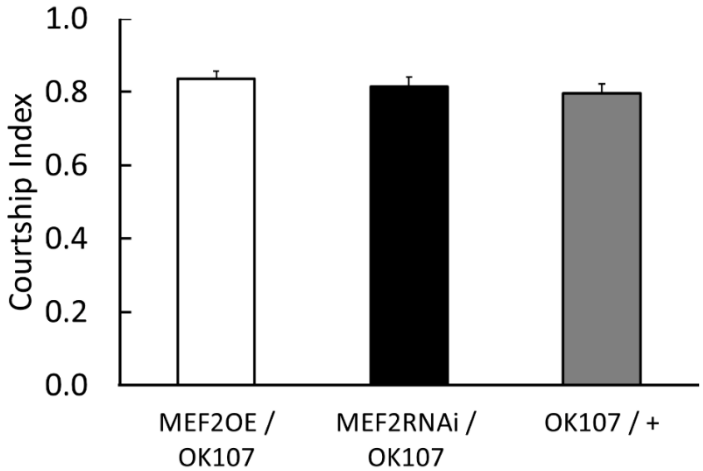

Figure 5.6 Courtship indices of flies with altered MEF2 activity.
Courtship indices showing courtship activity of male *Drosophila.* Bars indicate mean MI ±SEM.

Having determined that the courtship indices were unchanged from the driver-only control, LTM was tested. The results from this were unexpected given the

current paradigm; knockdown of MEF2 did not significantly impair memory when compared to a driver-only or construct only control (Figure 5.7) whereas the overexpression of MEF2 did impair long-term memory (Figure 5.8). This data suggests that in *Drosophila* HDAC4's impairment of memory is not through the repression of MEF2 directly. However, the nuclear co-localisation suggests that an interaction may be occurring between HDAC4 and MEF2 and that HDAC4 may be activating MEF2 rather than repressing it.

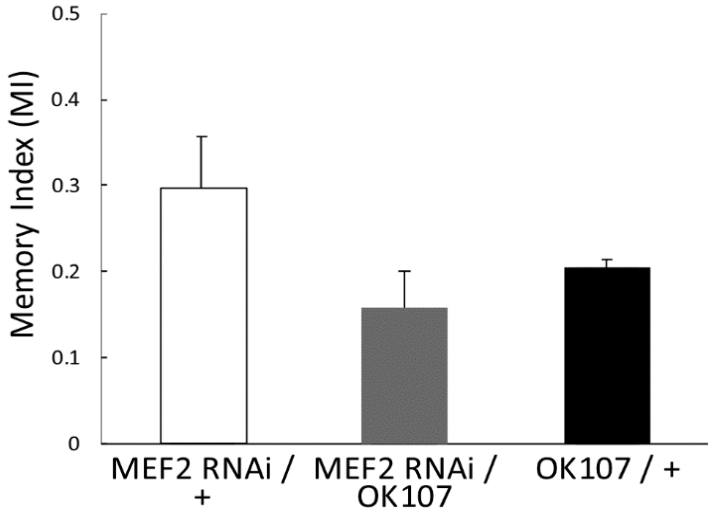

Figure 5.7 Memory indices of MEF2 KD flies and controls.
Memory indices from MEF2KD flies and controls giving an indication of the learning ability of male *Drosophila.* Bars indicate mean MI ±SEM. N > 50 for each genotype. P-Values are RNAi/+ : RNAi/OK107 = 0.119, RNAi/OK107 : OK107/+ = 0.897.

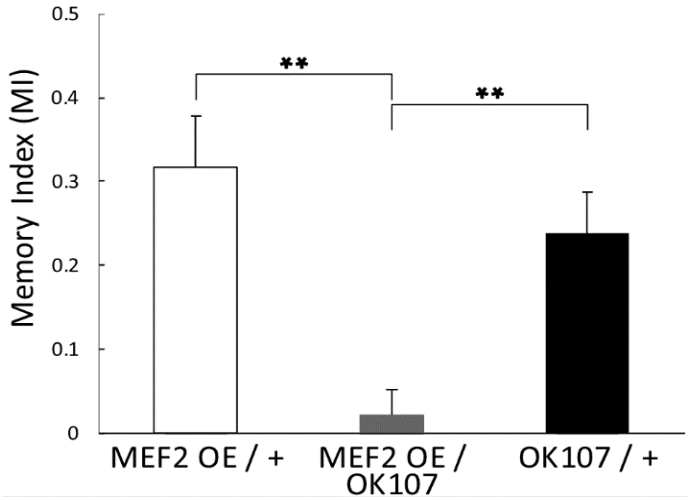

Figure 5.8 Memory indices of MEF2 OE flies and controls.
Memory indices from MEF2OE flies and driver or construct only controls indicating the memory performance of male *Drosophila.* Bars indicate mean MI ±SEM. ** = p > 0.01 using one-way ANOVA followed by Tukey's post-hoc significance test. N > 50 for each genotype. P-Values are MEF2/+ : MEF2/OK107 = 0.001. MEF2/OK107 : OK107/+ = 0.001.

5.5 Investigating a potential HDAC4-MEF2 interaction

It was previously determined that MEF2 is highly expressed in the mushroom body and that, when HDAC4 is overexpressed, MEF2 redistributes into DmHDAC4-containing punctate foci, suggesting they may physically interact (Fitzsimons *et al.*, 2013), this co-localisation was also shown to occur with hHDAC4-3SA. Alongside the investigation of MEF2 activity in *Drosophila* neuronal development and memory, the putative regulation of MEF2 by HDAC4 was also investigated. To measure the activity of MEF2 *in vivo* and subsequently characterise the effects of nuclear HDAC4 on MEF2 it was decided to use a luciferase reporter assay.

To investigate this, a fly line in which luciferase expression is induced in response to increased MEF2 activity was generated. This line harbours the firefly luciferase gene downstream of a MEF2 response element (MRE) and a minimal TATA-containing promoter. The MRE consists of three MEF2 recognition sequences, to which the DNA binding domain of MEF2 binds (Figure 5.9). As a control, a ΔMRE construct was also generated that harbours the same sequence but with mutations of three adenines to guanines, so it is unable to be bound by MEF2. Both constructs were generated by Helen Fitzsimons and transgenic flies were generated by GenetiVision (Texas, USA).

3xMRE 5′ TGT **TAC TAA AAA TAG** AAT GT**T ACT AAA AAT AG**A ATG T**TA CTA AAA ATA G**AA 3′

3xΔMRE 5′ TGT **TAC TAA GGG TAG** AAT GT**T ACT AAG GGT AG**A ATG T**TA CTA AGG GTA G**AA 3′

Figure 5.9 Sequences of the 3xMRE and 3xΔMRE DNA.
MEF2 response elements (MRE) are in bold and the altered sequence between the two sections is underlined.

To facilitate expression of a transgene such as MEF2 or HDAC4 in combination with MRE or ΔMRE-luciferase, the pan-neuronal elav-GAL4 driver was recombined into the same fly lines via standard crosses (Section 2.1.2). Elav-GAL4; MRE-luc and elav-GAL4; ΔMRE-luc females were crossed to UAS-

DmMEF2 males and the heads of progeny were processed for luciferase activity (Sections 2.13.1, 2.13.3) However, no luciferase assay was detected (Figure 5.10) suggesting that the MRE-luc cassette was unresponsive.

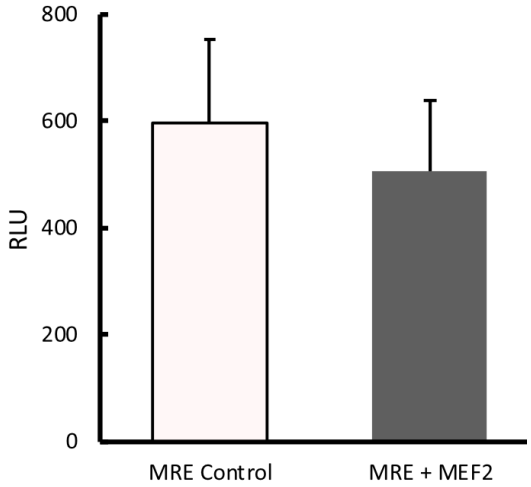

Figure 5.10 Initial testing of MRE-luciferase construct in flies.
In experiments where a consistent number of heads were lysed in reporter lysis buffer, MEF2 failed to induce greater expression than elav-MRE x CS (MRE Control). Bars represent mean Relative Luminescence Units (RLU) ±SEM. Experiment repeated in triplicate. N > 30 fly heads for each sample.

The MRE-luc cassette and UAS-DmMef2 constructs had both been confirmed via sequencing, therefore to determine whether the lack of induction was due to an issue with the UAS-DMEF2 construct or the cassette itself flies were generated in which a constitutively active MEF2-VP16 (described in Section 5.3) was expressed by the elav-driver (Figure 5.11).

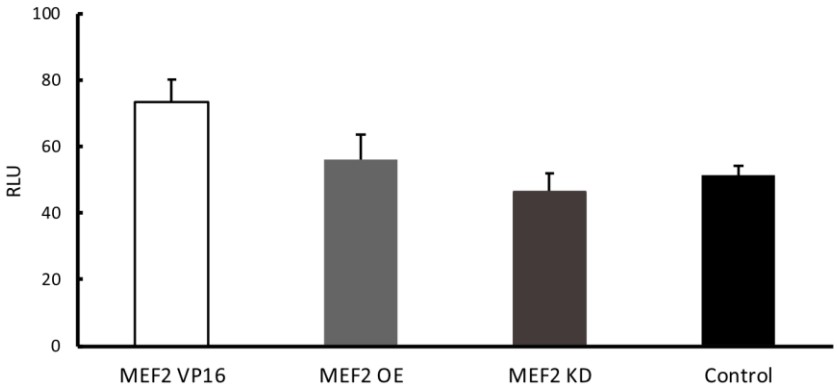

Figure 5.11 Luciferase activity in *Drosophila* heads expressing MEF2-related constructs.

Whole head lysate from flies harbouring MRE-luciferase and elav-driven construct. Bars represent mean RLU ±SEM. Results from duplicate experiments in which N > 30 fly heads per sample.

The MEF2-VP16 construct was unable to significantly induce MRE expression in flies, indeed, normal RLU readings are > 2 orders of magnitude greater than what was observed.

To further examine the integrity of the construct, it was transfected into a human cell line along with the MEF2-VP16 construct under control of the human CMV promoter (Section 2.9). The cells were processed an analysed for luciferase assay (Sections 2.13.2, 2.13.3). The resulting data showed that the MEF2-VP16 construct activated luciferase transcription, which confirmed that the MRE was able to be induced (Figure 5.12). Therefore, it was concluded that the MRE construct was functional in MCF7 but not *Drosophila.* It was reasoned that the minimal promoter, which consisted of a synthetic TATA box derived from the Strategene cre-luc plasmid, might be inactive in *Drosophila* and that it should be replaced with a *Drosophila* minimal promoter.

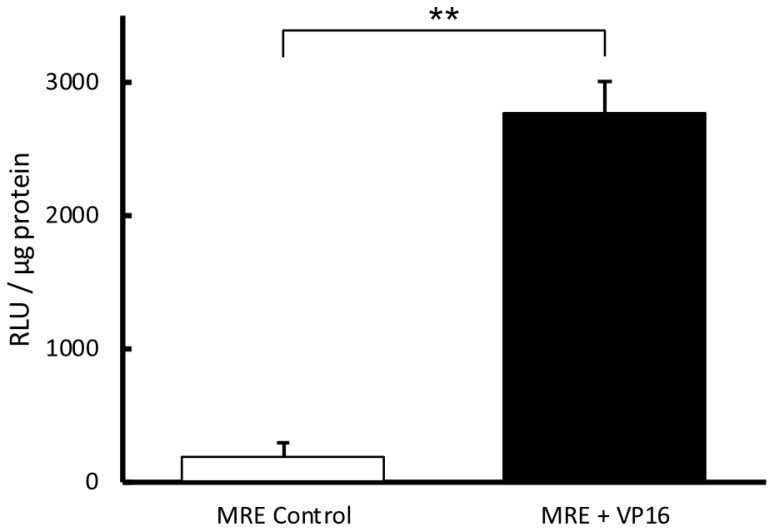

Figure 5.12 Initial testing of MRE-luciferase in human MCF7 cells.
MCF7 cells were transfected with the MRE-luc plasmid and either an empty vector as DNA loading control (Control) or MEF2-VP16 (VP16). Luminescence was measured and normalised to protein extracted from the cells. ** = $p < 0.01$, student's t-test. Bars represent mean RLU/µg protein ±SEM. Experiment repeated in triplicate with three transfections per repeat.

The *Drosophila* hsp70 minimal promoter was inserted in place of the minimal TATA in both MRE-luc and ΔMRE-luc (named hsp70MRE-luc and hsp70ΔMRE-luc) (Appendix 4). The plasmids were transfected into MCF7 cells with CMV-MEF2-VP16 and it was confirmed that the new hsp70MRE-luc was inducible by MEF2-VP16 and did not activate the ΔMRE, confirming specificity of activation (Figure 5.13). However, the hsp70MRE was not able to be activated using DmMEF2 in MCF7 cells (Figure 5.14).

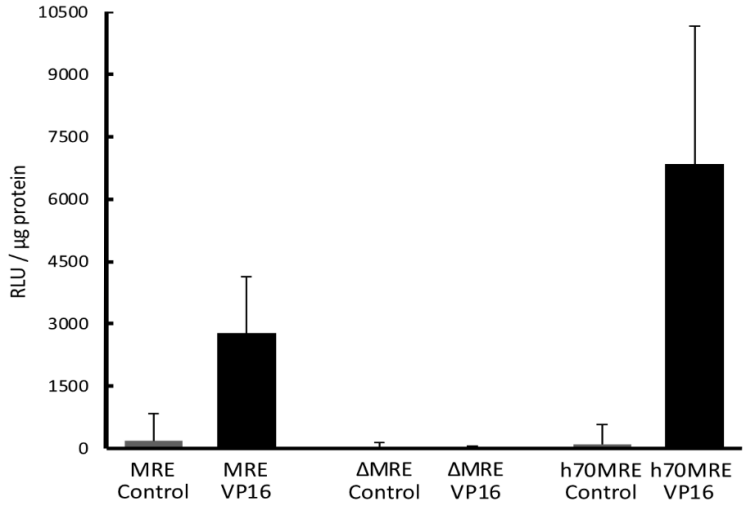

Figure 5.13 Comparing the original MRE-luciferase to the hspMRE-luciferase in MCF7 cells.

Normalised to the total protein, the hsp70-MRE-luciferase construct (h70MRE) exhibited much higher activation by the MEF2-VP16 (VP16) construct than was observed in the original MRE construct. Control indicates empty vector as DNA loading control. N = 3 for each pairing. Bars represent mean RLU/µg protein ±SEM.

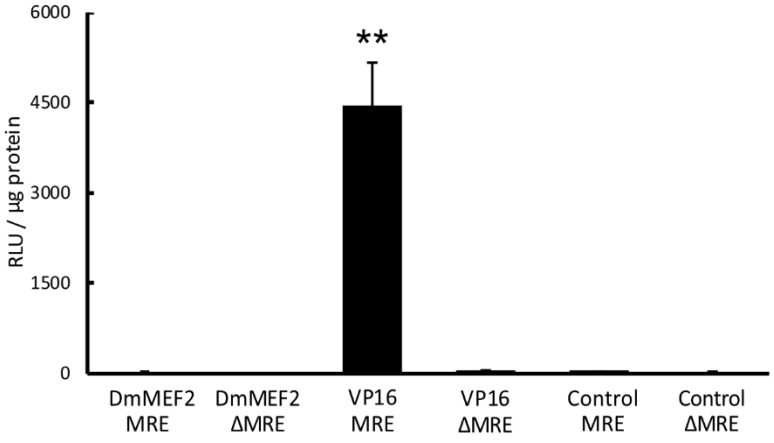

Figure 5.14 Activation of the MRE-luciferase in MCF7 cells.

Normalised to the total protein, it was determined that the hsp70MRE could not be activated to a measurable level by co-transfection of the *Drosophila* MEF2. Control indicates empty vector used as DNA loading control. N= 9 for each pair. ** indicates $p < 0.01$ from other samples, one-way ANOVA with post-hoc Tukey's HSD. Bars represent mean RLU/µg

New transgenic fly lines were generated by GenetiVision. These harboured the new hsp70MRE and hsp70ΔMRE constructs that were shown to work in tissue culture and had the same genetic background as the previously used fly line. These were recombined with elav-GAL4 fly lines to make flies homozygous for

both the elav-driver and the hsp70MRE-luciferase (or the hsp70ΔMRE luciferase). Luciferase assays on lysates from adult fly heads in which MEF2-VP16 was expressed resulted in robust induction of luciferase, confirming that MREhsp70-luc is functional in the *Drosophila* brain (Figure 5.15).

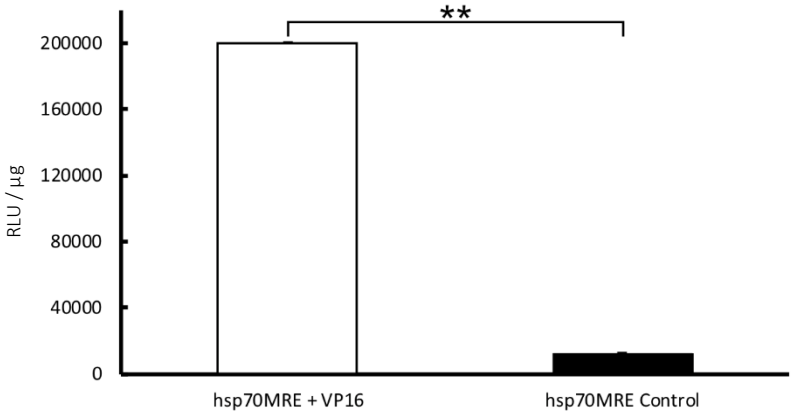

Figure 5.15 MEF2-VP16 activation of hsp70MRE-luciferase in *Drosophila*.
Drosophila harbouring elav; hsp70MRE-luciferase were crossed with either Canton S (Control) flies or flies harbouring a MEF2-VP16 under UAS control. The progeny were processed and the resulting luciferase activity was tested. Experiment was duplicated with each duplicate using > 20 fly heads. ** = $p < 0.01$, student's t-test. Bars represent mean RLU ±SEM.

Subsequently, the ability of MEF2 to activate the construct in *Drosophila* was investigated. However, heads overexpressing MEF2 showed no more luciferase activity than was observed in control samples (Figure 5.16), suggesting that under basal conditions in the adult brain, DmMEF2 appears to be minimally active.

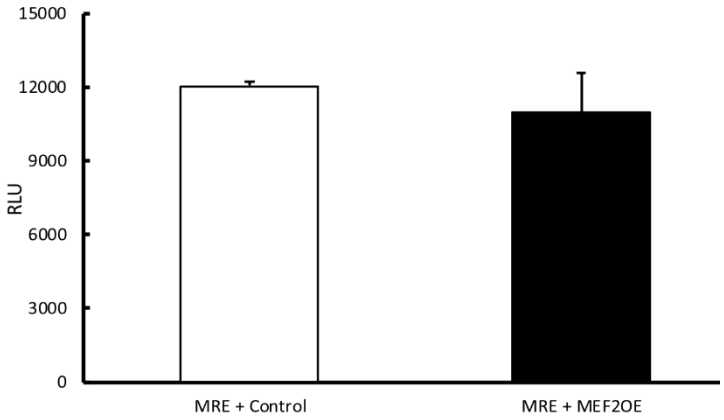

Figure 5.16 Activation of MRE-luciferase by DmMEF2 in *Drosophila*.
Drosophila harbouring elav; hsp70MRE-luciferase were crossed with either Canton S (Control) flies or flies harbouring a MEF2 construct under UAS control. The progeny were processed and the resulting luciferase activity was tested. Experiment was carried out in triplicate using extract from > 20 fly heads in each experiment. Bars represent mean RLU/µg protein ±SEM.

Having determined that MCF7 cells were not a suitable cell-type for DmMEF2-induced activation of the MRE-luciferase, further investigating was carried out in cultured HeLa cells. However, these also failed to show activation of the MRE-luc by either DmMEF2 and mouse MEF2 (MmMEF2) (Figure 5.17).

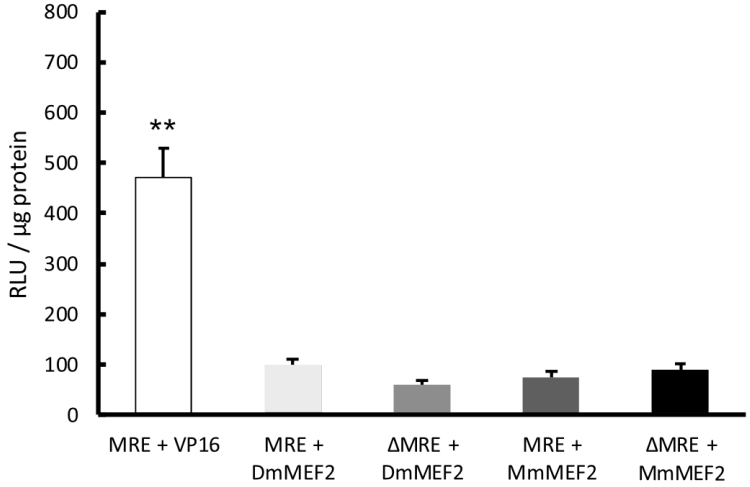

Figure 5.17 Activation of the MRE-luciferase in HeLa cells.
Total protein from HeLa cells lysed with reporter lysis buffer. Bars represent mean RLU/ µg protein ±SEM. N = 9 for each sample. ** = $p < 0.01$ following one-way ANOVA and Tukey's post-hoc significance test.

This effectively ruled out using tissue culture as a method to investigate the effects of HDAC4 on MEF2 activity as the only reliable activation was through

the MEF2-VP16 construct which does not contain the proposed HDAC4 binding site, therefore it would be unable to be repressed by HDAC4.

In previous research it has been shown that MEF2 is activated by calcium-dependent neuronal activation, as membrane depolarisation and calcium influx leads to MEF2 dephosphorylation via calcineurin resulting in activated MEF2 (Flavell *et al.*, 2006; Shalizi, 2006). On this basis, electrical stimulation of whole flies was carried out, based on techniques derived from olfactory conditioning with the rationale that this would activate MEF2 (Section 2.16). This stimulation induced an approximately four-fold increase in luciferase activity compared to the ΔMRE-luciferase control after 60 minutes (Figure 5.18).

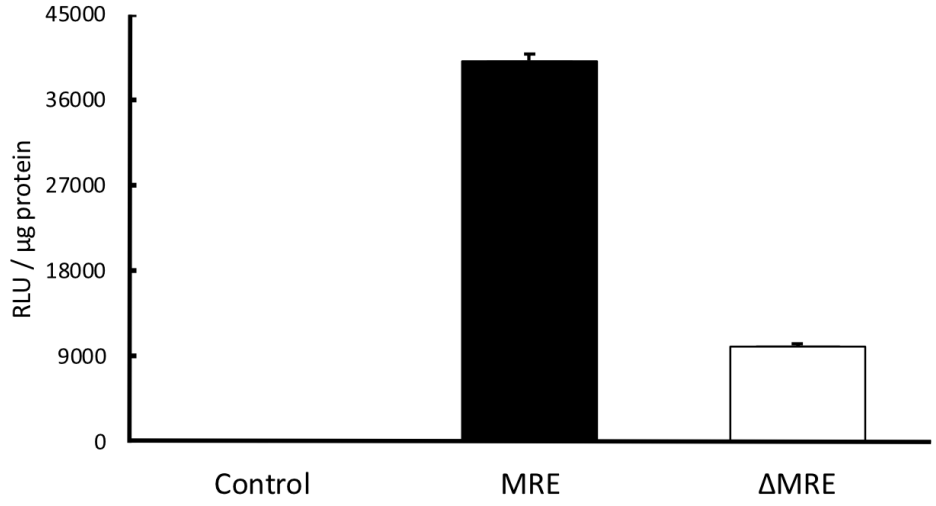

Figure 5.18 Luciferase activity 60 minutes post-electrical stimulation.
Normalised to the total protein, it was observed that inducing whole body neuron activation through electric shock induced MRE activity within 60 minutes after stimulation. Experiment was carried out in triplicate with each run using > 5 whole flies. Bars represent mean RLU/ µg protein ±SEM.

To more precisely control neuronal depolarisation, flies were obtained that carry a UAS-TrpA1 construct. TrpA1 encodes a temperature gated ion channel that initiates neuronal depolarisation above 25°C. Adult flies had TrpA1 activated by submerging a vial of flies into a 46°C water bath for four minutes, as has been carried out in previous work investigating TrpA1 in adult *Drosophila* (Neely *et al.*, 2011), detailed further in Section 2.17.

Lines were generated that each harboured the UAS-TrpA1 construct as well as a UAS-HDACv construct. These were crossed to the elav; MRE-Luc flies and the progeny were heated to induce TrpA1 signalling. Subsets of flies (~15 flies each sample) were taken at several intervals after induction to examine the activation of luciferase by TrpA1 induction over time (Figure 5.19).

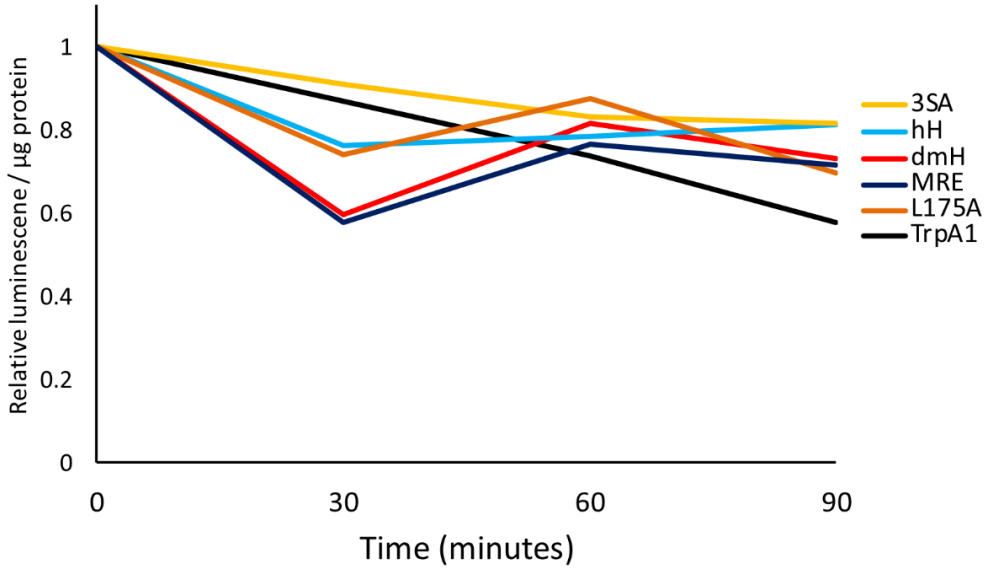

Figure 5.19 Luciferase activity of TrpA1 expressing flies.
Preliminary luciferase data from flies processed following induction of TrpA1 through heating. Fly lines are elav; MRE crossed with: Canton S (MRE, dark blue); TrpA1;L175A (L175A, orange); TrpA1; 3SA (3SA, yellow); TrpA1;hHDAC4 (hH, pale blue); TrpA1; DmHDAC4 (dmH, red); and TrpA1/+ (TrpA1, black). The TrpA1-only flies (black) exhibited a steady downward trend in MRE activation, while all other flies (including the MRE-only control, dark blue) showed a small uptick in MRE activation after 60 minutes. Data is normalised to both the protein in the measured sample and the base MRE-luciferase activity within the line (thus, all start at a value of 1).

The TrpA1 channel appeared functional as after the four-minute incubation, 100% of flies expressing TrpA1 had total body paralysis and were immobile, recovering gradually over the course of 30-60 minutes. A large proportion of the flies harbouring the MRE-luciferase but not expressing TrpA1 were also paralysed by the heat treatment but recovered within less than five minutes of returning to room temperature, suggesting the long-term paralysis was, as expected, due to the TrpA1 activation.

Unexpectedly, it turned out the TrpA1 had a repressive effect on MEF2 activity, as after heating the luciferase activity steadily decreased for the full 90-minutes tested. This was unexpected as it would cause activation of TrpA1 in all neurons and the activation of MEF2 is believed to be up-regulated by neuronal activation (Flavell *et al.*, 2006; Shalizi *et al.*, 2006). The effects of the HDAC4 variant co-expression on luciferase reporter activity were minimal, though the presence of any HDAC4 appeared to increase MEF2-induced activation of the MRE-luciferase. A slight up-tick is observed in most samples at the 60 minute interval but the trend reverts to a decline in luciferase activity following this. This could indicate that there is a spike in MEF2 activity between 60 and 90 minutes that could be enhanced repeated training in future experiments.

Having established that it is unlikely that HDAC4 acts through MEF2 to repress memory in *Drosophila*, another proposed candidate of HDAC4 regulation, CREB, was investigated.

5.6 Characterising CREB activity in cultured human cells

Another mechanism through which HDAC4 could regulate memory is through CREB. CREB activity has been shown to be essential for LTM formation (Perazzona *et al.*, 2004; Tully *et al.*, 1994; Yin *et al.*, 1994) as well as the maintenance of four-day LTM (Hirano *et al.*, 2016). Knockdown of CREB or repression of CREB activity impairs LTM (Dash *et al.*, 1990), which could be the means through which HDAC4 represses memory formation. Recently, it was shown that CREB and HDAC4 interact genetically in the rough eye screen (Schwartz, 2016). Additionally, HDAC4 has been shown to bind to CREB and repress CREB activity in vertebrates (Sen and Sen, 2016). CREB activity could be investigated in the same manner as the MEF2 activity, using a CRE-Luciferase construct (Stratagene, California, USA) co-transfected with various CREB constructs to assay the activity of CREB *in vivo*.

Initially, CREB was used to activate the CRE-luciferase construct in a simple transfection, using the CRE-luciferase co-transfected with empty vector as a control. The activation of CRE-luciferase could be enhanced by co-transfecting CREB with protein kinase A (PKA) that is known to phosphorylate and subsequently activate CREB (Bourne and Harris, 2011).

To investigate the potential interaction between HDAC4 and CREB, wt human HDAC4 (hHDAC4) or the nuclear accumulating 3SA were co-transfected with PKA and CREB was co-transfected with either human-HDAC4 (Figure 5.20). After normalising to co-transfected renilla luminescence to control for transfection efficiency the fold-activation of CRE-luciferase was calculated. This showed that, surprisingly, the nuclear accumulation of HDAC4-3SA increased the activity of CREB compared to the wt-hHDAC4. This suggests that HDAC4-associated memory impairment is not a result of the HDAC4-CREB interaction as increased CREB activity has previously been associated with improved rather than worsened memory function (Suzuki *et al.*, 2011; Serita *et al.*, 2017).

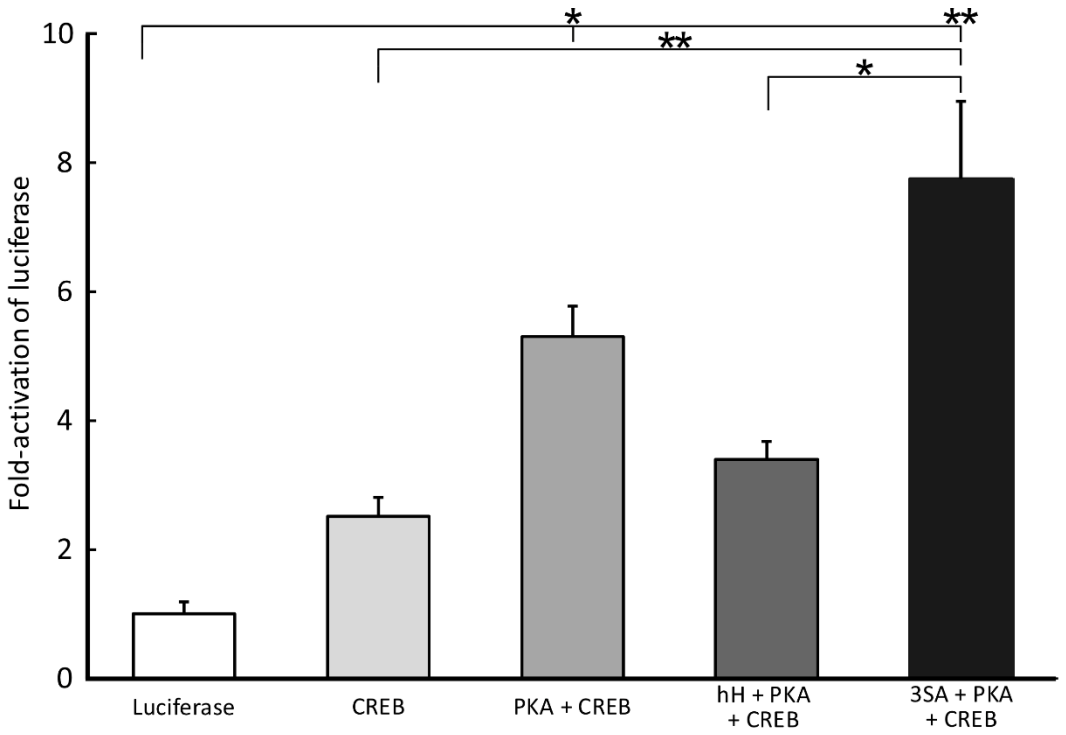

Figure 5.20 Fold-activation of luciferase by CRE in mammalian tissue culture.

* = $p < 0.05$ as determined by one-way ANOVA and Tukey's post-hoc significance test. Luminescence normalised to the basal CRE-luciferase activity. Bars indicate fold-activation of luciferase, normalised to transfection efficiency ±SEM. Experiment carried out in triplicate with three independent transfections per repeat. Significance reported using letter substitutions (A = luciferase, B = CREB, C = PKA + CREB, D = hH + PKA + CREB, E = 3SA + PKA + CREB). P-values are as follows: A : B = 0.848, A : C = 0.041 *, A : D = 0.606, A : E = 0.001 **, B : C = 0.220, B : D = 0.900, B : E = 0.001 **, C : D = 0.676, C : E = 0.216, D : E = 0.029 *.

5.7 Co-localisation of HDAC4 and CREB

Concurrently with the luciferase assays, the co-localisation of CREB and HDAC4 in *Drosophila* Kenyon cells was investigated. It has been previously established in vertebrate models that HDAC4 can bind CREB (Wu *et al.*, 2017), it was subsequently proposed that HDAC4 and CREB may co-localise in the *Drosophila* brain and that physical interaction may be the means through which HDAC4 regulates CREB activity.

Following the same experimental path as the investigation of MEF2, fly lines harbouring both GFP::HDACv and an HA-tagged DmCREB were generated. These were crossed with flies harbouring the OK107-GAL4 driver and Tubulin-GAL80^{ts}, as detailed before. The flies were dissected and probed with an α-GFP, an α-HA antibody, and DAPI before being imaged.

As is seen in Figure 5.21 – 5.23 the overexpression of HDAC4 does not appear to alter the distribution of the HA-tagged CREB in the way it did MEF2 as the distribution of CREB is unchanged between the nuclear and cytoplasmically localising variants of hHDAC4. This data suggests that HDAC4 does not physically interact with CREB in the same way it appears to with MEF2, this could suggest that HDAC4 interacts with CREB through an intermediary.

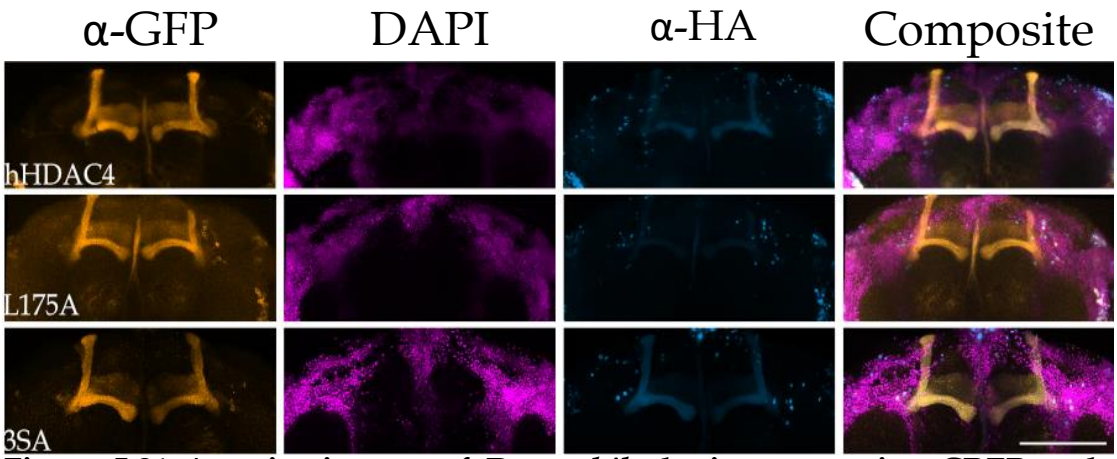

Figure 5.21 Anterior images of *Drosophila* brains expressing CREB and HDAC.

Fly brains co-expressing GFP::hHDACv and DmCREB::HA driven by OK107-GAL4 were stained and visualised using confocal microscopy. Staining is GFP (orange), DAPI (magenta), HA (blue), composite. Images show cytoplasmic presence of CREB in all three samples. Scale bar is 100 μm.

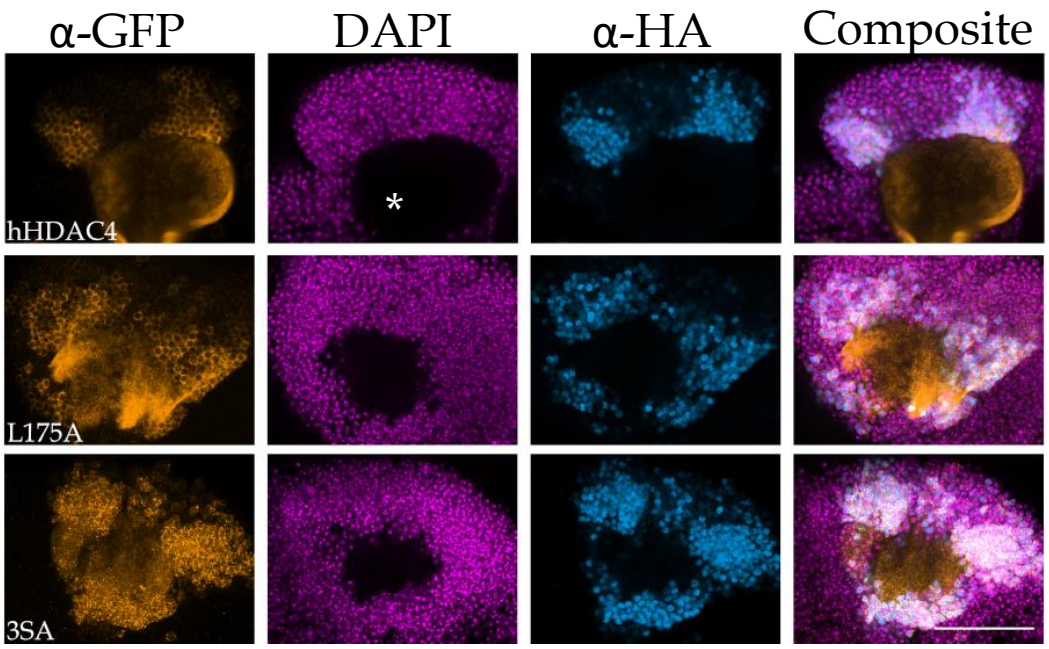

Figure 5.22 *Drosophila* calyces expressing CREB and HDAC4

Immunohistochemistry on whole mount fly brains using anti-GFP (orange), DAPI (magenta) and anti-HA (blue). Calyx is denoted with (*). Scale bar is 40 µm.

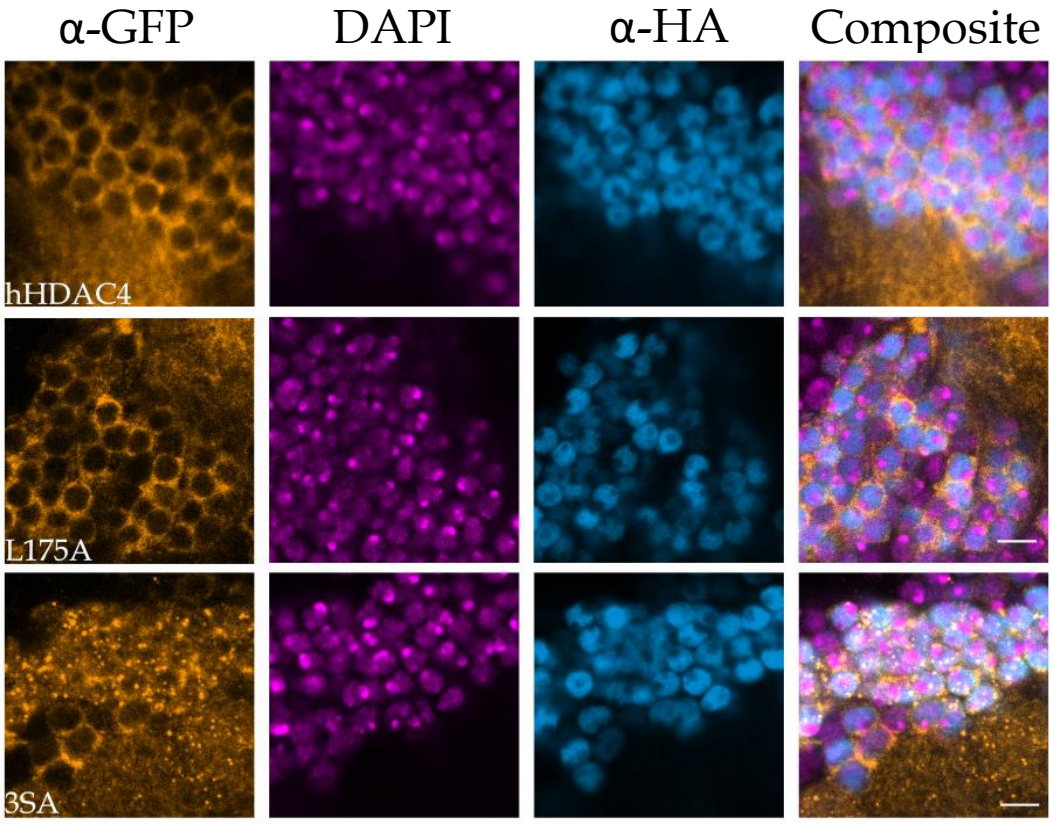

Figure 5.23 *Drosophila* Kenyon cell bodies expressing HDAC4 and CREB.

Immunohistochemistry on whole mount fly brains using anti-GFP (orange), DAPI (oagenta) and anti-HA (blue). Scale bar is 4 µm.

5.8 Discussion

The intent of this investigation was originally to determine both the effect of increased nuclear HDAC4 on MEF2 activity as well as to determine whether MEF2 played a role in *Drosophila* memory and development. The role of MEF2 in mouse learning and memory has been investigated in depth and MEF2 has been shown to be required for synaptic development and playing a complex role in memory, having been shown to both increase and decrease memory when its activity is reduced (Miska *et al.*, 1999; Flavell *et al.*, 2006; Barbosa *et al.*, 2008; Cole *et al.*, 2012) and it has been proposed that MEF2 is regulated by HDAC4 in vertebrates (Sando *et al.*, 2012). Thus, it was proposed that HDAC4 acts through MEF2 to supress memory formation and function in neuronal development.

Using the GFP-tagged HDAC4 variants, co-localisation of HDAC4 and MEF2 in the *Drosophila* brain was investigated. This showed that the nuclear accumulation of hHDAC4 lead to co-localisation of MEF2 with the nuclear puncta of 3SA, supporting the proposed interaction between MEF2 and HDAC4.

Subsequent investigation of both memory and development in flies overexpressing MEF2 or expressing an RNAi targeted to MEF2 showed that MEF2 overexpression impaired memory in *Drosophila*. However, knockdown of MEF2 did not significantly reduce learning when measured through the courtship suppression assay. If nuclear HDAC4 is acting to repress memory formation through MEF2, the knockdown of MEF2 should mimic the effects of increased nuclear HDAC4, thus, it can be proposed that HDAC4-mediation of MEF2 activity is not the prime cause of memory repression caused by increased nuclear HDAC4.

Analysis of mushroom body development using the same overexpression and knockdown lines showed mild disruption to neuronal development with both overexpression and knockdown of MEF2. In both cases, the average phenotype was less severe than those observed when DmHDAC4 or 3SA were expressed during development. This result suggests that MEF2 is required in development

but, much like HDAC4, a tight regulation of the abundance of MEF2 is required. Unlike the memory assay, the development assay does not suggest a lack of interaction between HDAC4 and MEF2. As MEF2 has a role in regulating axonal branching (Alchini *et al.*, 2017), it is probable that the effects of MEF2KD on brain development are reflective of HDAC4's repression of MEF2 activity during development affecting axonal pathing and branching.

Having established that MEF2 has a role in development that could be regulated by HDAC4, it was decided to look into the possible regulation of MEF2 by HDAC4 in *Drosophila*. It was determined that a luciferase reporter activated by a MEF2-response element (MRE) could permit the investigation of HDAC4's regulation of MEF2 (Andrés *et al.*, 1995; Maiti *et al.*, 2008; Kawashima *et al.*, 2009). A lengthy process of investigation and troubleshooting was carried out before it was determined that using the temperature-gated ion channel TrpA1, co-expressed with HDACv in fly lines harbouring the MRE-luciferase would permit the activation of luciferase by MEF2 in a fashion that could be altered by HDAC4. Using the TrpA1 construct it was observed that, while HDAC4 activity altered TrpA1-mediated activity of the MRE-luciferase construct it was not clear whether this was up- or down-regulating MEF2, if it was regulating it at all. This experiment bears repeating in the future, potentially expanding the time-frame over which MEF2 activity is measured.

Combined with the data from learning and memory assays carried out with MEF2 overexpression and knockdown, this suggests that HDAC4 may not act to repress MEF2 in adult *Drosophila* neurons, despite the observed co-localisation. However, the potential interaction between HDAC4 and MEF2 during development is supported. In earlier experiments (Section 3.4) it was observed that increased nuclear accumulated HDAC4 appeared increase the disruption of axonal development in a dose-dependent fashion. The increase of nuclear HDAC4 would permit greater HDAC4-mediated repression of MEF2 which would, in turn, impact axonal pathing and branching (Alchini *et al.*, 2017). However, given that knockdown of MEF2 did not induce as severe a phenotype

as the increased nuclear HDAC4, it is likely that HDAC4 works through other pathways in addition to the regulation of MEF2 during development.

As MEF2 was most likely not the prime transcriptional regulator targeted by HDAC4, subsequent investigation into another potential candidate was carried out. CREB is required for learning and memory (Tully *et al.*, 1994; Perazzona *et al.*, 2004) and it has been proposed that HDAC4 may bind to and repress CREB in vertebrates (Sen and Sen, 2016). Initial investigations in human tissue culture showed that the CRE-luciferase construct could be activated by CREB in a predictable manner that was further altered by established CREB-activator PKA.

To investigate a possible HDAC4-CREB interaction, wild-type and nuclear accumulated hHDAC4 were co-transfected with PKA and CREB. It was observed that the nuclear accumulated hHDAC4-3SA increased the activity of CREB compared to wt-hHDAC4. How HDAC4 might increase CREB activity is unclear, but it is suggested by this data that CREB may not one of the means through which nuclear HDAC4 repressed memory in *Drosophila* as it has been shown in previous publications that increased CREB activity leads to improved memory formation (Suzuki *et al.*, 2011; Serita *et al.*, 2017). As a result of this, the investigation of potential interactions between CREB and MEF2 was put on hold, in favour of a more exploratory investigation into the transcriptional changes induced by changes in the subcellular distribution of HDAC4.

6 INVESTIGATING THE EFFECTS OF ALTERED HDAC4 SUBCELLULAR DISTRIBUTION ON TRANSCRIPTION IN *DROSOPHILA*

6.1 Introduction

In the previous sections it was shown that the presence of increased nuclear hHDAC4 impairs both the development of neurons and the function of adult neurons in learning and memory. This disruption of normal function was observed to a lesser extent in brains overexpressing wt-HDAC4 and not observed at all in flies expressing the cytoplasmically restricted variant of HDAC4. This pattern strongly indicates that it is the nuclear activity of HDAC4 that leads to the effects observed when HDAC4 is overexpressed in the brain. It has previously been suggested that transcriptional regulation by HDAC4 may occur through the repression of MEF2 or CREB, however, results from this study suggest that this is not the case in *Drosophila*.

Previous RNA sequencing data from flies overexpressing wild-type DmHDAC4 in the adult brain showed that only a small number of genes were significantly differentially expressed in the presence of an overabundance of HDAC4 (Schwartz, 2016). This data suggested that HDAC4 is unlikely to be a global regulator of transcription. However, two factors complicate this. Firstly, as this protein undergoes nucleocytoplasmic shuttling it is uncertain whether the observed transcriptional changes were due to actions of HDAC4 within the nucleus or due to the alterations in transcription through cytoplasmic HDAC4, such as sequestration of HDAC4-regulated targets in the cytoplasm or regulation of signal transduction pathways that feed back into the nucleus. Secondly, it has been shown that DmHDAC4 is nuclear only in a subset of Kenyon cells, even when overexpressed (Fitzsimons *et al.*, 2013). This means that any transcriptional changes caused by DmHDAC4 in the nucleus are likely to be diluted as the transcriptome analysis was carried out on RNA from whole heads. Therefore, to examine whether nuclear localised DmHDAC4 observed to be associated with neurological deficits also causes transcriptional changes, RNASeq was

performed on flies overexpressing the L175A (cytoplasmically restricted) and 3SA (nuclear localised) variants. The rationale being that this should alleviate this dilution effect as well as the uncertainty over the subcellular reservoir responsible for any changes observed.

6.2 Preparation and QC of samples

To investigate the effects of altered HDAC4 subcellular distribution on transcription, elav-GAL4; tub-GAL80^{ts} females were crossed to males individually carrying UAS-hHDAC4-3AS and UAS-hHDAC4 L175A as well as to w{CS10} to provide a control line with the same genetic background but no UAS-HDAC4 construct. Thus, the genotypes of the groups are described in shorthand as follows:

elav / + ; Tub-GAL80^{ts} / +; UAS-hHDAC-3SA / +

elav / + ; Tub-GAL80^{ts} / +; UAS-hHDAC-L175A / +

elav / + ; Tub-GAL80^{ts} / +; + / +

Where + indicates wild-type chromosome.

Flies were raised at 18°C, at which temperature GAL80^{ts} is active and transgene expression is repressed (Section 1.3.2). After emerging from their pupal cases, adult flies were then incubated at 30°C for 72 hours to induce expression of 3SA and L175A in all neurons. The flies were then snap frozen in liquid nitrogen and their heads separated by vortexing (Section 2.4.1). RNA was extracted from the heads as described in section 2.4.3 and was then quantified and integrity was assessed via Labchip using capillary electrophoresis to ascertain the degradation of the RNA (if any), an example of this analysis is shown in Figure 6.1.

This method of diagnosis separates fragments of RNA based on size, with the rRNA subunits being the primary indicator. In insects, the 28S subunit of rRNA is cleaved into two subunits that migrate at about 18S (Winnebeck *et al.*, 2010) so high integrity insect RNA is characterised with two sharp peaks around 18S, and

a third at 5S with very low fluorescence between them. High concentrations of RNA will lead to a higher base-line of fluorescence. The RNA was shown to be of high quality, the sample was sent to Novogene where additional quality control and library assembly were carried out. Quality was investigated using a Qubit (Table 6.1) and agarose gel verification (Figure 6.2).

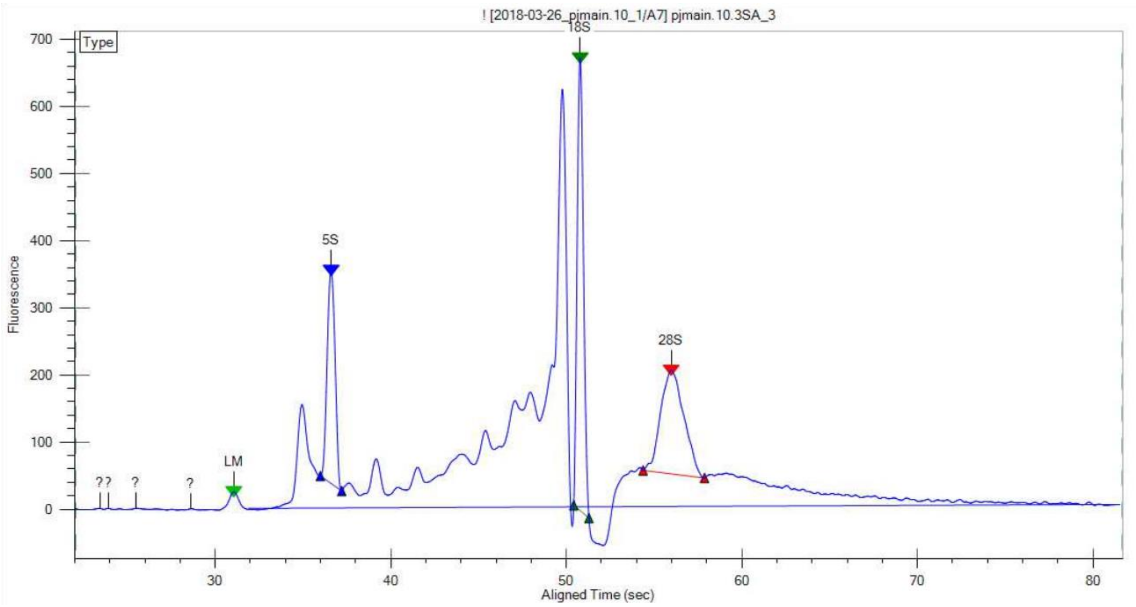

Figure 6.1 Trace from Labchip analysis of RNA integrity.
Clean 18S and 10S ribosomal subunits are shown (18S is labelled), this is characteristic of insect RNA where the 28S subunit is cleaved into two subunits that exhibit peaks around 18S. Relatively high peaks between the 5S and 18S subunits are due to the amount of RNA present.

This additional QC showed that one sample (3SA 1) had degraded somewhat during transit. Despite this, all were sequenced as it was decided that analysis of the read quality could be used to exclude the sample if it was substantially different.

The samples were sequenced using paired end sequencing and the library assembled before the data was sent to NBSeq for analysis and pairwise comparison of the samples.

Sample	Concentration (ng / µL)	260/280	260/230	RIN
L175A 1	438	2.19	2.305	6.8
L175A 2	378	2.172	2.03	7
L175A 3	236	2.145	1.662	7.3
L175A 4	274	2.076	2.016	7.1
3SA 1	352	2.071	1.778	3.9
3SA 2	386	2.169	1.969	5.8
3SA 3	366	2.128	2.153	6.7
3SA 4	327	2.145	2.046	5.6
CS 1	306	2.217	2.284	7
CS 2	260	2.203	1.884	7.1
CS 3	422	2.153	1.675	7
CS 4	280	2.188	1.842	7.1

Table 6.1 Qubit analysis of RNA samples.

The absorbance ration 260/280 indicates the relative contamination of the sample by protein and a result of >2.0 is considered "pure" for RNA. The 260/230 is a secondary measure and can help indicate an overabundance of phenolic compounds carried through from purification. A 260/230 ratio of > 1.8 is considered "pure". RIN is an RNA integrity number that indicates overall quality between 1 and 10.

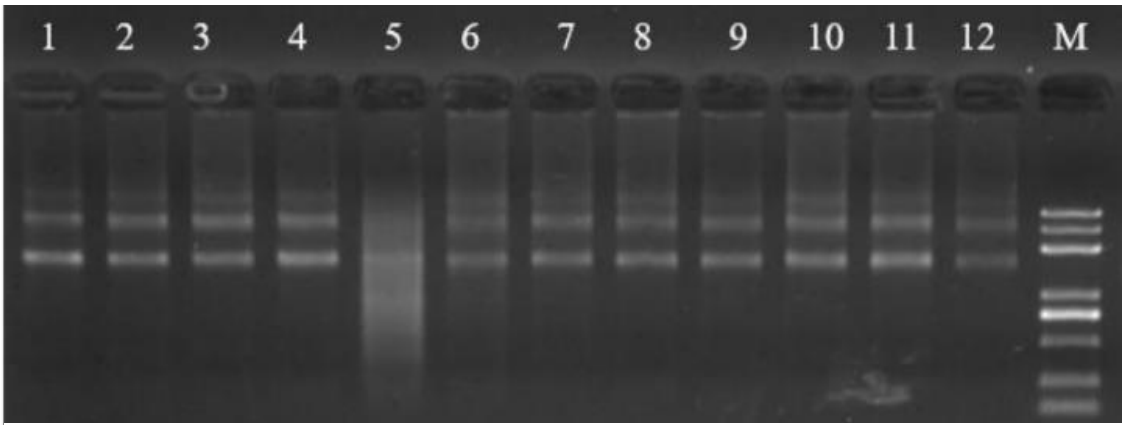

Figure 6.2 Agarose gel electrophoresis of RNA samples.

Samples are as follows: 1-4: L175A 1-4, 5-8: 3SA 1-4, 9-12: CS 1-4. M is the mass standard used by Novogene. Note degradation present in sample 5, 3SA 1.

6.3 Quality control and read verification

Following library assembly, the data was sent to NgBS (Dave Wheeler) where, to begin the process of data analysis, quality analysis of reads was carried out. Firstly, the reads were examined using *fastqc,* a programme that analyses the reads and analyses the quality based on data from the sequencing, allowing for trimming of reads of poor quality and removal of contaminants. The *fastqc* analysis showed that both the forward and reverse reads of each library were of high quality (Figure 6.3) and high sequencing depth (>30 million reads each). Small reads (<50 bp) were removed to prevent potential mapping errors (removing less than 1% of the total reads from each library) and the remaining dataset was used for analysis.

The filtered reads were mapped to the *Drosophila* genome (release 92) downloaded from ENSEMBL using HAT2 in stranded mapping mode. Overall mapping was high with greater than 94% of the reads in each library mapping at least once to the reference genome. Read counts were generated using HT-Seq v0.6.0, DESeq2 was used to generate positive fold changes between the treatment samples. This allowed a principle component analysis comparison between treatment groups in a pair-wise fashion (Figure 6.4). This comparison showed that the PC1 variance was extreme, indicating a technical variation rather than a treatment-derived variation, this allowed us to identify the fact that CS3 (rightmost red dot in each figure) appeared to have a disparate read quality, indicative that is was an outlier and should be ignored from future comparisons.

Having determined that the reads were reliable and of good quality and erroneous groups excluded, the sequencing data was checked for to verify the genotypes of the treatment groups, i.e. the presence of the 3SA and L175A variants. The sequences from the 3SA and L175A samples were aligned to human chromosome 2 and the presence of the 3SA and L175A mutations were confirmed (Figure 6.5) (See Appendix 3 – 11.4 for mutant sequences).

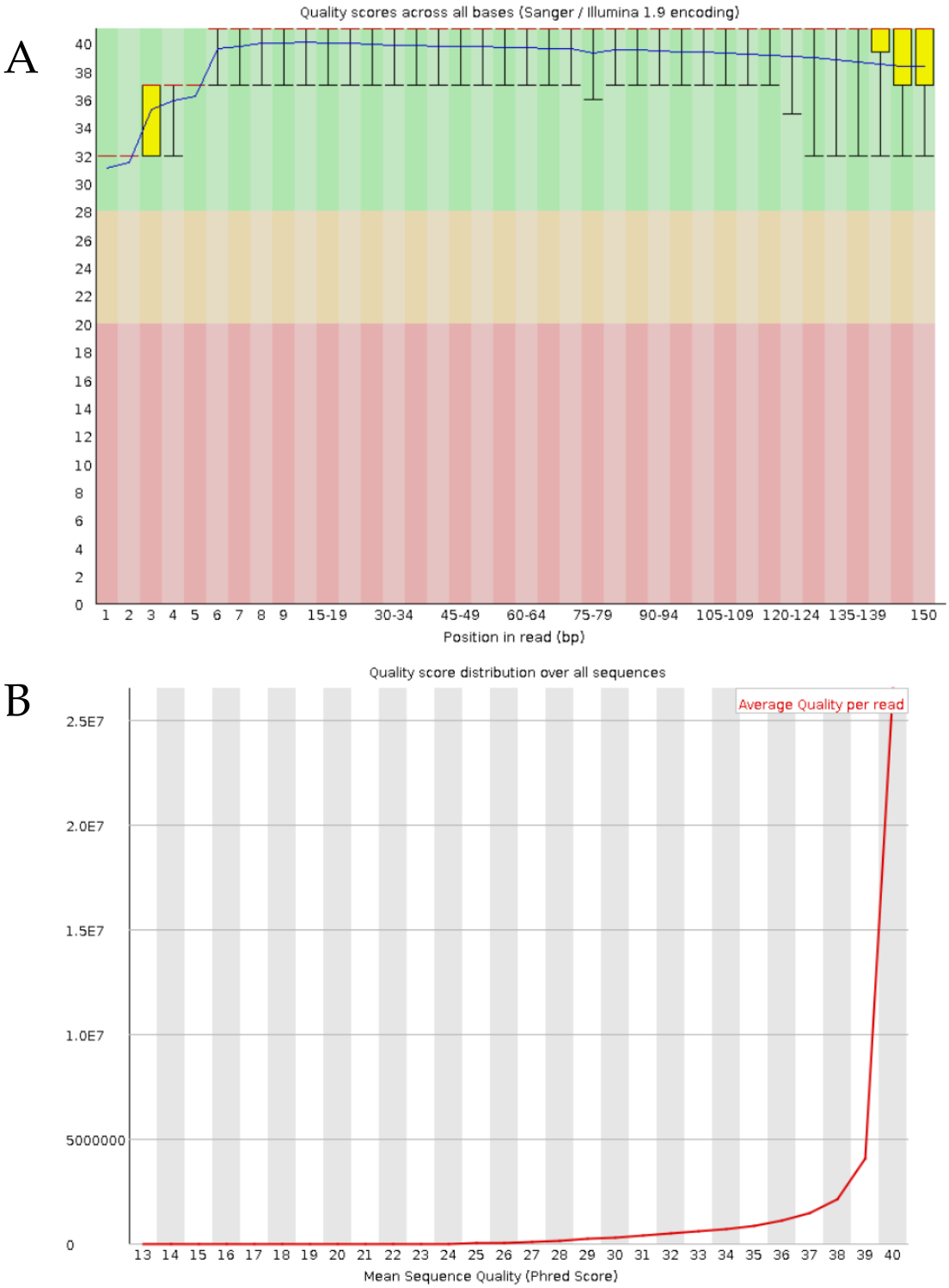

Figure 6.3 Sample of quality checking data from *fastqc* 0.6.0.

A) The quality score across all bases in segments of each read is shown, higher scores indicate higher quality. Quality is shown as a box and whisker plot with the red bar as the median value and the yellow box encompassing the inter-quartile range. Figure included is representative, further examples are present in Section 13 Appendix 5. B) The number of reads assigned the quality score shown on the x-axis, for reference a quality score of 27 indicates a 0.2% error rate.

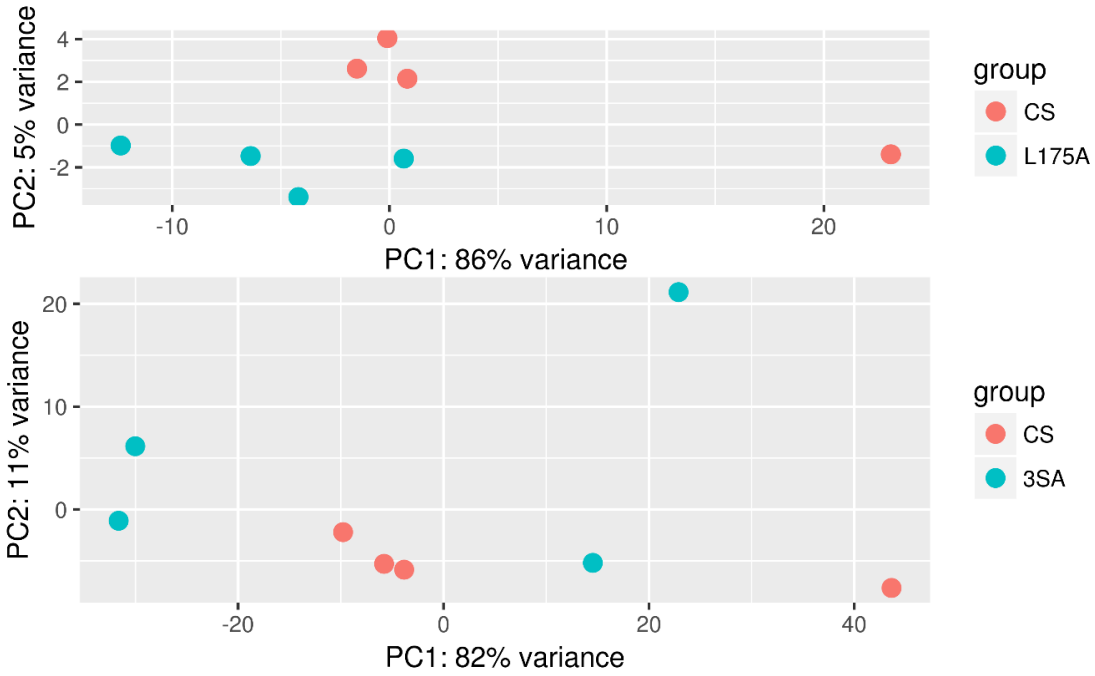

Figure 6.4 Pair-wise principal component analysis of the samples.
The fold-changes across all genes of the control samples (red) were compared to the treated groups (either 3SA or L175A) to view the similarity within the group. The PC1 axis denotes technical variation between samples and the PC2 axis denotes treatment variances between samples. The outlier from the control samples was excluded from future analysis.

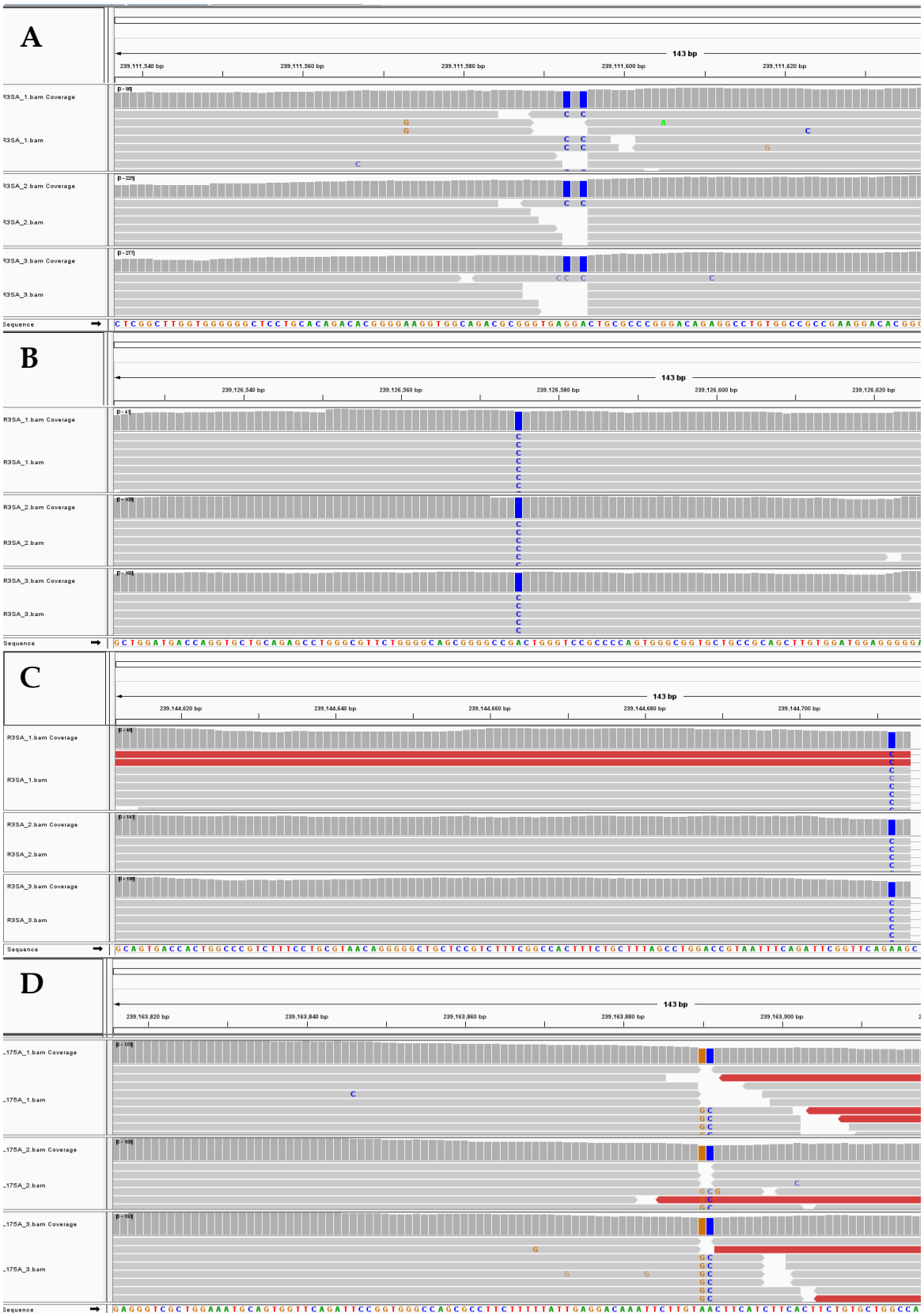

Figure 6.5 Variant sequences from read data aligned with human chromosome 2.
The read data was aligned with human chromosome 2 to verify the mutations in the HDAC4 variants. Sequence changes are highlighted in blue and orange, compared to wild-type sequence along the bottom of each image. A, B and C show the 3SA mutations and D shows the L175A mutant.

6.4 Analysis of differential expression between treatment groups

Following the completion of QC, the reads were compared to one another in a pairwise fashion to examine the differentially expressed transcripts. Both 3SA and L175A samples were compared with the control to determine the differences introduced by the overexpression of the variant and then the 3SA and L175A were compared to one another to identify the differences between nuclear and cytoplasmic subcellular distribution of HDAC4. These comparisons showed that, interestingly, both L175A and 3SA increased transcription of a greater number of genes than they repressed. Using a false discovery rate of 0.05, L175A induced changes in the expression of 612 genes and 3SA induced changes in expression of 140 genes. When comparing L175A and 3SA, only 29 genes were differentially expressed (Table 6.2).

L175A vs. Control		3SA vs. Control		L175A vs. 3SA	
Significant UP	376	Significant UP	101	Significant UP	17
Significant DOWN	236	Significant DOWN	39	Significant DOWN	12

Table 6.2 Overview of each sample comparison showing number of significant changes.

The number of genes significantly differentially expressed between the treatment groups is shown (FDR < 0.05). Compared to control flies, L175A expression altered the expression of 612 genes significantly (61% up-regulated, 39% down-regulated) and 3SA expression altered the expression of 140 genes significantly (72% up-regulated and 28% down-regulated). Comparing the transcriptomes of 3SA and L175A revealed that the expression of only 29 genes was significantly altered (59% up-regulated and 41% down-regulated).

6.5 Transcriptional changes induced by L175A

Principal component analysis after excluding CS3 shows tight grouping of the control group samples and a clear relationship (if not quite as internally consistent) between the L175A group, though some technical variance is present (Figure 6.6).

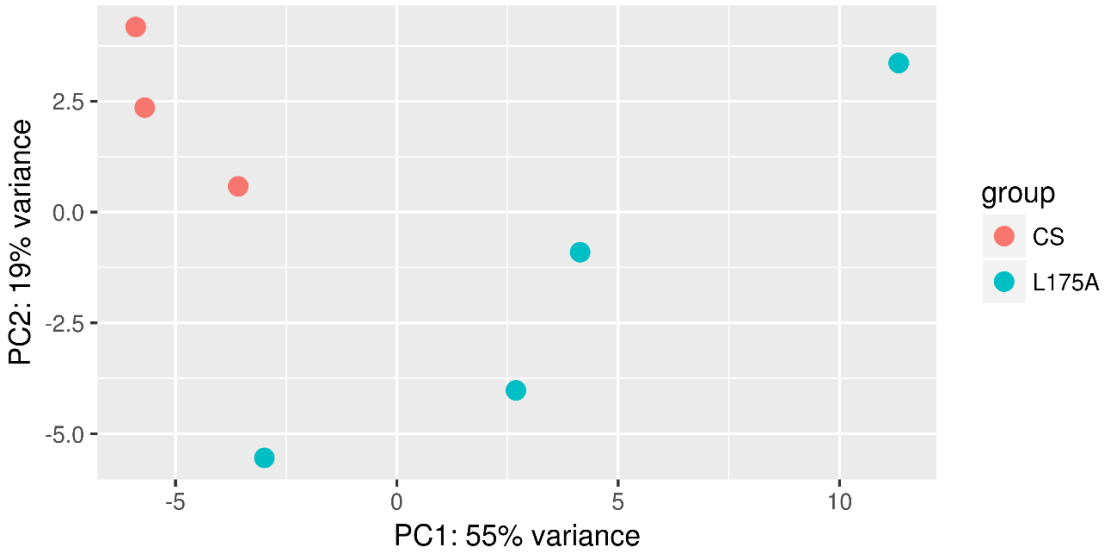

Figure 6.6 PCA of L175A treatment and control groups.
This analysis of variance between the samples shows variance by treatment along the vertical axis and variance by technical qualities (experimental variance) along the horizontal axis. This serves to identify groups within the samples tested and identifies that the treatment is different to the control along the treatment-derived axis.

Investigating the transcriptional differences between the two samples showed, as previously indicated, approximately 600 genes were significantly differentially expressed in the L175A group. The significance is determined by false-discovery rate which is, in interpretation, highly analogous to p-values as it is the calculated probability of the gene being identified by chance as opposed to being a real change in read count. The FDR is expressed as a proportion between 0 and 1 with 0.05 indicating a 5% chance that the result is a false discovery. Thus, when it is said that approximately 600 genes were significantly differentially expressed, what is meant is that approximately 600 genes had a false discovery rate (FDR) of less than 0.05.

The changes in expression observed are detailed below as a volcano plot to highlight the spread of the log_2-fold change in expression vs. the log_{10} of the false discovery rate, black dots indicate genes above the 0.05 cut-off for FDR and red dots indicate FDR < 0.05, i.e. significantly altered expression (Figure 6.7). It can be seen in this plot that a majority of the genes where the change in expression was deemed to be significant were up- or down-regulated by less than 2-fold (log_2-fold -1 to 1), with a comparatively small number of genes undergoing a change in expression of >2-fold.

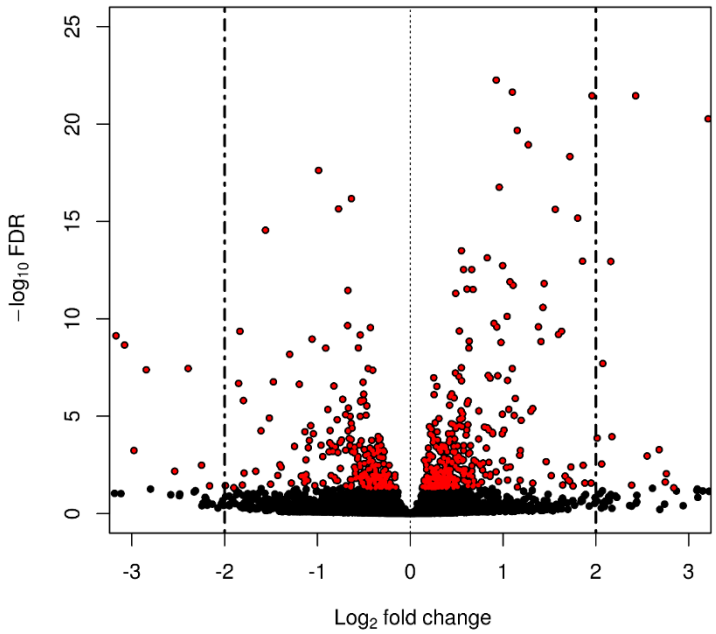

Figure 6.7 Volcano plot of identified genes in L175A vs control sample.
The volcano plot visualises the changes in transcription observed between the L175A and control, the horizontal axis indicates the Log_2-fold change of the gene and the vertical axis indicates the negative Log_{10} of the false discovery rate. Genes that are deemed significant (i.e. FDR < 0.05) are highlighted in red. Insignificantly altered genes are in black.

Finally, to further examine the consistency of the transcriptional profiles of each sample within each group, a heatmap was constructed showing relative expression of the 50 most significantly differentially expressed genes. The genes were grouped by similar expression patterns (left dendrogram) and by treatment group (top dendrogram) (Figure 6.8). This shows the normalised read counts (right) as a colour-coded heatmap in which warmer colours are higher levels of expression. This heatmap highlights the consistency of the read numbers within

the treatment groups, as well as showing that, though significant, many of the changes observed are not large changes in expression.

A shortlist of the 30 most significantly altered genes is shown below (Table 6.3). In this table the genes are listed in order of significance (increasing adjusted p-value) along with their annotation, FlyBase ID and several identified/proposed functions from FlyBase. The roles/functions are either experimentally demonstrated or predicted from sequence homology. Also included in the table is the $\log_2$-fold change.

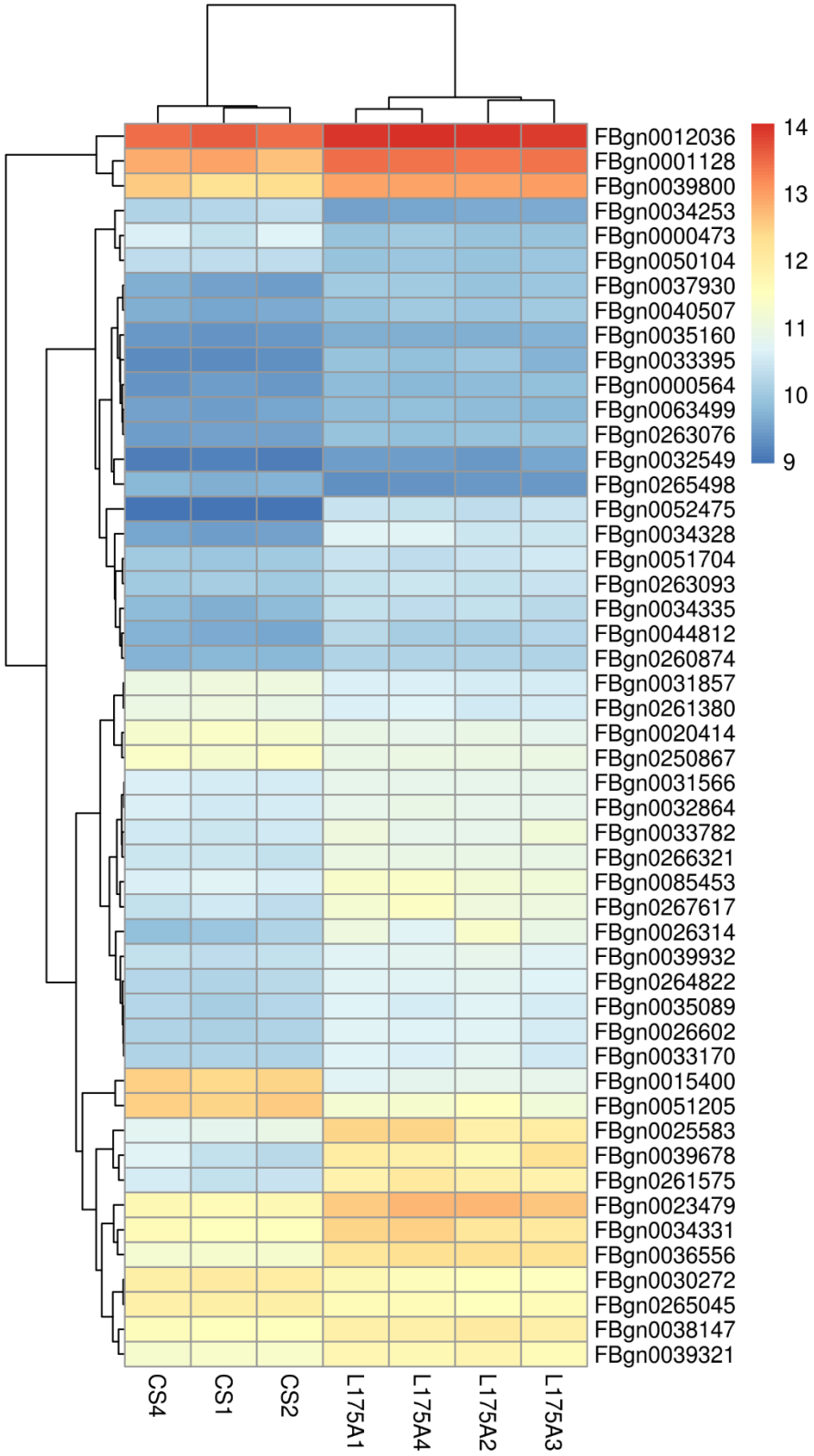

Figure 6.8 Heatmap of the 50 most significantly differentially expressed genes in L175A vs. control sample.

The warmth of the colour indicates higher levels of transcription, read counts are normalised by read depth and show the variability within each sample. The left dendrogram links genes based on transcriptional changes and the top dendrogram groups samples by similarity. The FlyBase ID for each gene is listed on the right. Key indicates Log_2 of read count. See 14 – Appendix 6 for table detailing molecular functions of these genes.

Annotation	FlyBaseID	log2Fold Change	Adjusted p-value	Molecular function / biological process
kek2	FBgn0015400	-2.283	4.55E-148	Not-negative regulation of epidermal growth factor receptor signalling pathway
CG5830	FBgn0036556	1.350	9.81E-69	Phosphoprotein phosphatase activity / RNA polymerase II CTD heptapeptide repeat phosphatase activity / regulation f transcription by RNA polymerase II
Tobi	FBgn0261575	2.293	6.12E-57	Hydrolase activity / carbohydrate metabolic process / glycoside catabolic process
Teq	FBgn0023479	1.262	2.28E-49	Chitin binding / serine-type endopeptidase activity / glucose homeostasis / long-term memory / positive regulation of insulin secretion / short-term memory
IM23	FBgn0034328	3.323	1.06E-48	Antibacterial response / defence against gram-positive bacteria
CG31205	FBgn0051205	-1.618	9.53E-33	Serine-type endopeptidase activity
CG10936	FBgn0034253	-2.299	1.16E-27	Unknown
CR44986	FBgn0266321	0.926	5.53E-23	Unknown
CR44030	FBgn0264822	1.100	2.30E-22	Unknown
IM2	FBgn0025583	1.958	3.56E-22	Defence response / response to bacteria
Obp99a	FBgn0039678	2.429	3.56E-22	Odorant binding / olfactory behaviour / response to pheromone / sensory perception of chemical stimulus (scent)
Cyp4p2	FBgn0033395	3.210	5.42E-21	Heme binding / iron ion binding / oxidoreductase activity
Ady43A	FBgn0026602	1.152	2.14E-20	Adenosine kinase activity

Ir76a	FBgn0260874	1.272	1.16E-19	Olfactory receptor activity / ligand-gated ion channel activity / detection of chemical stimulus involved in sensory perception of smel
mthl8 *	FBgn0052475	11.490	2.54E-19	G-protein coupled receptor activity / determination of adult lifespan / response to starvation
Klp54D	FBgn0263076	1.720	4.67E-19	Microtubule motor activity / microtubule binding / microtubule-based movement
NT5E-2	FBgn0050104	-0.988	2.39E-18	5'-nucleotidase activity / nucleotide binding / metal ion binding
CR43361	FBgn0263093	0.959	1.76E-17	Unknown
CG42238	FBgn0250867	-0.635	6.74E-17	Unknown
CG11321 / LUBEL	FBgn0031857	-0.773	2.26E-16	Linear polyubiquitin binding / ubiquitin protein ligase activity / heat acclimation / protein polyubiquitination
GstE1	FBgn0034335	1.563	2.41E-16	Glutathionine transferase activity / response to heat, oxidative stress
TotC	FBgn0044812	1.805	6.77E-16	Cellular response to heat, UV, oxidative stress and bacteria
Cyp6a2	FBgn0000473	-1.560	2.81E-15	Heme binding / iron ion binding / oxidoreductase activity / response to caffeine and DDT
CG10550	FBgn0039321	0.551	3.20E-14	Unknown
Fuss	FBgn0039932	0.829	7.40E-14	Co-SMAD binding / SMAD binding / imaginal disc-derived wing vein specification / negative regulation of BMP signalling pathway / neuron development

Eh	FBgn0000564	1.856	1.10E-13	Eclosion hormone activity / neuropeptide hormone activity / eclosion / ecdysis
Ugt35b	FBgn0026314	2.161	1.14E-13	UDP-glycosyltransferase activity / UDP-glucose metabolic process
CG34424 / Mthfs	FBgn0085453	0.996	1.86E-13	5-formyltetrahydrofolate cyclo-ligase activity / folic acid-containing compound biosynthetic process / tetrahydrofolate interconversion
Gpdh / Gdph1	FBgn0001128	0.662	2.97E-13	Glycerol-3-phosphate dehydrogenase activity / chromatin binding / ethanol metabolic process / flight behaviour / triglyceride metabolic process
CG2818	FBgn0031566	0.574	2.97E-13	Glycerophosphocholine phosphodiesterase activity / starch binding / glycerophospholipid catabolic process

Table 6.3 The 30 most significantly differentially expressed genes between the L175A and control groups.

Included are identifiers as well as details about proposed functions. Genes selected for further analysis are starred (*), a short briefing on these potential candidates for future research is present later in the chapter (6.10).

6.6 Transcriptional changes induced by 3SA

In contrast to the changes caused by L175A, the expression of 3SA induced relatively few transcriptional changes, many of which were similar to the changes observed in the L175A sample. Particularly noteworthy is the observation that, overall, the upregulated genes form a much higher proportion of significantly altered transcripts than in the L175A group, contrasting the suggestions in previous literature that HDAC4 acts largely as a transcriptional repressor (Fischle *et al.*, 2002; Flavell and Greenberg, 2008).

Principal component analysis of the 3SA and control groups appear similar to that comparing the L175A and Control with the treatment group exhibiting more technical variability. It is worth noting that the treatment variability (Y axis) is much greater within the 3SA groups than it was the L175A sample, indicating a less internally consistent dataset (Figure 6.9). This is likely due to the observed degradation of one of the 3SA samples, which evidently impaired sequencing marginally but was still included as the variance was not extreme compared to the other samples in the group. It was decided to retain all four samples rather

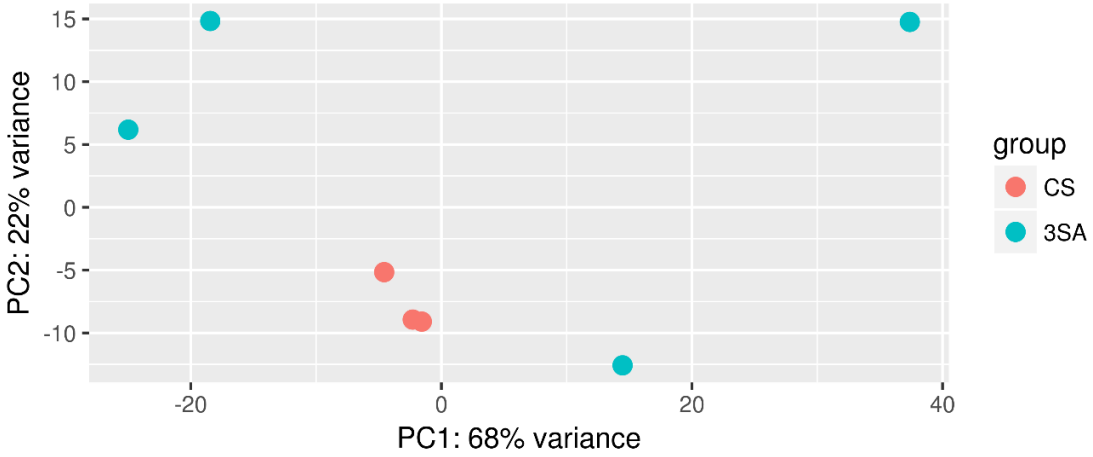

Figure 6.9 PCA of the 3SA and control samples.

This analysis of variance between the samples shows variance by treatment along the vertical axis and variance by technical qualities (experimental variance) along the horizontal axis. This serves to identify groups within the samples tested and identifies that the treatment is different to the control along the treatment-derived axis. The 3SA samples are significantly more disparate than the L175A and control (CS), with a large amount of variance on both the treatment and technical variance axes.

than eschew one after considering that there was no clear outlier (one differed by treatment variability and the other by technical variability), discussion with our RNASeq expert at NgBS lead to the conclusion that including all four was the best course for reliable data.

An analysis of the total transcription changes induced by the overexpression of 3SA can be seen in the volcano plot (Figure 6.10). This plot highlights that more genes were differentially up-regulated than down-regulated, as well as indicating that many of the genes which had significantly increased expression were increased by >4-fold.

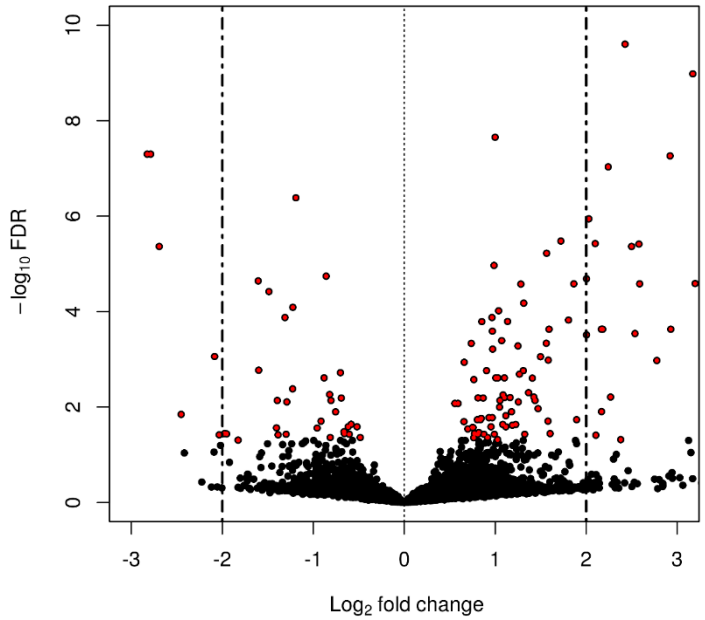

Figure 6.10 Volcano plot comparing 3SA and control samples.
The volcano plot visualises the changes in transcription observed between the 3SA and control, the horizontal axis indicates the Log_2-fold change of the gene and the vertical axis indicates the negative Log_{10} of the false discovery rate.

As a comparison of both the changes in transcription and a comparison of the groups a heatmap was generated showing the normalised read number for the 50 most significantly altered genes. The heatmap shows that the variance within the 3SA group is largely caused by a few genes with notably different read counts compared to the other 3SA samples but, aside from these few genes, the group is largely internally consistent (Figure 6.11). A shortlist of the 30 most significantly altered genes is shown below (Table 6.4).

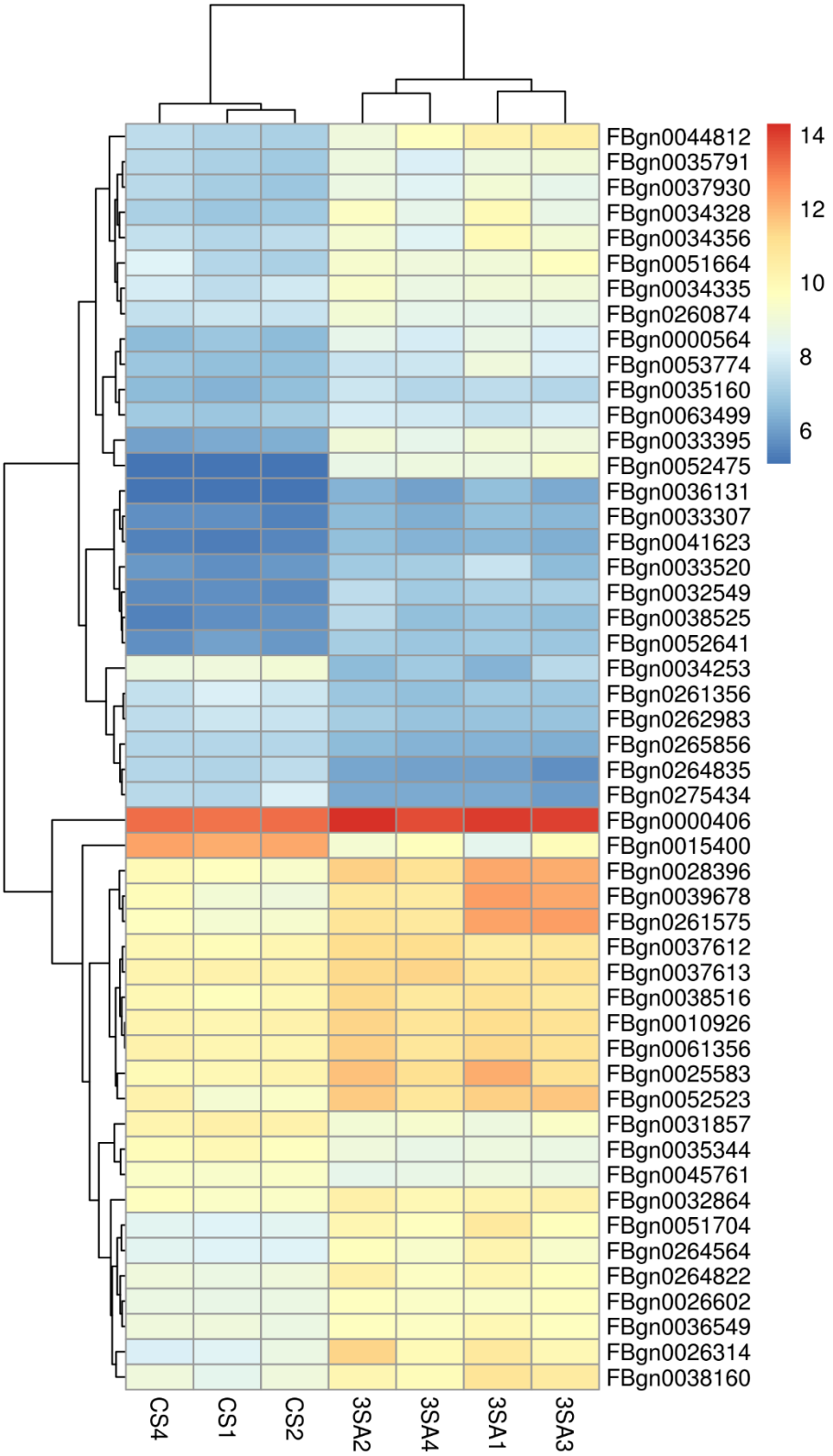

Figure 6.11 Heatmap of the 50 most significantly differentially expressed genes in 3SA vs. control sample.

The warmth of the colour indicates higher levels of transcription, read counts are normalised by read depth and show the variability within each sample. The left dendrogram links genes based on transcriptional changes and the top dendrogram groups samples by similarity. FlyBase IDs are listed on the right. Key indicates Log_2 of read count. See 14 – Appendix 6 for table detailing molecular functions of these genes.

Annotation	FlyBaseID	log2-Fold Change	Adjusted p-value	Molecular function / biological pathways
Cyp4p2	FBgn0033395	4.251	6.35E-41	Heme binding / iron ion binding / oxidoreductase activity
mthl8 *	FBgn0052475	11.145	2.93E-16	G-protein coupled receptor activity / determination of adult lifespan / response to starvation
CG4650	FBgn0032549	4.170	3.94E-12	Not Serine-type endopeptidase activity
kek2	FBgn0015400	-2.956	1.10E-11	Not-negative regulation of epidermal growth factor receptor signalling pathway
Eh	FBgn0000564	2.427	2.49E-10	Eclosion hormone activity / neuropeptide hormone activity / eclosion / ecdysis
TotC	FBgn0044812	3.172	1.04E-09	Cellular response to heat, UV, oxidative stress and bacteria
Ady43A	FBgn0026602	0.999	2.22E-08	Adenosine kinase activity
CR44043	FBgn0264835	-2.788	5.01E-08	Unknown
CR46266	FBgn0275434	-2.826	5.01E-08	Unknown
IM23	FBgn0034328	2.922	5.45E-08	Antibacterial response / defence against gram-positive bacteria
TotA	FBgn0028396	2.242	9.27E-08	Cellular response to heat, cold, mercury, UV, water deprivation
Cyp4d20	FBgn0035344	-1.191	4.13E-07	Heme binding / iron ion binding / oxidoreductase activity
CG31704	FBgn0051704	2.029	1.14E-06	Multicellular organism reproduction
CR43936	FBgn0264564	1.721	3.32E-06	Unknown
CG14715	FBgn0037930	2.099	3.75E-06	Unknown
CG32641	FBgn0052641	7.348	3.28E-05	Unknown
Ugt35b	FBgn0026314	2.580	3.85E-06	UDP-glycosyltransferase activity / UDP-glucose metabolic process

CG10936	FBgn0034253	2.499	4.31E-06	Unknown
CG14329	FBgn0038525	-2.694	4.31E-06	Unknown
GstE1	FBgn0034335	3.630	4.31E-06	Glutathionine transferase activity / response to heat, oxidative stress
l(3)07882	FBgn0010926	1.565	5.99E-06	snoRNA binding / ribosomal small subunit biogenesis
Or65c	FBgn0041623	0.987	1.08E-05	Odorant binding / olfactory receptor activity / detection of chemical stimulus involved in sensory perception of smell
CHKov1	FBgn0045761	4.112	1.81E-05	Unknown
CG8539	FBgn0035791	-0.859	1.81E-05	Unknown
CR44645	FBgn0265856	2.003	2.05E-05	Metallocarboxypeptidase activity / zinc ion binding / proteolysis
Prx2540-1	FBgn0033520	-1.606	2.27E-05	Unknown
CG9759	FBgn0038160	3.198	2.58E-05	Peroxidase activity / cell redox homeostasis / hydrogen peroxide catabolic process
Tobi	FBgn0261575	1.864	2.62E-05	Hydrolase activity / carbohydrate metabolic process / glycoside catabolic process
Ir76a	FBgn0260874	2.588	2.62E-05	Olfactory receptor activity / ligand-gated ion channel activity / detection of chemical stimulus involved in sensory perception of smell
CG12522	FBgn0036131	1.282	2.65E-05	Unknown

Table 6.4 The 30 most significantly differentially expressed genes between the 3SA and control groups.

Included are identifiers as well as details about proposed functions. Genes selected for further analysis are starred (*), a short briefing on these potential candidates for future research is present later in the chapter (6.10).

6.7 Differential expression between the L175A and 3SA groups

Having established the differences induced by L175A and 3SA when compared to the control group, the final piece of the puzzle is investigating the differences in transcription profile between the exclusively cytoplasmic L175A and the largely nuclear 3SA samples. This should highlight expression changes induced by the nucleocytoplasmic shuttling of HDAC4 and could indicate some of the pathways through which the nuclear-accumulated HDAC4 induces its abnormal phenotypes.

The PCA of the two treatment groups shows significant overlap between the two. This is unsurprising as both treatments had relatively high internal variance and are overexpressing mutants of the same protein that only differ in subcellular distribution (Figure 6.12).

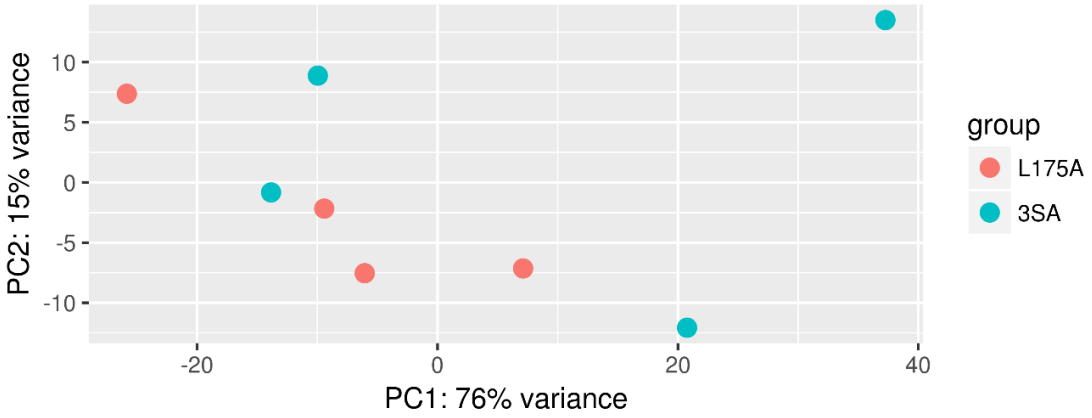

Figure 6.12 PCA of the 3SA and L175A samples.
This analysis of variance between the samples shows variance by treatment along the vertical axis and variance by technical qualities (experimental variance) along the horizontal axis. This serves to identify groups within the samples tested and identifies that the treatment is different to the control along the treatment-derived axis.

This similarity between the groups is easily visualised in the volcano plot as many of the data points are gathered at a very low $\log_{10}$FDR score on the Y-axis (Figure 6.13). Only 29 genes were differentially expressed between the two samples, 17 of which were up-regulated and 12 of which were down-regulated.

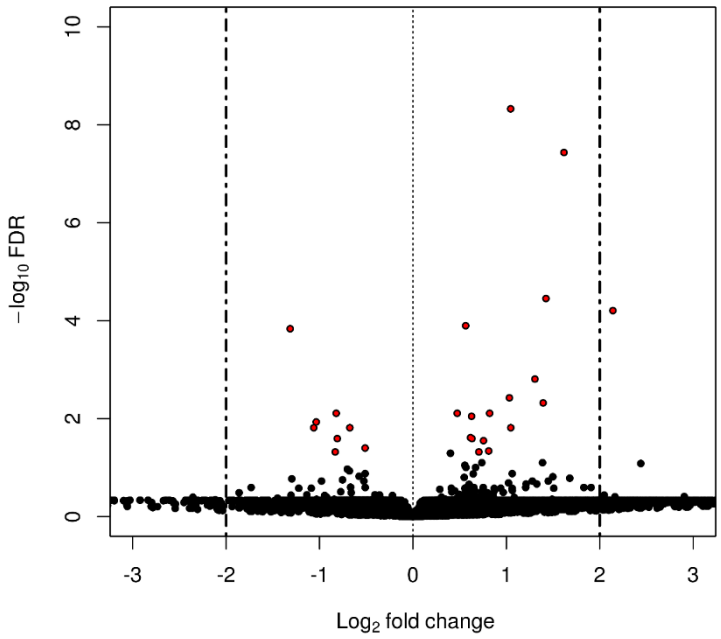

Figure 6.13 Volcano plot comparing L175A and 3SA samples.

The volcano plot visualises the changes in transcription observed between the L175A and 3SA samples, the horizontal axis indicates the Log_2-fold change of the gene and the vertical axis indicates the negative Log_{10} of the false discovery rate.

Finally, the heatmap analysis of reads showing the fifty most significantly different genes again highlights the similarities between the two treatments. It is worth noting that this format does include some 20 genes that were not significantly differentially expressed but is still useful in showing the groupings of the treatments, the consistency within the groups and the altered expression between treatments (Figure 6.14). A shortlist of the 30 most significantly altered genes is shown in Table 6.5.

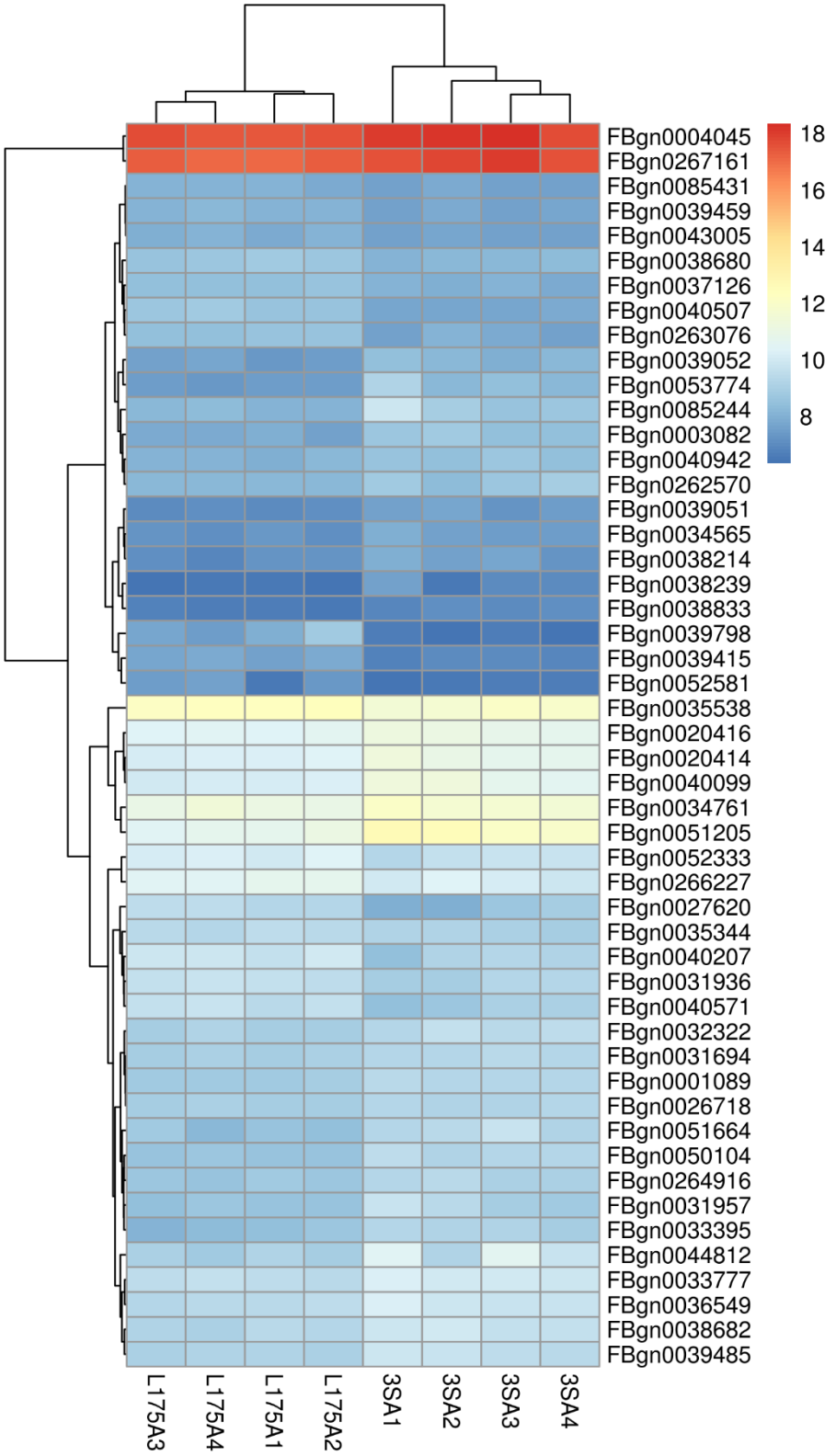

Figure 6.14 Heatmap of the 50 most significantly differentially expressed genes in L175A vs. 3SA samples.

The warmth of the colour indicates higher levels of transcription, read counts are normalised by read depth and show the variability within each sample. The left dendrogram links genes based on transcriptional changes and the top dendrogram groups samples by similarity. FlyBase IDs are listed on the right. Key indicates Log_2 of read count. See 14 – Appendix 6 for table detailing molecular functions of these genes.

Annotation	**FlyBaseID**	**log2Fold Change**	**Adjusted p-value**	**Molecular function / biological pathways**
ACXD *	FBgn0040507	-1.527	3.74E-15	Adenylyl cyclase
CG6142	FBgn0039415	-2.740	2.88E-11	Glucose-methanol-choline oxidoreductase
NT5E-2	FBgn0050104	1.046	4.72E-09	5'-nucleotidase activity / nucleotide binding / metal ion binding
CG31205	FBgn0051205	1.617	3.68E-08	Serine-type endopeptidase activity
CG11313	FBgn0039798	-6.228	5.30E-08	Serine-type endopeptidase activity
Phr	FBgn0003082	1.424	3.52E-05	Deoxyribodipyrimidine photo-lyase activity/photoreactive repair
CG33774	FBgn0053774	2.140	6.22E-05	Dolichyl-diphosphooligosaccharide-protein glycotransferase activity / protein N-linked glycosylation
Gal	FBgn0001089	0.565	1.27E-04	Beta-galactosidase activity / protein homodimerisation activity
Klp54D	FBgn0263076	-1.314	1.46E-04	Microtubule motor activity / microtubule binding / microtubule-based movement
CG31664	FBgn0051664	1.306	1.55E-03	Unknown
lectin-28C	FBgn0040099	1.033	3.76E-03	Galactose binding / transmembrane signalling receptor activity
CG6733	FBgn0039052	1.394	4.77E-03	Aminoacyclase activity / cellular amino acid metabolic process
Idgf3	FBgn0020414	0.821	7.78E-03	Imaginal disc growth factor receptor binding / chitin - based cuticle development / wound healing
Cyp4ac2	FBgn0031694	0.474	7.78E-03	Heme binding / iron ion binding / oxidoreductase activity
CG14567	FBgn0037126	-0.821	7.78E-03	Unknown
CG17574	FBgn0033777	0.628	0.009	Unknown

CG17193	FBgn0040571	-1.035	0.012	Unknown
Cyp4p2	FBgn0033395	1.047	0.015	Heme binding / iron ion binding / oxidoreductase activity
Cyp12a5	FBgn0038680	-0.675	0.015	Heme binding / iron ion binding / oxidoreductase activity
kat80 *	FBgn0040207	-1.062	0.015	Microtubule binding / microtubule depolymerisation / microtubule severing
CG16743	FBgn0032322	0.617	0.024	Unknown
CG10516	FBgn0036549	0.632	0.026	Ubiquitin-protein transferase activity / ubiquitin-dependent protein catabolic process
IntS12	FBgn0039459	-0.810	0.026	snRNA 3' end processing
CG5835	FBgn0038682	0.755	0.028	Unknown
Cyp4d20	FBgn0035344	-0.512	0.040	Heme binding / iron ion binding / oxidoreductase activity
CG43110	FBgn0262570	0.811	0.046	Serine-type endopeptidase activity
CG12643	FBgn0040942	0.706	0.048	Unknown
prt	FBgn0043005	-0.832	0.048	Serotonin:sodium symporter activity / male mating behaviour / olfactory learning
CG32581	FBgn0052581	-4.441	0.048	Ubiquitin protein ligase activity / ubiquitin-protein transferase activity / ubiquitin-dependent protein catabolic processes
fu12 *	FBgn0026718	0.402	0.051	1-acyllycerol-3-phosphate O-acyltransferase activity / behavioural response to ethanol

Table 6.5 The 30 most significantly differentially expressed genes between the L175A and 3SA groups.

Included are identifiers as well as details about proposed functions. Genes selected for further analysis are starred (*), a short briefing these potential candidates for future research is present later in the chapter (6.10).

6.8 GO-TERM analysis

Having investigated the changes in expression on a single gene level any overall trends that were induced in transcriptional changes by L175A and 3SA were examined via Gene Ontology (GO) term analysis. The Gene Ontology project is one that attempts to distil the function and relationships of genes to universal, understandable terms. The project has developed a definition of categories, properties and relations between genes (the ontology) to reduce complexity and permit organisation and interpretation of data. Gene ontology has three domains: Cellular components (CC); biological processes (BP) and molecular functions (MF).

For this, the identity of all differentially expressed genes with an FDR < 5% (i.e. significantly altered) were uploaded to the Database for Analysis, Visualisation and Integrated Discovery (DAVID, 6.8) (Huang *et al.*, 2009a, 2009b). This toolset allows for the identification of functional groups highly enriched in a sample, as well as identifying biological pathways that are highly represented in a given group. For simplicity and ease of interpretation in this brief overview, only a few of the outputs from interpretation of the data will be included in this chapter.

The data from the gene sets below is laid out below with the output separated based on gene-ontology term group, that is, separated into biological processes, molecular function or cellular component. DAVID further produces an output that groups these GO-terms into functional pathways but for initial investigations, the raw GO-term population was used as it is easier to visualise. GO-term analysis showed that expression of both L175A and 3SA both significantly altered oxidoreductase activity, carbohydrate binding, and heme binding pathways (Grouped under oxidoreductase activity for table legibility) (Table 6.6, Table 6.7). Interestingly, L175A expression also altered expression of a large number of cytoplasmic translation genes as well as sleep, synapse assembly and neuron cell-cell adhesion related terms.

Comparison between the L175A and 3SA groups yielded much less robust comparisons, this is most likely due to the relatively small number of differentially expressed genes. Differential expression of four genes that encode cytochrome P450 superfamily proteins were the source of all of the significant pathways that have possible roles in heme ion binding and oxidoreductase activity (Table 6.8).

Biological Process GO-terms	Gene count	% of total genes	P-Value	Fold enrichment	FDR (%)
Cytoplasmic translation	37	6.11	6.67E-26	9.53	1.05E-22
Oxidation-reduction process	36	5.94	1.04E-05	2.25	0.016302
'*de novo*' IMP biosynthetic process	5	0.83	3.13E-05	21.46	0.049076
Sleep	15	2.48	2.60E-04	3.17	0.405972
Centrosome duplication	14	2.31	2.66E-04	3.34	0.416745
Response to bacterium	9	1.49	3.39E-04	5.04	0.530692
Translation	39	6.44	0.002	1.67	2.98554
Glutathione metabolic process	8	1.32	0.002	4.38	3.164484
Regulation of locomotor rhythm	4	0.66	0.003	12.88	4.29232
Cellular component GO-terms					
Ribosome	34	5.61	1.66E-22	8.74	2.05E-19
Cytosolic large ribosomal subunit	20	3.30	3.39E-13	8.69	4.20E-10
Cytosolic small ribosomal subunit	17	2.81	4.09E-12	9.73	5.06E-09
Cytosolic ribosome	24	3.96	3.10E-08	3.95	3.84E-05
Extracellular region	46	7.59	3.31E-06	2.08	0.004093
Lipid particle	28	4.62	1.37E-05	2.55	0.01698
Small ribosomal subunit	6	0.99	3.60E-05	13.74	0.044531
Cell surface	12	1.98	2.61E-04	3.83	0.322646
Membrane	28	4.62	0.003	1.82	3.752708
Organelle membrane	10	1.65	0.004	3.19	4.688262
Molecular Function GO-terms					
Structural constituent of ribosome	41	6.75	1.39E-09	2.92	1.98E-06
Oxidoreductase activity	23	3.79	3.61E-05	2.71	0.052
rRNA binding	8	1.32	1.22E-04	6.74	0.175
Iron ion binding	16	2.64	0.002	2.46	2.924
Glutathione transferase activity	8	1.32	0.002	4.33	2.967

Table 6.6 GO-Term analysis from L175A expression.

All significantly differentially expressed genes were submitted to DAVID (6.8) for analysis, the resulting GO-terms were uncovered, only those with a false discovery rate (FDR) < 5% were included. Gene count and % of total genes are in reference to the number of genes submitted.

Biological Process GO-terms	Gene count	% of total genes	P-Value	Fold enrichment	FDR (%)
Response to bacterium	6	4.29	4.96E-05	14.64	0.06
Oxidation-reduction process	14	10	6.32E-05	3.81	0.08
Cellular Component GO-terms					
Organelle membrane	6	4.29	5.08E-04	8.96	0.51
Extracellular region	14	10	6.75E-04	2.97	0.67
Endoplasmic reticulum membrane	8	5.71	0.002472	4.27	2.44
Molecular Function GO-terms					
Monooxygenase activity	7	5	1.89E-04	8.21	0.23
Paired donor oxidoreductase activity	7	5	2.27E-04	7.94	0.27
Heme binding	8	5.71	2.62E-04	6.25	0.31
Carbohydrate binding	6	4.29	0.001	7.28	1.54
Iron ion binding	7	5	0.003	4.88	3.41

Table 6.7 GO-Term analysis from 3SA expression.

All significantly differentially expressed genes were submitted to DAVID (6.8) for analysis, the resulting GO-terms were uncovered, only those with a false discovery rate (FDR) < 5% were included. Gene count and % of total genes are in reference to the number of genes submitted.

Molecular Function GO-terms	Count	% of total genes	P-Value	Fold Enrichment	FDR (%)
Monooxygenase activity	4	13.79	9.67E-04	19.18	0.84
Paired donor oxidoreductase activity	4	13.79	0.001	18.55	0.93
Heme binding	4	13.79	0.003	12.79	2.67
Iron ion binding	4	13.79	0.004	11.41	3.67

Table 6.8 GO-Term analysis from comparing the 3SA sample to the L175A sample.

All significantly differentially expressed genes were submitted to DAVID (6.8) for analysis, the resulting GO-terms were uncovered, only those with a false discovery rate (FDR) < 5% were included. Gene count and % of total genes are in reference to the number of genes submitted.

Further investigation of the genes identified by the GO term analysis showed that four genes identified in the comparison between L175A and 3SA were altered in opposite directions with two of the genes being up-regulated and two of them being down-regulated by the nuclear accumulated HDAC4. Thus, it was decided to split the significantly differentially expressed genes in each dataset into two groups based on whether they were up-regulated or down-regulated and resubmit them to GO term analysis (Table 6.9, Table 6.10).

Up-regulated by L175A expression		**Down-regulated by L175A expression**	
Annotation Cluster 1 Enrichment Score: 15.64	Ribosomal proteins, cytoplasmic translation, centrosome duplication	**Annotation Cluster 1 Enrichment Score 2.11**	Glucose dehydrogenase, oxidoreductase activity
Annotation Cluster 2 Enrichment Score: 4.01	Purine biosynthesis, "*de novo*" IMP biosynthesis, purine metabolism		
Annotation Cluster 3 Enrichment Score: 3.82	rRNA binding, RNA binding		
Annotation Cluster 4 Enrichment Score: 2.76	ATP-"grasp-fold", ligase		
Annotation Cluster 5 Enrichment Score: 2.37	Cell surface, cell-cell adhesion, lipid metabolism, synaptic transmission		

Table 6.9 DAVID analysis of genes up- or down-regulated by L175A expression.

Up- and down-regulated genes from L175A expression data were separately submitted to DAVID and enriched pathways were clustered based on related annotations. Annotation clusters were condensed to representative key words from all terms. Five most enriched groups were selected from the clustering detected in the L175A up-regulated genes. Selection was made with a cut-off enrichment score of > 2.00.

Firstly, analysis of the genes upregulated by L175A expression (compared with control) identifies the presence of two groups of GO-terms related to molecular pathways and biological functions (Table 6.9). Group 1, with an enrichment score of 15.6, includes cytoplasmic translation, cytosolic ribosomes and other cytoplasmic translation machinery. Annotation clusters 2, 3 and 4 are enriched for purine biosynthesis, ribosomal RNA binding and ATP "grasp-fold" proteins that strongly suggest that DNA and protein synthesis is differentially regulated in the L175A sample. The fifth most enriched group includes genes that encode proteins with roles in neuron cell-cell adhesion, synapse assembly and lipid metabolism. The single significant (>2-fold enrichment) down-regulated cluster incorporates terms associated with glucose dehydrogenase and oxidoreductase activity, potentially part of cellular metabolism.

Genes up-regulated by 3SA		**Genes down-regulated by 3SA**
Annotation Cluster 1 Enrichment Score: 3.46	Response to bacterium, signal peptides, immunity, disulfide bonds	**No significant clusters discovered**
Annotation Cluster 2 Enrichment Score: 2.40	Oxidation-reduction pathway, oxidoreductase sites, Cytochrome P450 pathway, heme binding, monooxygenase activity	
Annotation Cluster 3 Enrichment Score: 2.05	Drug metabolism, xenobiotic metabolism	

Table 6.10 DAVID analysis of genes up- or down-regulated by 3SA expression.

Up- and down-regulated genes from 3SA expression data were separately submitted to DAVID and enriched pathways were clustered based on related annotations. Annotation clusters were condensed to representative key words from all terms. Selection was made with a cut-off enrichment score of > 2.00.

Dividing the up- and down- regulated genes from the 3SA sample showed 3 enriched annotation clusters in the up-regulated genes and no significant clusters

in the down-regulated genes (Table 6.10). The first of the three groups was enriched for immune-associated genes and bacterial defence-related genes. The second group showed enrichment of multiple facets of the oxidoreductase pathway and cytochrome P450 related terms. Finally, annotation cluster 3 showed enrichment for genes associated with drug and xenobiotics. These three groups are unexpected as they all indicate some sort of external threat to the fly which, if present, should have been consistent throughout treatment groups. The observation that no significant clusters were found to be down-regulated is surprising as it was previously assumed that nuclear HDAC4 was a major transcriptional repressor.

6.9 Comparisons to previous sequencing data

Previous work in our lab showed that HDAC4 does not appear to alter the transcription of many genes. RNASeq was carried out on RNA extracted from heads in which DmHDAC4 was overexpressed in all neurons, this indicated changes in expression of only a few dozen genes, shown in Table 6.11 (Schwartz, 2016). The second highest differentially expressed gene in this dataset was DmHDAC4, validating that the gene was indeed overexpressed significantly, despite the small number of significantly differentially expressed genes. It was therefore of interest to determine whether this set of genes was also regulated by human HDAC4, which may indicate functional conservation with respect to regulation of gene expression.

Annotation	**Flybase ID**	**Log_2 fold-change**	**p-value**	**Molecular function/Biological Process**
CG9676	FBgn0030773	1.17	5.00E-5	Serine-type endopeptidase activity/proteolysis
Histone deacetylase 4	FBgn0041210	1.09	5.00E-5	Histone deacetylase activity/long-term memory; regulation of transcription, DNA templated
CG11211	FBgn0041210	1.07	5.00E-5	Carbohydrate binding; mannose binding/unknown
CG15068	FBgn0040733	1.03	5.00E-5	Unknown/unknown
CG9377	FBgn0032507	0.95	5.00E-5	Unknown/unknown
UDP-glycosyltransferase 35b	FBgn0026314	0.94	5.00E-5	UDP glycosyltransferase activity, transferring hexosyl groups/UDP glucose metabolic process
CG8343	FBgn0040502	0.89	5.00E-5	Carbohydrate binding; mannose binding/unknown
CG8329	FBgn0036022	0.84	5.00E-5	Serine-type endopeptidase activity/proteolysis
Niemann-Pick type C-2g	FBgn0039800	0.80	5.00E-5	Sterol binding/hemolymph coagulation; mesoderm development; sterol transport
CG3088	FBgn0036015	0.71	5.00E-5	Unknown/unknown
Ornithine decarboxylase 1	FBgn0013307	0.69	5.00E-5	Ornithine decarboxylase activity/polyamine biosynthetic process

CG5840	FBgn0038516	0.68	5.00E-5	Pyrroline-5-carboxylate reductase activity/oxidation reduction process; proline biosynthetic process
*white**	FBgn0003996	0.67	5.00E-5	Eye pigment precursor/eye pigment precursor transporter activity
CG6503	FBgn0040606	0.67	5.00E-5	Unknown/unknown
Short spindle 7	FBgn0052667	0.66	5.00E-5	Unknown/mitotic spindle assembly; multicellular organism reproduction
Odorant-binding protein 99d	FBgn0039684	-1.68	5.00E-5	Odorant binding/autophagic cell death, inter-male aggressive behaviour
Larval serum protein 2	FBgn0002565	-1.38	5.00E-5	Nutrient reservoir activity/motor neuron axon guidance; synaptic target inhibition
CG9701	FBgn0036659	-1.35	5.00E-5	Hydrolase activity, hydrolysing O-glycosyl compounds/carbohydrate metabolic process
CG4757	FBgn0027584	-1.27	5.00E-5	Carboxylic ester hydrolase activity/unknown
CG18473	FBgn0037683	-1.27	5.00E-5	Aryldialkylphosphatase activity; hydrolase activity; zinc ion binding/catabolic process
CG6409	FBgn0036106	-0.90	5.00E-5	Unknown/GPI anchor biosynthetic process
Laminin A	FBgn0002526	-0.77	5.00E-5	Receptor binding/axon guidance; brain morphogenesis, cell adhesion by integrin; inter-male aggressive behaviour; locomotion involved in locomotory behaviour; negative regulation of synaptic growth at neuromuscular junction
Kekkon-2	FBgn0015400	-0.72	5.00E-5	Unknown/unknown
Carbonic anhydrase 2	FBgn0027843	-0.71	5.00E-5	Carbonate dehydratase activity; one carbon metabolic process
Activity-regulated	FBgn0033926	-0.69	5.00E-5	Nucleic acid binding/ zinc ion binding; behavioural

cytoskeleton associated protein 1				response to starvation; muscle system process
Odorant-binding protein 56d	FBgn0034470	-0.68	5.00E-5	Odorant binding/olfactory behaviour; response to pheromone; sensory perception of chemical stimulus
Homogentisate 1,2-dioxygenase	FBgn0040211	-0.55	1.50E-4	Homogentisate 1,2-dioxygenase activity; L-phenylalanine catabolic process; oxidation-reduction process, tyrosine catabolic and metabolic process
CG31205	FBgn0051205	-0.54	1.50E-4	Serine-type endopeptidase-activity/proteolysis

Table 6.11 RNASeq data from DmHDAC4 overexpression.
This data shows the changes in expression following the overexpression of *Drosophila* HDAC4 in the adult fly brain to a control line harbouring the driver but no construct. (Data adapted from Schwartz, 2016).

Comparing this data from overexpression of *Drosophila* HDAC4 to the RNASeq data from this project in which human 3SA or L175A mutants were expressed shows a significant overlap in expression changes. Importantly, many of these are differentially up- or down-regulated in the same direction (Table 6.12). This is an extra step in the validation of the previous results as it confirms that the human HDAC4 (which L175A and 3SA are both mutants of) facilitates similar transcriptional changes in the *Drosophila* model in a similar manner to the DmHDAC4, of the 26 genes (not including *w* and *DmHDAC4*) differentially expressed in the previous work, 14 were also differentially expressed in this project, approximately 54% of the total.

Annotation	FlyBase ID	L175A vs. Control	3SA vs. Control	L175A vs. 3SA	DmHDAC4OE vs. Control
Ugt35b	FBgn0026314	2.16	2.50	0.34	0.94
CG8343	FBgn0040502	0.89	1.50	0.63	0.89
CG8329	FBgn0036022	0.47	0.83	0.38	0.84
Npc2g	FBgn0039800	0.68	1.12	0.46	0.8
CG3088	FBgn0036015	0.56	1.23	0.69	0.71
Odc1	FBgn0013307	0.52	0.76	0.25	0.69

P5cr-2	FBgn0038516	0.59	1.14	0.55	0.68
w	FBgn0003996	0.26	0.27	0.02	0.67
CG6503	FBgn0040606	-0.27	0.33	0.61	0.67
ssp7	FBgn0052667	0.46	0.99	0.55	0.66
Obp99d	FBgn0039684	-2.85	-1.92	0.93	-1.68
CG4757	FBgn0027584	0.63	1.11	0.50	-1.27
CG18473	FBgn0037683	-0.94	-0.65	0.31	-1.27
kek2	FBgn0015400	-2.28	-2.96	-0.67	-0.72
CG31205	FBgn0051205	-1.62	-0.01	1.62	-0.54

Table 6.12 Comparison of log_2-fold changes in read counts from the overexpression of DmHDAC4 (Schwartz, 2016), L175A, and 3SA compared to controls.

The data from the DmHDAC4 overexpression RNASeq was used to search a dataset that constituted all genes that were significantly overexpressed in any one of the three analyses carried out in this project. DmHDAC4OE data from Schwartz, 2016.

The *white* gene in this data is carried on the pUASTattB plasmid used for transgenesis and is a selectable marker for transformants. The expression of the *white* gene is, as such, susceptible to position effects resulting from the chromatin environment of the insertion site in the genome. Altered expression levels of *white* between samples would indicate different availability of the construct to transcription machinery, a factor that could indicate insertion of the constructs into different genetic sites. The expression of white was consistent between the two samples (0.27 and 0.26-fold up-regulation respectively), this provides confidence that the observed changes in expression observed between the samples are due to real differences in their activity and not differences in expression levels.

A brief literature review was carried out on the genes that were common between the two transcriptomic analyses to determine potential candidates for future projects. Candidates highlighted for future investigation are those that were part of highly enriched pathways in the hHDAC4 analysis or those that may have a role in learning, memory and development.

Ugt35b

Ugt35b encodes a protein that is part of the UDP-glycosyltransferase family 35 which are part of the cytochrome P450 pathway. They function by catalysing the production of glycosides and are proposed to be part of the detoxification process for the removal of xeno- and endo-biotics in insects (Wang *et al.*, 1999b). This is interesting as it was noted that 3SA up-regulated genes with GO terms associated with drug and xenobiotic metabolism, suggesting *Ugt35b* could be the primary axis through which HDAC4 interacts with this pathway (Section 6.8). The UGT family is large, with some 30 genes identified as potential UGT genes in *Drosophila* (Luque and O'Reilly, 2002). This protein has not been well studied but has been suggested to be highly expressed in the adult fly, particularly the antennae and is potentially involved in olfactory perception in *Drosophila* (Wang *et al.*, 1999b; Ahn *et al.*, 2012).

CG31205

CG31205 encodes a protein of unknown function, however, Interpro designated functions based of functional domains suggest that it acts as a serine protease (Mitchell *et al.*, 2019). This is possibly a result of autonomous regulation of protein homeostasis in the neuron, acting to prevent the accumulation of HDAC4, a proposal supported by Backs *et al.,* (2011) in which the serine protease inhibiter was shown to inhibit the formation of a small N-terminal cleavage product from HDAC4 which contains the nuclear-localisation sequence and protein interaction domain. This was also one of the few genes that was significantly differentially expressed between the L175A and 3SA samples.

Obp99d

Obp99d encodes one of a large family of odorant binding proteins that are required for olfactory perception of *Drosophila* (Hekmat-Scafe *et al.*, 2002). The OBP family is composed of 52 members in *Drosophila* and are most likely involved in the solubilisation and transport of odorants (Vieira and Rozas, 2011). Obp99d is part of the Minus-C subfamily, so called because they do not contain

the six-conserved cysteine residues present in most OBPs but is something of an outlier in this group as Obdp99d does have these residues (Hekmat-Scafe *et al.*, 2002). Olfactory sensation is a commonly used medium for testing long- and short-term memory in *Drosophila* and could play a role in pheromone detection during courtship.

CG4757

CG4757 was first identified in a ChIP-MS study in 2013, focusing on male-specific lethal (MSL) enriched histone modifications (Wang *et al.*, 2013). It has subsequently been further studied and termed NDF (nucleosome-destabilising factor), acting to destabilise nucleosomes by stimulating acetylation of H3K56 by p300, increasing transcription (Fei *et al.*, 2018). This is the only gene that was regulated in the opposite direction between the *Drosophila* HDAC4 and the human variants, being up-regulated 1.55-fold and 2.16-fold by the expression of L175A and 3SA respectively and down-regulated 2.41-fold by overexpression of DmHDAC4.

kek2

kek2 or *kekkon 2* is one of family of genes that express proteins involved in transmembrane transport, initially characterised as a pair of proteins (Musacchio and Perrimon, 1996) it has since come to light that they are part of a family of six proteins that are Tyrosine Kinaseless (TyrK-less) tyrosine kinase receptors (MacLaren *et al.*, 2004; Mandai *et al.*, 2009). *Kek2* was up-regulated in induced seizure model that triggers neuronal activity (Guan *et al.*, 2009), interestingly, *mthl8* (a strongly up-regulated gene in the hHDAC4 analysis) was down-regulated in this study. This pattern of gene regulation is directly opposite to that observed in the 3SA and L175A overexpression samples in which *kek2* was down-regulated and *Mthl8* was up-regulated. This supports the existing paradigm that HDAC4-based repression of gene expression is alleviated through activity-induced nuclear export of HDAC4 and that increased nuclear abundance decreased *kek2* expression and nuclear export driven by neuronal stimulation may lead to increased *kek2* expression.

6.10 Candidate genes from RNASeq analysis

Following the transcriptome analysis, functional studies will ideally be performed on candidate genes in an effort to elucidate more information about these genes and the role they play in neuronal development and memory. In this section, several genes were investigated for potential roles in neurological development. Candidates for literature reviews were selected based on their relevance to neurological function as well as the availability of fly stocks. Additionally, genes that were differentially expressed between L175A and 3SA groups were of more interest as these could be the causative factors in the different phenotypes observed between nuclear and cytoplasmic HDAC4.

mthl8

mthl8 or *methuselah-like 8* is part of the Methuselah-like family of genes named after the *Drosophila* Methuselah G-protein coupled receptor. This group harbours 15 paralogs, *Mthl1-15*, each of which express proteins with an N-terminal ectodomain, a seven transmembrane domain and a short intracellular C-terminal domain (Araujo *et al.*, 2013). These proteins have generally been identified as playing a role in ageing and reproduction (West *et al.*, 2001) as well as being involved in the regulation of neurotransmitter release in the larval neuromuscular junction (Song *et al.*, 2002). The expression of *mthl8* appears to be variable, transcriptome analysis in adult *Drosophila* has previously shown very low levels of expression in the nervous system (Guan *et al.*, 2011). However, *Mthl8* has also been observed to be down-regulated in flies expressing a mutant of the erg K^+ ion channel known as sei that can be used to induce paralytic seizures in *Drosophila* (Titus *et al.*, 1997). This observed down-regulation showed that, in certain circumstances, the Mthl8 protein is expressed, suggesting that its role may not be exclusively in larval flies (Guan *et al.*, 2009).

The base read count of *mthl8* in the control sample in this study was 0, supporting results from Guan *et al.*, 2011 suggesting that adult flies do not express *mthl8* under normal conditions. Expression was induced by both the 3SA and L175A

HDAC4 variants, therefore further investigation as to whether *Mthl8* plays a role in neuronal development and whether alteration of its expression is a mechanism through which HDAC4 impairs development is warranted.

ACXD

ACXD or *adenylyl cyclase XD* (or AC10D) expresses a largely uncharacterised transmembrane adenylyl cyclase. Adenylyl cyclases have previously been characterised as key proteins in *Drosophila* learning and memory ever since the discovery of *Rutabaga* (Livingstone *et al.*, 1984; Ishikawa and Homcy, 1997). In the initial identifying study, it was shown that *acxd* is expressed highly at the end of embryogenesis, larval stage 3 and adult flies in both male and female flies, in contrast to the other three ACX genes which are expressed in male flies only (Cann *et al.*, 2000). This could suggest that ACXD has a more general role in learning and memory than the other ACX isoforms and could imply that ACXD is a primary target through which HDAC4 exerts its influence on memory and development.

fu12

fu12 encodes a 1-acylglycerol-3-phosphate-*O*-acyltransferase (AGPAT), specifically AGPAT2. AGPATs localise to the endoplasmic reticulum and lipid droplets within cells and are involved in the synthesis of triacylglycerides (Wilfling *et al.*, 2013). In *Drosophila* it has been suggested that multiple AGPATs play a role in ethanol response, undergoing a significant change in expression when the fly is exposed to ethanol (Morozova *et al.*, 2006; Urizar *et al.*, 2007; Kong *et al.*, 2010). Additionally, when expression of *fu12* is disrupted through transposon insertion, flies exhibit an increase in ethanol induced hyperactivity through a greater distance travelled during exposure (Kong *et al.*, 2010). Interestingly, the *Drosophila* homologue of HDAC1/2, *Rpd3* was shown to be significantly differentially expressed in two of these studies (Morozova *et al.*, 2006; Kong *et al.*, 2010). This is of note as *Rpd3* overexpression and knockdown in the fly brain has been shown to impair memory (Fitzsimons and Scott, 2011).

kat80

kat80 encodes one of the two subunits for katanin, a microtubule-severing protein. The second subunit of katanin is encoded by *kat60* in humans, a gene that has two paralogues in *Drosophila* (CG10229 and CG1193) (Goldstein and Gunawardena, 2000), neither of which were differentially expressed in any of the samples tested. The kat80 subunit is responsible for the targeting of the Katanin heterodimer and mediation of its disruption of the contacts within the microtubule lattice. Particularly interesting is that Katanin is essential for the neuronal morphogenesis, similarly to HDAC4 (McNally and Vale, 1993; McNally *et al.*, 2000; Yu *et al.*, 2008). Additionally, it has been observed that the microtubule trimming (and associated dendrite pruning) activity of the second subunit, Kat60, is down-regulated by over-expression of HDAC6 in cultured mammalian cells (Mao *et al.*, 2014) which could indicate that DmHDAC4 and DmHDAC6 are co-ordinated regulators of dendrite growth regulation.

npc2g

Niemann-pick type C-2 (*npc2*) genes encode proteins that are involved in cholesterol homeostasis. The Npc2g protein is responsible for the export of cholesterol from endosomal compartments, allowing the cholesterol to move to other membrane regions (Liscum and Faust, 1987; Patterson, 2003). Mutations in two of the human *NPC2* genes (*NPC1* and *NPC2*) result in Niemann-Pick type C disease, a disorder that causes hepatic and pulmonary failure as well as neurological disorders (Patterson, 2003). In *Drosophila*, there are eight known *npc2*-like genes (*npc2a-h*), *npc2g* has been shown to be expressed specifically in the head mesoderm and fat body (Huang *et al.*, 2007; Fisher *et al.*, 2012). This is unexpected as this gene was differentially expressed in the previous transcriptome analysis in our lab (Schwartz, 2016) and during both experiments, HDAC4 expression was driven by elav, which purportedly does not express in the mesoderm or fat body (Robinow and White, 1988). Thus, it must be assumed that the Npc2g-associated cholesterol metabolism may have a function in neurological activity that is affected by HDAC4.

6.11 Screening candidate genes for interactions with HDAC4

The candidates discussed in section 6.10 were selected to undergo screening to determine if they played a role in *Drosophila* development and/or interacted genetically with HDAC4. Co-expression of an RNAi targeting the gene of interest with each of the HDAC4 variants in the eye allows for the visualisation of potential developmental defects incurred and, if the genes interact, could result in a more severe disruption than by altering the levels of each protein on their own, as described in section 2.2.

To investigate possible interactions, a fly strain carrying a UAS-RNAi inverted repeat targeted to an individual candidate gene was crossed to GMR-GAL4, the progeny were raised at 25°C and adults were examined for deficits in eye development via light microscopy and scanning electron microscopy. Each line was also co-expressed with UAS-DmHDAC4, UAS-hHDAC4, UAS-L175A and UAS-3SA to determine whether there was a more severe disruption than either the RNAi or each HDACv alone.

Unfortunately, flies homozygous for GMR-GAL4; UAS-3SA were non-viable (referenced in Section 3. 4) and so only DmHDAC4, hHDAC4 and L175A could be co-expressed with the RNAi lines. Knockdown of *AXCD*, *fu12*, *kat80*, *mthl8*, and *npc2g* resulted in no impairments to ommatidial development (Figure 6.16 – 6.19, top row). Therefore, if any of genes interact in the same pathway as HDAC4 an enhancement of the HDAC4 phenotype would be expected.

Representative high magnification SEM images of the phenotypes resulting from expression of each HDACv or the GMR-driver alone are shown below (Figure 6.15).

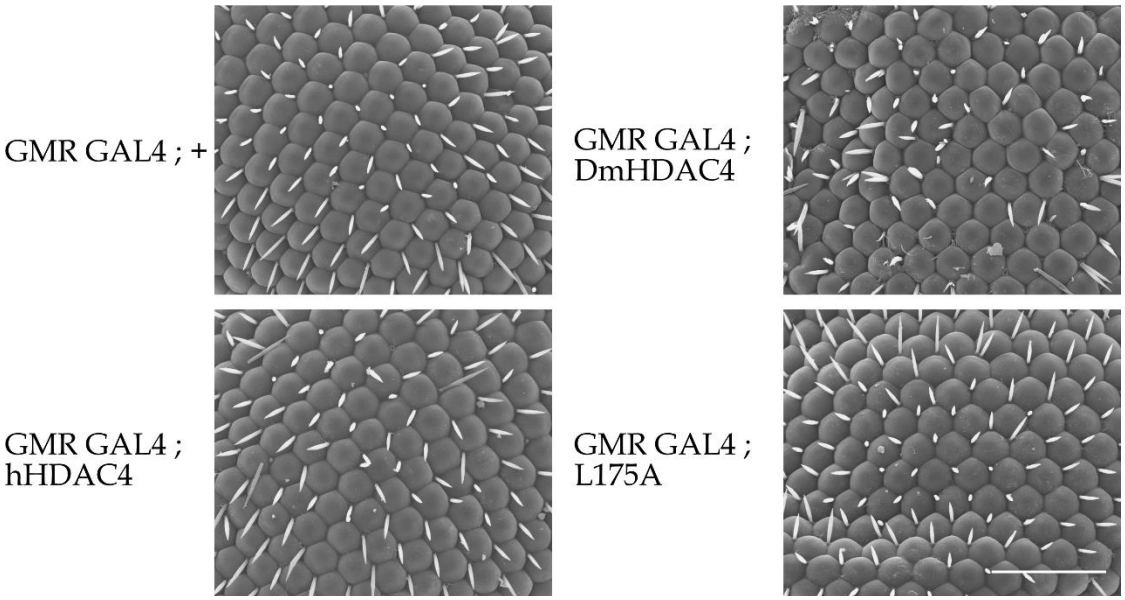

Figure 6.15 Representative image of GMR-driven HDACv in fly eyes.
Scanning electron microscopy of flies harbouring one copy of GMR driving either DmHDAC4, hHDAC4, or L175A. The control and L175A have almost no discernible disruption. hHDAC4 causes a mild disruption to bristle patterning. DmHDAC4 shows altered ommatidia shapes and clearly disrupted bristle patterning. Scale bar = 50 μm.

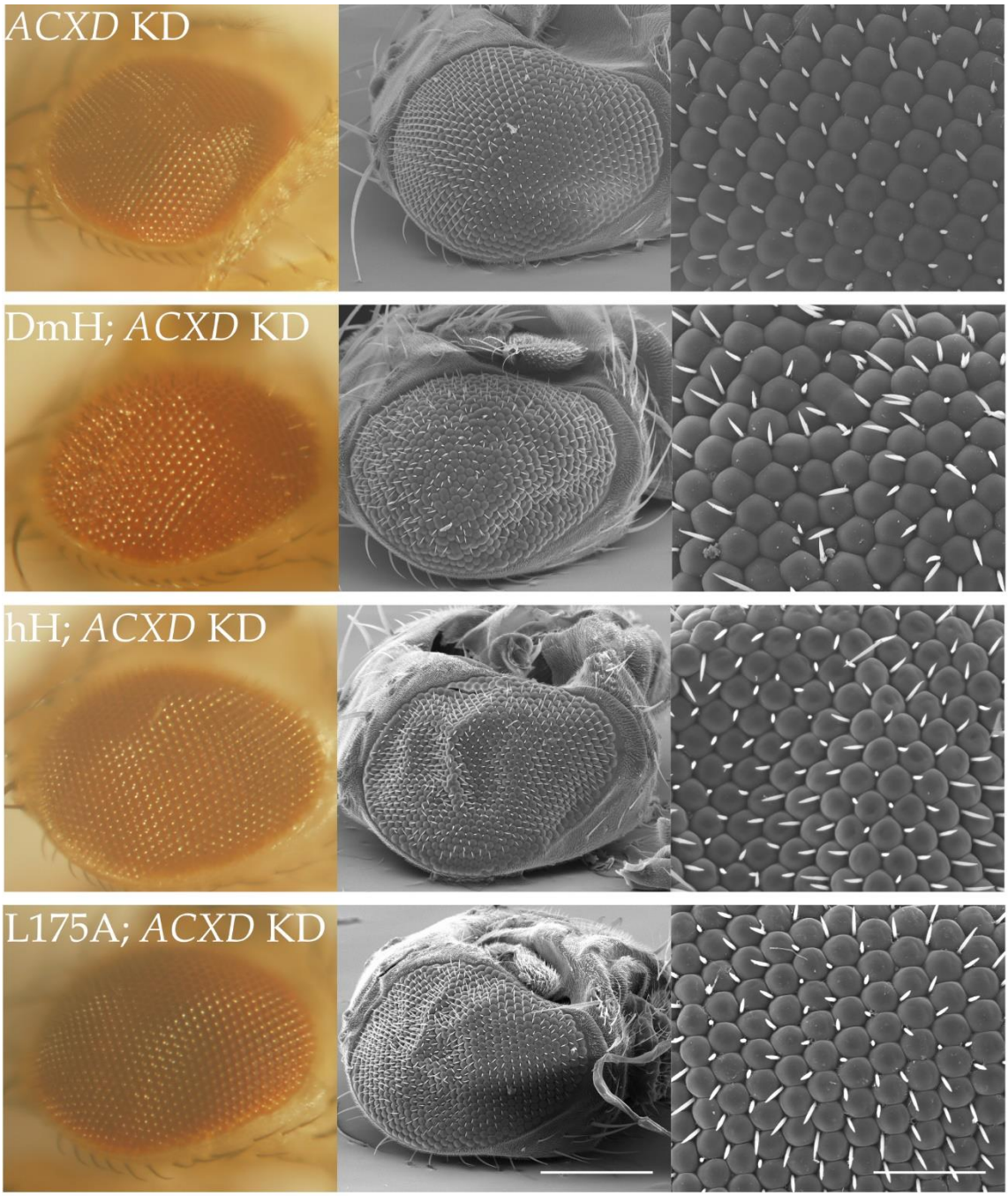

Figure 6.16 Representative images of *ACXD* KD in *Drosophila* eyes.
Light and scanning electron microscopy images of fly eyes expressing RNAi targeted to *acxd* as well as either DmHDAC4 (DmH; *ACXD* KD), hHDAC4 (hH; *ACXD* KD), L175A (L175A; *ACXD* KD) or on its own (*ACXD* KD). Expression of each construct is driven by the GMR-GAL4 driver. Scale bar for middle column is 200 µm and for the right-hand column is 50 µm.

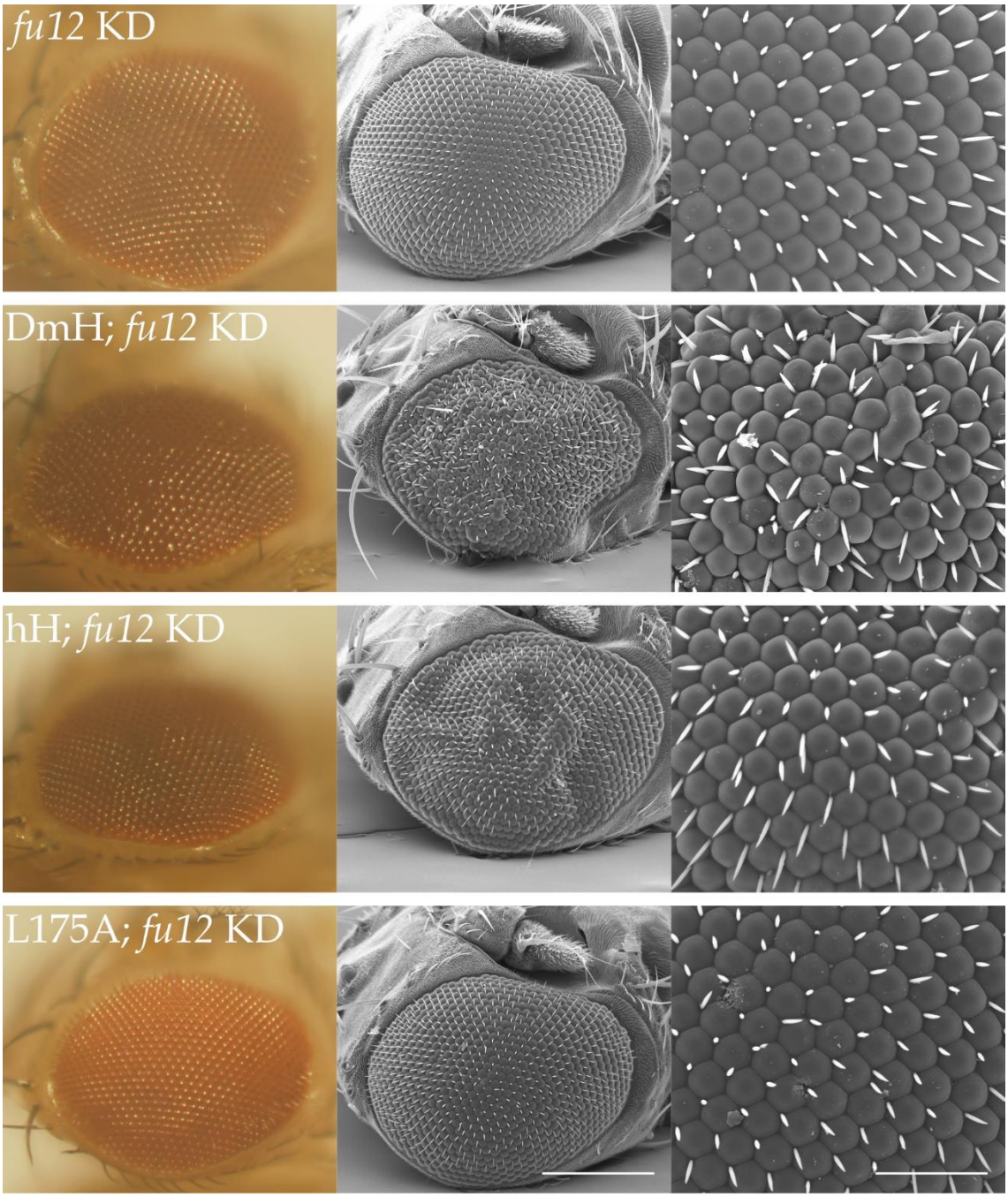

Figure 6.17 Representative images of *fu12* KD in *Drosophila* eyes.
Light and scanning electron microscopy images of fly eyes expressing RNAi targeted to *fu12* as well as either DmHDAC4 (DmH; *fu12* KD), hHDAC4 (hH; *fu12* KD), L175A (L175A; *fu12* KD) or on its own (*fu12* KD). Expression of each construct is driven by the GMR-GAL4 driver. Scale bar for middle column is 200 μm and for the right-hand column is 50 μm.

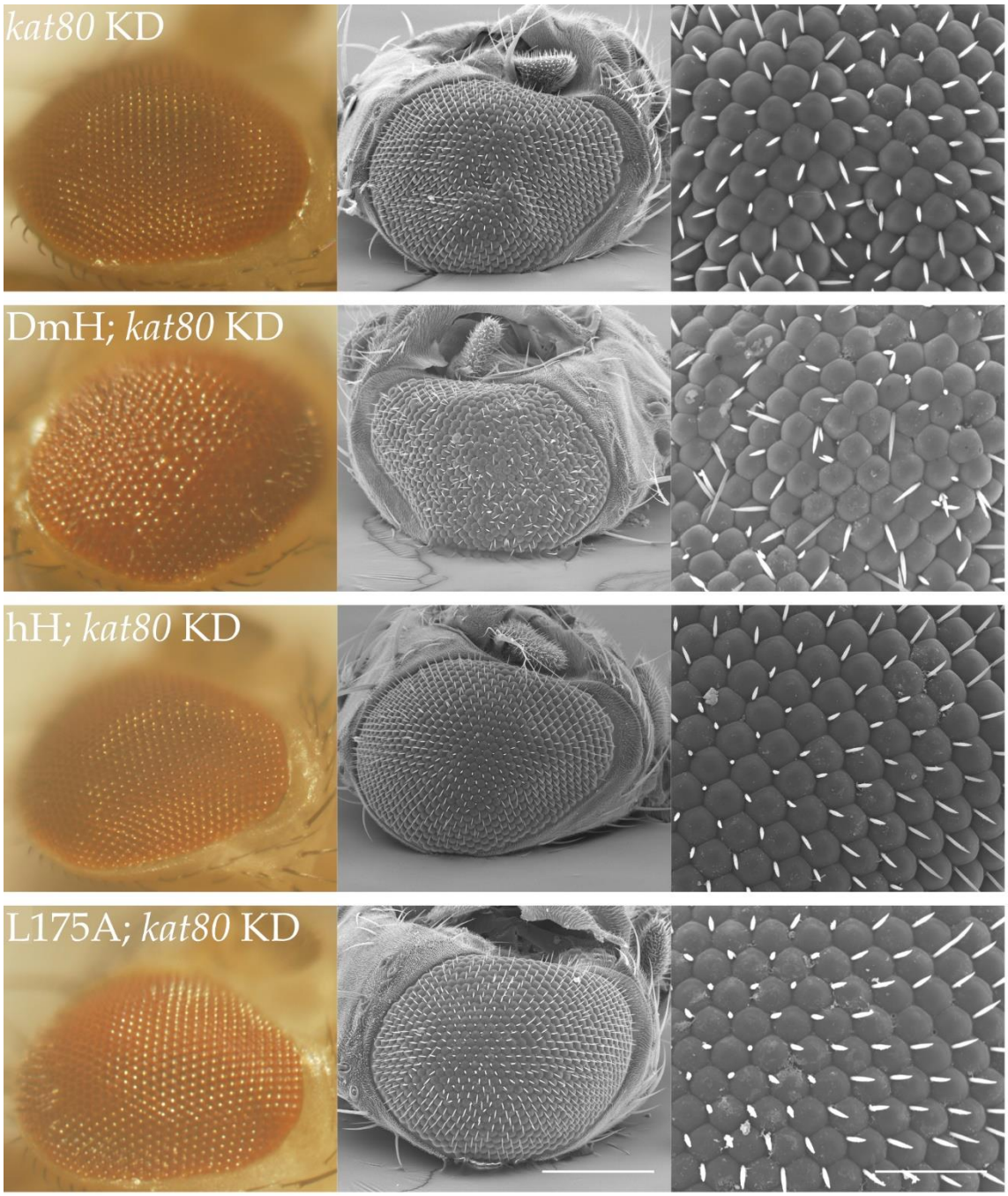

Figure 6.18 Representative images of *kat80* KD in *Drosophila* eyes.
Light and scanning electron microscopy images of fly eyes expressing RNAi targeted to *kat80* as well as either DmHDAC4 (DmH; *kat80* KD), hHDAC4 (hH; *kat80* KD), L175A (L175A; *kat80* KD) or on its own (*kat80* KD Expression of each construct is driven by the GMR-GAL4 driver. Scale bar for middle column is 200 μm and for the right-hand column is 50 μm.

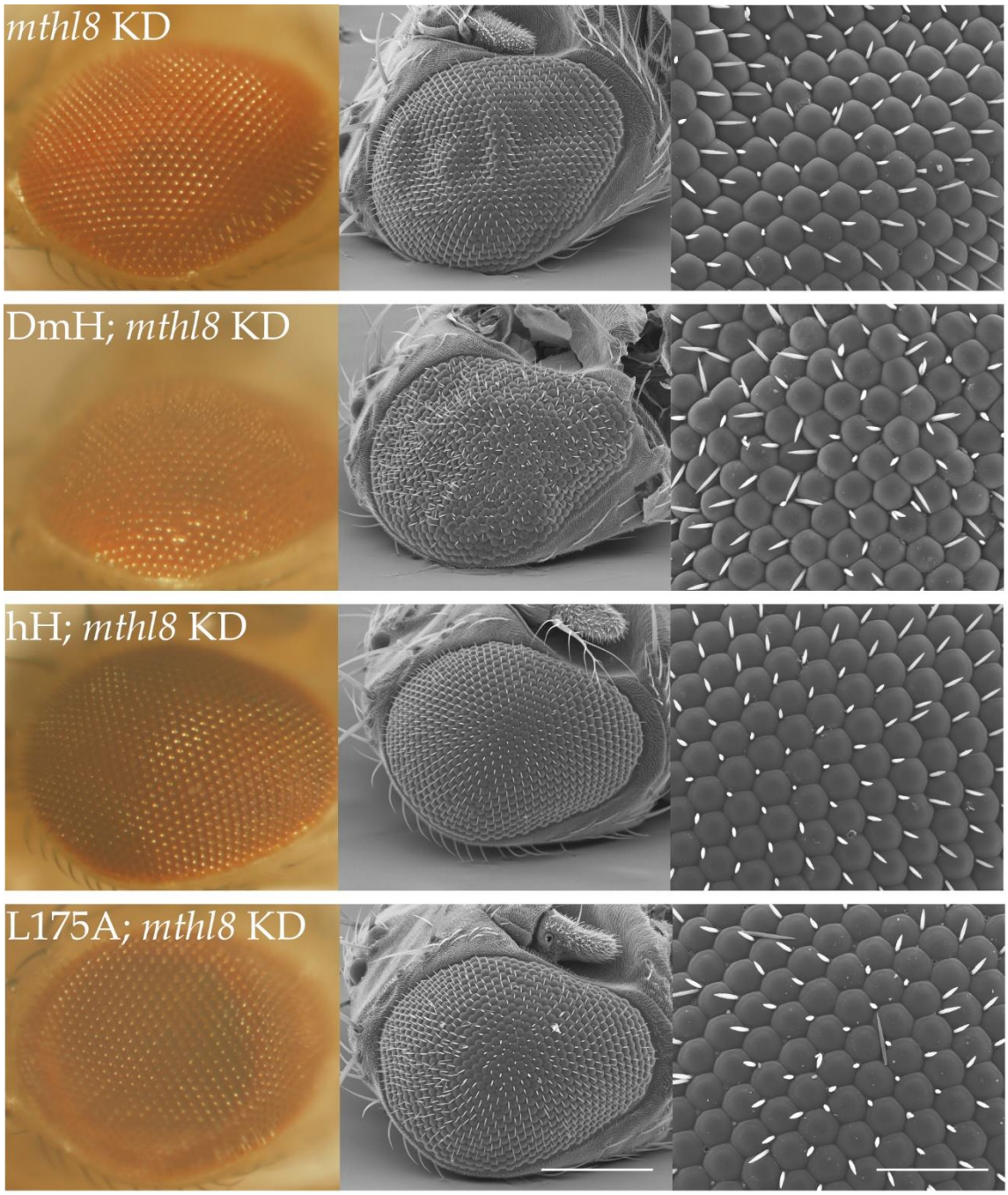

Figure 6.19 Representative images of *mthl8* KD in *Drosophila* eyes.
Light and scanning electron microscopy images of fly eyes expressing RNAi targeted to *mthl8* as well as either DmHDAC4 (DmH; *mthl8* KD), hHDAC4 (hH; *mthl8* KD), L175A (L175A; *mthl8* KD) or on its own (*mthl8* KD). Expression of each construct is driven by the GMR-GAL4 driver. Scale bar for middle column is 200 μm and for the right-hand column is 50 μm.

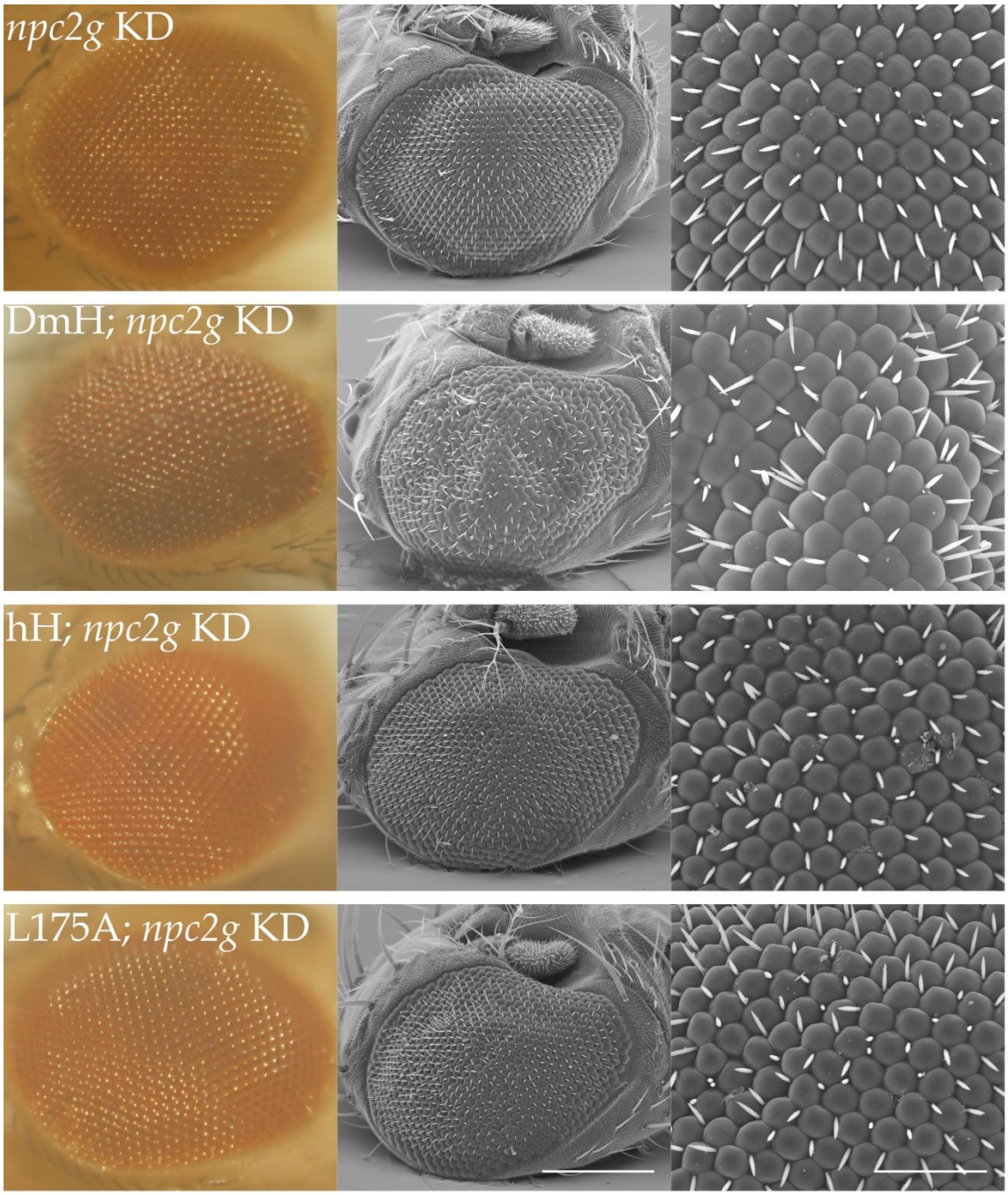

Figure 6.20 Representative images of *npc2g* KD in *Drosophila* eyes.
Light and scanning electron microscopy images of fly eyes expressing RNAi targeted to *npc2g* as well as either DmHDAC4 (DmH; *npc2g*), hHDAC4 (hH; *npc2g*), L175A (L175A; *npc2g*) or on its own (*npc2g* KD). Expression of each construct is driven by the GMR-GAL4 driver. Scale bar for middle column is 200 µm and for the right-hand column is 50 µm.

Comparing the eye phenotypes to the reference images in Figure 6.14 shows that none of the chosen candidate genes have an appreciable effect on eye development when individually expressed. However, some minor additive effects can be observed between the HDACv and *fu12* knockdown, *kat80*

knockdown, and *npc2g* knockdown. It was observed that *fu12* KD exacerbates the effects of DmHDAC4 OE with increased frequency of duplicate bristle growths and disrupted ommatidial patterning, including several sets of fused ommatidia (Figure 6.17). This is somewhat unexpected as it has been assumed that increased nuclear abundance is the main factor of developmental disruption caused by HDAC4 and *fu12* expression was up-regulated by 3SA compared the L175A.

Co-expression of *kat80* RNAi with DmHDAC4 had a similarly synergistic effect, not disrupting the development on its own but when co-expressed with DmHDAC4 resulted in more frequent duplicate bristles as well as occasional fused ommatidia (Figure 6.18). This is a result that is more neatly predicted by the RNASeq as *kat80* was down-regulated by 3SA when compared with L175A, thus, overexpression of the largely nuclear DmHDAC4 is most likely already reducing levels of *kat80* transcription and the RNAi reduces it further.

The knockdown of *npc2g* was the only candidate chosen for this preliminary screen that resulted in a synergistic effect when co-expressed with the hHDAC4 and L175A variants (Figure 6.20). Neither hHDAC4; L175A or *npc2g* KD alone had any obvious effect on eye development, whereas in both cases, when co-expressed the ommatidia formed more rounded shapes with deeper clefts between each facet, indicating a probable genetic interaction. This phenotype is not observed when *npc2g* RNAi is co-expressed with DmHDAC4, despite the fact that it is up-regulated by L175A, 3SA and DmHDAC4 OE alike. This lack of synergistic phenotype may be due to the subtle disruption caused by *npc2g* KD being masked by the much stronger phenotype of DmHDAC OE in the eye.

6.12 Discussion

This RNASeq data has provided a new insight to the role of HDAC4 in *Drosophila* neurons. It was previously suggested that the primary role of HDAC4 was repression of transcription factors in the nucleus that was alleviated by nuclear export of HDAC4 to permit the formation of LTM. It was proposed recently that this nuclear repression may not be the sole activity of HDAC4 as it was discovered OE and KD of HDAC4 in the *Drosophila* brain impaired LTM formation, showing that HDAC4 is both required for and a repressor of memory formation (Fitzsimons *et al.*, 2013).

Previous transcription analysis was carried out in our lab in which DmHDAC4 was overexpressed in fly brains. The observed changes in transcription were surprisingly minimal given HDAC4's proposed role as a transcriptional repressor. It was proposed, initially, that the reason only a small number of genes were significantly altered was because, as DmHDAC4 is only nuclear in a subset of cells, the transcription repression and subsequent changes were being diluted by the number of neurons without nuclear HDAC4. Thus, this project attempted to abrogate this dilution effect by comparing two variants of HDAC4 that were highly abundant in the nucleus or the cytoplasm across all neurons.

The data shows a large number of genes were differentially regulated in the fly lines expressing 3SA and L175A. >600 genes are significantly differentially expressed between the L175A sample and the control, with >200 significantly differentially expressed between the 3SA and control. Despite the abundance of differentially expressed genes only a small number were significant between the flies expressing 3SA and those expressing L175A. The differences between these two constructs support the observations in previous RNASeq work in our lab which showed that DmHDAC4 is not a global regulator of transcription but regulates a small subset of genes in a specific manner (Schwartz, 2016).

The presence of transcriptional changes at all is somewhat intriguing as the L175A HDAC4 variant is restricted to the cytoplasm (Section 3.2). While some of

these changes could be induced by the altered levels of protein (the cell responding to elevated levels of cytoplasmic HDAC4 by importing endogenous DmHDAC4 into the nucleus, for example), the scope of the differential expression implies a cytoplasmically-linked activity for HDAC4 in transcription regulation, perhaps by sequestering transcription factors at the nuclear periphery or in the cytoplasm.

The fact that most of the genes that were differentially expressed between L175A and control were also differentially expressed between 3SA and control is potentially reflective of the observation that, despite the mutation of the 14-3-3ζ binding regions and subsequent nuclear abundance, the 3SA variant of hHDAC4 still retains a high cytoplasmic presence. This indicates that the 29 differentially expressed genes are due to the actions of HDAC4 in the nucleus. It can thus be assumed that the other genes that are differentially expressed are due to cytoplasmic hHDAC4.

The observation that only 29 genes were differentially expressed between L175A and 3SA shows that the nuclear abundance of hHDAC4 does not widely affect transcription. This is interesting as the phenotypes observed when the nuclear abundance of hHDAC4 is increased (in the 3SA expressing brains) are drastic, both during development and in memory with severe mushroom body defects and severely impaired long-term memory formation. One possible answer is that expression of 3SA leads to a form of transcription-independent disruption to development, perhaps through the formation of protein aggregates that prevent appropriate transport of subcellular components or, possibly, that the nuclear accumulation of the 3SA leads to an overload of the protein degradation pathways, resulting in a build-up of other factors that are required for normal development. The role of HDAC4 as post-translational modifier has been suggested previously, particularly due to its interaction with the SUMOylation machinery (Gregoire and Yang, 2005; Wilkinson *et al.*, 2010; Schwartz *et al.*, 2016). It is possible that the nuclear accumulation of HDAC4 leads to abnormal SUMOylation of nuclear proteins, leading to their rapid degradation or

interfering with binding to affect cellular protein balance in a non-transcriptional fashion.

After initial GO-term analysis to highlight affected pathways, it was decided to split the significantly altered genes into groups up- and those down-regulated by 3SA and L175A independently. This allowed for a much clearer analysis of the potential role of nuclear and cytoplasmic HDAC4 in *Drosophila* brains.

In the L175A vs. Control sample, five pathways from the up-regulated genes were identified as having an enrichment score greater than two (Table 6.9). Of these, the top four had initially confusing properties. The first, overwhelmingly most highly enriched group, was composed of ribosomal and translational proteins. The third was similar, being highly enriched for rRNA binding proteins. These suggest that cytoplasmic HDAC4 is acting to recruit translational machinery. The fourth-most enriched was enriched for so-called ATP- "grasp-fold" proteins. Brief investigation into these suggest that they may be related to the ribosomal/translational machinery and ATP-"grasp-fold" proteins are exclusively related to carboxylic acid nucleoside substitutions, a reaction that is common in amino acid synthesis. Finally, the second-most enriched annotation group is enriched for IMP biosynthesis and purine metabolism. IMP biosynthesis is the synthesis of inosine monophosphate, the first nucleotide formed during the synthesis of purine (Zalkin and Dixon, 1992). Thus, of the five significantly altered pathways, four were related to translation of protein synthesis, suggesting that the cytoplasmic HDAC4 is capable and, perhaps, responsible for shifting the neuron into a sort of "ready-state" in which the induction of protein synthesis following neuronal activation is able to be rapidly engaged. The final group was enriched for cell-cell adhesion, synaptic transmission and other terms typically associated with neuron function. This implies that cytoplasmic HDAC4 has an active role in promoting increased axonal development and synaptic transmission, though this may be a minor facet of its main activity in cellular metabolism.

Furthering the hypothesis that cytoplasmic HDAC4 is engaging in a metabolic shift is that the sole significantly enriched group of genes down-regulated by L175A is comprised of oxidoreductase and glucose dehydrogenase-related terms, suggesting a minor downturn in the catabolic pathways of the neurons (Table 6.9).

Finally, the 3SA up-regulated genes that were sorted into three ontological groups (Table 6.10). The first and third of these were somewhat perplexing, relating to bacterial defence and immune response, and drug/xenobiotic metabolism. This is potentially a mis-identification based on structural identification as several of the genes identified are associated with olfactory perception in *Drosophila* and, as such, have similar structural components to enzymes involved in drug metabolism due to their binding and transport of organic, volatile compounds (Wang *et al.*, 1999b; Vieira and Rozas, 2011; Ahn *et al.*, 2012).

The second-most enriched group was highly enriched for oxidoreductases, heme-binding proteins and cytochrome P450 pathway. On its own, this would be unsurprising as these pathways were highlighted in the grouped analysis, but the inverse was observed in the L175A sample, in which down-regulated genes showed enriched pathways for oxidoreductase pathways and cytochrome functions. This further supports the hypothesis that cytoplasmic HDAC4 prepares the neuron for protein synthesis, reducing the production of energy in the short-term to enable the rapid production of the many components involved in signal transduction and synaptic transmission of neurotransmitters. Oxidoreductase proteins have been shown to be down-regulated in ageing *Drosophila* (Pacifico *et al.*, 2018), correlating with deteriorating neuronal function. At first glance this appears to contradict the up-regulation shown in 3SA, but it seems that the down-regulation observed in aged flies is due to the up-regulated developmental processes (as is seen in L175A), reflective of increased cellular repair pathways as more rapid degradation occurs. Thus, up-regulating energy

generation processes disrupts cellular development, supporting the observed data in flies expressing highly nuclear HDAC4.

It was proposed in previous work in our lab that cytoplasmic HDAC4 plays an important role in neuronal function due to its interaction with cytoplasmic proteins (Schwartz, 2016). The data from transcription analysis supports this in two ways. Firstly, the abundance of transcriptional changes induced by the cytoplasmic restriction of HDAC4 suggest that the transcriptional role of HDAC4 is not exclusively nuclear and that it may act to sequester transcription factors away from the nucleus. The second is that, despite the >600 genes differentially expressed in the presence of L175A, no developmental or memory phenotypes were observed when L175A was expressed in *Drosophila*. This could suggest that cytoplasmic HDAC4 is playing an essential role in development and memory and it could be this that causes disruptions to neuronal function when HDAC4 is knocked down (Fitzsimons *et al.*, 2013).

Comparing the RNASeq results from this project to the transcription changes observed in the previous transcription analysis from our lab shows the conservation of HDAC4's activity between *Drosophila* and humans with 54% of the genes observed to be significantly altered by DmHDAC4 present in this screen (Table 6.11). Brief investigation of these suggested that many of them have potential roles in learning and memory and are excellent candidates for further investigation (Sections 6.9, 6.10).

Several candidate genes were selected for a brief investigation to determine if they were involved in development. Using the rough eye phenotype screen, five RNAi lines were co-expressed with HDAC4v to see if they had a synergistic effect on development. However, only three of the candidate genes showed increased disruption when co-expressed with any of the HDACv, *fu12*, *kat80* and *npc2g* knockdown resulted in synergistic effects when co-expressed with one or more of the HDAC4 variants. Of these, only *npc2g* KD showed an increased severity of phenotype with the wt-hHDAC4 and L175A, Npc2g is involved in cholesterol metabolism via endocytosis and has previously been shown to be expressed in

the head mesoderm and fat bodies (Huang *et al.*, 2007; Fisher *et al.*, 2012). It is the former that likely causes its interaction with GMR-driven HDACv as the development of the eye is a complex process involving the interactions of mesodermal and endodermal tissues, in addition to cell-cell interactions (Franzdóttir *et al.*, 2009). The previous data on the expression pattern of *npc2g* seems to conflict the data from this and previous RNASeq work as the leave-driver does not express in fat bodies, however, as insect fat bodies are highly involved in energy economies (Arrese and Soulages, 2010; Lee *et al.*, 2018b), the presence of this cholesterol managing protein could reflect the fact that HDAC4 is altering the basic metabolism of the cell, increasing it to a "ready state" and thus, exerting increased demands on the fly metabolism.

This is somewhat supported by the interaction between *fu12* KD and DmHDAC4 OE. As discussed earlier (Section 6.10) *fu12* is an AGPAT protein involved in the synthesis of triacylglycerides (Wilfling *et al.*, 2013). The *fu12* gene was down-regulated in the L175A sample and not significantly changed in the 3SA sample. As triacylglycerides are a form of long-term energy storage, this again suggests that cytoplasmic HDAC4 are acting to put the neuron in a "ready state". The increased severity of the eye phenotype observed could be a result of an imbalanced lipid metabolism as the DmHDAC4 is expressed. However, this does not explain why no such interaction was seen with L175A expression. It is possible that the effects are minor enough that the lack of disruption caused by L175A means that this change in lipid metabolism does not cause enough of a change on its own to be observed in the eye but could be investigated in the future, perhaps in conjunction with other metabolic pathways.

The final observed synergistic interaction was between DmHDAC4 and *kat80* KD. This was, perhaps, the most likely of the interactions given the current understanding of the activity of HDAC4 as the katanin heterodimer (of which Kat80 forms half) is essential for neuronal morphogenesis (McNally and Vale, 1993; McNally *et al.*, 2000; Yu *et al.*, 2008). *kat80* expression was also up-regulated in the L175A and down-regulated by 3SA (significantly when compared with the

L175A sample but not compared to control). As, of the three HDACv tested, DmHDAC4 was the only one with a significant nuclear presence the further knockdown of *kat80* expression logically resulted in a worsened phenotype when neuronal development is assayed. Indeed, further work investigating the role of HDAC4 in MB development would be a logical step in future projects.

The brief foray into characterising potential candidates for interactions with HDAC4 indicated some surprising results, suggesting that HDAC4 has a role in neuronal metabolism regulation rather than purely memory and development. This is supported by the GO-term analysis which suggested that metabolic pathways and biosynthesis may be increased by the cytoplasmic presence of HDAC4. While no key player in the role of HDAC4 in disease models was identified, many potential candidates were identified that bear further investigating. Additionally, the role of HDAC4 as a metabolic regulator is a novel proposition which could explain the severity of the effects of HDAC4 overexpression, despite its relatively small suite of apparent targets.

7 SUMMARY AND FUTURE DIRECTIONS

HDAC4 is a class IIa HDAC that has been implicated in learning, development and memory (Li *et al.*, 2012; Sando *et al.*, 2012; Morris *et al.*, 2012; Fitzsimons *et al.*, 2013). In mammalian systems it has been demonstrated that the nucleocytoplasmic shuttling of HDAC4 is mediated by neuronal activation and its nuclear exit may relieve repression of MEF2, CREB or other transcription factors (Chawla *et al.*, 2003; Backs *et al.*, 2011; Sando *et al.*, 2012) but this interaction has been poorly studied in *Drosophila*. Subsequently, this project aimed to elucidate the function and action of the nuclear and cytoplasmic pools of HDAC4 by altering the nuclear and cytoplasmic abundance of HDAC4 using DmHDAC4, hHDAC4 and two subcellular distribution mutants of hHDAC4, as discussed in section 3.1.

7.1 Increased nuclear but not cytoplasmic HDAC4 significantly impairs memory and development in *Drosophila*.

This study began with the intent to observe and characterise the effects of increasing the abundance of HDAC4 in the nucleus and cytoplasm separately both in the adult *Drosophila* brain and during development. To fulfil this, GFP-tagged variants of the DmHDAC4, hHDAC4-wt, hHDAC4-L175A and hHDAC-3SA were developed and the proposed subcellular distribution of each variant verified using confocal microscopy (Section 3.3). It was shown that the GFP-DmHDAC4 was largely cytoplasmic but localised to nuclear puncta, as observed previously (Fitzsimons *et al.*, 2013). Additionally, it was shown that the hHDAC4-wt and hHDAC4-L175A were almost entirely cytoplasmic but the 3SA variant exhibited extensive nuclear localisation and a high frequency of nuclear puncta. However, 3SA was also present in the cytoplasm and axons of the Kenyon cells. This is different to what has been observed in mammalian tissue culture, in which a 3SA variant was very tightly restricted to the nucleus (Backs *et al.*, 2011). This suggests a that a different regulatory system exists in *Drosophila* for the nuclear export of HDAC4 that is not present in mammals, a hypothesis supported by the

lack of NES in DmHDAC4 compared to hHDAC4 (Miska *et al.*, 1999). This unknown system may be a target for future investigations into the regulation of nucleocytoplasmic balance of HDAC4.

Having verified the subcellular distribution of the variants, the role of subcellular distribution of HDAC4 in neuronal development and long-term memory was investigated. By expressing each variant in the brain or eye throughout development, it was determined that DmHDAC4 impaired development of both organs, this supports previous research in our lab, in which overexpression of DmHDAC4 impaired mushroom body development (Schwartz, 2016). The nuclear-localising hHDAC4-3SA severely disrupted the brain and eye during development while, the cytoplasmic hHDAC4-L175A and hHDAC4-wt did not significantly alter development (Section 3.3). It is worth noting that the hHDAC4-wt is, like the L175A variant, almost completely cytoplasmic and it is this distribution that is most likely the cause for the minor phenotype. The primary investigation into the effects of nuclear and cytoplasmic overabundance of HDAC4 was consistent with predominant findings from mammalian studies in that the increased nuclear HDAC4 was the predominant cause of pathologies in systems with an excess of HDAC4. This supports the current paradigm as it has been shown in several different studies that nuclear accumulation of HDAC4 is deleterious to neuronal survival (Li *et al.*, 2012; Sando *et al.*, 2012; Wu *et al.*, 2017), indeed, nuclear HDAC4 has been identified as a causative factor in one case of BDMR, which is otherwise caused by haploinsufficiency of HDAC4 (Williams *et al.*, 2010; Morris *et al.*, 2012). The observation that L175A did not significantly alter eye development supports previous research in which the knockdown of HDAC4 reduced photoreceptor survival, an effect that was deemed to be due to the depletion of cytoplasmic HDAC4, suggesting that cytoplasmic HDAC4 is somehow required for maintenance of neuronal integrity (Chen and Cepko, 2009).

Following developmental investigation, each variant was expressed exclusively in the adult mushroom body and long-term memory was tested, measured using

the courtship suppression assay. This showed that, as previously identified (Fitzsimons *et al.*, 2013), expression of DmHDAC4 severely impaired long-term memory formation. It was also shown that wt- hHDAC4 and nuclear hHDAC4-3SA severely impaired long-term memory formation whereas the totally cytoplasmic L175A did not significantly impair long-term memory (Section 4.2). This data supported the current literature that indicates increased nuclear as the primary causative factor in the deleterious effects caused by overabundant HDAC4 (Morris *et al.*, 2012; Fitzsimons, 2015).

In this work, it has been shown that nuclear HDAC4 is deleterious to both development and memory, further investigation could be carried out using split-GAL4 lines, this technique is covered in section 1.3.2 but, briefly, it allows for much finer spatial regulation of expression in *Drosophila.* Using the split-GAL4 driver system could permit the identification of the Kenyon cells in which DmHDAC4 is present in the nucleus as it is currently unknown if this distribution is based cellular identity or whether it is a stochastic distribution that is in constant flux. Furthermore, to overcome one of the limitations of this study, split-GAL4 lines could be used to investigate the role of HDAC4 in the output neurons of the mushroom body. These have been shown, extensively, to be involved in memory (Aso *et al.*, 2014b; Berry *et al.*, 2018; Pavlowsky *et al.*, 2018) and the role of subcellular distribution of HDAC4 in the output neurons is currently unknown.

Recently, class IIa HDAC-specific HDAC inhibitors have been developed that could act to prevent the deleterious effects of nuclear-accumulated HDAC4, either through inhibition of enzymatic activity or through the prevention of nuclear import (Hsu *et al.*, 2017; Choi *et al.*, 2018). These could be trialled in the *Drosophila* model to investigate their potential to alleviate the disruption induced by nuclear accumulation of HDAC4.

7.2 HDAC4 does not appear to act through MEF2 or CREB in the repression of *Drosophila* memory.

Having confirmed that an overabundance of specifically nuclear HDAC4 impaired memory and disrupted development two candidate targets of HDAC4 regulation, MEF2 and CREB, were investigated (Cole *et al.*, 2012; Sen and Sen, 2016) to determine the means through which HDAC4 altered neuronal function. MEF2 was shown to be required in development, as knockdown of MEF2 resulted in mild developmental disruption (Section 5.3). Overexpression of MEF2 also showed mild disruption to development, however, overexpressed MEF2 also impaired long-term memory when expressed in the adult *Drosophila* brain, unlike knockdown of MEF2 (Section 5.4). This suggested that HDAC4 may not act through MEF2 to repress memory formation but that the two proteins could interact during development. This is surprising as it has been shown in mammalian systems that the activity-induced nuclear export of HDAC4 leads to MEF2 activation and subsequent memory formation (Backs *et al.*, 2011; Jayathilaka *et al.*, 2012). However, the role of MEF2 is not strictly pro-memory. Increased MEF2 activity has been shown to repress dendrite formation and reduce synapse development, acting to increase the specificity of novel synapse formation through trimming of dendrites (Bailey and Kandel, 1993; Flavell *et al.*, 2006; Shalizi *et al.*, 2006). This suggests that the role of HDAC4 and MEF2 in memory may not be as simple as first proposed as excessive dendritic trimming during development can result in neurodevelopmental disorders, such as schizophrenia (Lewis and Levitt, 2002).

As MEF2 has been shown to be involved in dendrite growth and neuronal differentiation (Mao *et al.*, 1999; Gaudilliere *et al.*, 2002; Lam and Chawla, 2007) the observation that it is required in brain development is expected. This could indicate that HDAC4 and MEF2 interact during development, an interaction supported by the observed co-localisation of hHDAC4-3SA and MEF2 in nuclear puncta (Section 5.2).

Evaluation of MEF2 activity with a luciferase reporter indicated that the system was potentially more complex than had been expected. Overexpression of wild-type *Drosophila* MEF2 did not activate MRE-luciferase in *Drosophila*. However, activation of neurons through electrical stimulation did result in activation of luciferase, suggesting that the DmMEF2 requires a co-factor or activity dependent modification to be functional in *Drosophila*. The use of temperature gated ion channels (Rosenzweig *et al.*, 2004) permitted a preliminary investigation into the HDAC4-moderated role of MEF2 in activated neurons. This did not produce any clear results but did indicate that HDAC4 may not have a primarily repressive interaction with MEF2 in *Drosophila* brains (Section 5.5). To further this investigation, the TrpA1 activation assays could be continued further, perhaps using repeat heat/cool cycles to more realistically replicate training-based neuron activation. Additionally, optogenetic methods such as the use of channel rhodopsins could provide a means to activate neurons in *Drosophila* in a less invasive manner. Channel rhodopsins are transmembrane proteins that initiate ion exchange when exposed to specific wavelengths of light, these can be used in a similar manner to the TrpA1 channel but instead of heat inducing neuron depolarisation, light is the trigger (Inoue, 2016). This would permit the spaced-stimulation of neurons that is reflective of the training required for long-term memory and would also allow for induction of neuronal activity without the physiological stress of exposure to excess heat.

The investigation into the interaction between HDAC4 and MEF2 during memory suggests that MEF2 is not the primary axis through which HDAC4 regulates memory formation. However, it is likely that the two still interact as the co-localisation of 3SA and MEF2 was observed in KC nuclei and it has been shown that mammalian HDAC4 physically interacts with DmMEF2 in cultured tissue (Lu *et al.*, 2000). This could be verified in *Drosophila* through the co-immunoprecipitation experiments with HDAC4 and MEF2.

A second candidate target of HDAC4 in memory formation is CREB. It was observed in Kenyon cell bodies that, unlike MEF2, no strong co-localised puncta

were observed (Section 5.7). However, expression of the nuclear hHDAC4-3SA led to increased CREB activity when compared to hHDAC4-wt as measured by a CRE-luciferase promoter in cultured mammalian cells. This is in direct contrast to results from a study in mouse brains, in which exposure of the mouse to isoflurane resulted in increased nuclear HDAC4. This nuclear import was suggested to prevent CBP from binding to CREB, leading to a subsequent reduction in CREB activity (Sen and Sen, 2016). The CREB and hHDACs were co-transfected with PKA to activate CREB activity in the cultured cells (Gonzalez and Montminy, 1989) the high levels of PKA may have induced HDAC4 proteolysis, as has been observed previously in cultured neurons (Backs *et al.*, 2011). This N-terminal cleavage can remove the protein binding domain of HDAC4, possibly preventing the interaction proposed by Sen and Sen (2016). While this does not explain the difference between hHDAC4-wt and hHDAC4-3SA activation of CREB, it does bear noting that neither of these were statistically significant from the PKA+CREB co-transfection (Section 5.6). However, the unexpected up-regulation of CREB activity combined with the lack of co-localisation with CREB in the nucleus suggested that CREB was also not a likely candidate through which nuclear HDAC4 exerts its negative effects on memory (Suzuki *et al.*, 2011; Serita *et al.*, 2017).

It is worth noting that CREB was not studied in the *Drosophila* model beyond the subcellular distribution, it has been relatively well established that CREB is required for memory across many species (Silva *et al.*, 1998; Kandel, 2012; Kida and Serita, 2014). Furthermore, it has been shown in the γ-lobes of *Drosophila* that CREB is required for the formation of long-term memory (Akalal *et al.*, 2010). However, the interplay between HDAC4 and CREB merits further investigation. It has been shown that CREB binding protein (CBP) is important to neuronal function that its activity is modified by SUMOylation, a pathway HDAC4 is highly likely to modulate (Kuo *et al.*, 2005; Ryan *et al.*, 2010; Chatterjee *et al.*, 2013; Schwartz *et al.*, 2016). Additionally, while no strong co-localisation was observed between CREB and HDAC4, this does not mean the two do not interact in *Drosophila*. It would be prudent, therefore, to investigate the possible physical

interaction by attempting to pull-down CREB with HDAC4 or vice-versa in a co-immunoprecipitation.

7.3 Transcriptional effects of increased nuclear or cytoplasmic HDAC4 in the *Drosophila* brain.

Due to the fact that MEF2 and CREB seemed unlikely to be the primary axis through which HDAC4 regulates memory and development, it was determined that HDAC4 might be interacting through previously unidentified pathways.

Heads from flies expressing either the nuclear hHDAC4-3SA or the cytoplasmic hHDAC4-L175A in all neurons underwent RNASeq to analyse the changes in transcription caused by an overabundance of nuclear or cytoplasmic hHDAC4 respectively. This RNASeq and the subsequent analysis showed that nuclear HDAC4 altered transcription of only approximately 30 genes and that cytoplasmic HDAC4 appeared to affect transcription of a much greater range of genes (Sections 6.1 – 6.4).

Analysis of the GO-terms of the genes regulated hHDAC4-L175A and hHDAC4-3SA suggested that cytoplasmic HDAC4 could be acting to prepare the neurons for cellular activity, escalating metabolic activity and preparing pathways involved in translation and protein synthesis. This could be reflective of a form of preparation for increased neuronal activity, a process with a very high energy requirement (Dienel, 2012; Didier *et al.*, 2018). In addition to this, the increased abundance of cytoplasmic HDAC4 increased transcription of genes related to neuron connection and synapse formation (Section 6.8). This were not significantly down-regulated by the expression of 3SA suggesting that it is cytoplasmic abundance rather than lack of nuclear abundance that leads to these changes. The GO-term analysis of L175A induced changes showed that cytoplasmic HDAC4 activated the transcription of many genes involved in elevating the cell to a "ready state" for high metabolic activity. It appears to do this by reducing the preparation of energy storage pathways and instead activating protein and DNA synthesis pathways. Intriguingly, there is some

evidence that HDAC4 has a role in insulin sensitivity and metabolism. Much of this appears to be through regulation of the forkhead box O1 and 3 (FOXO1, FOXO3) proteins in conjunction with HDAC5, though more recent work has identified HDAC4 and 5 as regulators of GLUT4, a key glucose transporter (Mihaylova *et al.*, 2011; Niu *et al.*, 2017). Furthermore, it has been suggested that the HDAC4 modulation of insulin-related factors is associated with SUMOylation activity due to the inability of mammalian HDAC4 to deacetylate without the recruitment of Class I HDACs (Ozcan *et al.*, 2016). This data supports the hypothesis that at least a portion of the role of cytoplasmic HDAC4 is regulation of neuronal metabolism.

This is possibly reflective of a role for HDAC4 as a metabolic regulator in neurons, a cell-type that has been shown to have extremely high energy requirements (Dienel, 2012). It is possible that the nuclear exclusion of HDAC4 is required for memory function both to reduce the nuclear abundance of HDAC4 but also to increase the cytoplasmic presence and prepare the neuronal metabolism for protein synthesis and membrane recycling. The effect of accumulated nuclear or cytoplasmic HDAC4 on neuronal metabolism could potentially be investigated in the same manner HAT activity was (Section 1.4.2) through the tracking of isotope tagged metabolites. Use of ^{13}C-enriched glucose has been used in multiple studies to investigate cellular metabolism (Chokkathukalam *et al.*, 2014; Jang *et al.*, 2018; Lee *et al.*, 2018a) and could indicate if a nuclear or cytoplasmic abundance of HDAC4 alters the metabolic turnover of an organism.

It is not clear how cytoplasmic HDAC4 is regulating transcription, whether it is through the sequestration of transcriptional regulators, through competitive binding for nuclear import factors or through another, as yet unconsidered means. It is possible that a screen of likely targets for cytoplasmic HDAC4 could be carried out using fluorescence resonance energy transfer (FRET) to detect proteins in close proximity. An array of donor-chromophore tagged transcription factors, in conjunction with an acceptor-chromophore tagged L175A could be

expressed pairwise in the *Drosophila* Kenyon cells and, if fluorescence from the acceptor is detected it can be proposed an interaction is occurring, allowing for further investigation.

From the RNASeq data, several candidates were highlighted for further investigation, these were screened for interactions with HDAC4 during development using an eye phenotype screen (Section 5.11). In this, it was shown that knockdown of three (*kat80, fu12* and *npc2g*) had synergistic effects with HDAC4 expression but only knockdown of *npc2g* showed an enhanced rough-eye phenotype when expressed with cytoplasmic hHDAC4. *npc2g* encodes a protein involved in the metabolism and recycling of cholesterol, this could suggest a role for HDAC4 in the recycling of synaptic vesicles, a pathway which has high cholesterol turnover (Krivoi and Petrov, 2019).

Finally, these results strongly suggest that the deleterious effects of hDHAC4-3SA on learning and development are not primarily due to transcriptional changes. It is possible, instead, that the nuclear accumulation of 3SA results in the formation of aggregates in the nucleus. Several types of protein aggregates have been identified and HDAC4 has been shown to localise in some of these. Nuclear speckles are nuclear domains enriched in mRNA splicing factors that could modify mRNA abundance through alternative splicing (Spector and Lamond, 2011), these occur in regions of the nucleus without high densities of DNA, as was observed in immunohistochemistry images of 3SA subcellular distribution. Alternatively, Lewy and Marinesco bodies are cytoplasmic and nuclear inclusions observed in Parkinson's Disease (PD) that have been shown to harbour HDAC4 in the brains of individuals with PD (Takahashi-Fujigasaki and Fujigasaki, 2006; Abbott *et al.*, 2017), supporting this is evidence that nuclear HDAC4 exerts neurotoxicity in PD model mice (Wu *et al.*, 2017). Two other factors suggest this may be relevant to the current project and that is the presence of both SUMO-1 and a 14-3-3 chaperone protein in the Marinesco bodies. The 14-3-3ζ protein is responsible for the nuclear export of HDAC4 but may also have a role in preventing the aggregation of HDAC4. It could be that if the binding of

14-3-3ζ to HDAC4 is interrupted by the 3SA mutation the mutated HDAC4 begins to form Lewy and Marinesco body-like clusters that are in some way responsible for the disruption of development and memory observed in this project.

SUMOylation of proteins has been a recurring theme in the story of HDAC4, It has been suggested that HDAC4 could act as an E3 ligase, conjugating SUMO proteins to target proteins (Gregoire and Yang, 2005; Yang *et al.*, 2011; Henley *et al.*, 2014) and it has been shown that DmHDAC4 and Ubc9, the SUMO E2 enzyme interact in *Drosophila* (Schwartz *et al.*, 2016). It may be that nuclear HDAC4-mediated SUMOylation (or lack of cytoplasmic SUMOylation) is interrupting normal neuronal function by interrupting key protein-protein interactions SUMOylation.

7.4 Conclusion

In the work described in this thesis, it was shown that increased nuclear HDAC4 disrupts learning and development, as well as appearing to interact with MEF2 in *Drosophila*. However, the HDAC4-mediated repression of MEF2 proposed in mammals appears not to be the primary cause of memory impairment in flies with an excess of nuclear HDAC4.

Subsequently, it was demonstrated that many transcriptional changes induced by HDAC4 overexpression are due to cytoplasmic, rather than nuclear, HDAC4 and that these genes suggest that cytoplasmic HDAC4 acts to prepare the neuron for activity by increasing metabolism and preparing protein translation and synthesis pathways. This could clarify similarities observed in BDMR patients, in whom haploinsufficiency and nuclear restriction of HDAC4 are both causative factors.

This work has confirmed the role of nuclear HDAC4 as deleterious to development and memory and has opened up many new avenues for investigation into the role of cytoplasmic HDAC4 and its putative role in neuronal metabolism.

8 BIBLIOGRAPHY

Abbott, R.D., Nelson, J.S., Ross, G.W., Uyehara-Lock, J.H., Tanner, C.M., Masaki, K.H., Launer, L.J., White, L.R., and Petrovitch, H. (2017). Marinesco bodies and substantia nigra neuron density in Parkinson's disease. Neuropathol. Appl. Neurobiol. *43*, 621–630.

Abe, T., and Zukin, R.S. (2008). Epigenetic targets of HDAC inhibition in neurodegenerative and psychiatric disorders. Curr. Opin. Pharmacol. *8*, 57–64.

Abel, T., and Lattal, K.M. (2001). Molecular mechanisms of memory acquisition, consolidation and retrieval. Curr. Opin. Neurobiol. *11*, 180–187.

Aceves-Piña, E.O., and Quinn, W.G. (1979). Learning in normal and mutant *Drosophila* larvae. Science *206*, 93–96.

Adams, M.D., Celniker, S.E., Holt, R.A., Evans, C.A., Gocayne, J.D., Amanatides, P.G., Scherer, S.E., Li, P.W., Hoskins, R.A., Galle, R.F., et al. (2000). The genome sequence of *Drosophila melanogaster*. Science *287*, 2185–2195.

Ahn, S.-J., Vogel, H., and Heckel, D.G. (2012). Comparative analysis of the UDP-glycosyltransferase multigene family in insects. Insect Biochem. Mol. Biol. *42*, 133–147.

Akalal, D.B.G., Yu, D.H., and Davis, R.L. (2010). A late-phase, long-term memory trace forms in the gamma neurons of *Drosophila* mushroom bodies after olfactory classical conditioning. J. Neurosci. *30*, 16699–16708.

Akhtar, M.W., Kim, M.-S., Adachi, M., Morris, M.J., Qi, X., Richardson, J.A., Bassel-Duby, R., Olson, E.N., Kavalali, E.T., and Monteggia, L.M. (2012). *in vivo* analysis of MEF2 transcription factors in synapse regulation and neuronal survival. Plos One *7*, e34863.

Alarcon, J.M., Malleret, G., Touzani, K., Vronskaya, S., Ishii, S., Kandel, E.R., and Barco, A. (2004). Chromatin acetylation, memory, and LTP are impaired in CBP+/- mice: A model for the cognitive deficit in Rubinstein-Taybi syndrome and its amelioration. Neuron *42*, 947–959.

Alchini, R., Sugo, N., and Yamamoto, N. (2011). Histone deacetylase 9 (HDAC9) regulates thalamocortical axon branching by shuttling from the nucleus to cytoplasm in an activity-dependent fashion. Neurosci. Res. *71*, E46–E47.

Alchini, R., Sato, H., Matsumoto, N., Shimogori, T., Sugo, N., and Yamamoto, N. (2017). Nucleocytoplasmic shuttling of histone deacetylase 9 controls activity-dependent thalamocortical axon branching. Sci. Rep. *7*, 6024.

Alivisatos, A.P., Chun, M., Church, G.M., Greenspan, R.J., Roukes, M.L., and Yuste, R. (2012). The brain activity map project and the challenge of functional connectomics. Neuron *74*, 970–974.

Allfrey, V.G., Faulkner, R., and Mirsky, A.E. (1964). Acetylation and methylation of histones and their possible role in the regulation of RNA synthesis. Proc. Natl. Acad. Sci. U. S. A. *51*, 786–794.

Alonso, A. del C., Grundke-Iqbal, I., and Iqbal, K. (1996). Alzheimer's disease hyperphosphorylated tau sequesters normal tau into tangles of filaments and disassembles microtubules. Nat. Med. *2*, 783–787.

Alzheimer's Association (2018). 2018 Alzheimer's disease facts and figures - Alzheimer's & dementia: The Journal of the Alzheimer's Association. J. Alzheimers Assoc. *14*, 367–429.

American Psychiatric Association (2013). Diagnostic and statistical manual of mental disorders (5th ed.) (Arlington, VA).

Andrés, V., Cervera, M., and Mahdavi, V. (1995). Determination of the consensus binding site for MEF2 expressed in muscle and brain reveals tissue-specific sequence constraints. J. Biol. Chem. *270*, 23246–23249.

Araujo, A.R., Reis, M., Rocha, H., Aguiar, B., Morales-Hojas, R., Macedo-Ribeiro, S., Fonseca, N.A., Reboiro-Jato, D., Reboiro-Jato, M., Fdez-Riverola, F., et al. (2013). The *Drosophila melanogaster methuselah* gene: A novel gene with ancient functions. Plos One *8*, e63747.

Arrese, E.L., and Soulages, J.L. (2010). Insect fat body: energy, metabolism, and regulation. Annu. Rev. Entomol. *55*, 207–225.

Aso, Y., Grubel, K., Busch, S., Friedrich, A.B., Siwanowicz, I., and Tanimoto, H. (2009). The mushroom body of adult *Drosophila* characterized by GAL4 drivers. J. Neurogenet. *23*, 156–U29.

Aso, Y., Hattori, D., Yu, Y., Johnston, R.M., Iyer, N.A., Ngo, T.-T., Dionne, H., Abbott, L., Axel, R., Tanimoto, H., et al. (2014a). The neuronal architecture of the mushroom body provides a logic for associative learning. eLife *3*, e04577.

Aso, Y., Sitaraman, D., Ichinose, T., Kaun, K.R., Vogt, K., Belliart-Guérin, G., Plaçais, P.-Y., Robie, A.A., Yamagata, N., Schnaitmann, C., et al. (2014b). Mushroom body output neurons encode valence and guide memory-based action selection in *Drosophila*. eLife *3*, e04580.

Attwell, P.J.E., Cooke, S.F., and Yeo, C.H. (2002). Cerebellar function in consolidation of a motor memory. Neuron *34*, 1011–1020.

Backs, J., Worst, B.C., Lehmann, L.H., Patrick, D.M., Jebessa, Z., Kreusser, M.M., Sun, Q., Chen, L., Heft, C., Katus, H.A., et al. (2011). Selective repression of MEF2 activity by PKA-dependent proteolysis of HDAC4. J. Cell Biol. *195*, 403–415.

Bailey, C., and Kandel, E. (1993). Structural-changes accompanying memory storage. Annu. Rev. Physiol. *55*, 397–426.

Barbosa, A.C., Kim, M.-S., Ertunc, M., Adachi, M., Nelson, E.D., McAnally, J., Richardson, J.A., Kavalali, E.T., Monteggia, L.M., Bassel-Duby, R., et al. (2008). MEF2C, a transcription factor that facilitates learning and memory by negative regulation of synapse numbers and function. Proc. Natl. Acad. Sci. U. S. A. *105*, 9391–9396.

Barco, A., Bailey, C.H., and Kandel, E.R. (2006). Common molecular mechanisms in explicit and implicit memory. J. Neurochem. *97*, 1520–1533.

Bellen, H.J., Tong, C., and Tsuda, H. (2010). 100 years of *Drosophila* research and its impact on vertebrate neuroscience: a history lesson for the future. Nat. Rev. Neurosci. *11*, 514–522.

Berger, T., Alger, B., and Thompson, R. (1976). Neuronal substrate of classical-conditioning in hippocampus. Science *192*, 483–485.

Berry, J.A., Cervantes-Sandoval, I., Nicholas, E.P., and Davis, R.L. (2012). Dopamine is required for learning and forgetting in *Drosophila*. Neuron *74*, 530–542.

Berry, J.A., Phan, A., and Davis, R.L. (2018). Dopamine neurons mediate learning and forgetting through bidirectional modulation of a memory trace. Cell Rep. *25*, 651–662.e5.

Black, B.L., and Olson, E.N. (1998). Transcriptional Control of Muscle Development by Myocyte Enhancer Factor-2 (mef2) Proteins. Annu. Rev. Cell Dev. Biol. *14*, 167–196.

Black, B.L., Ligon, K.L., Zhang, Y., and Olson, E.N. (1996). Cooperative transcriptional activation by the neurogenic basic helix-loop-jelix protein MASH1 and members of the myocyte enhancer factor-2 (MEF2) family. J. Biol. Chem. *271*, 26659–26663.

Bliek, A.M. van der, and Meyerowrtz, E.M. (1991). Dynamin-like protein encoded by the *Drosophila shibire* gene associated with vesicular traffic. Nature *351*, 411.

Bolger, T.A., and Yao, T.P. (2005). Intracellular trafficking of histone deacetylase 4 regulates neuronal cell death. J. Neurosci. *25*, 9544–9553.

Bottomley, M.J., Lo Surdo, P., Di Giovine, P., Cirillo, A., Scarpelli, R., Ferrigno, F., Jones, P., Neddermann, P., De Francesco, R., Steinkuhler, C., et al. (2008).

Structural and functional analysis of the human HDAC4 catalytic domain reveals a regulatory structural zinc-binding domain. J. Biol. Chem. *283*, 26694–26704.

Bourne, J.N., and Harris, K.M. (2011). Coordination of size and number of excitatory and inhibitory synapses results in a balanced structural plasticity along mature hippocampal CA1 dendrites during LTP. Hippocampus *21*, 354–373.

Bradford, A., Kunik, M.E., Schulz, P., Williams, S.P., and Singh, H. (2009). Missed and delayed diagnosis of dementia in primary care: prevalence and contributing factors. Alzheimer Dis. Assoc. Disord. *23*, 306–314.

Brand, A.H., and Perrimon, N. (1993). Targeted gene expression as a means of altering cell fates and generating dominant phenotypes. Development *118*, 401–415.

Brandl, A., Heinzel, T., and Kraemer, O.H. (2009). Histone deacetylases: salesmen and customers in the post-translational modification market. Biol. Cell *101*, 193–205.

Brindle, P., Linke, S., and Montminy, M. (1993). Protein-kinase-A-dependent activator in transcription factor CREB reveals new role for CREM repressers. Nature *364*, 821–824.

Broide, R.S., Redwine, J.M., Aftahi, N., Young, W., Bloom, F.E., and Winrow, C.J. (2007). Distribution of histone deacetylases 1-11 in the rat brain. J. Mol. Neurosci. *31*, 47–58.

Bruckert, H., Marchetti, G., Ramialison, M., and Besse, F. (2015). *Drosophila* Hrp48 is required for Mushroom Body axon growth, branching and guidance. PLOS ONE *10*, e0136610.

Cann, M.J., Chung, E., and Levin, L.R. (2000). A new family of adenylyl cyclase genes in the male germline of *Drosophila melanogaster*. Dev. Genes Evol. *210*, 200–206.

Cervantes-Sandoval, I., Phan, A., Chakraborty, M., and Davis, R.L. (2017). Reciprocal synapses between mushroom body and dopamine neurons form a positive feedback loop required for learning. eLife *6*.

Chatterjee, S., Mizar, P., Cassel, R., Neidl, R., Selvi, B.R., Mohankrishna, D.V., Vedamurthy, B.M., Schneider, A., Bousiges, O., Mathis, C., et al. (2013). A novel activator of CBP/p300 acetyltransferases promotes neurogenesis and extends memory duration in adult mice. J. Neurosci. *33*, 10698–10712.

Chawla, S., Vanhoutte, P., Arnold, F.J.L., Huang, C.L.H., and Bading, H. (2003). Neuronal activity-dependent nucleocytoplasmic shuttling of HDAC4 and HDAC5. J. Neurochem. *85*, 151–159.

Chen, B., and Cepko, C.L. (2009). HDAC4 regulates neuronal survival in normal and diseased retinas. Science *323*, 256–259.

Chen, C.-C., Wu, J.-K., Lin, H.-W., Pai, T.-P., Fu, T.-F., Wu, C.-L., Tully, T., and Chiang, A.-S. (2012a). Visualizing long-term memory formation in two neurons of the *Drosophila* brain. Science *335*, 678–685.

Chen, S.X., Cherry, A., Tari, P.K., Podgorski, K., Kwong, Y.K.K., and Haas, K. (2012b). The transcription factor MEF2 directs developmental visually driven functional and structural metaplasticity. Cell *151*, 41–55.

Chen, T., Zhu, J., Yang, L.-K., Feng, Y., Lin, W., and Wang, Y.-H. (2017). Glutamate-induced rapid induction of Arc/Arg3.1 requires NMDA receptor-mediated phosphorylation of ERK and CREB. Neurosci. Lett. *661*, 23–28.

Chen, Y.C., Hsu, W.L., Ma, Y.L., Tai, D.J.C., and Lee, E.H.Y. (2014). CREB SUMOylation by the E3 Ligase PIAS1 enhances spatial memory. J. Neurosci. *34*, 9574–9589.

Choi, S.Y., Kee, H.J., Jin, L., Ryu, Y., Sun, S., Kim, G.R., and Jeong, M.H. (2018). Inhibition of class IIa histone deacetylase activity by gallic acid, sulforaphane, TMP269, and panobinostat. Biomed. Pharmacother. *101*, 145–154.

Chokkathukalam, A., Kim, D.-H., Barrett, M.P., Breitling, R., and Creek, D.J. (2014). Stable isotope-labeling studies in metabolomics: new insights into structure and dynamics of metabolic networks. Bioanalysis *6*, 511–524.

Choudhuri, S. (2011). From Waddington's epigenetic landscape to small noncoding RNA: some important milestones in the history of epigenetics research. Toxicol. Mech. Methods *21*, 252–274.

Claridge-Chang, A., Roorda, R.D., Vrontou, E., Sjulson, L., Li, H., Hirsh, J., and Miesenböck, G. (2009). Writing memories with light-addressable reinforcement circuitry. Cell *139*, 405–415.

Claßen, G., and Scholz, H. (2018). Octopamine shifts the behavioral response from indecision to approach or aversion in *Drosophila melanogaster*. Front. Behav. Neurosci. *12*.

Cole, C.J., Mercaldo, V., Restivo, L., Yiu, A.P., Sekeres, M.J., Han, J.H., Vetere, G., Pekar, T., Ross, P.J., Neve, R.L., et al. (2012). MEF2 negatively regulates learning-induced structural plasticity and memory formation. Nat. Neurosci. *15*, 1255 – NIL_121.

Conti, M., and Beavo, J. (2007). Biochemistry and physiology of cyclic nucleotide Phosphocliesterases: Essential components in cyclic nucleotide signaling. Annu. Rev. Biochem. *76*, 481–511.

Craig, T.J., and Henley, J.M. (2012). Protein SUMOylation in spine structure and function. Curr. Opin. Neurobiol. *22*, 480–487.

Crittenden, J.R., Skoulakis, E.M.C., Han, K.A., Kalderon, D., and Davis, R.L. (1998). Tripartite mushroom body architecture revealed by antigenic markers. Learn. Mem. *5*, 38–51.

Crook, T., Bartus, R.T., Ferris, S.H., Whitehouse, P., Cohen, G.D., and Gershon, S. (1986). Age-associated memory impairment: Proposed diagnostic criteria and measures of clinical change — report of a national institute of mental health work group. Dev. Neuropsychol. *2*, 261–276.

Darcy, M.J., Calvin, K., Cavnar, K., and Ouimet, C.C. (2010). Regional and subcellular distribution of HDAC4 in mouse brain. J. Comp. Neurol. *518*, 722–740.

Dash, P., Hochner, B., and Kandel, E. (1990). Injection of the cAMP-responsive element into the nucleus of *Aplysia* sensory neurons blocks long-term facilitation. Nature *345*, 718–721.

Davis, R.L. (2005). Olfactory memory formation in *Drosophila*: From molecular to systems neuroscience. Annu. Rev. Neurosci. *28*, 275–302.

Davis, R.L. (2011). Traces of *Drosophila* Memory. Neuron *70*, 8–19.

Delcuve, G.P., Khan, D.H., and Davie, J.R. (2012). Roles of histone deacetylases in epigenetic regulation: emerging paradigms from studies with inhibitors. Clin. Epigenetics *4*, 5.

De Roo, M., Klauser, P., Garcia, P.M., Poglia, L., and Muller, D. (2008). Spine dynamics and synapse remodeling during LTP and memory processes. In Essence of Memory, W.S. Sossin, J.C. Lacaille, V.F. Castellucci, and S. Belleville, eds. (Amsterdam: Elsevier Science Bv), pp. 199–207.

Deupree, D., Bradley, J., and Turner, D. (1993). Age-related alterations in potentiation in the CA1 region in F344 rats. Neurobiol. Aging *14*, 249–258.

Didier, S., Sauvé, F., Domise, M., Buée, L., Marinangeli, C., and Vingtdeux, V. (2018). AMP-activated protein kinase controls immediate early genes expression following synaptic activation through the PKA/CREB pathway. Int. J. Mol. Sci. *19*, 3716.

Dienel, G.A. (2012). Fueling and imaging brain activation. ASN Neuro *4*, AN20120021.

Dietz, K.C., and Casaccia, P. (2010). HDAC inhibitors and neurodegeneration: At the edge between protection and damage. Pharmacol. Res. *62*, 11–17.

Dietzl, G., Chen, D., Schnorrer, F., Su, K.-C., Barinova, Y., Fellner, M., Gasser, B., Kinsey, K., Oppel, S., Scheiblauer, S., et al. (2007). A genome-wide transgenic RNAi library for conditional gene inactivation in *Drosophila*. Nature *448*, 151–156.

Dudai, Y., Jan, Y.N., Byers, D., Quinn, W.G., and Benzer, S. (1976). *dunce*, a mutant of *Drosophila* deficient in learning. Proc. Natl. Acad. Sci. *73*, 1684–1688.

Dujardin, F. (1850). Mémoire sur le système nerveux des insectes. Ann Sci Nat Zool *14*, 195–206.

Ejima, A., and Griffith, L.C. (2011). Assay for Courtship Suppression in *Drosophila*. Cold Spring Harb. Protoc. *2011*, pdb.prot5575.

Emptage, N.J., and Carew, T.J. (1993). Long-term synaptic facilitation in the absence of short-term facilitation in *Aplysia* neurons. Science *262*, 253–256.

Ergorul, C., and Eichenbaum, H. (2004). The Hippocampus and memory for "what," "where," and "when." Learn. Mem. *11*, 397–405.

Fei, J., Ishii, H., Hoeksema, M.A., Meitinger, F., Kassavetis, G.A., Glass, C.K., Ren, B., and Kadonaga, J.T. (2018). NDF, a nucleosome-destabilizing factor that facilitates transcription through nucleosomes. Genes Dev. *32*, 682–694.

Fischle, W., Dequiedt, F., Fillion, M., Hendzel, M.J., Voelter, W., and Verdin, E. (2001). Human HDAC7 histone deacetylase activity is associated with HDAC3 in vivo. J. Biol. Chem. *276*, 35826–35835.

Fischle, W., Dequiedt, F., Hendzel, M.J., Guenther, M.G., Lazar, M.A., Voelter, W., and Verdin, E. (2002). Enzymatic activity associated with class IIHDACs is dependent on a multiprotein complex containing HDAC3 and SMRT/N-CoR. Mol. Cell *9*, 45–57.

Fisher, B., Weiszmann, R., Frise, E., Hammonds, A., Tomancak, P., Beaton, A., Berman, B., Quan, E., Shu, S., Lewis, S., et al. (2012). Berkeley *Drosophila* Genome Project.

Fitzsimons, H.L. (2015). The Class IIa histone deacetylase HDAC4 and neuronal function: Nuclear nuisance and cytoplasmic stalwart? Neurobiol. Learn. Mem. *123*, 149–158.

Fitzsimons, H.L., and Scott, M.J. (2011). Genetic modulation of Rpd3 Expression impairs long-term courtship memory in *Drosophila*. Plos One *6*, e29171.

Fitzsimons, H.L., Schwartz, S., Given, F.M., and Scott, M.J. (2013). The histone deacetylase HDAC4 regulates long-term memory in *Drosophila*. Plos One *8*, e83903.

Flavell, S.W., and Greenberg, M.E. (2008). Signaling Mechanisms Linking Neuronal Activity to Gene Expression and Plasticity of the Nervous System. Annu. Rev. Neurosci. *31*, 563–590.

Flavell, S.W., Cowan, C.W., Kim, T.K., Greer, P.L., Lin, Y.X., Paradis, S., Griffith, E.C., Hu, L.S., Chen, C.F., and Greenberg, M.E. (2006). Activity-dependent regulation of MEF2 transcription factors suppresses excitatory synapse number. Science *311*, 1008–1012.

Flavell, S.W., Kim, T.-K., Gray, J.M., Harmin, D.A., Hemberg, M., Hong, E.J., Markenscoff-Papadimitriou, E., Bear, D.M., and Greenberg, M.E. (2008). Genome-wide analysis of MEF2 transcriptional program reveals synaptic target genes and neuronal activity-dependent polyadenylation site selection. Neuron *60*, 1022–1038.

Franzdóttir, S.R., Engelen, D., Yuva-Aydemir, Y., Schmidt, I., Aho, A., and Klämbt, C. (2009). Switch in FGF signalling initiates glial differentiation in the *Drosophila* eye. Nature *460*, 758–761.

Freeman, M. (1996). Reiterative use of the EGF receptor triggers differentiation of all cell types in the *Drosophila* eye. Cell *87*, 651–660.

Freymuth, P.S., and Fitzsimons, H.L. (2017). The ERM protein Moesin is essential for neuronal morphogenesis and long-term memory in *Drosophila*. Mol. Brain *10*, 41.

Frost, W.N., Castellucci, V.F., Hawkins, R.D., and Kandel, E.R. (1985). Monosynaptic connections made by the sensory neurons of the gill- and siphon-withdrawal reflex in *Aplysia* participate in the storage of long-term memory for sensitization. Proc. Natl. Acad. Sci. *82*, 8266–8269.

Fuenzalida-Uribe, N., and Campusano, J.M. (2018). Unveiling the dual role of the dopaminergic system on locomotion and the innate value for an aversive olfactory stimulus in *Drosophila*. Neuroscience *371*, 433–444.

Gaudilliere, B., Shi, Y., and Bonni, A. (2002). RNA interference reveals a requirement for myocyte enhancer factor 2A in activity-dependent neuronal survival. J. Biol. Chem. *277*, 46442–46446.

Gershey, E., Vidali, G., and Allfrey, V. (1968). Chemical studies of histone acetylation - occurrence of epsilon-N-acetyllysine in F2a1 histone. J. Biol. Chem. *243*, 5018 – &.

Gervasi, N., Tchenio, P., and Preat, T. (2010). PKA dynamics in a *Drosophil* a learning center: coincidence detection by Rutabaga adenylyl cyclase and spatial regulation by Dunce phosphodiesterase. Neuron *65*, 516–529.

Glozak, M.A., and Seto, E. (2009). Acetylation/deacetylation modulates the stability of DNA replication licensing factor Cdt1. J. Biol. Chem. *284*, 11446–11453.

Goldstein, L.S.B., and Gunawardena, S. (2000). Flying through the *Drosophila* Cytoskeletal Genome. J. Cell Biol. *150*, F63–F68.

Gonzalez, G.A., and Montminy, M.R. (1989). Cyclic AMP stimulates somatostatin gene transcription by phosphorylation of CREB at serine 133. Cell *59*, 675–680.

Gregoire, S., and Yang, X.J. (2005). Association with class IIa histone deacetylases upregulates the sumoylation of MEF2 transcription factors. Mol. Cell. Biol. *25*, 2273–2287.

Gregoretti, I., Lee, Y.-M., and Goodson, H.V. (2004). Molecular evolution of the histone deacetylase family: functional implications of phylogenetic analysis. J. Mol. Biol. *338*, 17–31.

Griffith, L.C., and Ejima, A. (2009). Courtship learning in Drosophila melanogaster: Diverse plasticity of a reproductive behavior. Learn. Mem. *16*, 743–750.

Grozinger, C.M., Hassig, C.A., and Schreiber, S.L. (1999). Three proteins define a class of human histone deacetylases related to yeast Hda1p. Proc. Natl. Acad. Sci. U. S. A. *96*, 4868–4873.

Guan, J.S., Haggarty, S.J., Giacometti, E., Dannenberg, J.H., Joseph, N., Gao, J., Nieland, T.J.F., Zhou, Y., Wang, X.Y., Mazitschek, R., et al. (2009). HDAC2 negatively regulates memory formation and synaptic plasticity. Nature *459*, 55 – NIL_58.

Guan, Z., Buhl, L.K., Quinn, W.G., and Littleton, J.T. (2011). Altered gene regulation and synaptic morphology in *Drosophila* learning and memory mutants. Learn. Mem. *18*, 191–206.

Guenther, M.G., Barak, O., and Lazar, M.A. (2001). The SMRT and N-CoR Corepressors Are Activating Cofactors for Histone Deacetylase 3. Mol. Cell. Biol. *21*, 6091–6101.

Guo, L., Han, A., Bates, D.L., Cao, J., and Chen, L. (2007). Crystal structure of a conserved N-terminal domain of histone deacetylase 4 reveals functional insights into glutamine-rich domains. Proc. Natl. Acad. Sci. U. S. A. *104*, 4297–4302.

Guven-Ozkan, T., and Davis, R.L. (2014). Functional neuroanatomy of *Drosophila* olfactory memory formation. Learn. Mem. *21*, 519–526.

Haggarty, S.J., and Tsai, L.-H. (2011). Probing the role of HDACs and mechanisms of chromatin-mediated neuroplasticity. Neurobiol. Learn. Mem. *96*, 41–52.

Hamada, F.N., Rosenzweig, M., Kang, K., Pulver, S.R., Ghezzi, A., Jegla, T.J., and Garrity, P.A. (2008). An internal thermal sensor controlling temperature preference in *Drosophila*. Nature *454*, 217–220.

Han, P., Levin, L., Reed, R., and Davis, R. (1992). Preferential expression of the *Drosophila rutabaga* gene in mushroom bodies, neural centers for learning in insects. Neuron *9*, 619–627.

Hawkins, R.D., Kandel, E.R., and Bailey, C.H. (2006). Molecular mechanisms of memory storage in *Aplysia*. Biol. Bull. *210*, 174–191.

Haynes, P.R., Christmann, B.L., and Griffith, L.C. (2015). A single pair of neurons links sleep to memory consolidation in *Drosophila melanogaster* . eLife *4*, e03868.

Hebert, L.E., Weuve, J., Scherr, P.A., and Evans, D.A. (2013). Alzheimer disease in the United States (2010-2050) estimated using the 2010 census. Neurology *80*, 1778–1783.

Heisenberg, M. (1985). 3 Genes on the 2nd chromosome, affecting the structure of the mushroom bodies. Biol. Chem. Hoppe. Seyler *366*, 118–118.

Heisenberg, M. (1998). What do the mushroom bodies do for the insect brain? An introduction. Learn. Mem. *5*, 1–10.

Hekmat-Scafe, D.S., Scafe, C.R., McKinney, A.J., and Tanouye, M.A. (2002). Genome-wide analysis of the odorant-binding protein gene family in *Drosophila melanogaster*. Genome Res. *12*, 1357–1369.

Henikoff, S., and Matzke, M.A. (1997). Epigenetics: Exploring and explaining epigenetic effects. Trends Genet. *13*, 293–295.

Henley, J.M., Craig, T.J., and Wilkinson, K.A. (2014). Neuronal SUMOylation: mechanisms, physiology, and roles in neuronal dysfunction. Physiol. Rev. *94*, 1249–1285.

Herskovits, A.Z., and Guarente, L. (2013). Sirtuin deacetylases in neurodegenerative diseases of aging. Cell Res. *23*, 746–758.

Hige, T., Aso, Y., Rubin, G.M., and Turner, G.C. (2015). Plasticity-driven individualization of olfactory coding in mushroom body output neurons. Nature *526*, 258–262.

Hirano, Y., Ihara, K., Masuda, T., Yamamoto, T., Iwata, I., Takahashi, A., Awata, H., Nakamura, N., Takakura, M., Suzuki, Y., et al. (2016). Shifting transcriptional machinery is required for long-term memory maintenance and modification in *Drosophila* mushroom bodies. Nat. Commun. *7*, 13471.

Hsu, K.-C., Liu, C.-Y., Lin, T.E., Hsieh, J.-H., Sung, T.-Y., Tseng, H.-J., Yang, J.-M., and Huang, W.-J. (2017). Novel class IIa-selective histone deacetylase inhibitors discovered using an *in silico* virtual screening approach. Sci. Rep. *7*, 3228.

Huang, D.W., Sherman, B.T., and Lempicki, R.A. (2009a). Systematic and integrative analysis of large gene lists using DAVID bioinformatics resources. Nat. Protoc. *4*, 44–57.

Huang, D.W., Sherman, B.T., and Lempicki, R.A. (2009b). Bioinformatics enrichment tools: paths toward the comprehensive functional analysis of large gene lists. Nucleic Acids Res. *37*, 1–13.

Huang, X., Warren, J.T., Buchanan, J., Gilbert, L.I., and Scott, M.P. (2007). *Drosophila* Niemann-Pick Type C-2 genes control sterol homeostasis and steroid biosynthesis: a model of human neurodegenerative disease. Development *134*, 3733–3742.

Iliadi, K.G., Iliadi, N., and Boulianne, G.L. (2017). *Drosophila* mutants lacking octopamine exhibit impairment in aversive olfactory associative learning. Eur. J. Neurosci. *46*, 2080–2087.

Inoue, K. (2016). The study and application of photoreceptive membrane protein, rhodopsin. Bull. Chem. Soc. Jpn. *89*, 1416–1424.

Ishikawa, Y., and Homcy, C.J. (1997). The adenylyl cyclases as integrators of transmembrane signal transduction. Circ. Res. *80*, 297–304.

Ito, K., Awano, W., Suzuki, K., Hiromi, Y., and Yamamoto, D. (1997). The *Drosophila* mushroom body is a quadruple structure of clonal units each of which contains a virtually identical set of neurones and glial cells. Development *124*, 761–771.

Izquierdo, I., Medina, J.H., Izquierdo, L.A., Barros, D.M., de Souza, M.M., and Mello e Souza, T. (1998). Short- and long-term memory are differentially regulated by monoaminergic systems in the rat brain. Neurobiol. Learn. Mem. *69*, 219–224.

Izquierdo, I., Medina, J.H., Vianna, M.R.M., Izquierdo, L.A., and Barros, D.M. (1999). Separate mechanisms for short- and long-term memory. Behav. Brain Res. *103*, 1–11.

Izquierdo, L.A., Vianna, M., Barros, D.M., Mello e Souza, T., Ardenghi, P., Sant' Anna, M.K., Rodrigues, C., Medinam, J.H., and Izquierdo, I. (2000). Short- and long-term memory are differentially affected by metabolic inhibitors given into hippocampus and entorhinal cortex. Neurobiol. Learn. Mem. *73*, 141–149.

Izquierdo, L.A., Barros, D.M., Vianna, M.R.M., Coitinho, A., Silva, T.D. de, Choi, H., Moletta, B., Medina, J.H., and Izquierdo, I. (2002). Molecular pharmacological dissection of short- and long-term memory. Cell. Mol. Neurobiol. *22*, 269–287.

Janczura, K.J., Volmar, C.-H., Sartor, G.C., Rao, S.J., Ricciardi, N.R., Lambert, G., Brothers, S.P., and Wahlestedt, C. (2018). Inhibition of HDAC3 reverses Alzheimer's disease-related pathologies in vitro and in the 3xTg-AD mouse model. Proc. Natl. Acad. Sci. *115*, E11148–E11157.

Jang, C., Chen, L., and Rabinowitz, J.D. (2018). Metabolomics and Isotope Tracing. Cell *173*, 822–837.

Jayathilaka, N., Han, A., Gaffney, K.J., Dey, R., Jarusiewicz, J.A., Noridomi, K., Philips, M.A., Lei, X., He, J., Ye, J., et al. (2012). Inhibition of the function of class IIa HDACs by blocking their interaction with MEF2. Nucleic Acids Res. *40*, 5378–5388.

Jeon, E.-J., Lee, K.-Y., Choi, N.-S., Lee, M.-H., Kim, H.-N., Jin, Y.-H., Ryoo, H.-M., Choi, J.-Y., Yoshida, M., Nishino, N., et al. (2006). Bone morphogenetic protein-2 stimulates Runx2 acetylation. J. Biol. Chem. *281*, 16502–16511.

Kandel, E.R. (2001). Neuroscience - The molecular biology of memory storage: A dialogue between genes and synapses. Science *294*, 1030–1038.

Kandel, E.R. (2012). The molecular biology of memory: cAMP, PKA, CRE, CREB-1, CREB-2, and CPEB. Mol. Brain *5*, 14.

Kandel, E.R., and Tauc, L. (1965). Heterosynaptic facilitation in neurones of the abdominal ganglion of *Aplysia depilans*. J. Physiol. *181*, 1–27.

Kao, H.Y., Downes, M., Ordentlich, P., and Evans, R.M. (2000). Isolation of a novel histone deacetylase reveals that class I and class. Genes Dev. *14*, 55–66.

Kassis, H., Shehadah, A., Li, C., Zhang, Y., Cui, Y., Roberts, C., Sadry, N., Liu, X., Chopp, M., and Zhang, Z.G. (2016). Class IIa histone deacetylases affect neuronal remodeling and functional outcome after stroke. Neurochem. Int. *96*, 24–31.

Kataoka, S., Takuma, K., Hara, Y., Maeda, Y., Ago, Y., and Matsuda, T. (2013). Autism-like behaviours with transient histone hyperacetylation in mice treated prenatally with valproic acid. Int. J. Neuropsychopharmacol. *16*, 91–103.

Kawashima, T., Okuno, H., Nonaka, M., Adachi-Morishima, A., Kyo, N., Okamura, M., Takemoto-Kimura, S., Worley, P.F., and Bito, H. (2009). Synaptic activity-responsive element in the Arc/Arg3.1 promoter essential for synapse-to-nucleus signaling in activated neurons. Proc. Natl. Acad. Sci. U. S. A. *106*, 316–321.

Keene, A.C., Stratmann, M., Keller, A., Perrat, P.N., Vosshall, L.B., and Waddell, S. (2004). Diverse odor-conditioned memories require uniquely timed dorsal paired medial neuron output. Neuron *44*, 521–533.

Keleman, K., Krüttner, S., Alenius, M., and Dickson, B.J. (2007). Function of the *Drosophila* CPEB protein Orb2 in long-term courtship memory. Nat. Neurosci. *10*, 1587–1593.

Keleman, K., Vrontou, E., Krüttner, S., Yu, J.Y., Kurtovic-Kozaric, A., and Dickson, B.J. (2012). Dopamine neurons modulate pheromone responses in *Drosophila* courtship learning. Nature *489*, 145–149.

Kida, S., and Serita, T. (2014). Functional roles of CREB as a positive regulator in the formation and enhancement of memory. Brain Res. Bull. *105*, 17–24.

Kim, M.S., Akhtar, M.W., Adachi, M., Mahgoub, M., Bassel-Duby, R., Kavalali, E.T., Olson, E.N., and Monteggia, L.M. (2012). An essential role for histone deacetylase 4 in synaptic plasticity and memory formation. J. Neurosci. *32*, 10879–10886.

Kim, T., Park, J.K., Kim, H.-J., Chung, J.-H., and Kim, J.W. (2010). Association of histone deacetylase genes with schizophrenia in Korean population. Psychiatry Res. *178*, 266–269.

Kleinsmith, L., Allfrey, V., and Mirsky, A. (1966). Phosphorylation of nuclear protein early in course of gene activation in lymphocytes. Science *154*, 780 – &.

Koenig, J., and Ikeda, K. (1978). Characterization of temperature induced firing pattern of dorsal longitudinal flight-muscle in *Drosophila* mutant *shibire*. Fed. Proc. *37*, 527–527.

Koester, J., and Kandel, E.R. (1977). Further identification of neurons in the abdominal ganglion of *Aplysia* using behavioral criteria. Brain Res. *121*, 1–20.

Kong, E.C., Allouche, L., Chapot, P.A., Vranizan, K., Moore, M.S., Heberlein, U., and Wolf, F.W. (2010). Ethanol-regulated genes that contribute to ethanol sensitivity and rapid tolerance in *Drosophila*. Alcohol. Clin. Exp. Res. *34*, 302–316.

Krivoi, I.I., and Petrov, A.M. (2019). Cholesterol and the safety factor for neuromuscular transmission. Int. J. Mol. Sci. *20*, 1046.

Kumar, A., Kumar Singh, S., Kumar, V., Kumar, D., Agarwal, S., and Rana, M.K. (2015). Huntington's disease: An update of therapeutic strategies. Gene *556*, 91–97.

Kuo, H.-Y., Chang, C.-C., Jeng, J.-C., Hu, H.-M., Lin, D.-Y., Maul, G.G., Kwok, R.P.S., and Shih, H.-M. (2005). SUMO modification negatively modulates the transcriptional activity of CREB-binding protein via the recruitment of Daxx. Proc. Natl. Acad. Sci. U. S. A. *102*, 16973–16978.

LaBar, K.S., and Cabeza, R. (2006). Cognitive neuroscience of emotional memory. Nat. Rev. Neurosci. *7*, 54–64.

Lahm, A., Paolini, C., Pallaoro, M., Nardi, M.C., Jones, P., Neddermann, P., Sambucini, S., Bottomley, M.J., Lo Surdo, P., Carfi, A., et al. (2007). Unraveling the hidden catalytic activity of vertebrate class Ila histone deacetylases. Proc. Natl. Acad. Sci. U. S. A. *104*, 17335–17340.

Lam, B.Y.H., and Chawla, S. (2007). MEF2D expression increases during neuronal differentiation of neural progenitor cells and correlates with neurite length. Neurosci. Lett. *427*, 153–158.

Lam, B.Y.H., Zhang, W., Ng, D.C.-H., Maruthappu, M., Roderick, H.L., and Chawla, S. (2010). CREB-dependent Nur77 induction following depolarization in PC12 cells and neurons is modulated by MEF2 transcription factors. J. Neurochem. *112*, 1065–1073.

Lashley, K. (1950). In search of the engram. Symp. Soc. Exp. Biol. *4*, 454–482.

Laverty, C., Li, F., Belikoff, E.J., and Scott, M.J. (2011). Abnormal dosage compensation of reporter genes driven by the *Drosophila* Glass Multiple Reporter (GMR) enhancer-promoter. PLOS ONE *6*, e20455.

Lee, D.-K., Na, E., Park, S., Park, J.H., Lim, J., and Kwon, S.W. (2018a). *in vitro* tracking of intracellular metabolism-derived cancer volatiles via isotope labeling. ACS Cent. Sci. *4*, 1037–1044.

Lee, G.J., Han, G., Yun, H.M., Lim, J.J., Noh, S., Lee, J., and Hyun, S. (2018b). Steroid signaling mediates nutritional regulation of juvenile body growth via IGF-binding protein in *Drosophila*. Proc. Natl. Acad. Sci. *115*, 5992–5997.

Levenson, J.M., and Sweatt, J.D. (2006). Epigenetic mechanisms: a common theme in vertebrate and invertebrate memory formation. Cell. Mol. Life Sci. *63*, 1009–1016.

Levenson, J.M., O'Riordan, K.J., Brown, K.D., Trinh, M.A., Molfese, D.L., and Sweatt, J.D. (2004). Regulation of histone acetylation during memory formation in the hippocampus. J. Biol. Chem. *279*, 40545–40559.

Lewis, D.A., and Levitt, P. (2002). Schizophrenia as a disorder of neurodevelopment. Annu. Rev. Neurosci. *25*, 409–432.

Li, J., Chen, J., Ricupero, C.L., Hart, R.P., Schwartz, M.S., Kusnecov, A., and Herrup, K. (2012). Nuclear accumulation of HDAC4 in ATM deficiency promotes neurodegeneration in ataxia telangiectasia. Nat. Med. *18*, 783–U182.

Li, J.W., Wang, J., Wang, J.X., Nawaz, Z., Liu, J.M., Qin, J., and Wong, J.M. (2000). Both corepressor proteins SMRT and N-CoR exist in large protein complexes containing HDAC3. Embo J. *19*, 4342–4350.

Liscum, L., and Faust, J.R. (1987). Low density lipoprotein (LDL)-mediated suppression of cholesterol synthesis and LDL uptake is defective in Niemann-Pick type C fibroblasts. J. Biol. Chem. *262*, 17002–17008.

Litke, C., Bading, H., and Mauceri, D. (2018). Histone deacetylase 4 shapes neuronal morphology via a mechanism involving regulation of expression of Vascular Endothelial Growth Factor D. J. Biol. Chem. jbc.RA117.001613.

Liu, X., and Davis, R.L. (2009). The GABAergic anterior paired lateral neuron suppresses and is suppressed by olfactory learning. Nat. Neurosci. *12*, 53–59.

Liu, C., Placais, P.-Y., Yamagata, N., Pfeiffer, B.D., Aso, Y., Friedrich, A.B., Siwanowicz, I., Rubin, G.M., Preat, T., and Tanimoto, H. (2012). A subset of dopamine neurons signals reward for odour memory in *Drosophila*. Nature *488*, 512 – +.

Livingstone, M.S., Sziber, P.P., and Quinn, W.G. (1984). Loss of calcium/calmodulin responsiveness in adenylate cyclase of *rutabaga*, a *Drosophila* learning mutant. Cell *37*, 205–215.

Loriol, C., Khayachi, A., Poupon, G., Gwizdek, C., and Martin, S. (2013). Activity-dependent regulation of the sumoylation machinery in rat hippocampal neurons. Biol. Cell *105*, 30–45.

Lu, J.R., McKinsey, T.A., Zhang, C.L., and Olson, E.N. (2000). Regulation of skeletal myogenesis by association of the MEF2 transcription factor with class II histone deacetylases. Mol. Cell *6*, 233–244.

Luan, H., Peabody, N.C., Vinson, C.R., and White, B.H. (2006). Refined spatial manipulation of neuronal function by combinatorial restriction of transgene expression. Neuron *52*, 425–436.

Luque, T., and O'Reilly, D.R. (2002). Functional and phylogenetic analyses of a putative *Drosophila melanogaster* UDP-glycosyltransferase gene. Insect Biochem. Mol. Biol. *32*, 1597–1604.

MacLaren, C.M., Evans, T.A., Alvarado, D., and Duffy, J.B. (2004). Comparative analysis of the Kekkon molecules, related members of the LIG superfamily. Dev. Genes Evol. *214*, 360–366.

Maiti, D., Xu, Z., and Duh, E.J. (2008). Vascular endothelial growth factor induces MEF2C and MEF2-dependent activity in endothelial cells. Invest. Ophthalmol. Vis. Sci. *49*, 3640–3648.

Majdzadeh, N., Wang, L., Morrison, B.E., Bassel-Duby, R., Olson, E.N., and D'Mello, S.R. (2008). HDAC4 inhibits cell-cycle progression and protects neurons from cell death. Dev. Neurobiol. *68*, 1076–1092.

Malik, B.R., and Hodge, J.J.L. (2014). *Drosophila* adult olfactory shock learning. Jove-J. Vis. Exp. e50107.

Mandai, K., Guo, T., Hillaire, C.S., Meabon, J.S., Kanning, K.C., Bothwell, M., and Ginty, D.D. (2009). LIG family receptor tyrosine kinase-associated proteins modulate growth factor signals during neural development. Neuron *63*, 614–627.

Manjila, S.B., Kuruvilla, M., Ferveur, J.-F., Sane, S.P., and Hasan, G. (2019). Extended flight bouts require disinhibition from GABAergic mushroom body neurons. Curr. Biol. *29*, 283 – +.

Mao, C.-X., Xiong, Y., Xiong, Z., Wang, Q., Zhang, Y.Q., and Jin, S. (2014). Microtubule-severing protein Katanin regulates neuromuscular junction development and dendritic elaboration in *Drosophila*. Development *141*, 1064–1074.

Mao, Z., Bonni, A., Xia, F., Nadal-Vicens, M., and Greenberg, M.E. (1999). Neuronal Activity-Dependent Cell Survival Mediated by Transcription Factor MEF2. Science *286*, 785–790.

Marks, P.A., Rifkind, R.A., Richon, V.M., Breslow, R., Miller, T., and Kelly, W.K. (2001). Histone deacetylases and cancer: causes and therapies. Nat. Rev. Cancer *1*, 194–202.

Marks, P.A., Miller, T., and Richon, V.M. (2003). Histone deacetylases. Curr. Opin. Pharmacol. *3*, 344–351.

Masek, P., and Keene, A.C. (2016). Gustatory processing and taste memory in *Drosophila*. J. Neurogenet. *30*, 112–121.

Matthews, K.A., Kaufman, T.C., and Gelbart, W.M. (2005). Research resources for *Drosophila*: the expanding universe. Nat. Rev. Genet. *6*, 179–193.

Mayr, B., and Montminy, M. (2001). Transcriptional regulation by the phosphorylation-dependent factor CREB. Nat. Rev. Mol. Cell Biol. *2*, 599–609.

McBride, S.M.J., Giuliani, G., Choi, C., Krause, P., Correale, D., Watson, K., Baker, G., and Siwicki, K.K. (1999). Mushroom body ablation impairs short-term memory and long-term memory of courtship conditioning in *Drosophila melanogaster*. Neuron *24*, 967–977.

McGaugh, J.L., Cahill, L., and Roozendaal, B. (1996). Involvement of the amygdala in memory storage: Interaction with other brain systems. Proc. Natl. Acad. Sci. *93*, 13508–13514.

McGuire, S.E., Mao, Z., and Davis, R.L. (2004). Spatiotemporal gene expression targeting with the TARGET and gene-switch systems in *Drosophila*. Sci STKE *2004*, pl6–pl6.

McKinsey, T.A., Zhang, C.L., and Olson, E.N. (2001). Identification of a signal-responsive nuclear export sequence in class. Mol. Cell. Biol. *21*, 6312–6321.

McKinsey, T.A., Zhang, C.L., and Olson, E.N. (2002). MEF2: a calcium-dependent regulator of cell division, differentiation and death. Trends Biochem. Sci. *27*, 40–47.

McNally, F.J., and Vale, R.D. (1993). Identification of katanin, an ATPase that severs and disassembles stable microtubules. Cell *75*, 419–429.

McNally, K.P., Bazirgan, O.A., and McNally, F.J. (2000). Two domains of p80 katanin regulate microtubule severing and spindle pole targeting by p60 katanin. J. Cell Sci. *113 (Pt 9)*, 1623–1633.

McQuown, S.C., Barrett, R.M., Matheos, D.P., Post, R.J., Rogge, G.A., Alenghat, T., Mullican, S.E., Jones, S., Rusche, J.R., Lazar, M.A., et al. (2011). HDAC3 is a critical negative regulator of long-term memory formation. J. Neurosci. *31*, 764–774.

Mihaylova, M.M., Vasquez, D.S., Ravnskjaer, K., Denechaud, P.-D., Yu, R.T., Alvarez, J.G., Downes, M., Evans, R.M., Montminy, M., and Shaw, R.J. (2011). Class IIa histone deacetylases are hormone-activated regulators of FOXO and mammalian glucose homeostasis. Cell *145*, 607–621.

Mishkin, M., and Appenzeller, T. (1987). The anatomy of memory. Sci. Am. *256*, 80–89.

Miska, E.A., Karlsson, C., Langley, E., Nielsen, S.J., Pines, J., and Kouzarides, T. (1999). HDAC4 deacetylase associates with and represses the MEF2 transcription factor. Embo J. *18*, 5099–5107.

Mitchell, A.L., Attwood, T.K., Babbitt, P.C., Blum, M., Bork, P., Bridge, A., Brown, S.D., Chang, H.-Y., El-Gebali, S., Fraser, M.I., et al. (2019). InterPro in 2019: improving coverage, classification and access to protein sequence annotations. Nucleic Acids Res. *47*, D351–D360.

Moffat, S.D., Zonderman, A.B., and Resnick, S.M. (2001). Age differences in spatial memory in a virtual environment navigation task. Neurobiol. Aging *22*, 787–796.

Montague, S.A., and Baker, B.S. (2016). Memory elicited by courtship conditioning requires mushroom body neuronal subsets similar to those utilized in appetitive memory. PLOS ONE *11*, e0164516.

Morozova, T.V., Anholt, R.R., and Mackay, T.F. (2006). Transcriptional response to alcohol exposure in *Drosophila melanogaster*. Genome Biol. *7*, R95.

Morris, M.J., and Monteggia, L.M. (2013). Unique functional roles for class I and class II histone deacetylases in central nervous system development and function. Int. J. Dev. Neurosci. *31*, 370–381.

Morris, B., Etoubleau, C., Bourthoumieu, S., Reynaud-Perrine, S., Laroche, C., Lebbar, A., Yardin, C., and Elsea, S.H. (2012). Dose dependent expression of HDAC4 causes variable expressivity in a novel inherited case of brachydactyly mental retardation syndrome. Am. J. Med. Genet. A. *158A*, 2015–2020.

Murata, T., Kurokawa, R., Krones, A., Tatsumi, K., Ishii, M., Taki, T., Masuno, M., Ohashi, H., Yanagisawa, M., Rosenfeld, M.G., et al. (2001). Defect of histone acetyltransferase activity of the nuclear transcriptional coactivator CBP in Rubinstein-Taybi syndrome. Hum. Mol. Genet. *10*, 1071–1076.

Murphy, M.P., and LeVine III, H. (2010). Alzheimer's Disease and the amyloid-β peptide. J. Alzheimers Dis. *19*, 311–323.

Musacchio, M., and Perrimon, N. (1996). The *Drosophila kekkon* genes: Novel members of both the leucine-rich repeat and immunoglobulin superfamilies expressed in the CNS. Dev. Biol. *178*, 63–76.

Neely, G.G., Keene, A.C., Duchek, P., Chang, E.C., Wang, Q.-P., Aksoy, Y.A., Rosenzweig, M., Costigan, M., Woolf, C.J., Garrity, P.A., et al. (2011). TrpA1 regulates thermal nociception in *Drosophila*. Plos One *6*, e24343.

Neuner, S.M., Wilmott, L.A., Hoffmann, B.R., Mozhui, K., and Kaczorowski, C.C. (2016). Hippocampal proteomics defines pathways associated with memory decline and resilience in normal aging and Alzheimer's disease mouse models. Behav. Brain Res.

Nighorn, A., Healy, M., and Davis, R. (1991). The cyclic-AMP phosphodiesterase encoded by the *Drosophila dunce* gene is concentrated in the mushroom body neuropil. Neuron *6*, 455–467.

Niu, Y., Wang, T., Liu, S., Yuan, H., Li, H., and Fu, L. (2017). Exercise-induced GLUT4 transcription via inactivation of HDAC4/5 in mouse skeletal muscle in an AMPK alpha 2-dependent manner. Biochim. Biophys. Acta-Mol. Basis Dis. *1863*, 2372–2381.

Nyugen, T., Wang, J., and Schulz, R. (2002). Mutations within the conserved MADS box of the D-MEF2 muscle differentiation factor result in a loss of DNA binding ability and lethality in *Drosophila*. Differentiation *70*, 438–446.

Okabe, M., and Ito, K. (2002). Color Universal Design (CUD) / Colorblind Barrier Free.

osnimf Synapse Figure.

Ozcan, L., Ghorpade, D.S., Zheng, Z., de Souza, J.C., Chen, K., Bessler, M., Bagloo, M., Schrope, B., Pestell, R., and Tabas, I. (2016). Hepatocyte DACH1 is increased in obesity via nuclear exclusion of HDAC4 and promotes hepatic insulin resistance. Cell Rep. *15*, 2214–2225.

Pacifico, R., MacMullen, C.M., Walkinshaw, E., Zhang, X., and Davis, R.L. (2018). Brain transcriptome changes in the aging *Drosophila melanogaster* accompany olfactory memory performance deficits. PloS One *13*, e0209405.

Pandey, U.B., and Nichols, C.D. (2011). Human disease models in *Drosophila melanogaster* and the role of the fly in therapeutic drug discovery. Pharmacol. Rev. *63*, 411–436.

Paroni, G., Fontanini, A., Cernotta, N., Foti, C., Gupta, M.P., Yang, X.-J., Fasino, D., and Brancolini, C. (2007). Dephosphorylation and caspase processing generate distinct nuclear pools of histone deacetylase 4. Mol. Cell. Biol. *27*, 6718–6732.

Paroni, G., Cernotta, N., Dello Russo, C., Gallinari, P., Pallaoro, M., Foti, C., Talamo, F., Orsatti, L., Steinkuhler, C., and Brancolini, C. (2008). PP2A regulates HDAC4 nuclear import. Mol. Biol. Cell *19*, 655–667.

Patterson, M.C. (2003). A riddle wrapped in a mystery: understanding Niemann-Pick disease, type C. The Neurologist *9*, 301–310.

Pavlowsky, A., Schor, J., Plaçais, P.-Y., and Preat, T. (2018). A GABAergic feedback shapes dopaminergic input on the *Drosophila* mushroom body to promote appetitive long-term memory. Curr. Biol. *28*, 1783–1793.e4.

Perazzona, B., Isabel, G., Preat, T., and Davis, R.L. (2004). The role of cAMP response element-binding protein in *Drosophila* long-term memory. J. Neurosci. *24*, 8823–8828.

Perez, F. (2013). Serial Cloner 2.6.1.

Petrij, F., Dauwerse, H., Blough, R., Giles, R., van der Smagt, J.J., Wallerstein, R., Maaswinkel-Mooy, P., van Karnebeek, C.D., van Ommen, G.-J.B., van Haeringen, A., et al. (2000). Diagnostic analysis of the Rubinstein-Taybi syndrome: five cosmids should be used for microdeletion detection and low number of protein truncating mutations. J. Med. Genet. *37*, 168–176.

Pinsker, H., Kupferma.i, Castellu.v, and Kandel, E. (1970). Habituation and dishabituation of gill-withdrawal reflex in *Aplysia*. Science *167*, 1740 – &.

Pinto, D., Delaby, E., Merico, D., Barbosa, M., Merikangas, A., Klei, L., Thiruvahindrapuram, B., Xu, X., Ziman, R., Wang, Z., et al. (2014). Convergence of genes and cellular pathways dysregulated in autism spectrum disorders. Am. J. Hum. Genet. *94*, 677–694.

Plaçais, P.-Y., Trannoy, S., Isabel, G., Aso, Y., Siwanowicz, I., Belliart-Guérin, G., Vernier, P., Birman, S., Tanimoto, H., and Preat, T. (2012). Slow oscillations in two pairs of dopaminergic neurons gate long-term memory formation in *Drosophila*. Nat. Neurosci. *15*, 592–599.

Price, L., Said, K., and Haaland, K.Y. (2004). Age-associated memory impairment of logical memory and visual reproduction. J. Clin. Exp. Neuropsychol. *26*, 531–538.

Prince, M., Wimo, A., Guerchet, M., Ali, G.-C., Wu, Y.-T., Prina, M., and Alzheimer's Disease International (2015). Global Alzheimer's report, 2015.

Przedborski, S. (2017). The two-century journey of Parkinson disease research. Nat. Rev. Neurosci. *18*, 251–259.

Qiu, Y.H., and Davis, R.L. (1993). Genetic dissection of the learning memory gene *dunce* of *Drosophila melanogaster*. Genes Dev. *7*, 1447–1458.

Quinn, W., Harris, W., and Benzer, S. (1974). Conditioned behavior in *Drosophila melanogaster*. Proc. Natl. Acad. Sci. U. S. A. *71*, 708–712.

Ramon y Cajal Santiago (1894). The Croonian lecture.—La fine structure des centres nerveux. Proc. R. Soc. Lond. *55*, 444–468.

Ranganayakulu, G., Zhao, B., Dokidis, A., Molkentin, J.D., Olson, E.N., and Schulz, R.A. (1995). A series of mutations in the D-MEF2 transcription factor reveal multiple functions in larval and adult myogenesis in *Drosophila*. Dev. Biol. *171*, 169–181.

Ray, M., and Lakhotia, S.C. (2015). The commonly used eye-specific sev-GAL4 and GMR-GAL4 drivers in *Drosophila melanogaster* are expressed in tissues other than eyes also. J. Genet. *94*, 407–416.

Revenga, M. de la F., Ibi, D., Saunders, J.M., Cuddy, T., Ijaz, M.K., Toneatti, R., Kurita, M., Holloway, T., Shen, L., Seto, J., et al. (2018). HDAC2-dependent antipsychotic-like effects of chronic treatment with the HDAC inhibitor SAHA in mice. Neuroscience *388*, 102–117.

Robinow, S., and White, K. (1988). The locus *elav* of *Drosophila melanogaster* is expressed in neurons at all developmental stages. Dev. Biol. *126*, 294–303.

Rosenzweig, E.S., Rao, G., McNaughton, B.L., and Barnes, C.A. (1997). Role of temporal summation in age-related long-term potentiation-induction deficits. Hippocampus *7*, 549–558.

Rosenzweig, M., Brennan, K.M., Tayler, T.D., and Garrity, P.A. (2004). *Drosophila* dTRPA1 controls thermosensory behavior. Mol. Biol. Cell *15*, 362A – 362A.

Rosenzweig, M.R., Bennett, E.L., Colombo, P.J., Lee, D.W., and Serrano, P.A. (1993). Short-term, intermediate-term, and long-term memories. Behav. Brain Res. *57*, 193–198.

Rumbaugh, G., Sillivan, S.E., Ozkan, E.D., Rojas, C.S., Hubbs, C.R., Aceti, M., Kilgore, M., Kudugunti, S., Puthanveettil, S.V., Sweatt, J.D., et al. (2015). Pharmacological selectivity within Class I histone deacetylases predicts effects on synaptic function and memory rescue. Neuropsychopharmacology *40*, 2307–2316.

Ryan, C.M., Kindle, K.B., Collins, H.M., and Heery, D.M. (2010). SUMOylation regulates the nuclear mobility of CREB binding protein and its association with nuclear bodies in live cells. Biochem. Biophys. Res. Commun. *391*, 1136–1141.

Sando, R., Gounko, N., Pieraut, S., Liao, L.J., Yates, J., and Maximov, A. (2012). HDAC4 governs a transcriptional program essential for synaptic plasticity and memory. Cell *151*, 821–834.

Saumweber, T., Rohwedder, A., Schleyer, M., Eichler, K., Chen, Y., Aso, Y., Cardona, A., Eschbach, C., Kobler, O., Voigt, A., et al. (2018). Functional architecture of reward learning in mushroom body extrinsic neurons of larval *Drosophila*. Nat. Commun. *9*.

Schmitt, M., and Matthies, H. (1979). Biochemical studies on histones of the central nervous-system .3. Incorporation of [acetate-C-14 into the histones of different rat-brain regions during a learning-experiment. Acta Biol. Med. Ger. *38*, 683–689.

Schwaerzel, M., Monastirioti, M., Scholz, H., Friggi-Grelin, F., Birman, S., and Heisenberg, M. (2003). Dopamine and octopamine differentiate between aversive and appetitive olfactory memories in *Drosophila*. J. Neurosci. *23*, 10495–10502.

Schwartz, S. (2016). Investigating the role of histone deacetylase HDAC4 in long-term memory formation : a thesis presented in partial fulfilment of the requirements for the degree of Doctor of Philosophy in Genetics at Massey University, Manawatu, New Zealand. Thesis. Massey University.

Schwartz, S., Truglio, M., Scott, M.J., and Fitzsimons, H.L. (2016). Long-Term Memory in Drosophila Is Influenced by Histone Deacetylase HDAC4 Interacting with SUMO-Conjugating Enzyme Ubc9. Genetics *203*, 1249–1264.

Segal, M. (1973). Dissecting a short-term memory circuit in the rat brain. I. Changes in entorphinal unit activity and responsiveness of hippocampal units in the process of classical conditioning. Brain Res. *64*, 281–292.

Sen, T., and Sen, N. (2016). Isoflurane-induced inactivation of CREB through histone deacetylase 4 is responsible for cognitive impairment in developing brain. Elsevier Neurobiol. Dis. *96*, 12–21.

Serita, T., Fukushima, H., and Kida, S. (2017). Constitutive activation of CREB in mice enhances temporal association learning and increases hippocampal CA1 neuronal spine density and complexity. Sci. Rep. *7*, 42528.

Seufert, W., Futcher, B., and Jentsch, S. (1995). Role of a ubiquitin-conjugating enzyme in degradation of S- and M-phase cyclins. Nature *373*, 78.

Shalizi, A., Gaudilliere, B., Yuan, Z.Q., Stegmuller, J., Shirogane, T., Ge, Q.Y., Tan, Y., Schulman, B., Harper, J.W., and Bonni, A. (2006). A calcium-regulated MEF2 surnoylation switch controls postsynaptic differentiation. Science *311*, 1012–1017.

Shen, X., Chen, J., Li, J., Kofler, J., and Herrup, K. (2016). Neurons in vulnerable regions of the Alzheimer's Disease brain display reduced ATM signaling. Eneuro *3*, ENEURO.0124–15.2016.

Shen, Y., Wei, W., and Zhou, D.-X. (2015). Histone acetylation enzymes coordinate metabolism and gene expression. Trends Plant Sci. *20*, 614–621.

Shu, S.Y., Wu, Y.M., Bao, X.M., and Leonard, B. (2003). Interactions among memory-related centers in the brain. J. Neurosci. Res. *71*, 609–616.

Siegel, R., and Hall, J. (1979). Conditioned-responses in courtship behavior of normal and mutant *Drosophila*. Proc. Natl. Acad. Sci. U. S. A. *76*, 3430–3434.

Silva, A.J., Kogan, J.H., Frankland, P.W., and Kida, S. (1998). CREB and memory. Annu. Rev. Neurosci. *21*, 127–148.

Sivachenko, A., Li, Y., Abruzzi, K.C., and Rosbash, M. (2013). The transcription factor MEF2 links the *Drosophila* core clock to FAS2, neuronal morphology, and circadian behavior. Neuron *79*, 281–292.

Sokolowski, M.B. (2001). Drosophila: Genetics meets behaviour. Nat. Rev. Genet. *2*, 879–890.

Soler, C., Han, J., and Taylor, M.V. (2012). The conserved transcription factor MEF2 has multiple roles in adult *Drosophila* musculature formation. Development *139*, 1270–1275.

Song, W., Ranjan, R., Dawson-Scully, K., Bronk, P., Marin, L., Seroude, L., Lin, Y.J., Nie, Z.P., Atwood, H.L., Benzer, S., et al. (2002). Presynaptic regulation of neurotransmission in *Drosophila* by the G protein-coupled receptor Methuselah. Neuron *36*, 105–119.

Spector, D.L., and Lamond, A.I. (2011). Nuclear Speckles. Cold Spring Harb. Perspect. Biol. *3*, a000646.

Suzuki, A., Fukushima, H., Mukawa, T., Toyoda, H., Wu, L.-J., Zhao, M.-G., Xu, H., Shang, Y., Endoh, K., Iwamoto, T., et al. (2011). Upregulation of CREB-

mediated transcription enhances both short- and long-term memory. J. Neurosci. *31*, 8786–8802.

Swank, M.W., and Sweatt, J.D. (2001). Increased histone acetyltransferase and lysine acetyltransferase activity and biphasic activation of the ERK/RSK cascade in insular cortex during novel taste learning. J. Neurosci. Off. J. Soc. Neurosci. *21*, 3383–3391.

Takahashi-Fujigasaki, J., and Fujigasaki, H. (2006). Histone deacetylase (HDAC) 4 involvement in both Lewy and Marinesco bodies. Neuropathol. Appl. Neurobiol. *32*, 562–566.

Takehara-Nishiuchi, K. (2014). Entorhinal cortex and consolidated memory. Neurosci. Res. *84*, 27–33.

Takuma, K., Hara, Y., Kataoka, S., Kawanai, T., Maeda, Y., Watanabe, R., Takano, E., Hayata-Takano, A., Hashimoto, H., Ago, Y., et al. (2014). Chronic treatment with valproic acid or sodium butyrate attenuates novel object recognition deficits and hippocampal dendritic spine loss in a mouse model of autism. Pharmacol. Biochem. Behav. *126*, 43–49.

Thurmond, J., Goodman, J.L., Strelets, V.B., Attrill, H., Gramates, L.S., Marygold, S.J., Matthews, B.B., Millburn, G., Antonazzo, G., Trovisco, V., et al. (2019). FlyBase 2.0: the next generation. Nucleic Acids Res. *47*, D759–D765.

Titus, S.A., Warmke, J.W., and Ganetzky, B. (1997). The Drosophila erg K+ channel polypeptide is encoded by the seizure locus. J. Neurosci. *17*, 875–881.

Tomchik, S.M., and Davis, R.L. (2009). Dynamics of learning-related cAMP signaling and stimulus integration in the *Drosophila* olfactory pathway. Neuron *64*, 510–521.

Tompkins, L., Siegel, R.W., Gailey, D.A., and Hall, J.C. (1972). Conditioned courtship in *Drosophila*. Behav. Genet. *13*, 565–578.

Tully, T., and Quinn, W. (1985). Classical-conditioning and retention in normal and mutant *Drosophila-Melanogaster*. J. Comp. Physiol. -Sens. Neural Behav. Physiol. *157*, 263–277.

Tully, T., Preat, T., Boynton, S.C., and Del Vecchio, M. (1994). Genetic dissection of consolidated memory in *Drosophila*. Cell *79*, 35–47.

Tulving, E., and Markowitsch, H.J. (1998). Episodic and declarative memory: Role of the hippocampus. Hippocampus *8*, 198–204.

Urizar, N.L., Yang, Z., Edenberg, H.J., and Davis, R.L. (2007). *Drosophila* Homer is required in a small set of neurons including the ellipsoid body for normal ethanol sensitivity and tolerance. J. Neurosci. *27*, 4541–4551.

Uttl, B., and Graf, P. (1993). Episodic spatial memory in adulthood. Psychol. Aging *8*, 257–273.

Valiati, F.E., Vasconcelos, M., Lichtenfels, M., Petry, F.S., de Almeida, R.M.M., Schwartsmann, G., Schroeder, N., de Farias, C.B., and Roesler, R. (2017). Administration of a histone deacetylase inhibitor into the basolateral amygdala enhances memory consolidation, delays extinction, and increases hippocampal BDNF Levels. Front. Pharmacol. *8*, 415.

Vance, D.E., and Wright, M.A. (2009). Positive and negative neuroplasticity: Implications for age-related cognitive declines. J. Gerontol. Nurs. *35*, 11–17.

Vecsey, C.G., Hawk, J.D., Lattal, K.M., Stein, J.M., Fabian, S.A., Attner, M.A., Cabrera, S.M., McDonough, C.B., Brindle, P.K., Abel, T., et al. (2007). Histone deacetylase inhibitors enhance memory and synaptic plasticity via CREB: CBP-dependent transcriptional activation. J. Neurosci. *27*, 6128–6140.

Vega, R.B., Matsuda, K., Oh, J., Barbosa, A.C., Yang, X.L., Meadows, E., McAnally, J., Pomajzl, C., Shelton, J.M., Richardson, J.A., et al. (2004). Histone deacetylase 4 controls chondrocyte hypertrophy during skeletogenesis. Cell *119*, 555–566.

Venken, K.J.T., and Bellen, H.J. (2007). Transgenesis upgrades for *Drosophila melanogaster*. Development *134*, 3571–3584.

Venken, K.J.T., He, Y., Hoskins, R.A., and Bellen, H.J. (2006). P[acman]: A BAC transgenic platform for targeted insertion of large DNA fragments in *D. melanogaster*. Science *314*, 1747–1751.

Verlinden, H. (2018). Dopamine signalling in locusts and other insects. Insect Biochem. Mol. Biol. *97*, 40–52.

Vianna, M.R.M., Izquierdo, L.A., Barros, D.M., Medina, J.H., and Izquierdo, I. (1999). Intrahippocampal infusion of an inhibitor of protein kinase A separates short- from long-term memory. Behav. Pharmacol. *10*, 223–227.

Vieira, F.G., and Rozas, J. (2011). Comparative genomics of the odorant-binding and chemosensory protein gene families across the arthropoda: Origin and evolutionary history of the chemosensory system. Genome Biol. Evol. *3*, 476–490.

Villain, H., Florian, C., and Roullet, P. (2016). HDAC inhibition promotes both initial consolidation and reconsolidation of spatial memory in mice. Sci. Rep. *6*, 27015.

Viswanath, V., Story, G.M., Peier, A.M., Petrus, M.J., Lee, V.M., Hwang, S.W., Patapoutian, A., and Jegla, T. (2003). Ion channels: Opposite thermosensor in fruitfly and mouse. Nature *423*, 822–823.

Vogt, K., Aso, Y., Hige, T., Knapek, S., Ichinose, T., Friedrich, A.B., Turner, G.C., Rubin, G.M., and Tanimoto, H. (2016). Direct neural pathways convey distinct visual information to *Drosophila* mushroom bodies. eLife *5*.

Wang, A.H., and Yang, X.J. (2001). Histone deacetylase 4 possesses intrinsic nuclear import and export signals. Mol. Cell. Biol. *21*, 5992–6005.

Wang, A.H., Bertos, N.R., Vezmar, M., Pelletier, N., Crosato, M., Heng, H.H., Th'ng, J., Han, J.H., and Yang, X.J. (1999a). HDAC4, a human histone deacetylase related to yeast HDA1, is a transcriptional corepressor. Mol. Cell. Biol. *19*, 7816–7827.

Wang, C.I., Alekseyenko, A.A., LeRoy, G., Elia, A.E., Gorchakov, A.A., Britton, L.-M.P., Elledge, S.J., Kharchenko, P.V., Garcia, B.A., and Kuroda, M.I. (2013). Chromatin proteins captured by ChIP–mass spectrometry are linked to dosage compensation in *Drosophila*. Nat. Struct. Mol. Biol. *20*, 202–209.

Wang, Q., Hasan, G., and Pikielny, C.W. (1999b). Preferential expression of biotransformation enzymes in the olfactory organs of *Drosophila melanogaster*, the antennae. J. Biol. Chem. *274*, 10309–10315.

Wang, Y., Mamiya, A., Chiang, A., and Zhong, Y. (2008). Imaging of an early memory trace in the *Drosophila* mushroom body. J. Neurosci. *28*, 4368–4376.

West, A.P., LLamas, L.L., Snow, P.M., Benzer, S., and Bjorkman, P.J. (2001). Crystal structure of the ectodomain of Methuselah, a *Drosophila* G protein-coupled receptor associated with extended lifespan. Proc. Natl. Acad. Sci. U. S. A. *98*, 3744–3749.

Wilfling, F., Wang, H., Haas, J.T., Krahmer, N., Gould, T.J., Uchida, A., Cheng, J.-X., Graham, M., Christiano, R., Fröhlich, F., et al. (2013). Triacylglycerol synthesis enzymes mediate lipid droplet growth by relocalizing from the ER to lipid droplets. Dev. Cell *24*, 384–399.

Wilkinson, K.A., and Henley, J.M. (2010). Mechanisms, regulation and consequences of protein SUMOylation. Biochem. J. *428*, 133–145.

Wilkinson, K.A., Nakamura, Y., and Henley, J.M. (2010). Targets and consequences of protein SUMOylation in neurons. Brain Res. Rev. *64*, 195–212.

Wilkniss, S.M., Jones, M.G., Korol, D.L., Gold, P.E., and Manning, C.A. (1997). Age-related differences in an ecologically based study of route learning. Psychol. Aging *12*, 372–375.

Williams, S.R., Aldred, M.A., Kaloustian, V.M.D., Halal, F., Gowans, G., McLeod, D.R., Zondag, S., Toriello, H.V., Magenis, R.E., and Elsea, S.H. (2010). Haploinsufficiency of HDAC4 causes Brachydactyly Mental Retardation Syndrome, with brachydactyly type E, developmental delays, and behavioral problems. Am. J. Hum. Genet. *87*, 219–228.

Winnebeck, E.C., Millar, C.D., and Warman, G.R. (2010). Why does insect RNA look degraded? J. Insect Sci. *10*.

World Health Organisation (2016). Global health burdens.

Wu, C.-L., Shih, M.-F.M., Lee, P.-T., and Chiang, A.-S. (2013). An octopamine-mushroom body circuit modulates the formation of anesthesia-resistant memory in *Drosophila*. Curr. Biol. *23*, 2346–2354.

Wu, Q., Yang, X., Zhang, L., Zhang, Y., and Feng, L. (2017). Nuclear accumulation of histone deacetylase 4 (HDAC4) exerts neurotoxicity in models of parkinson's disease. Mol. Neurobiol. *54*, 6970–6983.

Yamagata, N., Hiroi, M., Kondo, S., Abe, A., and Tanimoto, H. (2016). Suppression of dopamine neurons mediates reward. Plos Biol. *14*, e1002586.

Yang, Y., Tse, A.K.W., Li, P., Ma, Q., Xiang, S., Nicosia, S.V., Seto, E., Zhang, X., and Bai, W. (2011). Inhibition of androgen receptor activity by histone deacetylase 4 through receptor SUMOylation. Oncogene *30*, 2207–2218.

Yin, J.C.P., Wallach, J.S., Del Vecchio, M., Wilder, E.L., Zhou, H., Quinn, W.G., and Tully, T. (1994). Induction of a dominant negative CREB transgene specifically blocks long-term memory in *Drosophila*. Cell *79*, 49–58.

Youn, H., Kirkhart, C., Chia, J., and Scott, K. (2018). A subset of octopaminergic neurons that promotes feeding initiation in *Drosophila melanogaster*. PLOS ONE *13*, e0198362.

Yu, D., Keene, A.C., Srivatsan, A., Waddell, S., and Davis, R.L. (2005). *Drosophila* DPM neurons form a delayed and branch-specific memory trace after olfactory classical conditioning. Cell *123*, 945–957.

Yu, W., Qiang, L., Solowska, J.M., Karabay, A., Korulu, S., and Baas, P.W. (2008). The microtubule-severing proteins spastin and katanin participate differently in the formation of axonal branches. Mol. Biol. Cell *19*, 1485–1498.

Zalkin, H., and Dixon, J.E. (1992). *de novo* purine nucleotide biosynthesis. In Progress in Nucleic Acid Research and Molecular Biology, W.E. Cohn, and K. Moldave, eds. (Academic Press), pp. 259–287.

Zhang, T., Branch, A., and Shen, P. (2013). Octopamine-mediated circuit mechanism underlying controlled appetite for palatable food in *Drosophila*. Proc. Natl. Acad. Sci. *110*, 15431–15436.

Zhu, B., Zhao, L., Luo, D., Xu, D., Tan, T., Dong, Z., Tang, Y., Min, Z., Deng, X., Sun, F., et al. (2018). Furin promotes dendritic morphogenesis and learning and memory in transgenic mice. Cell. Mol. Life Sci. *75*, 2473–2488.

Zovkic, I.B., and Sweatt, J.D. (2013). Epigenetic mechanisms in learned fear: Implications for PTSD. Neuropsychopharmacology *38*, 77–93.

Zwarts, L., Vanden Broeck, L., Cappuyns, E., Ayroles, J.F., Magwire, M.M., Vulsteke, V., Clements, J., Mackay, T.F.C., and Callaerts, P. (2015). The genetic basis of natural variation in mushroom body size in Drosophila melanogaster. Nat. Commun. *6*, 10115.

9 APPENDIX 1 FLY STOCKS

Stock Name	Genotype	Source
UAS-Luc	*y[1] v[1]; P{y[+t7.7] v[+t1.8]=UAS-LUC.VALIUM10}attP2*	BDSC 35788
UAS-hHDAC4	*y[1] w[67c23]; P{y[+t7.7]=CaryP}attP2, w[m+C]=UAS-hHDAC4,*	Genetivision, USA
UAS-hHDAC4 3SA	*y[1] w[67c23]; P{y[+t7.7]=CaryP}attP2, w[m+C]=UAS-hHDAC4 3SA*	Genetivision, USA
UAS-hHDAC4 L175A	*y[1] w[67c23]; P{y[+t7.7]=CaryP}attP2, w[m+C]=UAS-hHDAC4 L175A*	Genetivision, USA
UAS-DmHDAC4	*y[1] w[67c23]; P{y[+t7.7]=CaryP}attP2, w[m+C]=UAS-DmHDAC4*	Genetivision, USA
MRE-luc	*y[1] w[1118]; PBac{y[+]-attP-3B}VK00037 w[m+C]=MRE-luc*	Genetivision, USA
delta-luc	*y[1] w[1118]; PBac{y[+]-attP-3B}VK00037 w[m+C]=delta-luc*	Genetivision, USA
UAS-myc-MEF2	*w; M{3xP3-RFP.attP'}ZH-68E myc-MEF2OE/TM6,Tb*	Helen Fitzsimons
GMR-GAL4; hHDAC4	*w[*]; P{w[+mC]=GAL4-ninaE.GMR}12; P{y[+t7.7]=CaryP}attP2, w[m+C]=UAS-hHDAC4,*	Helen Fitzsimons
GMR-GAL4; HDAC4 L175A	*w[*]; P{w[+mC]=GAL4-ninaE.GMR}12; P{y[+t7.7]=CaryP}attP2, w[m+C]=UAS-hHDAC4 L175A*	Helen Fitzsimons
GMR-GAL4; DmHDAC4	*w[*]; P{w[+mC]=GAL4-ninaE.GMR}1; P{y[+t7.7]=CaryP}attP2, w[m+C]=UAS-DmHDAC4*	Helen Fitzsimons
MEF2-VP16	*y[1] w[67c23]; PBac{y+-attP-3B}VK37, UAS-MEF2DBD-VP16. Insert into VK37(2L) 22A3*	Genetivision, USA
MRE-hsp70-luc	*PBac{y+-attP-3B}VK37, MRE-hsp70-luc. Insert into VK37(2L) 22A3*	Genetivision, USA
dMRE-hsp70-luc	*PBac{y+-attP-3B}VK37, dMRE-hsp70-luc. Insert into VK37(2L) 22A3*	Genetivision, USA
GFP-hHDAC4 (WT)	*w[1118];PBac{y+-attP-3B}VK37, UAS-GFP-hHDAC4. Insert into VK37(2L) 22A3*	Genetivision, USA
UAS-DmMEF2-HA	*w[1118]; PBac{y+-attP-3B}VK22, UAS-DmMEF2-HA. Insert into VK22(2R) 57F5*	Genetivision, USA
UAS-DmCREB-ATG2-HA	*w[1118]; PBac{y+-attP-3B}VK22, UAS-DmCREB-ATG-HA. Insert into VK22(2R) 57F5*	Genetivision, USA
UAS-GFP-hHDAC4-3SA	*w[1118];PBac{y+-attP-3B}VK37, UAS-GFP-hHDAC4 3SA. Insert into VK37(2L) 22A3*	Genetivision, USA
UASGFP-hHDAC4-L175A	*w[1118];PBac{y+-attP-3B}VK37, UAS-GFP-hHDAC4-L175A. Insert into VK37(2L) 22A3*	Genetivision, USA
UAS-GFP-DmHDAC4 (WT)	*w[1118];PBac{y+-attP-3B}VK37, UAS-GFP-DmHDAC4.*	Patrick Main

UAS-GFP-hHDAC4 (WT), UAS0DmMEF2-HA	*PBac{y+-attP-3B}VK37, UAS-GFP-DmHDAC4*	Helen Fitzsimons
UAS-GFP-hHDAC4-L175A, UAS-DmMEF2-HA	*PBac{y+-attP-3B}VK37, UAS-GFP-hHDAC4-L175A*	Helen Fitzsimons
UAS-GFP	*w*; P{w+mC=UAS-2xEGFP}AH2*	BDSC 6874
UAS-GFP-hHDAC4-3SA, UAS-DmMEF2-HA	*PBac{y+-attP-3B}VK37, UAS-GFP-hHDAC4 3SA*	Helen Fitzsimons
UAS-GFP-hHDAC4 (WT), UAS-DmCREB-ATG2-HA	*PBac{y+-attP-3B}VK37, UAS-GFP-DmHDAC4*	Helen Fitzsimons
UAS-GFP-hHDAC4-L175A, UAS-DmCREB-ATG2-HA	*PBac{y+-attP-3B}VK37, UAS-GFP-hHDAC4-L175A*	Helen Fitzsimons
UAS-GFP-hHDAC4-3SA, UAS-DmCREB-ATG2-HA	*PBac{y+-attP-3B}VK37, UAS-GFP-hHDAC4 3SA*	Helen Fitzsimons
UAS-TrpA1	*w[*]; P{y[+t7.7] w[+mC]=UAS-TrpA1(B).K}attP16*	BDSC 26263
UAS-CD8::GFP	*y1w*; P{UAS-mCD8::GFP.L}LL5*	BDSC 5137
UAS-GFP-hHDAC4-3SA, UAS-TrpA1	*w[1118];PBac{y+-attP-3B}VK37, UAS-GFP-hHDAC4 3SA, w[+mC]=UAS-TrpA1(B).K}attP16*	Helen Fitzsimons
UAS-GFP-hHDAC4-L175A, UAS-TrpA1	*w[1118];PBac{y+-attP-3B}VK37, UAS-GFP-hHDAC4 L175A, w[+mC]=UAS-TrpA1(B).K}attP16*	Helen Fitzsimons
UAS-GFP-hHDAC4 (WT), UAS-TrpA1	*w[1118];PBac{y+-attP-3B}VK37, UAS-GFP-hHDAC4 (WT), w[+mC]=UAS-TrpA1(B).K}attP16*	Helen Fitzsimons
UAS-GFP-DmHDAC4 (WT), UAS-TrpA1	*w[1118];PBac{y+-attP-3B}VK37, UAS-GFP-DmHDAC4, , w[+mC]=UAS-TrpA1(B).K}attP16*	Helen Fitzsimons

Table 9.1 UAS-construct fly lines used in this project, their genotype, and source

Stock Name	Genotype	Source
w1118	*w[1118]*	BDSC 9752
wCS10	*w[CS10]*	R. Davis
wCS10; Cyo/Sco	*w[CS10]; Cyo/Sco*	R. Davis
wCS10; TM3, Sb	*w[CS10]; TM3,Sb*	R. Davis
wCS10; TM2, Ubx/ TMB6B-P	*W[CS10]; Tm2,Ubx/TM6B-P, Tb*	R. Davis
Canton special (CS10)	*Wild type Canton S strain*	R. Davis
elav^{C155};tub-GAL80^{ts}	*w[CS10]; P{w[+mW.hs]=GawB}elav[C155], P{w+mC=tubP-GAL80ts}10; Cantonized*	Helen Fitzsimons
VK37 attP	*y[1] w[1118]; PBac{y[+]-attP-3B}VK00037 22A3 2L*	BDSC 9752
CyO; TM2/TM6B, Tb[1]	*w[1118]/Dp(1;Y)y[+]; CyO/Bl[1]; TM2/TM6B, Tb[1]*	BDSC 3704
elav; MRE-hsp70-luc	*w[CS10];P{w[+mW.hs]=GawB}elav[C155]; PBac{y+-attP-3B}VK37, MRE-hsp70-luc. Insert into VK37(2L) 22A3*	Helen Fitzsimons
Tub-Gal80^{ts}	*w*; P{w+mC=tubP-GAL80ts}10; TM2/TM6B, Tb1; Gal80ts*	BDSC 7108
OK107-Gal4/Tub-Gal80^{ts}	*w(CS10); P{w+mC=tubP-GAL80ts}10; P{w+mW.hs=GawB}OK107*	Helen Fitzsimons
elav^{C155}-GAL4	*w[CS10];P{w[+mW.hs]=GawB}elav[C155]*	BDSC 458
GMR-GAL4	*w[*]; P{w[+mC]=GAL4-ninaE.GMR}12*	BDSC 1104
elav^{C155}-GAL4; UAS-CD8::GFP	*P{w[+mW.hs]=GawB}elav[C155], P{w[+mC]=UAS-mCD8::GFP.L}Ptp4E[LL4], P{ry[+t7.2]=hsFLP}1, w[*]*	BDSC 5146

Table 9.2 GAL4-driver lines, control lines and balancer fly lines used in this project, their genotype, and source

Stock	Genotype	Source
UAS-MEF2 RNAi	*w[CS10]; P{attP,y[+],w[3'}{GD5039}v15550*	VDRC 15550
UAS-Fu12 RNAi	*y[1] sc[*] v[1]; P{y[+t7.7] v[+t1.8]=TRiP.HMC04917}attP40*	BDSC 57728
UAS-Mthl8 RNAi	*y[1] v[1]; P{y[+t7.7] v[+t1.8]=TRiP.HMJ22590}attP40*	BDSC 60373
UAS-ACXD RNAi	*y[1] sc[*] v[1]; P{y[+t7.7] v[+t1.8]=TRiP.HMC05344}attP40*	BDSC 62871
UAS-Npc2g RNAi	*y[1] sc[*] v[1]; P{y[+t7.7] v[+t1.8]=TRiP.HMS05304}attP40*	BDSC 63030
UAS-kat80 RNAi	*y[1] sc[*] v[1]; P{y[+t7.7] v[+t1.8]=TRiP.HMC06296}attP40*	BDSC 66000

Table 9.3 UAS-RNAi fly lines used in this project, their genotype, and source

10 Appendix 2 Details on GFP::HDAC4v cloning

A brief overview of the generation of the GFP::HDACv constructs was provided in 3.1.2. This section contains details on the restriction enzymes, specific constructs and plasmid maps.

A GFP construct with specific restriction sites based on the sequences of each of the constructs and the pUAST-attB vector. Site-directed mutagenesis was carried out by GenScript (New Jersey, USA), to alter the sequence for insertion of the L175A construct.

GFP oligo sequence

5′ GGA TCC ATG GTG AGC AAG GGC GAG GAG CTG TTC ACC GGG GTG
GTG CCC ATC CTG GTC GAG CTG GAC GGC GAC GTA AAC GGC CAC AAG
TTC AGC GTG TCC GGC GAG GGC GAG GGC GAT GCC ACC TAC GGC AAG
CTG ACC CTG AAG TTC ATC TGC ACC ACC GGC AAG CTG CCC GTG CCC
TGG CCC ACC CTC GTG ACC ACC CTG ACC TAC GGC GTG CAG TGC TTC
AGC CGC TAC CCC GAC CAC ATG AAG CAG CAC GAC TTC TTC AAG TCC
GCC ATG CCC GAA GGC TAC GTC CAG GAG CGC ACC ATC TTC TTC AAG
GAC GAC GGC AAC TAC AAG ACC CGC GCC GAG GTG AAG TTC GAG GGC
GAC ACC CTG GTG AAC CGC ATC GAG CTG AAG GGC ATC GAC TTC AAG
GAG GAC GGC AAC ATC CTG GGG CAC AAG CTG GAG TAC AAC TAC AAC
AGC CAC AAC GTC TAT ATC ATG GCC GAC AAG CAG AAG AAC GGC ATC
AAG GTG AAC TTC AAG ATC CGC CAC AAC ATC GAG GAC GGC AGC GTG
CAG CTC GCC GAC CAC TAC CAG CAG AAC ACC CCC ATC GGC GAC GGC
CCC GTG CTG CTG CCC GAC AAC CAC TAC CTG AGC ACC CAG TCC GCC
CTG AGC AAA GAC CCC AAC GAG AAG CGC GAT CAC ATG GTC CTG CTG
GAG TTC GTG ACC GCC GCC GGG ATC ACT CTC GGC ATG GAC GAG CTG
TAC AAG GCG GCC GCA GAT CTT GGA GGT CTA GA 3′

Where green is the GFP ORF

Orange is the BamHI site for insertion, will be destroyed upon ligation with BglII site in pUAST.

Yellow is the NotI Restriction site

Red is the *BglII* Restriction site

Blue is the *XbaI* Restriction site that will be reconstructed upon re-ligation

Site Directed Mutagenesis:

CAG CTG TAC AAG ~~GCG GCC GCA~~ GAT CTT GGA GGT CTA GA

GT TTA AAC

Disrupting the *NotI* and *BglII* sites with a *PmeI* cut site.

This sequence was inserted into the pUAS-attB vector by GenScript (New Jersey, USA) and used as the host sequence for insertion of each construct. The different cut-sites were necessary to ensure that the constructs were in-frame with the GFP.

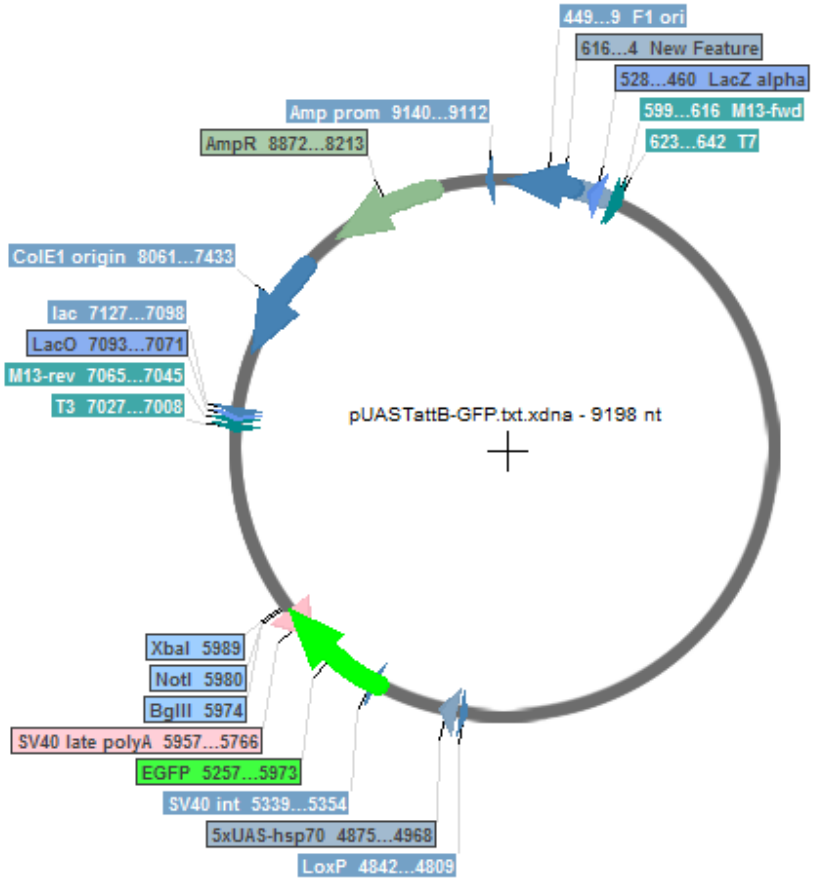

Figure 10.1 Diagram of the pUAST-attB-GFP plasmid.
EGFP sequence highlighted in bright green. pUAST-attB-GFPPmeI is identical apart from site directed mutagenesis at 3' end of GFP sequence

Restriction digest plans were as shown in Table 10.1, digest output shown in Figure 10.2

Construct	Vector digest	Insert digest
hHDAC4 and hHDAC4-3SA	*XbaI, NotI*	*NotI*
hHDAC4-L175A	*PmeI, XbaI*	*PmeI, XbaI*
DmHDAC4	*BglII, XbaI*	*BglII, XbaI*

Table 10.1 Restriction digest plan for digestion of vector and excision of HDACv inserts

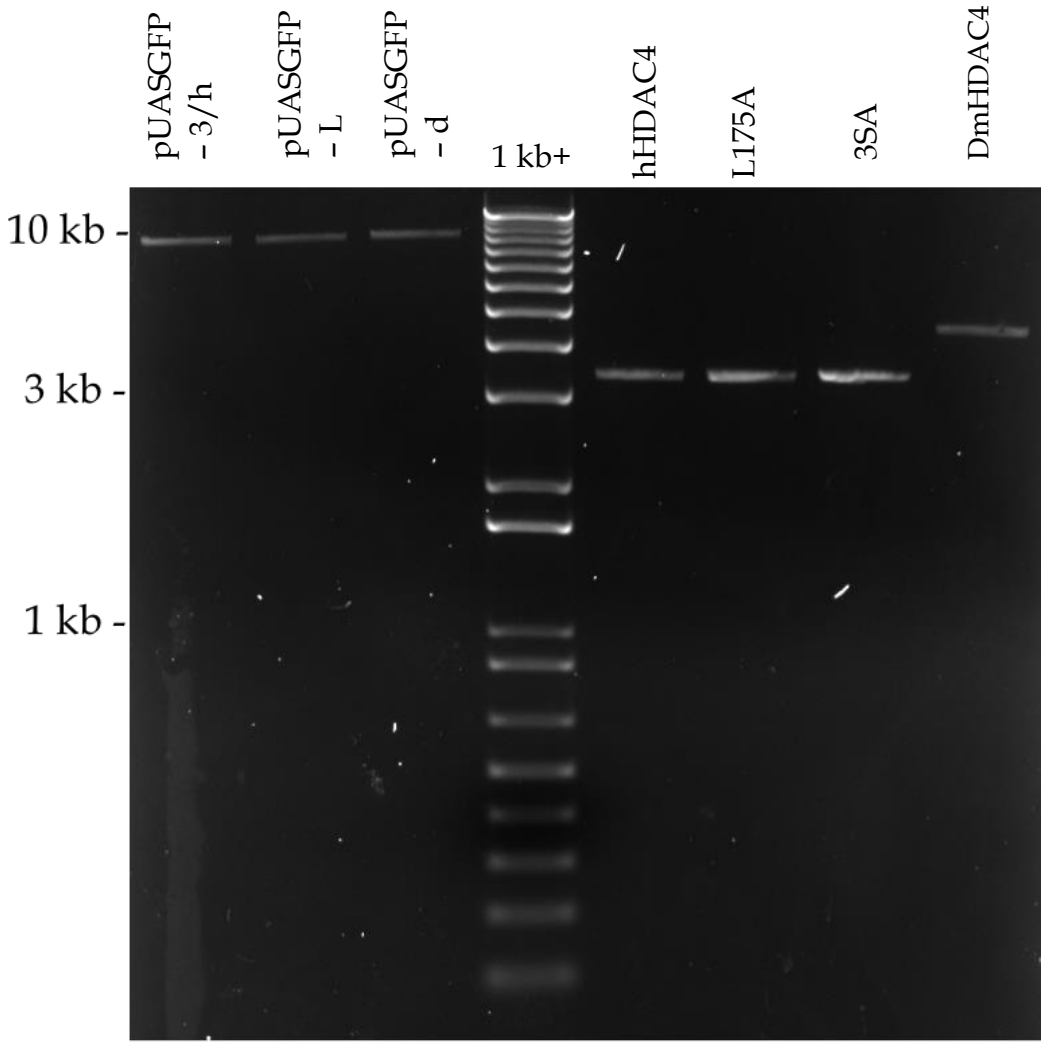

Figure 10.2 Agarose gel electrophoresis of digested vectors and inserts

Vector digests are labelled with the first letter of the intended insert. Inserts are labelled as appropriate.

Verification of the digests was carried out before purification. It was noted that the hHDAC4 and hHDAC4-3SA inserts could be inserted in the reverse orientation, making the internal digest extremely important in determining orientation of the insert (see Figure 3.3). Final plasmid constructs are shown below (Figures 10.3, 10.4, and 10.5), 3SA and hHDAC4 constructs are interchangeable barring the mutations required for 3SA variant.

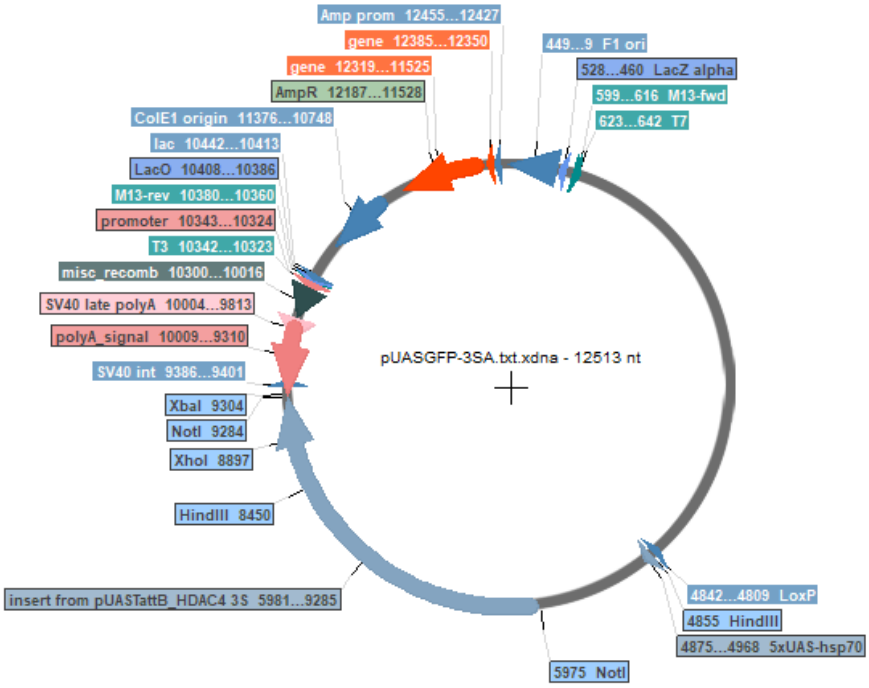

Figure 10.3 pUAST-attB-GFP-3SA plasmid map.
Figure made in SerialCloner 2.6.1 (Perez, 2013).

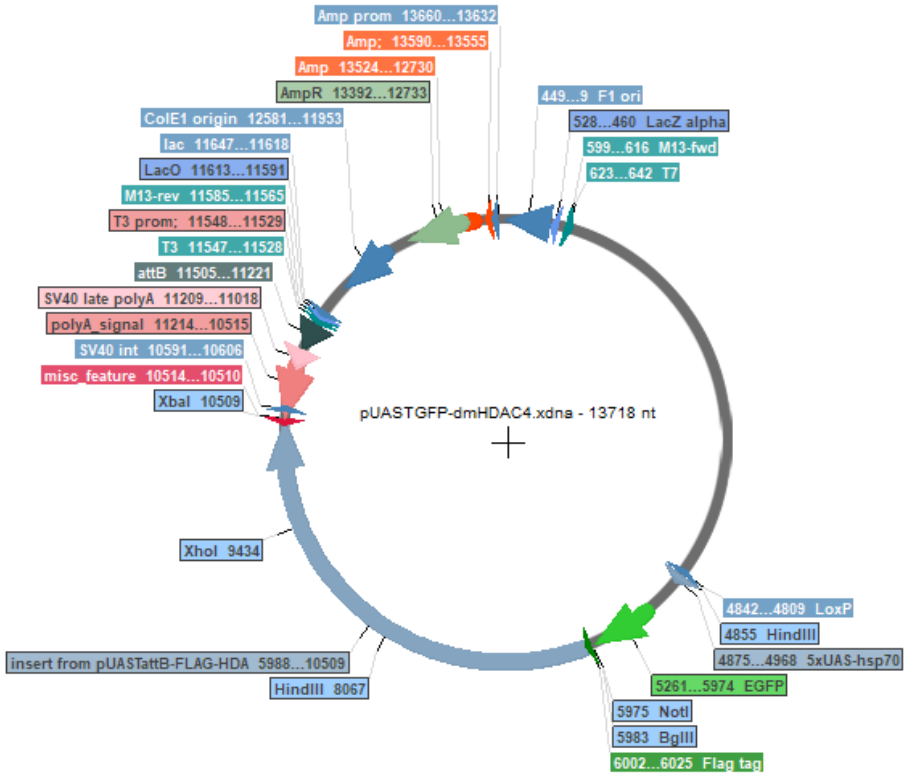

Figure 10.4 pUAST-attB-GFP-DmHDAC4 plasmid map.
Figure made in SerialCloner 2.6.1 (Perez, 2013).

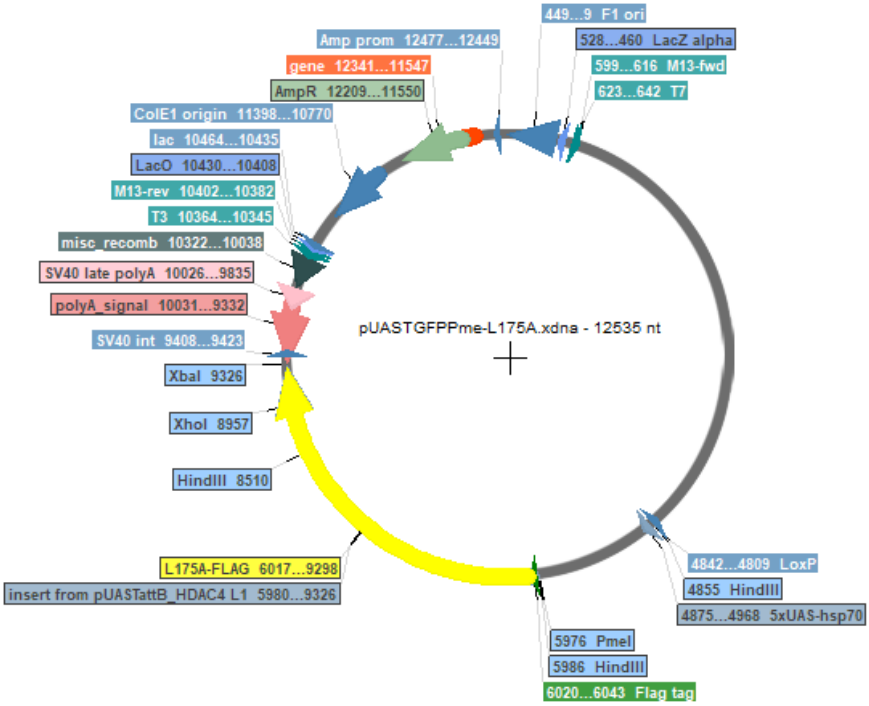

Figure 10.5 pUAST-attB-GFP-L175A plasmid map.
Figure made in SerialCloner 2.6.1 (Perez, 2013).

11 Appendix 3 Primers, plasmids and sequences

11.1 PCR Primers

Primer Name	Sequence 5′ > 3′	Usage
Hsp70min F	ATCT AGA TCT GAG CGC CGG AGT ATA AAT AG	Generation of the hsp70 minimal promoter fragment
Hsp70min R	ATC GCT CGA GGG ATC CCA ATT CCC TAT TCA GAG TTC	Generation of the hsp70 minimal promoter fragment
MRE F	CTA GCG ATA TCT GTT ACT AAA AAT AGA ATG TTA CTA AAA ATA GAA TGT TAC TAA AAA TAG AAA	Generation of 3xMRE sequence for Luciferase activation
MRE R	GAT CTT TCT ATT TTT AGT AAC ATT CTA TTT TTA GTA ACA TTC TAT TTT TAG TAA CAG ATA TCG	Generation of 3xMRE sequence for Luciferase activation
ΔMRE F	CTA GCG ATA TCT GTT ACT AAG GGT AGA ATG TTA CTA AGG GTA GAA TGT TAC TAA GGG TAG AAA	Generation of 3xΔMRE sequence for Luciferase control
ΔMRE R	GAT CTT TCT ACC CTT AGT AAC ATT CTA CCC TTA GTA ACA TTC TAC CCT TAG TAA CAG ATA TCG	Generation of 3xΔMRE sequence for Luciferase control
pUASTForSeq	GCA ACT ACT GAA ATC TGC CAA G	Verifying ORF-integrity in pUAST-attB-GFP-HDACv plasmids
pUASRevSeq	TCA TCA GTT CCA TAG GTT GG	Verifying ORF-integrity in pUAST-attB-GFP-HDACv plasmids
GFPEndFor	GAC AAC CAC TAC CTG AGC AG	Verifying ORF-integrity in pUAST-attB-GFP-HDACv plasmids

Table 11.1 PCR Primers used in this project, primers are from Sigma Aldrich

11.2 Plasmids

Plasmid Identifier	Description	Source
pCDNA3.1 – DmMEF2	*Drosophila* MEF2 with cytomegalovirs (CMV) promoter	Helen Fitzsimons
pCDNA3.1 – MmMEF2C-HA	Mouse MEF2C with CMV promoter	Addgene #32515
pCDNA3.1 – MEF2-VP16	MEF2-DNA binding domain with VP16 transactivation domain under CMV promoter	Gift from Sangeeta Chawla, University of York
pCDNA3.1 – hHDAC4	Human HDAC4 under CMV promoter	Gift from Sasha Mouravlev, University of Auckland)
pCDNA3.1 – hHDAC4-L175A	Human HDAC4 with L175A mutation under CMV promoter	Gift from Xiang-Jiao Yang, McGill University
pCDNA3.1 – hHDAC4-3SA	Human HDAC4 with 3SA mutations under CMV promoter	Gift from Sasha Mouravlev, University of Auckland
pAM/CBA-HA-mCREB-WPRE-BGH	Mouse CREB under the CMV enhancer/chicken beta-actin (CBA) promoter	Gift from Sasha Mouravlev, University of Auckland
pAM/CBA-PKA-WPRE-BGH	Human PKA under the CMV enhancer/chicken beta-actin (CBA) promoter	Gift from Sasha Mouravlev, University of Auckland
pUAST-attB	Plasmid containing a UAS and the attB site for phiC31 integration	Max Scott, Massey University
CRE-Luciferase	Plasmid harbouring CRE-Luciferase	Stratagen
pattB-MRE-Luciferase	MRE-Luciferase construct with attB site for phiC31 integration	Helen Fitzsimons
pUAST-attB-GFP-DmHDAC4	pUAST-attB plasmid with GFP-fused *Drosophila* HDAC4	Patrick Main - See Appendix 2
pUAST-attB-GFP-hHDAC4	pUAST-attB plasmid with GFP-fused human HDAC4	Patrick Main - See Appendix 2
pUAST-attB-GFP-L175A	pUAST-attB plasmid with GFP-fused human HDAC4-L175A	Patrick Main - See Appendix 2
pUAST-attB-GFP-3SA	pUAST-attB plasmid with GFP-fused human HDAC4-3SA	Patrick Main - See Appendix 2
hsp70MRE-Luciferase	3xMEF2 Response element fused to luciferase reporter, preceded by *Drosophila* hsp70 minimal promoter	Helen Fitzsimons - See Appendix 4
hsp70ΔMRE-Luciferase	The same as hsp70MRE-Luciferase but with the 3xMRE interrupted, see source	Helen Fitzsimons - See Appendix 4

Table 11.2 Plasmids used in this project

11.3 Antibodies

Name	Target	Source organism	Source	Concentration
1D4 anti-Fasciclin II	Fasciclin (FasII)	Mouse	Developmental Studies Hybridoma Bank (DSHB)	IHC 1: 2,000
Ab290	GFP-tag	Rabbit	AbCam	IHC 1 : 10,000 WB 1 : 4,000
Anti-HA High Affinity (3F10)	HA-tag	Rat	Sigma Aldrich	IHC 1 : 500 WB 1 : 4,000
9E10 c-myc	Myc-tag	Mouse	DSHB	IHC 1 : 50 WB 1 : 500
12G10 αTubulin	Tubulin	Mouse	DSHB	WB 1 : 500
Anti-FLAG M2 antibody	FLAG	Rabbit	Sigma Aldrich	IHC 1 : 5,000

Table 11.3 Primary antibodies used in immunohistochemistry (IHC) and Western blotting (WB).

Name	Target Species	Origin	Source	Concentration
Anti-Rat 555	Rat	Goat	Sigma Aldrich	IHC 1 : 500
Anti-Rat 647	Rat	Goat	Sigma Aldrich	IHC 1 : 500
Anti-Rabbit 488	Rabbit	Goat	Sigma Aldrich	IHC 1 : 500
Anti-Mouse 488	Mouse	Goat	Sigma Aldrich	IHC 1 : 500
Anti-Mouse 555	Mouse	Goat	Sigma Aldrich	IHC 1 : 500
Mouse HRP	Mouse	Goat	Sigma Aldrich	WB 1 : 10,000
Rabbit HRP	Rabbit	Goat	Sigma Aldrich	WB 1 : 20,000
Rat HRP	Rat	Goat	Abcam	WB 1 : 40,000

Table 11.4 Secondary antibodies used in immunohistochemistry (IHC) and Western blotting (WB).

11.4 HDAC4 variant sequences

hHDAC4 - 3SA

The codons responsible for S -> A mutation are highlighted in red and underlined.

5′

ATGAGCTCCCAAAGCCATCCAGATGGACTTTCTGGCCGAGACCAGCCAGTGGAGCTGCT
GAATCCTGCCCGCGTGAACCACATGCCCAGCACGGTGGATGTGGCCACGGCGCTGCCTC
TGCAAGTGGCCCCCTCGGCAGTGCCCATGGACCTGCGCCTGGACCACCAGTTCTCACTG
CCTGTGGCAGAGCCGGCCCTGCGGGAGCAGCAGCTGCAGCAGGAGCTCCTGGCGCTCAA
GCAGAAGCAGCAGATCCAGAGGCAGATCCTCATCGCTGAGTTCCAGAGGCAGCACGAGC
AGCTCTCCCGGCAGCACGAGGCGCAGCTCCACGAGCACATCAAGCAACAACAGGAGATG
CTGGCCATGAAGCACCAGCAGGAGCTGCTGGAACACCAGCGGAAGCTGGAGAGGCACCG
CCAGGAGCAGGAGCTGGAGAAGCAGCACCGGGAGCAGAAGCTGCAGCAGCTCAAGAACA
AGGAGAAGGGCAAAGAGAGTGCCGTGGCCAGCACAGAAGTGAAGATGAAGTTACAAGAA
TTTGTCCTCAATAAAAAGAAGGCGCTGGCCCACCGGAATCTGAACCACTGCATTTCCAG
CGACCCTCGCTACTGGTACGGGAAAACGCAGCACAGTTCCCTTGACCAGAGTTCTCCAC
CCCAGAGCGGAGTGTCGACCTCCTATAACCACCCGGTCCTGGGAATGTACGACGCCAAA
GATGACTTCCCTCTTAGGAAAACAGC**TGC**TGAACCGAATCTGAAATTACGGTCCAGGCT
AAAGCAGAAAGTGGCCGAAAGACGGAGCAGCCCCCTGTTACGCAGGAAAGACGGGCCAG
TGGTCACTGCTCTAAAAAAGCGTCCGTTGGATGTCACAGACTCCGCGTGCAGCAGCGCC
CCAGGCTCCGGACCCAGCTCACCCAACAACAGCTCCGGGAGCGTCAGCGCGGAGAACGG
TATCGCGCCCGCCGTCCCCAGCATCCCGGCGGAGACGAGTTTGGCGCACAGACTTGTGG
CACGAGAAGGCTCGGCCGCTCCACTTCCCCTCTACACATCGCCATCCTTGCCCAACATC
ACGCTGGGCCTGCCTGCCACCGGCCCCTCTGCGGGCACGGCGGGCCAGCAGGACGCCGA
GAGACTCACCCTTCCCGCCCTCCAGCAGAGGCTCTCCCTTTTCCCCGGCACCCACCTCA
CTCCCTACCTGAGCACCTCGCCCTTGGAGCGGGACGGAGGGGCAGCGCACAGCCCTCTT
CTGCAGCACATGGTCTTACTGGAGCAGCCACCGGCACAAGCACCCCTCGTCACAGGCCT
GGGAGCACTGCCCCTCCACGCACAGTCCTTGGTTGGTGCAGACCGGGTGTCCCCCTCCA
TCCACAAGCTGCGGCAGCACCGCCCACTGGGGCGGACCCAG**GCG**GCCCCGCTGCCCCAG
AACGCCCAGGCTCTGCAGCACCTGGTCATCCAGCAGCAGCATCAGCAGTTTCTGGAGAA
ACACAAGCAGCAGTTCCAGCAGCAGCAACTGCAGATGAACAAGATCATCCCCAAGCCAA
GCGAGCCAGCCCGGCAGCCGGAGAGCCACCCGGAGGAGACGGAGGAGGAGCTCCGTGAG
CACCAGGCTCTGCTGGACGAGCCCTACCTGGACCGGCTGCCGGGGCAGAAGGAGGCGCA
CGCACAGGCCGGCGTGCAGGTGAAGCAGGAGCCCATTGAGAGCGATGAGGAAGAGGCAG
AGCCCCCACGGGAGGTGGAGCCGGGCCAGCGCCAGCCCAGTGAGCAGGAGCTGCTCTTC
AGACAGCAAGCCCTCCTGCTGGAGCAGCAGCGGATCCACCAGCTGAGGAACTACCAGGC
GTCCATGGAGGCCGCCGGCATCCCCGTGTCCTTCGGCGGCCACAGGCCTCTGTCCCGGG
CGCAG**GCG**TCACCCGCGTCTGCCACCTTCCCCGTGTCTGTGCAGGAGCCCCCCACCAAG
CCGAGGTTCACGACAGGCCTCGTGTATGACACGCTGATGCTGAAGCACCAGTGCACCTG
CGGGAGTAGCAGCAGCCACCCCGAGCACGCCGGGAGGATCCAGAGCATCTGGTCCCGCC
TGCAGGAGACGGGCCTCCGGGGCAAATGCGAGTGCATCCGCGGACGCAAGGCCACCCTG
GAGGAGCTACAGACGGTGCACTCGGAAGCCCACACCCTCCTGTATGGCACGAACCCCCT
CAACCGGCAGAAACTGGACAGTAAGAAACTTCTAGGCTCGCTCGCCTCCGTGTTCGTCC
GGCTCCCTTGCGGTGGTGTTGGGGTGGACAGTGACACCATATGGAACGAGGTGCACTCG
GCGGGGGCAGCCCGCCTGGCTGTGGGCTGCGTGGTAGAGCTGGTCTTCAAGGTGGCCAC
AGGGGAGCTGAAGAATGGCTTTGCTGTGGTCCGCCCCCCTGGACACCATGCGGAGGAGA
GCACGCCCATGGGCTTTTGCTACTTCAACTCCGTGGCCGTGGCAGCCAAGCTTCTGCAG
CAGAGGTTGAGCGTGAGCAAGATCCTCATCGTGGACTGGGACGTGCACCATGGAAACGG

GACCCAGCAGGCTTTCTACAGCGACCCTAGCGTCCTGTACATGTCCCTCCACCGCTACG
ACGATGGGAACTTCTTCCCAGGCAGCGGGGCTCCTGATGAGGTGGGCACAGGGCCCGGC
GTGGGTTTCAACGTCAACATGGCTTTCACCGGCGGCCTGGACCCCCCCATGGGAGACGC
TGAGTACTTGGCGGCCTTCAGAACGGTGGTCATGCCGATCGCCAGCGAGTTTGCCCCGG
ATGTGGTGCTGGTGTCATCAGGCTTCGATGCCGTGGAGGGCCACCCCACCCCTCTTGGG
GGCTACAACCTCTCCGCCAGATGCTTCGGGTACCTGACGAAGCAGCTGATGGGCCTGGC
TGGCGGCCGGATTGTCCTGGCCCTCGAGGGAGGCCACGACCTGACCGCCATTTGCGACG
CCTCGGAAGCATGTGTTTCTGCCTTGCTGGGAAACGAGCTTGATCCTCTCCCAGAAAAG
GTTTTACAGCAAAGACCCAATGCAAACGCTGTCCGTTCCATGGAGAAAGTCATGGAGAT
CCACAGCAAGTACTGGCGCTGCCTGCAGCGCACAACCTCCACAGCGGGGCGTTCTCTGA
TCGAGGCTCAGACTTGCGAGAACGAAGAAGCCGAGACGGTCACCGCCATGGCCTCGCTG
TCCGTGGGCGTGAAGCCCGCCGAAAAGAGACCAGATGAGGAGCCCATGGAAGAGGAGCC
GCCCCTGGGGGATTATAAAGATGATGATGATAAATAAGAATTCGTTAA

FLAG-hHDAC4-L175A

The codon responsible for L175A mutation is highlighted in red and under-lined.

5′
ATGGACTACAAGGACGACGATGACAAAGAATTCTCCCAAAGCCATCCAGATGGACTTTC
TGGCCGAGACCAGCCAGTGGAGCTGCTGAATCCTGCCCGCGTGAACCACATGCCCAGCA
CGGTGGATGTGGCCACGGCGCTGCCTCTGCAAGTGGCCCCCTCGGCAGTGCCCATGGAC
CTGCGCCTGGACCACCAGTTCTCACTGCCTGTGGCAGAGCCGGCCCTGCGGGAGCAGCA
GCTGCAGCAGGAGCTCCTGGCGCTCAAGCAGAAGCAGCAGATCCAGAGGCAGATCCTCA
TCGCTGAGTTCCAGAGGCAGCACGAGCAGCTCTCCCGGCAGCACGAGGCGCAGCTCCAC
GAGCACATCAAGCAACAACAGGAGATGCTGGCCATGAAGCACCAGCAGGAGCTGCTGGA
ACACCAGCGGAAGCTGGAGAGGCACCGCCAGGAGCAGGAGCTGGAGAAGCAGCACCGGG
AGCAGAAGCTGCAGCAGCTCAAGAACAAGGAGAAGGGCAAAGAGAGTGCCGTGGCCAGC
ACAGAAGTGAAGATGAAG**GCA**CAAGAATTTGTCCTCAATAAAAAGAAGGCGCTGGCCCA
CCGGAATCTGAACCACTGCATTTCCAGCGACCCTCGCTACTGGTACGGGAAAACGCAGC
ACAGTTCCCTTGACCAGAGTTCTCCACCCCAGAGCGGAGTGTCGACCTCCTATAACCAC
CCGGTCCTGGGAATGTACGACGCCAAAGATGACTTCCCTCTTAGGAAAACAGCTTCTGA
ACCGAATCTGAAATTACGGTCCAGGCTAAAGCAGAAAGTGGCCGAAAGACGGAGCAGCC
CCCTGTTACGCAGGAAAGACGGGCCAGTGGTCACTGCTCTAAAAAAGCGTCCGTTGGAT
GTCACAGACTCCGCGTGCAGCAGCGCCCCAGGCTCCGGACCCAGCTCACCCAACAACAG
CTCCGGGAGCGTCAGCGCGGAGAACGGTATCGCGCCCGCCGTCCCCAGCATCCCGGCGG
AGACGAGTTTGGCGCACAGACTTGTGGCACGAGAAGGCTCGGCCGCTCCACTTCCCCTC
TACACATCGCCATCCTTGCCCAACATCACGCTGGGCCTGCCTGCCACCGGCCCCTCTGC
GGGCACGGCGGGCCAGCAGGACGCCGAGAGACTCACCCTTCCCGCCCTCCAGCAGAGGC
TCTCCCTTTTCCCCGGCACCCACCTCACTCCCTACCTGAGCACCTCGCCCTTGGAGCGG
GACGGAGGGGCAGCGCACAGCCCTCTTCTGCAGCACATGGTCTTACTGGAGCAGCCGCC
GGCACAAGCACCCCTCGTCACAGGCCTGGGAGCACTGCCCCTCCACGCACAGTCCTTGG
TTGGTGCAGACCGGGTGTCCCCCTCCATCCACAAGCTGCGGCAGCACCGCCCACTGGGG
CGGACCCAGTCGGCCCCGCTGCCCCAGAACGCCCAGGCTCTGCAGCACCTGGTCATCCA
GCAGCAGCATCAGCAGTTTCTGGAGAAACACAAGCAGCAGTTCCAGCAGCAGCAACTGC
AGATGAACAAGATCATCCCCAAGCCAAGCGAGCCAGCCCGGCAGCCGGAGAGCCACCCG
GAGGAGACGGAGGAGGAGCTCCGTGAGCACCAGGCTCTGCTGGACGAGCCCTACCTGGA
CCGGCTGCCGGGGCAGAAGGAGGCGCACGCACAGGCCGGCGTGCAGGTGAAGCAGGAGC
CCATTGAGAGCGATGAGGAAGAGGCAGAGCCCCCACGGGAGGTGGAGCCGGGCCAGCGC
CAGCCCAGTGAGCAGGAGCTGCTCTTCAGACAGCAAGCCCTCCTGCTGGAGCAGCAGCG
GATCCACCAGCTGAGGAACTACCAGGCGTCCATGGAGGCCGCCGGCATCCCCGTGTCCT

TCGGCGGCCACAGGCCTCTGTCCCGGGCGCAGTCCTCACCCGCGTCTGCCACCTTCCCC
GTGTCTGTGCAGGAGCCCCCCACCAAGCCGAGGTTCACGACAGGCCTCGTGTATGACAC
GCTGATGCTGAAGCACCAGTGCACCTGCGGGAGTAGCAGCAGCCACCCCGAGCACGCCG
GGAGGATCCAGAGCATCTGGTCCCGCCTGCAGGAGACGGGCCTCCGGGGCAAATGCGAG
TGCATCCGCGGACGCAAGGCCACCCTGGAGGAGCTACAGACGGTGCACTCGGAAGCCCA
CACCCTCCTGTATGGCACGAACCCCCTCAACCGGCAGAAACTGGACAGTAAGAAACTTC
TAGGCTCGCTCGCCTCCGTGTTCGTCCGGCTCCCTTGCGGTGGTGTTGGGGTGGACAGT
GACACCATATGGAACGAGGTGCACTCGGCGGGGGCAGCCCGCCTGGCTGTGGGCTGCGT
GGTAGAGCTGGTCTTCAAGGTGGCCACAGGGGAGCTGAAGAATGGCTTTGCTGTGGTCC
GCCCCCCTGGACACCATGCGGAGGAGAGCACGCCCATGGGCTTTTGCTACTTCAACTCC
GTGGCCGTGGCAGCCAAGCTTCTGCAGCAGAGGTTGAGCGTGAGCAAGATCCTCATCGT
GGACTGGGACGTGCACCATGGAAACGGGACCCAGCAGGCTTTCTACAGCGACCCTAGCG
TCCTGTACATGTCCCTCCACCGCTACGACGATGGGAACTTCTTCCCAGGCAGCGGGGCT
CCTGATGAGGTGGGCACAGGGCCCGGCGTGGGTTTCAACGTCAACATGGCTTTCACCGG
CGGCCTGGACCCCCCCATGGGAGACGCTGAGTACTTGGCGGCCTTCAGAACGGTGGTCA
TGCCGATCGCCAGCGAGTTTGCCCCGGATGTGGTGCTGGTGTCATCAGGCTTCGATGCC
GTGGAGGGCCACCCCACCCCTCTTGGGGGCTACAACCTCTCCGCCAGATGCTTCGGGTA
CCTGACGAAGCAGCTGATGGGCCTGGCTGGCGGCCGGATTGTCCTGGCCCTCGAGGGAG
GCCACGACCTGACCGCCATTTGCGACGCCTCGGAAGCATGTGTTTCTGCCTTGCTGGGA
AACGAGCTTGATCCTCTCCCAGAAAAGGTTTTACAGCAAAGACCCAATGCAAACGCTGT
CCGTTCCATGGAGAAAGTCATGGAGATCCACAGCAAGTACTGGCGCTGCCTGCAGCGCA
CAACCTCCACAGCGGGGCGTTCTCTGATCGAGGCTCAGACTTGCGAGAACGAAGAAGCC
GAGACGGTCACCGCCATGGCCTCGCTGTCCGTGGGCGTGAAGCCCGCCGAAAAGAGACC
AGATGAGGAGCCCATGGAAGAGGAGCCGCCCCTGTAGCACTCCCTCGAAGCTGCTGTTG
GTACCTCTAG

12 Appendix 4 hsp70MRE and hsp70ΔMRE development

The plasmid harbouring the hsp70MRE (and, subsequently, the hsp70ΔMRE) was generated by insertion of the hsp70 minimal promoter from a pUAS-attB plasmid into the pattB-MRE by generating a PCR product using primers hsp70minR and hsp70minF (Table 11.1, Appendix 3) and ligating the product in between the unique *Bgl II* and *Xho I* after the MRE.

Following the generation of this intermediary, the luciferase gene was excised from a pMIR-report plasmid using *Bam HI* and *SpeI* and ligated into the *Bam HI* and *Xba I* digested intermediary. The final product harbours an attB integrase site, an hsp70 minimal promoter, the 3xMEF2-binding MRE sequence and a *luciferase* gene. Plasmid map detailed below (Figure 12.1). The ΔMRE followed the same generation process but uses the ΔMRE fragment.

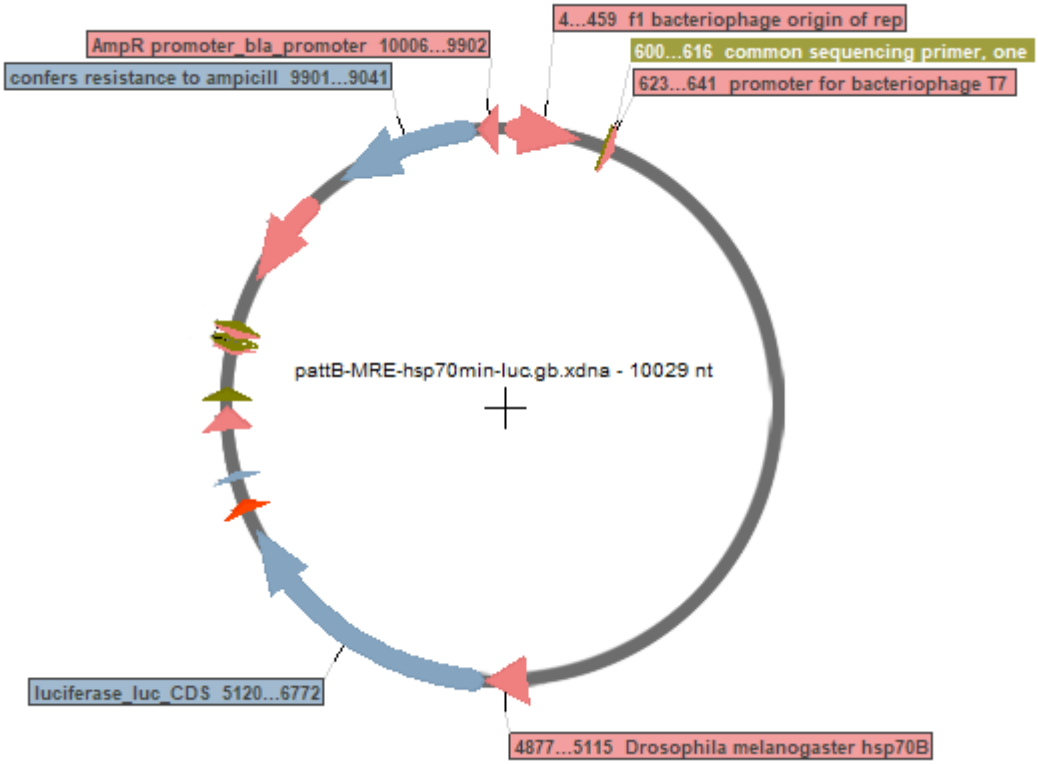

Figure 12.1 Map of the hsp70MRE-luciferase plasmid.
Image generated by SerialCloner 2.6.1 (Perez, 2013)

13 APPENDIX 5 RNASEQ QUALITY CONTROL

Samples are labelled in the figure captions, final digit indicates “forward” and “reverse” paired end sequencing.

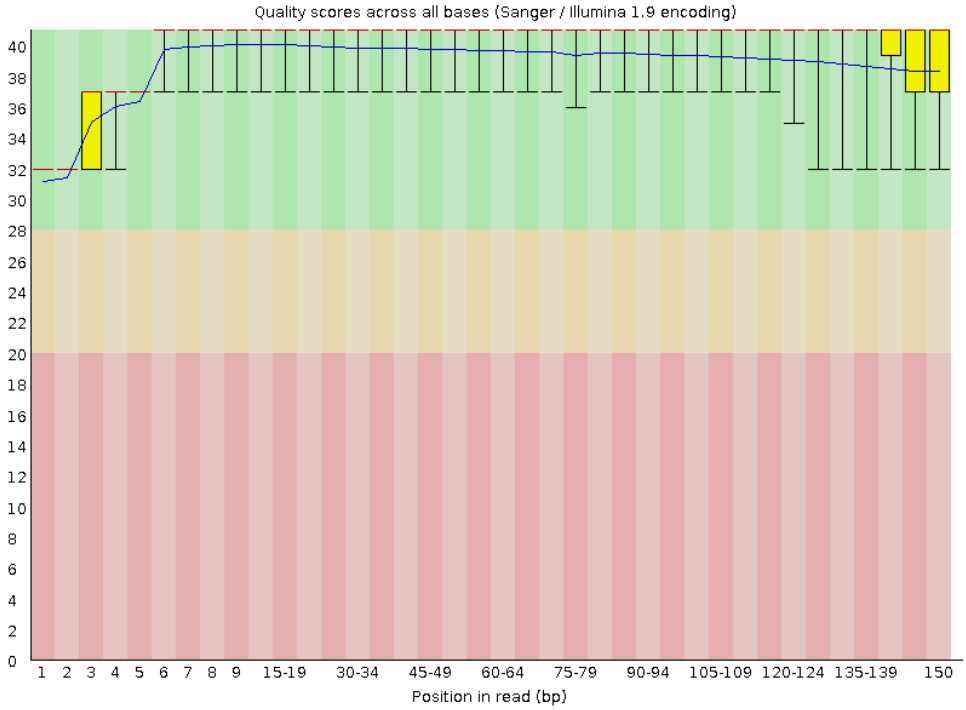

Figure 13.1 Per read quality analysis for sample 3SA_1_1

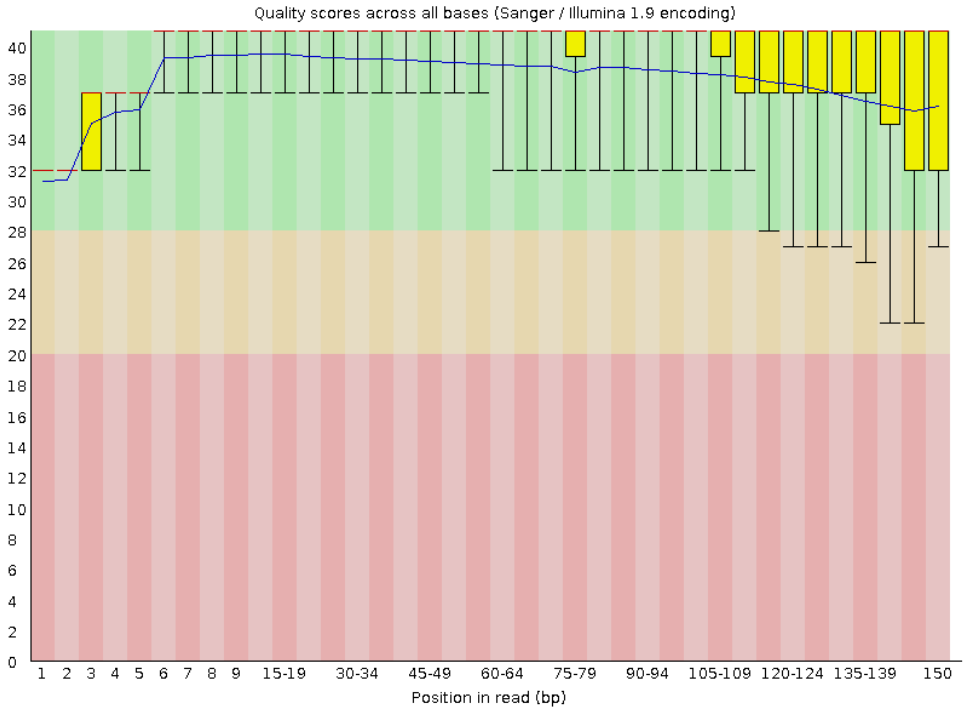

Figure 13.2 Per read quality analysis for sample 3SA_1_2

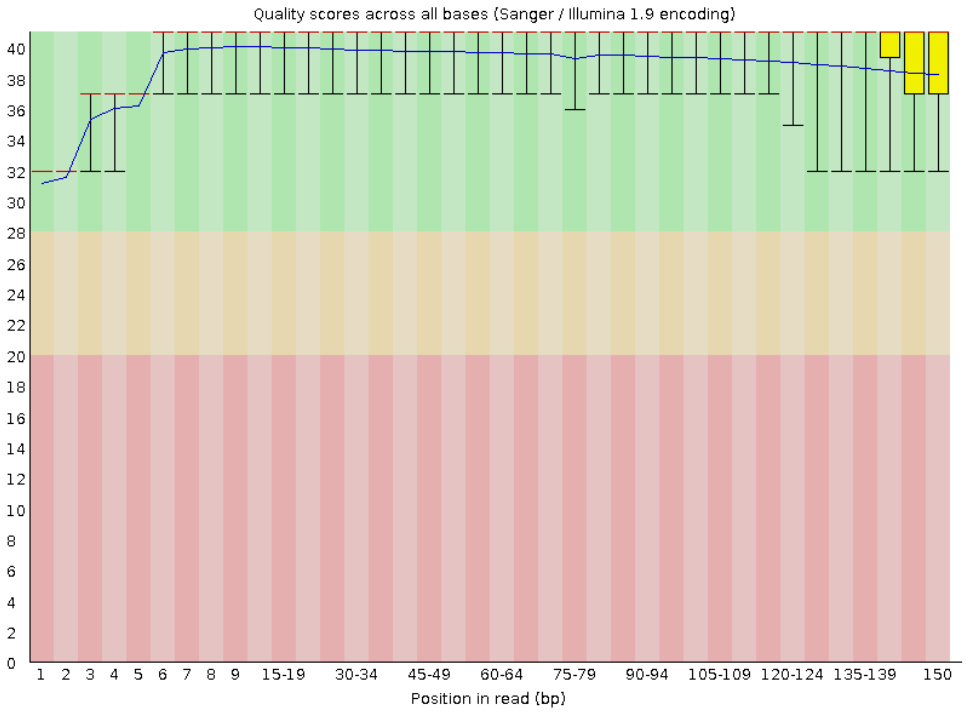

Figure 13.3 Per read quality analysis for sample 3SA_2_1

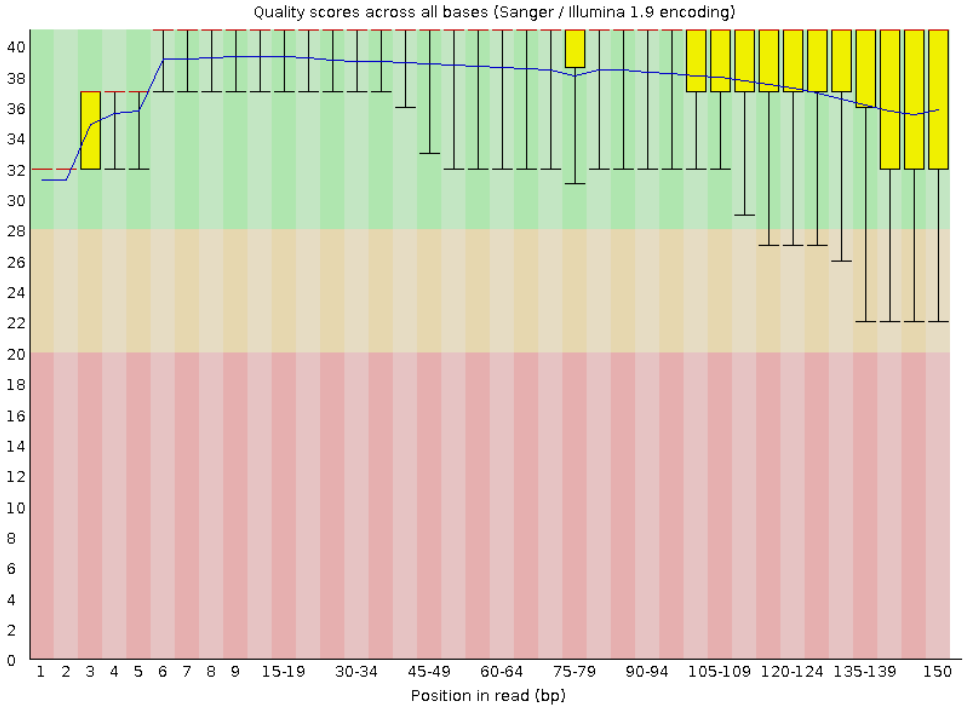

Figure 13.4 Per read quality analysis for sample 3SA_2_2

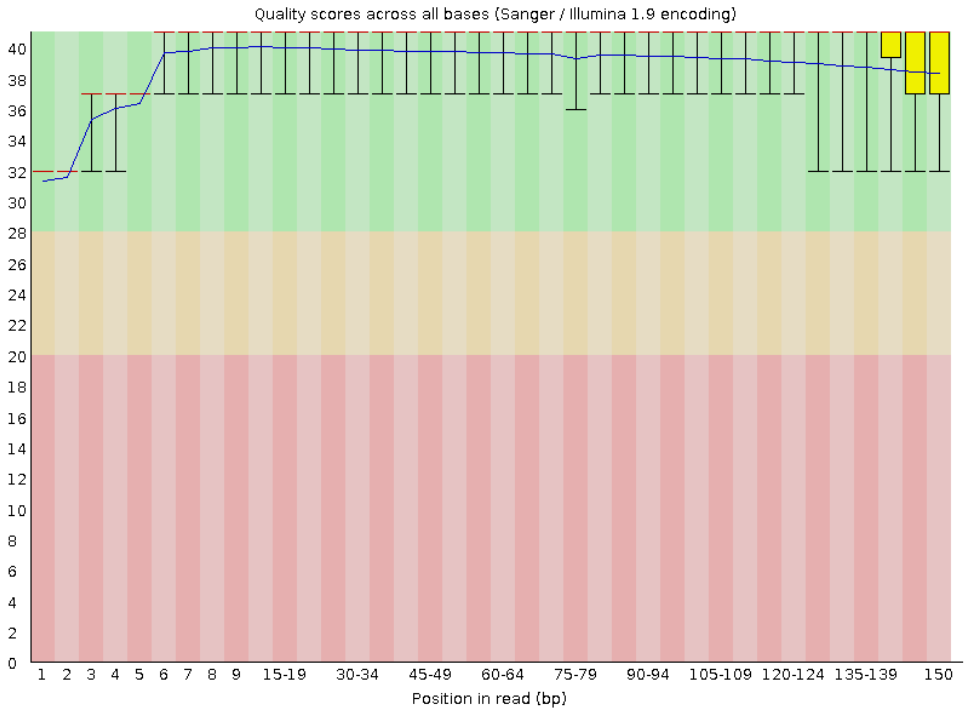

Figure 13.5 Per read quality analysis for sample 3SA_3_1

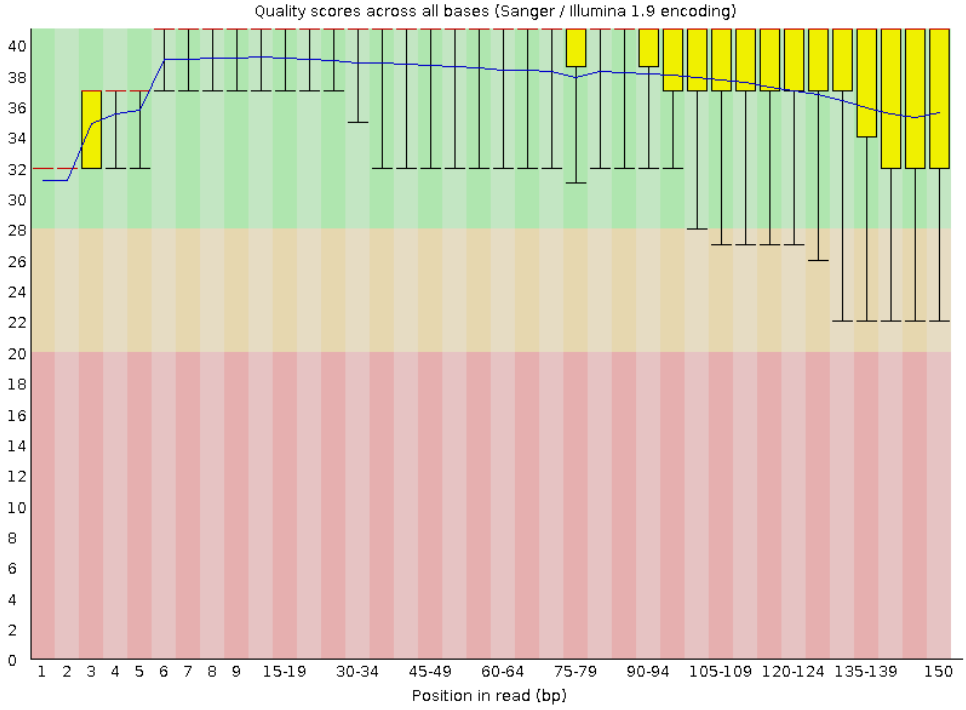

Figure 13.6 Per read quality analysis for sample 3SA_3_2

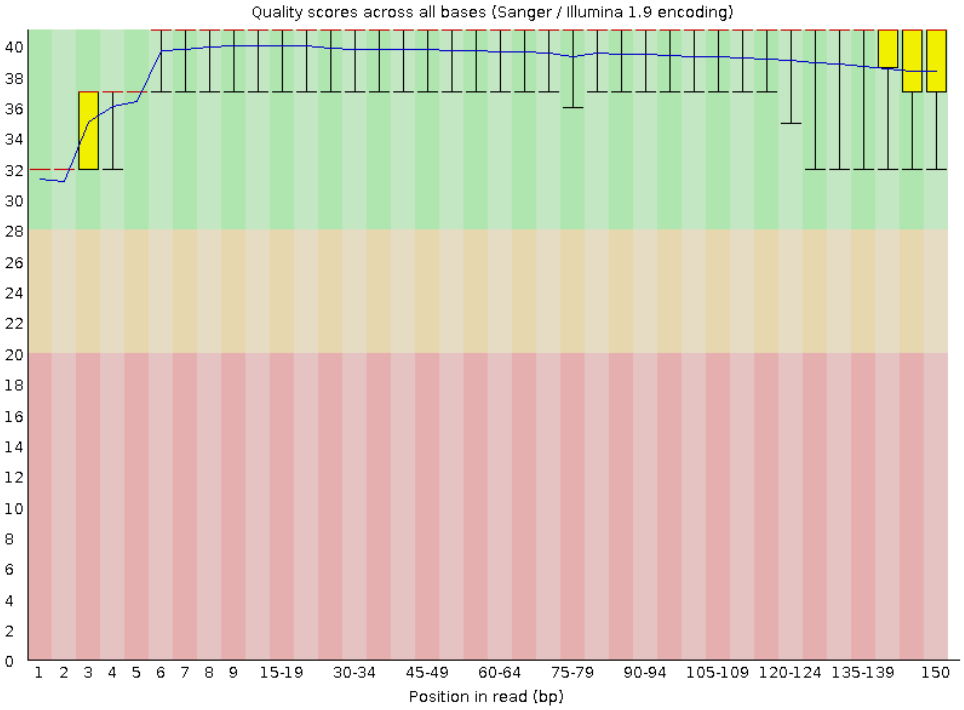

Figure 13.7 Per read quality analysis for sample 3SA_4_1

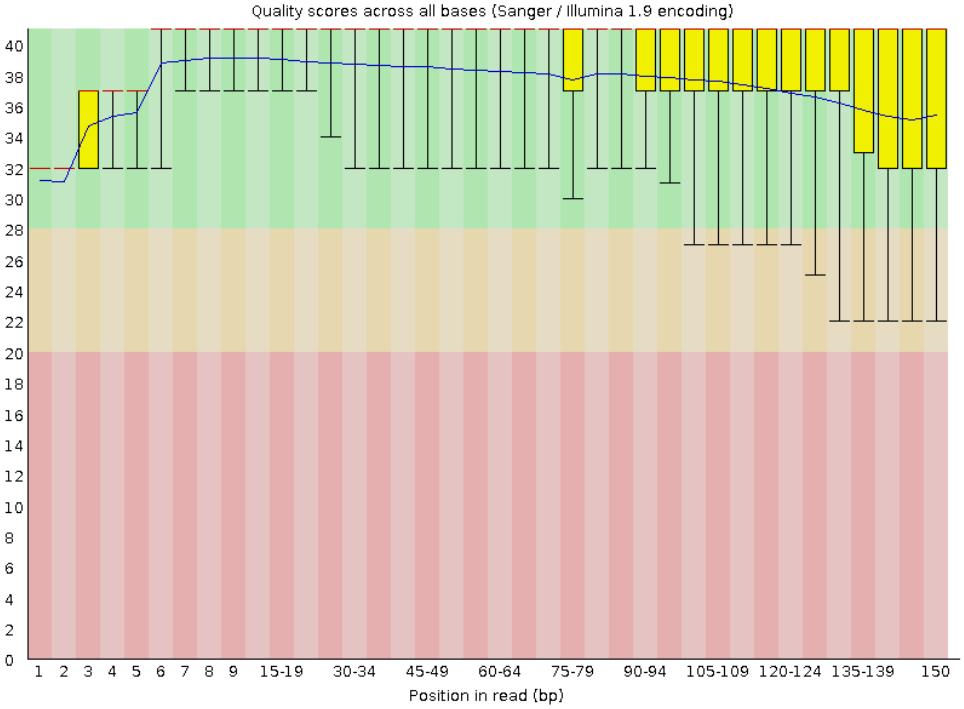

Figure 13.8 Per read quality analysis for sample 3SA_4_2

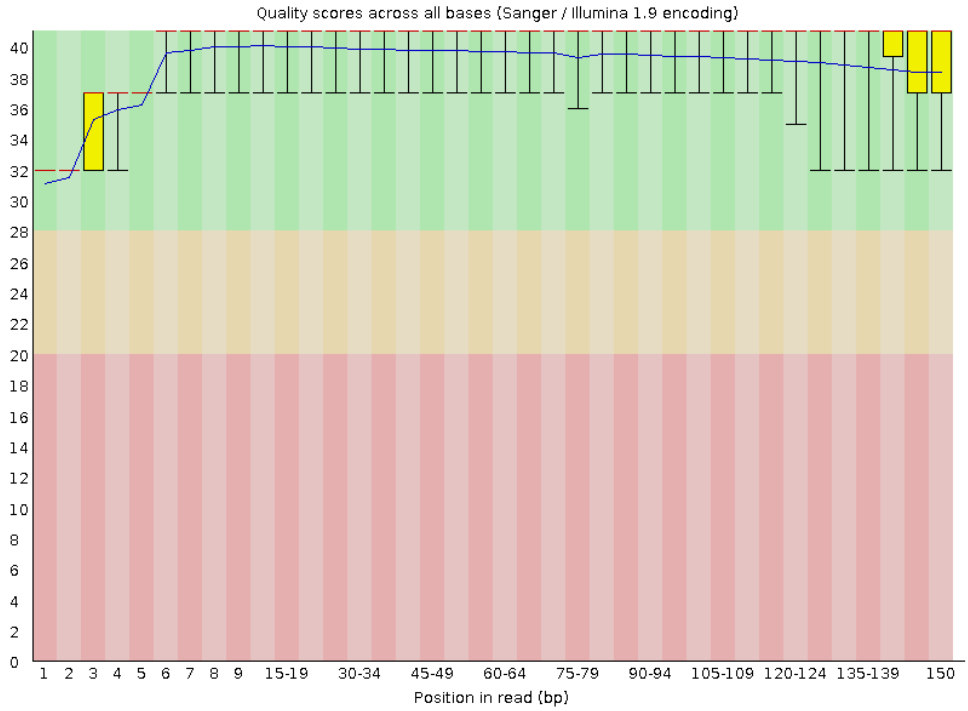

Figure 13.9 Per read quality analysis for sample CS_1_1

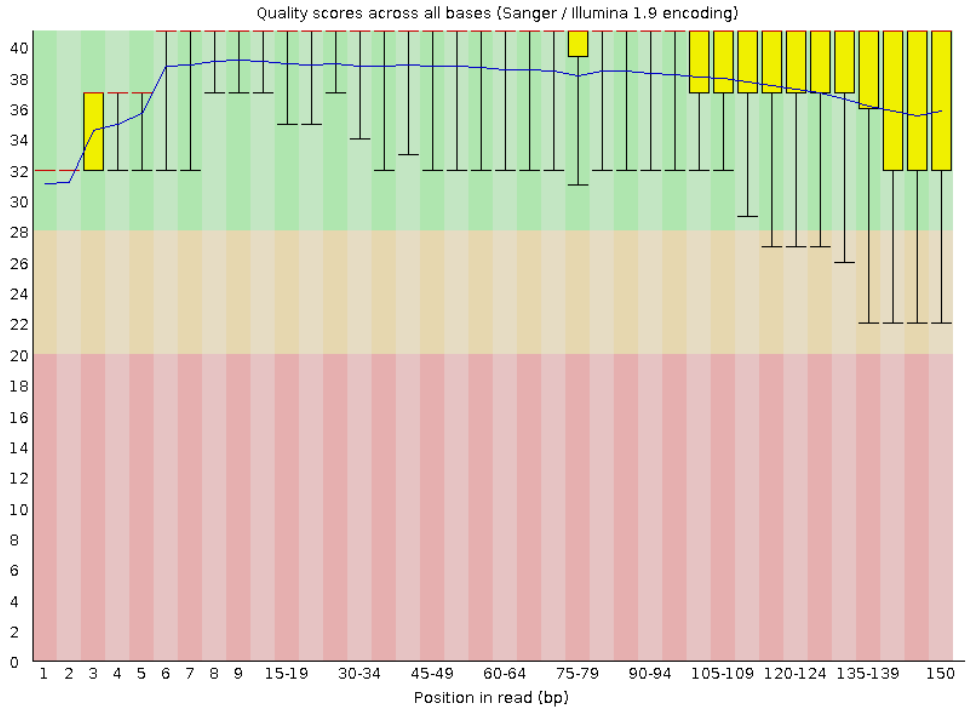

Figure 13.10 Per read quality analysis for sample CS_1_2

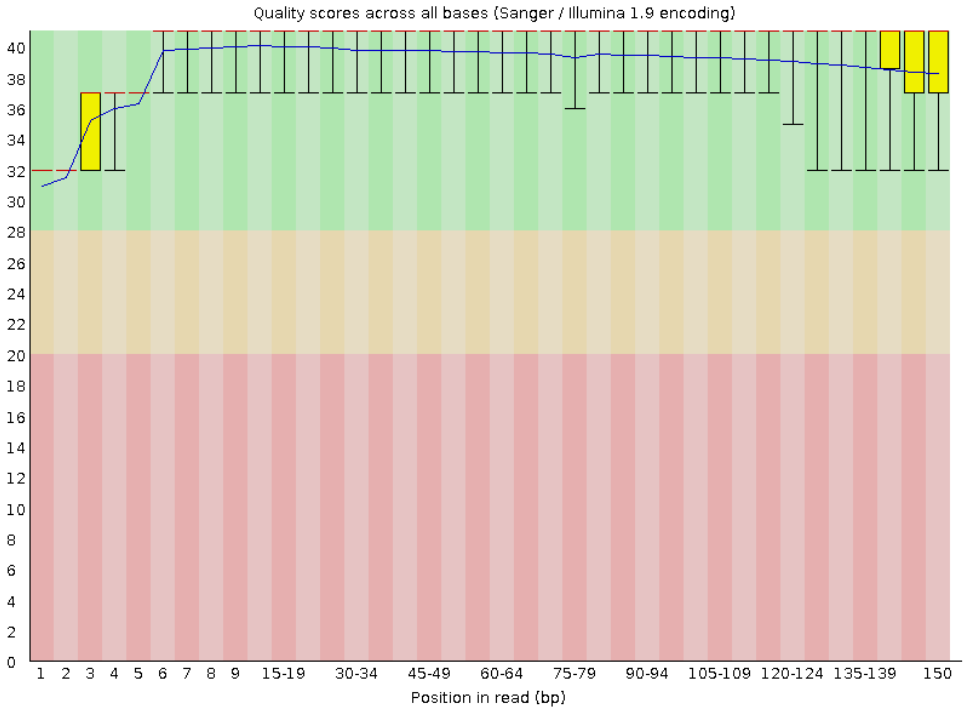

Figure 13.11 Per read quality analysis for sample CS_2_1

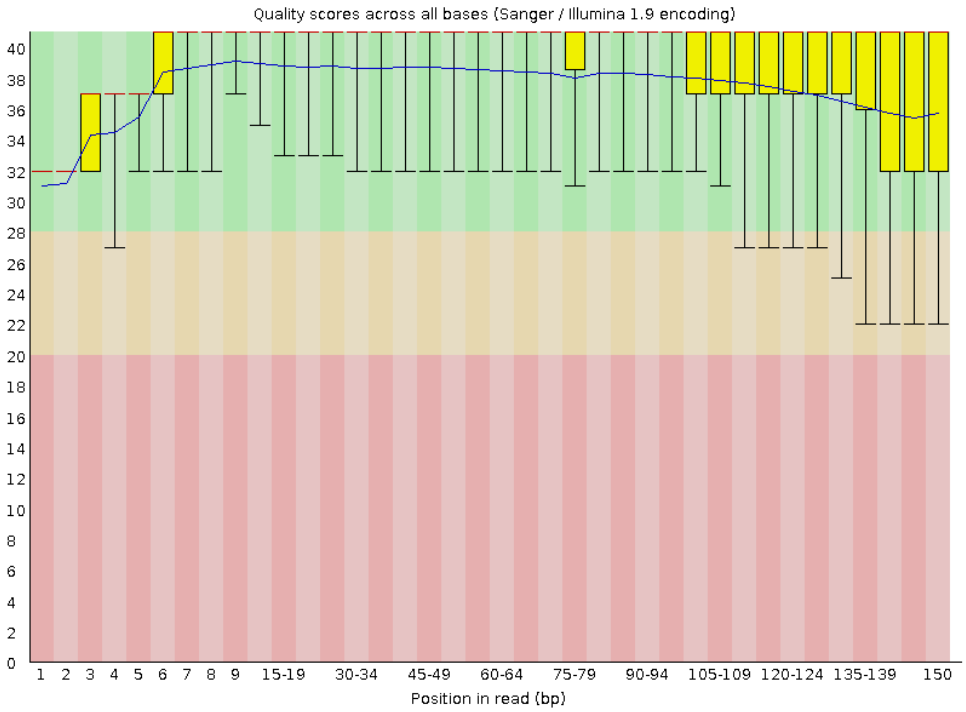

Figure 13.12 Per read quality analysis for sample CS_2_2

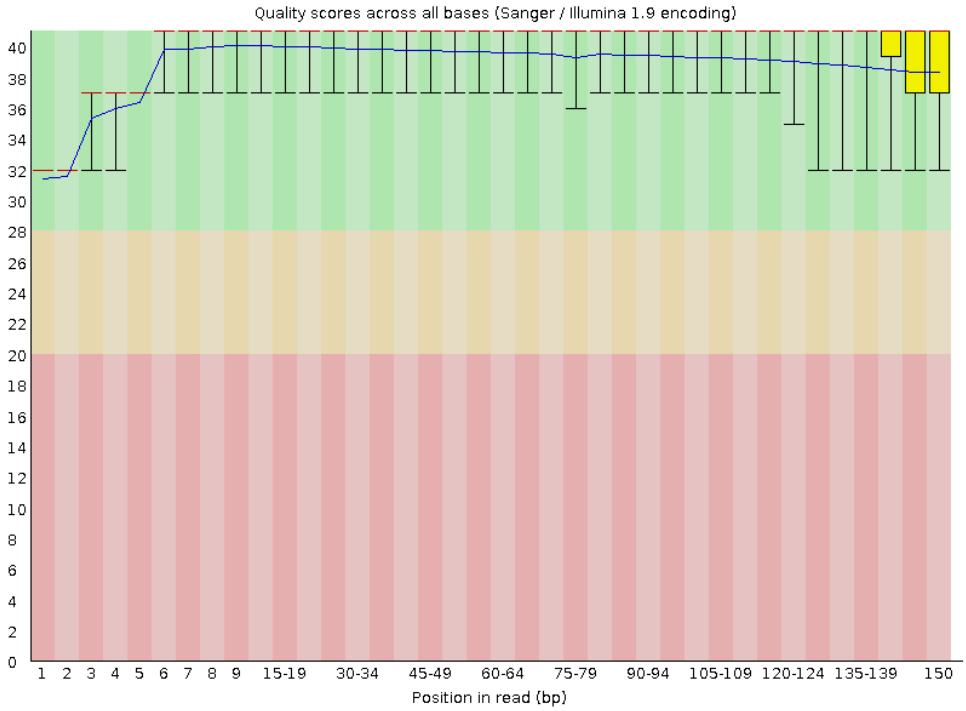

Figure 13.13 Per read quality analysis for sample CS_3_1

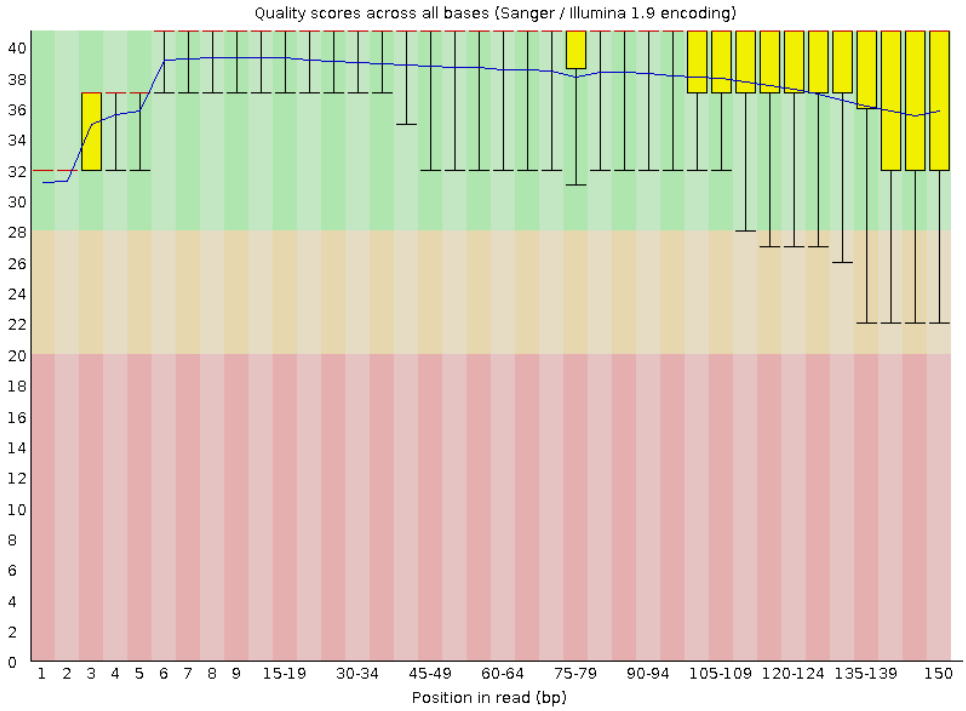

Figure 13.14 Per read quality analysis for sample CS_3_2

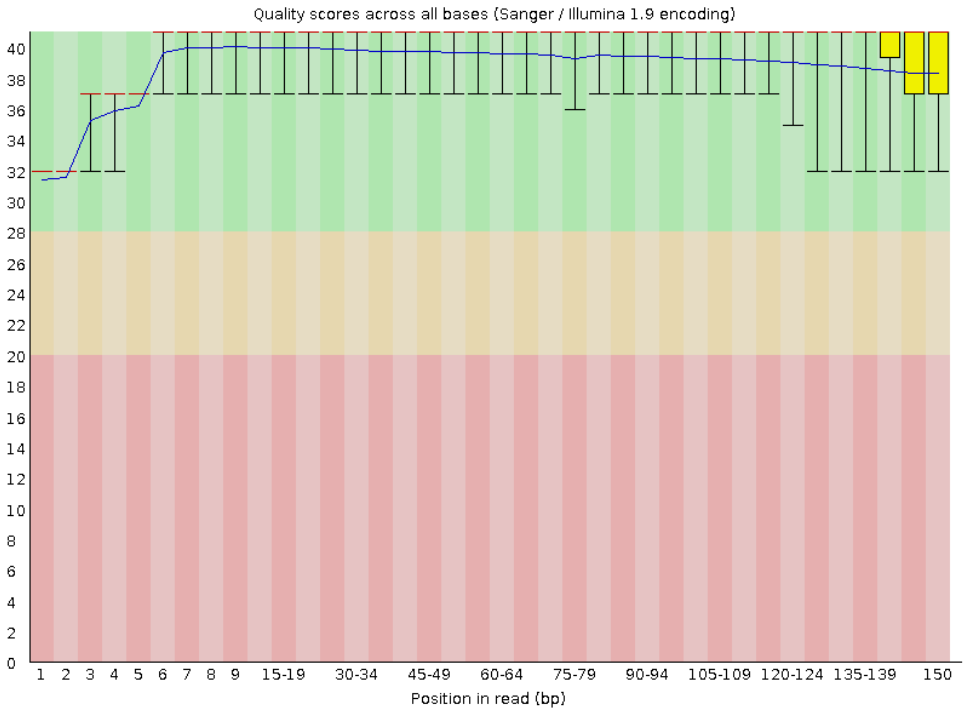

Figure 13.15 Per read quality analysis for sample CS_4_1

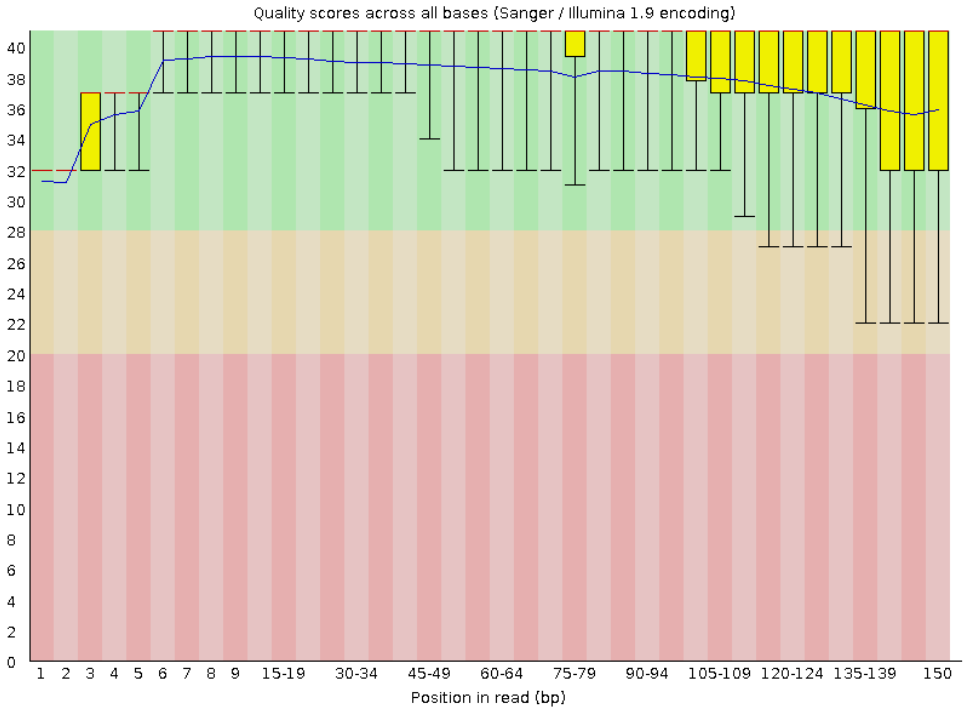

Figure 13.16 Per read quality analysis for sample CS_4_2

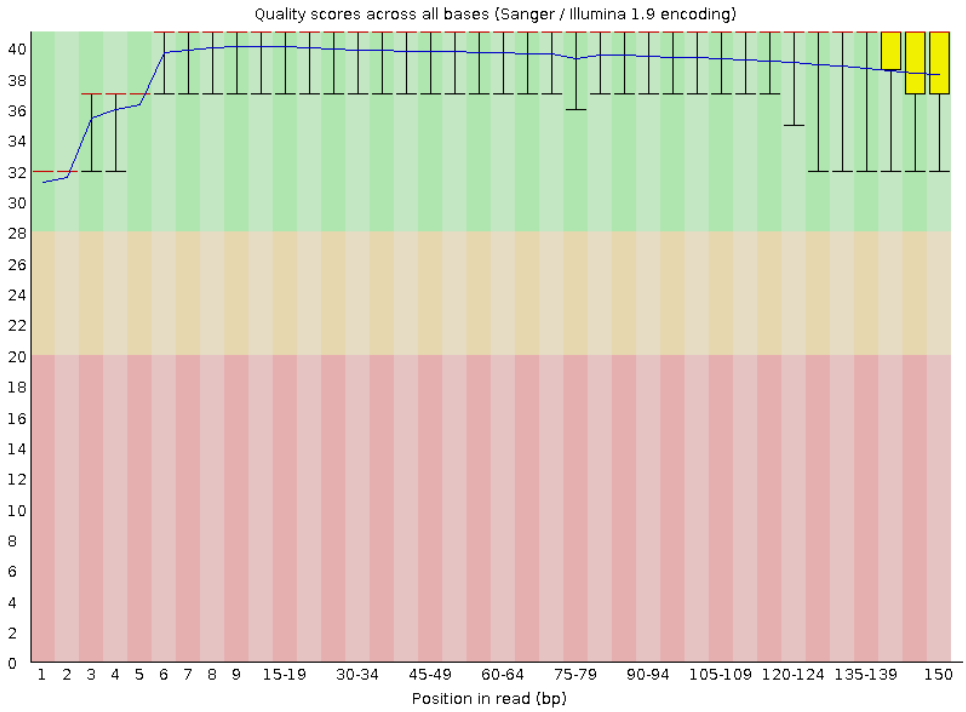

Figure 13.17 Per read quality analysis for sample L175A_1_1

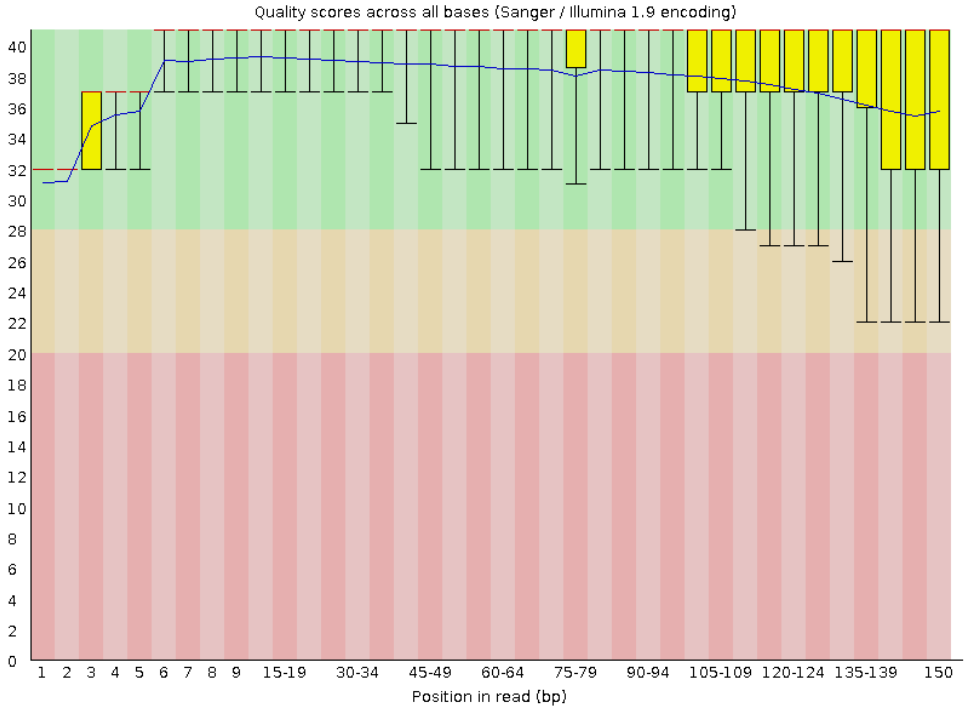

Figure 13.18 Per read quality analysis for sample L175A_1_2

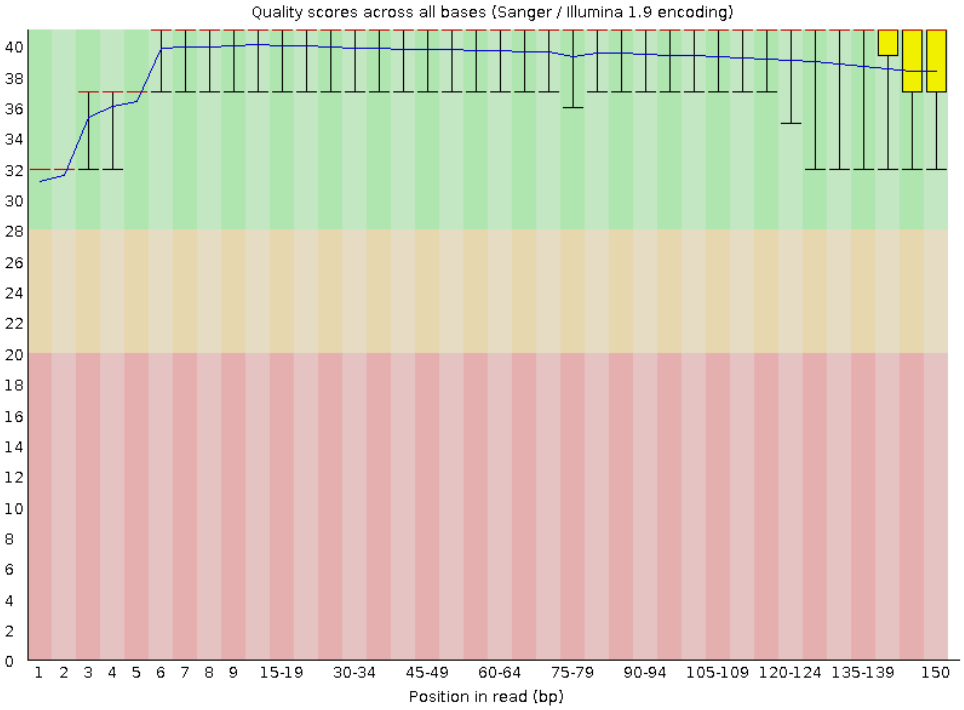

Figure 13.19 Per read quality analysis for sample L175A_2_1

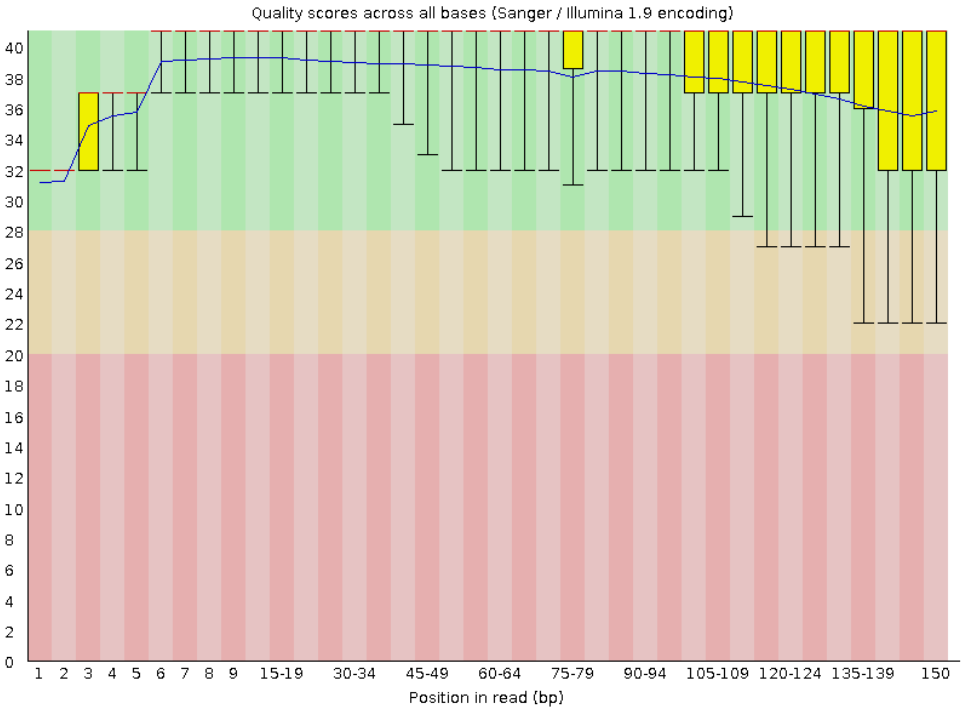

Figure 13.20 Per read quality analysis for sample L175A_2_2

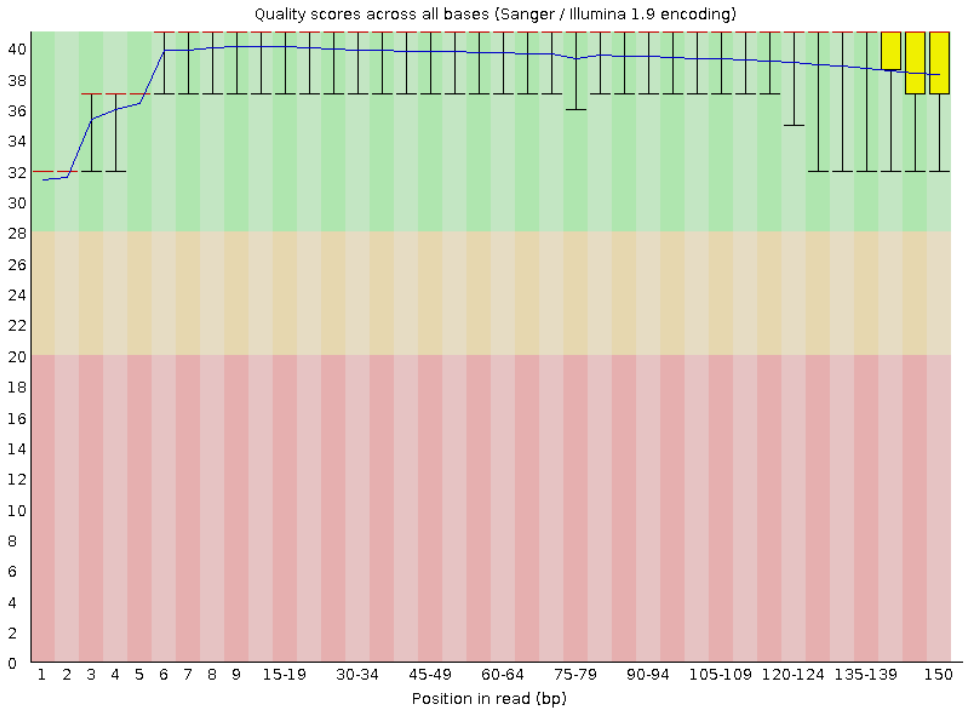

Figure 13.21 Per read quality analysis for sample L175A_3_1

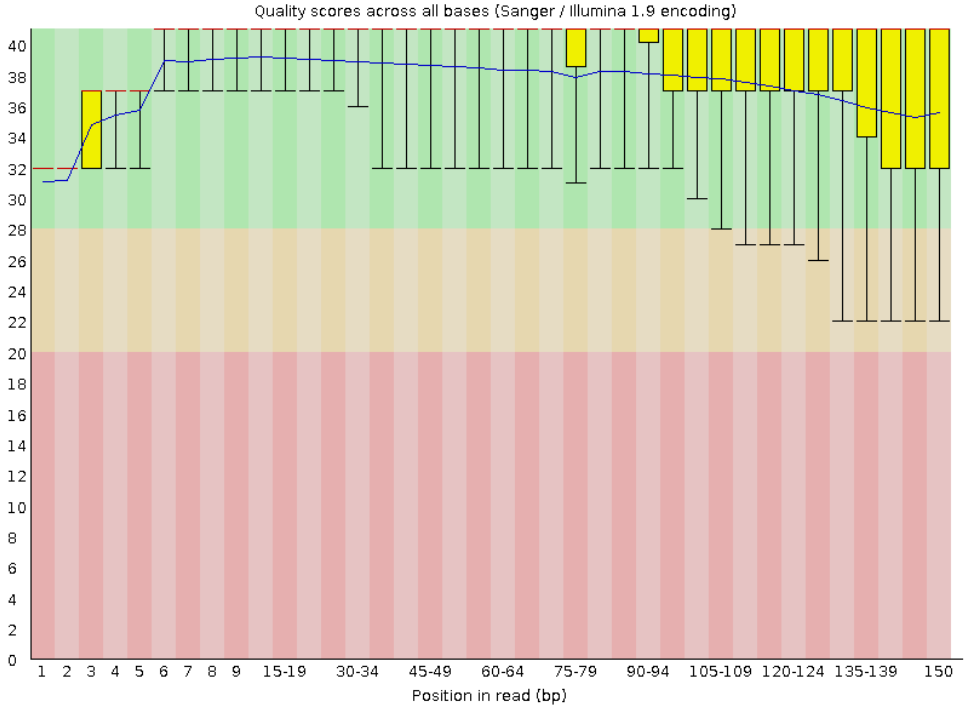

Figure 13.22 Per read quality analysis for sample L175A_3_2

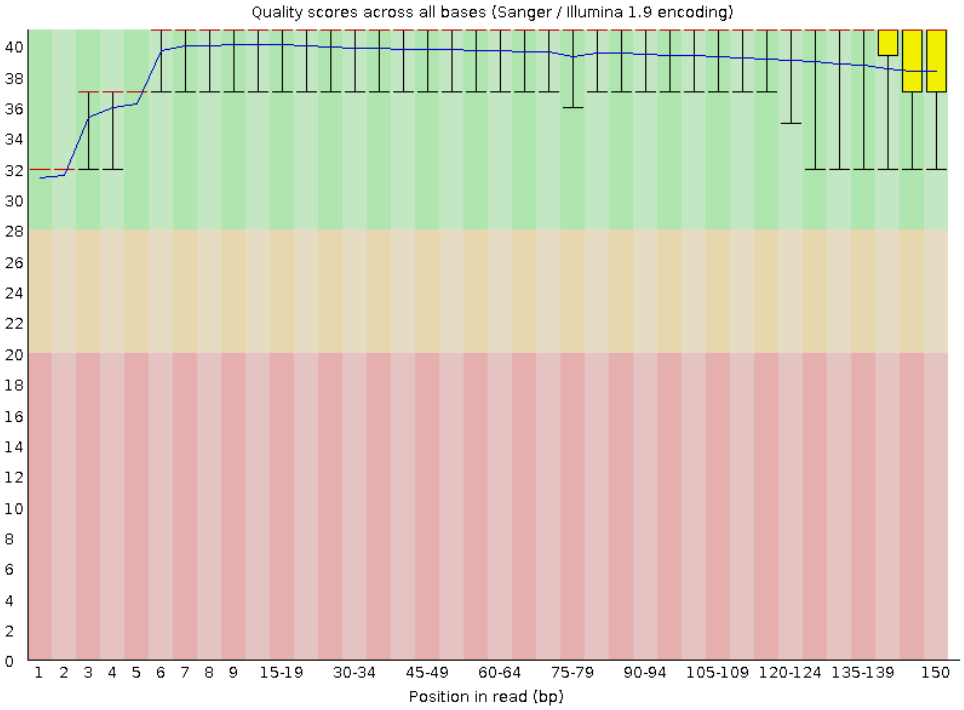

Figure 13.23 Per read quality analysis for sample L175A_4_1

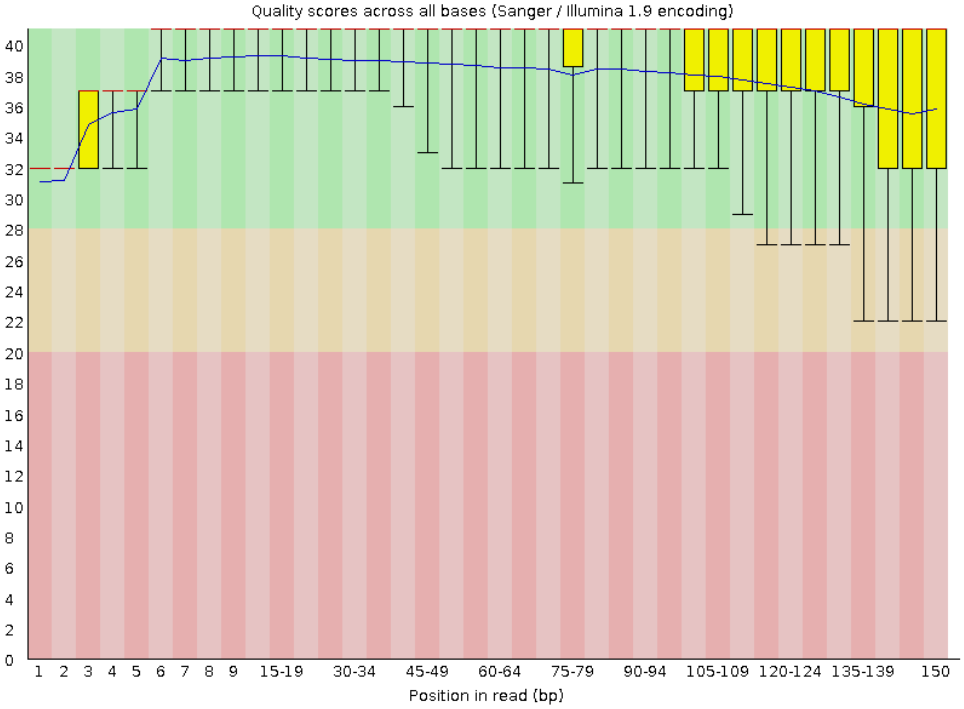

Figure 13.24 Per read quality analysis for sample L175A_4_2

14 Appendix 6 Most significantly differentially expressed RNASeq genes identified in differential expression heatmaps

FlyBase ID	Gene Name	Molecular / biological functions
FBgn0012036	Aldh	Aldehyde dehydrogenase
FBgn0001128	Gpdh	glycerol-3-phosphate dehydrogenase activity / chromatin binding / ethnaol metabolic process / flight behaviour / triglyceride metabolic process
FBgn0039800	Npc2g	Sterol binding / cholesterol transport
FBgn0034253	CG10936	Unknown
FBgn0000473	Cyp6a2	heme binding / iron ion binding / oxidoreductase activity / response to caffeine and DDT
FBgn0050104	NT5E-2	5'-nucleotidase activity / nucleotide binding / metal ion binding
FBgn0037930	CG14715	Unknown
FBgn0040507	ACXD	Adenylyl Cyclase
FBgn0035160	hng3	DNA Binding / transcription factor
FBgn0033395	Cyp4p2	heme binding / iron ion binding / oxidoreductase activity
FBgn0000564	Eh	Eclosion hormone activity / neuropeptide hormone activity / eclosion / ecdysis
FBgn0063499	GstE10	Glutathionine transferase activity
FBgn0263076	Klp54D	Microtubule motor activity / microtubule binding / microtubule-based movement
FBgn0032549	CG4650	Not Serine-type endopeptidase activity
FBgn0265498	CR44367	Unknown
FBgn0052475	mthl8	G-Protein coupled receptor activity / determination of adult lifespan / response to starvation
FBgn0034328	IM23	Antibacterial response / defense against gram-positive bacteria
FBgn0051704	CG31704	Multicellular organism reproduction
FBgn0263093	CR43361	Unknown
FBgn0034335	GstE1	Glutathionine transferase activity / response to heat, oxidative stress

FBgn0044812	TotC	Cellular response to heat, UV, oxidative stress and bacteria
FBgn0260874	Ir76a	Olfactory receptor activity / ligand-gated ion channel activity / detection of chemical stimulus involved in sensory perception of smel
FBgn0031857	CG11321	Linear polyubiquitin binding / ubiquitin protein ligase activity / heat acclimation / protein polyubiquitination
FBgn0261380	mRpL37	Structural constituent of ribosome / translation
FBgn0020414	Idgf3	imaginal disc growth factor receptor binding / chitin - based cuticle development / wound healing
FBgn0250867	CG42238	Unknown
FBgn0031566	CG2818	glycerophosphocholine phosphodiesterase activity / starch binding / glycerophospholipid catabolic process
FBgn0032864	CG2493	Serine-type endopeptidase activity
FBgn0033782	sug	cellular response to starvation / transcription regulation / CNS development
FBgn0266321	CR44986	Unknown
FBgn0085453	CG34424	5-formyltetrahydrofolate cyclo-ligase actvity / folic acid-containing compound biosynhetic process / tetrahydrofolate interconversion
FBgn0267617	CR45955	Unknown
FBgn0026314	Ugt35b	UDP-Glycosyltransferase activity / UDP-glucose metabolic proces
FBgn0039932	fuss	co-SMAD binding / SMAD binding / imaginal disc-derived wing vein specification / negative regulation of BMP signalling pathway / neuron development
FBgn0264822	CR44030	Unknown
FBgn0035089	Phk-3	metamorphosis / response to bacterium
FBgn0026602	Ady43A	Adenosine kinase activity
FBgn0033170	sPLA2	arachidonic acid secretion / phospholipid metabolic process
FBgn0015400	kek2	Not negative regulation of epidermal growth factor receptor singaling pathway
FBgn0051205	CG31205	Serine-type endopeptidase activity
FBgn0025583	IM2	Defense response / response to bacteria

FBgn0039678	Obp99a	Odorant binding / olfactory behaviour / response to pheromone / sensory perception of chemical stimulus (scent)
FBgn0261575	tobi	Hydrolase activity / carbohydrate metabolic process / glycoside catabolic process
FBgn0023479	teq	Chitin Binding / serine-type endopeptidase activity / glucose homeostasis / long-term memory / positive regulation of insulin secretion / short-term memory
FBgn0034331	CG15067	Unknown
FBgn0036556	CG5830	Phosphoprotein phopsphatase activity / RNA polymerase II CTD heptapeptide repeat phosphatase activity / regulation f transcription by RNA polymerase II
FBgn0030272	CG15201	Unknown
FBgn0265045	Strn-Mlck	Protein phosphorylation / positive regulation of microfilament motor activity
FBgn0038147	CCHa2	Neuropeptide signalling pathway
FBgn0039321	CG10550	Unknown

Table 14.1 50 most significantly differentially expressed genes from CS vs. L175A.

Genes presented in the same order as derived by deseq2 grouping observed in Figure 6.8, intended as reference chart for ease of interpretation.

FlyBase ID	Gene Name	Molecular / biological functions
FBgn0044812	TotC	Cellular response to heat, UV, oxidative stress and bacteria
FBgn0035791	CG8539	Unknown
FBgn0037930	CG14715	Unknown
FBgn0034328	IM23	Antibacterial response / defense against gram-positive bacteria
FBgn0034356	CG10924	Response to glucose / gluconeogenesis / glycerol synthesis / response to lipids
FBgn0051664	CG31664	Unknown
FBgn0034335	GstE1	Glutathionine transferase activity / response to heat, oxidative stress
FBgn0260874	Ir76a	Olfactory receptor activity / ligand-gated ion channel activity / detection of chemical stimulus involved in sensory perception of smel
FBgn0000564	Eh	Eclosion hormone activity / neuropeptide hormone activity / eclosion / ecdysis
FBgn0053774	CG33774	Dolichyl-diphosphooligosaccharide-protein glycotransferase activity / protein N-linked glycosylation
FBgn0035160	hng3	DNA Binding / transcription factor
FBgn0063499	GstE10	Glutathionine metabolic process
FBgn0033395	Cyp4p2	heme binding / iron ion binding / oxidoreductase activity
FBgn0052475	mthl8	G-Protein coupled receptor activity / determination of adult lifespan / response to starvation
FBgn0036131	CG12522	Unknown
FBgn0033307	CG14752	Unknown
FBgn0041623	Or65c	Odorant binding / olfactory receptor activity / detection of chemical stimulus involved in sensory perception of smell
FBgn0033520	Prx2540-1	Unknown
FBgn0032549	CG4650	Not Serine-type endopeptidase activity
FBgn0038525	CG14329	Unknown
FBgn0052641	CG32641	Unknown

FBgn0034253	CG10936	Unknown
FBgn0261356	CG42633	Unknown
FBgn0262983	CG43291	Unknown
FBgn0265856	CR44645	Metallocarboxypeptidase activity / Zinc ion binding / proteolysis
FBgn0264835	CR44043	Unknown
FBgn0275434	CR46266	Unknown
FBgn0000406	Cyt-b5-r	Lipid metabolic process
FBgn0015400	kek2	Not negative regulation of epidermal growth factor receptor singaling pathway
FBgn0028396	TotA	Cellular response to heat, cold, mercury, UV, water deprivation
FBgn0039678	Obp99a	Odorant binding / olfactory behaviour / response to pheromone / sensory perception of chemical stimulus (scent)
FBgn0261575	tobi	Hydrolase activity / carbohydrate metabolic process / glycoside catabolic process
FBgn0037612	CG8112	Cholesterol esterification / cholesterol homeostasis / cholesterol metabolic process
FBgn0037613	Cks85A	endomitic cell cycle / mitotic cell cycle
FBgn0038516	P5cr-2	L-Proline biosynthetic process / oxidation reduction process
FBgn0010926	l(3)07882	snoRNA bidning / ribosomal small subunit biogenesis
FBgn0061356	CG18003	Lactate oxidation
FBgn0025583	IM2	Defense response / response to bacteria
FBgn0052523	CG32523	Proteolysis
FBgn0031857	CG11321	Linear polyubiquitin binding / ubiquitin protein ligase activity / heat acclimation / protein polyubiquitination
FBgn0035344	Cyp4d20	heme binding / iron ion binding / oxidoreductase activity
FBgn0045761	CHKov1	Unknown
FBgn0032864	CG2493	Proteolysis
FBgn0051704	CG31704	Multicellular organism reproduction
FBgn0264564	CR43936	Unknown
FBgn0264822	CR44030	Unknown

FBgn0026602	Ady43A	Adenosine kinase activity
FBgn0036549	CG10516	Ubiquitin-protein transferase activity / ubiquitin-dependent protein catabolic process
FBgn0026314	Ugt35b	UDP-Glycosyltransferase activity / UDP-glucose metabolic proces
FBgn0038160	CG9759	Peroxidase activity / Cell redox homeostasis / hydrogen peroxide catabolic process

Table 14.2 50 most significantly differentially expressed genes from CS vs. 3SA.

Genes presented in the same order as derived by deseq2 grouping observed in Figure 6.11, intended as reference chart for ease of interpretation.

FlyBase ID	Gene Name	Molecular / biological functions
FBgn0004045	Yp1	Lipid catabolic processes / sex differentiation
FBgn0267161	CR45601	Unknown
FBgn0085431	CG34402	Unknown
FBgn0039459	IntS12	snRNA 3' end processing
FBgn0043005	prt	serotonin:sodium symporter activity / male mating behaviour / olfactory learning
FBgn0038680	Cyp12a5	heme binding / iron ion binding / oxidoreductase activity
FBgn0037126	CG14567	Unknown
FBgn0040507	ACXD	Adenylyl Cyclase
FBgn0263076	Klp54D	Microtubule motor activity / microtubule binding / microtubule-based movement
FBgn0039052	CG6733	Aminoacyclase activity / cellular amino acid metabolic process
FBgn0053774	CG33774	Dolichyl-diphosphooligosaccharide-protein glycotransferase activity / protein N-linked glycosylation
FBgn0085244	CG34215	Viral response
FBgn0003082	phr	deoxyribodipyrimidine photo-lyase activity/photoreactive repair
FBgn0040942	CG12643	Unknown
FBgn0262570	CG43110	Serine-type endopeptidase activity
FBgn0039051	CG17109	Aminoacyclase activity / cellular amino acid metabolic process
FBgn0034565	CG15650	Unknown
FBgn0038214	CG9616	Unknown
FBgn0038239	CG14850	Unknown
FBgn0038833	CG15696	Transcription regulation
FBgn0039798	CG11313	Serine-type endopeptidase activity
FBgn0039415	CG6142	Glucose-methanol-choline oxidoreductase
FBgn0052581	CG32581	Ubiquitin protein ligase activity / ubiquitin-protein tansferase activity / ubiquitin-dependent protein catabolic processes

FBgn0035538	DopEcR	response to ethanol / associative learning / adenylate cyclase-activating G protein-coupled receptor signalling pathway
FBgn0020416	Idgf1	imaginal disc growth factor receptor binding / chitin - based cuticle development / wound healing
FBgn0020414	Idgf3	imaginal disc growth factor receptor binding / chitin - based cuticle development / wound healing
FBgn0040099	lectin-28C	Galactose binding / transmembrane signalling receptor activity
FBgn0034761	CG4250	Unknown
FBgn0051205	CG31205	Serine-type endopeptidase activity
FBgn0052333	CG32333	cellular lipid metabolic process
FBgn0266227	CR44922	Unknown
FBgn0027620	Acf	Chromatin assembly / negative regulation of transcription / nucleosome assembly, mobilisation and positioning / nervous system development
FBgn0035344	Cyp4d20	heme binding / iron ion binding / oxidoreductase activity
FBgn0040207	kat80	microtubule binding / microtubule depolymerisation / microtubule severing
FBgn0031936	CG13794	Neurotransmitter transport
FBgn0040571	CG17193	Unknown
FBgn0032322	CG16743	Unknown
FBgn0031694	Cyp4ac2	heme binding / iron ion binding / oxidoreductase activity
FBgn0001089	Gal	beta-galactosidase activity / protein homodimerisation activity
FBgn0026718	fu12	1-acyllycerol-3-phosphate O-acyltransferase activity / behavioural response to ethanol
FBgn0051664	CG31664	Unknown
FBgn0050104	NT5E-2	5'-nucleotidase activity / nucleotide binding / metal ion binding
FBgn0264916	CR44107	Unknonw
FBgn0031957	TwdlE	Chitin-based cuticle development
FBgn0033395	Cyp4p2	heme binding / iron ion binding / oxidoreductase activity

FBgn0044812	TotC	Cellular response to heat, UV, oxidative stress and bacteria
FBgn0033777	CG17574	Unknown
FBgn0036549	CG10516	Ubiquitin-protein transferase activity / ubiquitin-dependent protein catabolic process
FBgn0038682	CG5835	Unknown
FBgn0039485	CG17189	Unknown

Table 14.3 50 most significantly differentially expressed genes from L175A vs. 3SA.

Genes presented in the same order as derived by deseq2 grouping observed in Figure 6.14, intended as reference chart for ease of interpretation.